New approaches towards understanding trypanosome mitosis

Owen Stretton, MSc, BSc

Thesis submitted to the University of Nottingham

towards the degree of Doctor of Philosophy

September 2016

Abstract

The protozoan parasite, *Trypanosoma brucei* has an unusual genome, consisting of an unusually large number of chromosomes. It is composed of 11 large diploid chromosomes and over 100 small linear chromosomes, known as intermediate chromosomes and minichromosomes. These smaller chromosomes contain a portion of a library of genes required for antigenic variation and, therefore, evasion of the host's immune response. Despite their number, all chromosomes are separated with fidelity during mitosis, through interaction with the mitotic spindle. Animal and fungal model organisms have been widely used to study mitosis and the proteins involved. *T. brucei*, however, belongs to a group of organisms that diverged from the animal-fungus lineage at or close to the eukaryotic root. Mitosis in trypanosomes differs from that observed in model organisms, including an apparent lack of conserved microtubule motor proteins that drive spindle function and a reduced number of kinetochores. It is, therefore, not well understood how trypanosomes segregate their genomes.

In this thesis, I will present the development of an RNA interference based library methodology for the investigation of microtubule motor function. This system uses a combinatorial library that accounts for interactions, such as redundancy, which can occur between motors. I demonstrate that motor redundancy can occur in trypanosomes, by knocking down flagellar kinesin-2 motors. The library approach allows for exploration of an individual motor's contribution to fitness and, by combining the library with a negative selection marker tag of individual chromosomes, the motor's role in chromosome segregation. The use of a negative selection marker also allows for quantification of chromosome loss, as I demonstrate by quantifying the losses caused by depletion of the mitotic motor KIN13-1 and the kinetochore protein KKIP1. I also present the development of a cell line to be used in validating the results of the library experiments. The production of a tag that uses KIN13-1 to label the mitotic spindle, for later observations of spindle defects, is presented. Finally, I present the development of a chromosome label that uses arrays of Lac operator repeats and fluorescently labelled Lac repressor protein to tag DNA elements, to follow

chromosomes through the cell cycle. I demonstrate this label's use in detecting chromosome loss and non-disjunction events after knockdown of KIN13-1 and KKIP1. I then use it to demonstrate interactions between chromosomes and kinetochores during mitosis. These data provide evidence that refutes a "lateral stacking" model for chromosome segregation.

Declaration

I declare that this thesis is the result of my own work, except where included data is explicitly mentioned, which has been undertaken during my period of registration for this degree at The University of Nottingham.

Acknowledgements

Thanks to Prof Tomo Tanaka (University of Dundee), for supplying the pAFS52 and pT1045 plasmids used in this work, to Dr Catarina Gadelha (University of Nottingham), for providing the pSiG-BG, pSiG-HhsfG and pBES-H-2 plasmids, and to Prof Rita Tewari (University of Nottingham), for loaning an Amaxa™ Nucleofector™ when required. Thanks also to the Deep Seq laboratory and Dr Sunir Malla (University of Nottingham), in particular, for providing next generation sequencing expertise.

I am grateful to all members of the Allers, Friel, Gadelha, Huett, Nieduszynski and Wickstead labs for their aid and contributions and for sharing supplies and equipment. I am particularly grateful to my supervisor, Bill Wickstead, for his support throughout my studies.

This work was supported by the University of Nottingham School of Life Sciences and the BBSRC new investigator grant awarded to Bill Wickstead.

Abbreviations

APC/C	anaphase promoting complex
BES	bloodstream expression site
BLE	bleomycin resistance marker
BSD	blasticidin S resistance marker
BSF	bloodstream form
CCAN	constitutive centromere-associated network
CDS	coding DNA sequence
CENP	centromere protein
CPC	chromosomal passenger complex
dsDNA	double stranded DNA
dsRNA	double stranded RNA
ESB	expression site body
FAZ	flagellum attachment zone
FISH	fluorescence *in situ* hybridisation
FP	flagellar pocket
γ-TURC	γ-tubulin ring complex
GFP	green fluorescent protein
HYG	hygromycin resistance marker
HSV-TK	herpes simplex virus thymidine kinase
IC	intermediate chromosome
IFT	intraflagellar transport
LacI	Lac repressor protein
LacO	Lac operator
KKIP	KKT-interacting protein
KKT	kinetoplastid kinetochore protein
LECA	last eukaryotic common ancestor
MBC	megabase chromosome
MC	minichromosome
MCAK	mitotic centromere associated kinesin
MCC	mitotic checkpoint complex

MTOC	microtubule organising centre
NAT1/SAT	nourseothricin resistance markers
NE	nuclear envelope
NEBD	nuclear envelope breakdown
NEO	neomycin resistance marker
NPC	nuclear pore complex
PCF	procyclic form
PFGE	pulsed field gel electrophoresis
PFR	paraflagellar rod
PFR1	paraflagellar rod protein 1
PFR2	paraflagellar rod protein 2
PUR	puromycin resistance marker
RIT-seq	RNAi target sequencing
RNAi	RNA interference
SAC	spindle assembly checkpoint
sfGFP	superfolder GFP
siRNA	short interfering RNA
SSR	strand switch region
ssu rRNA/DNA	small subunit ribosomal RNA/DNA
SV40	simian vacuolating virus 40
TGS	transcriptional gene silencing
UTR	untranslated region
VSG	variant surface glycoprotein
YFP	yellow fluorescent protein

Table of Contents

1. Introduction 1

1.1. *Trypanosoma brucei* 2

1.1.1. An introduction to *Trypanosoma brucei* 2

1.1.2. The evolutionary history of trypanosomes 4

1.1.3. The microtubule cytoskeleton of *Trypanosoma brucei* 7

1.1.4. The genome of *Trypanosoma brucei* 13

1.2. Mitosis in model systems 17

1.2.1. Open and closed mitosis 17

1.2.2. The canonical mitotic spindle 20

1.2.3. The kinetochore 24

1.2.4. Tension sensing at metaphase 27

1.2.5. The separation of sister chromatids at anaphase 30

1.3. Mitosis in *Trypanosoma brucei* 31

1.3.1. The mitotic spindle in *Trypanosoma brucei* 31

1.3.2. Segregation of trypanosome chromosomes 36

1.3.3. The trypanosome kinetochore lacks many components present in model systems 40

1.4. Kinesin motors 46

1.4.1. The kinesin superfamily 46

1.4.2. Kinesins perform a number of roles in mitosis 51

1.4.3. Kinesin motor interactions 59

1.4.4. The phylogenetic distribution of kinesins 61

1.4.5. Kinesins in trypanosomes 63

1.5. Trypanosomatid genetic modification technology 66

1.5.1. Established selection markers used for experimentation in trypanosomatids 66

1.5.2. The use of episomal constructs for genetic manipulation 69

1.5.3. Direct modification of trypanosomatid genomes 71

1.5.4. Tetracycline inducible systems 72
1.5.5. RNA interference 73
1.5.6. Recent advances in CRISPR technologies in trypanosomes .. 75
1.5.7. Genome wide genetic modification 76

2. Aims 79

3. Materials and Methods 80

3.1. Combinatorial library production 80
3.1.1. Microtubule motor coding sequence PCR 80
3.1.2. Plasmid library production 80
3.1.3. Plasmid library analysis 81
3.2. Production of plasmids 83
3.2.1. For the knockdown of kinesin-2 proteins by RNAi 83
3.2.2. For the knockdown of other proteins 84
3.2.3. For integration of *HSV-TK* chromosome labels 84
3.2.4. For the creation of a KIN13-1-GFP mitotic spindle tag 85
3.2.5. For the production of fluorescently labelled LacI 85
3.2.6. For the integration of a LacO chromosome tag 88
3.2.7. For the generation of fluorescently labelled kinetochore protein 90
3.3. Cell lines 91
3.4. Southern blotting 93
3.5. Analysis of LacO repeat integration 94
3.5.1. Diagnostic PCR 94
3.5.2. G418 sensitivity analysis 95
3.6. Western blotting 95
3.7. Growth analysis 96
3.8. Microscopy 97
3.8.1. Attachment and mounting of samples 97
3.8.2. Immunofluorescence 97
3.8.3. Imaging 98

3.9. K-N Counts 98
3.10. Minichromosome loss assay 98
3.11. Analysis of the distribution of fluorescent foci 99
3.11.1. Counts of LacI/LacO foci 99
3.11.2. Kinetochore-chromosome distance measurements 99
4. A combinatorial library for assessment of motor function in *Trypanosoma brucei* 100
4.1. Redundancy of trypanosomal motor proteins 100
4.1.1. Individual molecular motors do not significantly contribute to the fitness of trypanosomes in high-throughput screens ... 100
4.1.2. Kinesin-2 motors are essential for flagellar function in model organisms 105
4.1.3. Knockdown of both kinesin-2 motors is required to generate a growth phenotype in *Trypanosoma brucei* 107
4.1.4. The *KIN2A/B* knockdown phenotype is not the result of a gross change to the cell cycle 109
4.1.5. *KIN2A/B* knockdown prevents normal flagellum synthesis 114
4.1.6. Summary 116
4.2. Generation of combinatorial libraries 117
4.2.1. A method for generating libraries of random pairwise combinations for use in RNA interference 117
4.2.2. Producing the kinesin combinatorial library 121
4.2.3. The pan-kinesin library contains all possible pairwise combinations 125
4.2.4. Cells expressing hairpin RNA sequences do not phenocopy individual kinesin knockdown 131
4.2.5. Hairpins have a greater effect on the trypanosome cell cycle 133
4.2.6. Hairpins should be excluded from library analysis 137
4.2.7. Summary 138

5. "Reporter" cell lines for library analysis 139

5.1. A negative selection marker for chromosome loss 139

5.1.1. *HSV-TK* as a negative selection marker in trypanosomes ... 139

5.1.2. Transcriptionally active *HSV-TK* can be targeted to minichromosomes in bloodstream form cells..... 142

5.1.3. Minichromosome loss caused by kinesin knockdown can be detected using negative selection..... 144

5.1.4. Adapting *HSV-TK* constructs for use in procyclic form cells 147

5.1.5. Minichromosome loss can be detected with less sensitivity in procyclic form cells 152

5.1.6. Summary..... 154

5.2. Cell lines for validation of mitotic mutants 155

5.2.1. KIN13-1 can be used as a spindle label 155

5.2.2. A strategy for the production of a minichromosome label 159

5.2.3. Directing labelled LacI to the nucleus reduces protein levels... 161

5.2.4. Altering 3' untranslated regions does not increase labelled LacI expression 166

5.2.5. Changes to the nuclear localisation signal raise LacI protein levels..... 168

5.2.6. The use of sfGFP to label LacI also restores expression levels.. 170

5.2.7. A "LacI/LacO system" for observing trypanosome chromosomes 173

5.2.8. Summary..... 182

6. The movement of individual chromosomes through the *Trypanosoma brucei* cell cycle 183

6.1. Observing trypanosomal chromosome movement..... 183

6.1.1. Chromosome and minichromosome tags display similar localisations during the cell cycle 183

6.1.2. Distribution of fluorescent foci is consistent with kinetochore interaction 187
6.1.3. Distances between chromosomes and kinetochores vary throughout mitosis 196
6.1.4. Summary 199
6.2. Disrupting normal chromosome movement 200
6.2.1. Fluorescently labelled chromosomes can be used to detect chromosome loss and nondisjunction events 200
6.2.2. KKIP1 knockdown adversely affects kinetochore function . 205
6.2.3. Summary 208
7. Discussion 209
7.1. Redundancy in trypanosome kinesins 209
7.2. The increased efficiency of hairpin RNAi constructs 211
7.3. Combinatorial RNAi libraries 212
7.4. An assay for minichromosome loss frequency 215
7.5. A LacI/LacO system to monitor trypanosome chromosome movement 216
7.6. Trypanosome chromosomes share kinetochores 218
7.7. Summary 220
8. References 221

1. Introduction

Accurate replication and segregation of genomes is essential for all three domains of life: Bacteria, Archaea and Eukarya. In all eukaryotes, genome segregation, called mitosis, is executed by the mitotic spindle, a complex, macromolecular machine. The means by which the spindle separates chromosomes are largely based on the depolymerisation and polymerisation of microtubules. The mechanisms of mitosis have been extensively studied in animal, yeast and plant model systems. These organisms, however, form a very small fraction of the eukaryote domain as a whole. Some research has been performed into a few more divergent organisms, revealing vastly differing mitotic mechanisms and spindles (reviewed in Drechsler and McAinsh, 2012; Makarova and Oliferenko, 2016). Given the differences in mitosis that are known to exist among eukaryotes, model systems are unlikely to be representative of the mitotic machinery employed by all eukaryotes or the last eukaryotic common ancestor (LECA). An understanding of mitosis across eukaryotes would help in understanding mitosis in LECA and how it evolved into the systems we see today. In this thesis I describe the development of strategies for investigations into the roles of molecular motors in the mitotic spindle in, the divergent eukaryote, *Trypanosoma brucei*.

1.1. *Trypanosoma brucei*

1.1.1. An introduction to *Trypanosoma brucei*

Trypanosoma brucei is a flagellate, protozoan parasite. It is transmitted by the tsetse fly (genus *Glossina*) and is limited to the fly's range in sub-Saharan Africa. It is responsible for the fatal human African trypanosomiasis (HAT), or sleeping sickness, and animal African trypanosomiasis (AAT), or nagana, a wasting disease of livestock (Fèvre et al., 2008; Yaro et al., 2016). The species is comprised of three subspecies, *T. b. gambiense*, *T. b. rhodesiense* and *T. b. brucei*. Only *T. b. gambiense* and *T. b. rhodesiense* are capable of infecting humans, due to innate resistances to trypanolytic factors in the blood of humans and other primates (Pays et al., 2006). The former causes the majority of cases of HAT, particularly in West Africa, producing a less severe form of the disease, whereas the latter causes a more acute, more severe form, mainly in East Africa (Fèvre et al., 2008; WHO, 2012). HAT causes substantial morbidity and mortality, its burden estimated at 1.6 million disability-adjusted life years (DALYs) (WHO, 2012). AAT is also a significant burden, rendering ~7 million km^2 of land unsuitable for raising livestock and causes annual agricultural production losses of over 4.5 billion US dollars (Yaro et al., 2016).

T. brucei has a life cycle that consists of a number of stages, allowing it to adapt to its hosts, the key stages of which are shown in Figure 1. Briefly, the mammalian host becomes infected by metacyclic trypomastigote form *T. brucei* when an infected tsetse fly takes a blood meal. The parasite differentiates into long slender bloodstream form (BSF) trypomastigotes and begins multiplying within blood vessels. They then differentiate into short stumpy BSF cells and cease division, in preparation for tsetse fly colonisation. When a fly feeds, short stumpy trypanosomes are ingested and transform into the procyclic form (PCF), in the tsetse midgut, and begin dividing again. Eventually PCF cells leave the midgut and colonise the insect's salivary gland, as epimastigotes. They then transform into metacyclic trypomastigotes, stopping division, in preparation for host infection, completing the life cycle (Smyth, 1994; Vickerman, 1985).

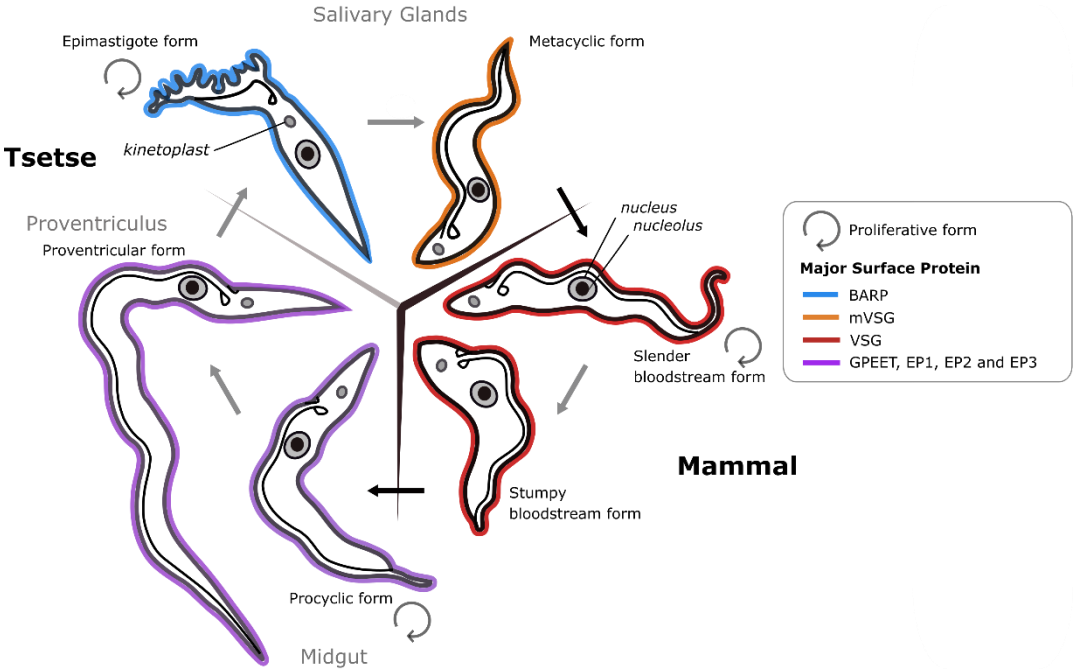


Figure 1. Diagram of the *T. brucei* life cycle showing key stages. The colours outlining the cell represent the major constituent of the trypanosome's surface coat. Courtesy of Jennifer McDonald.

1.1.2. The evolutionary history of trypanosomes

T. brucei belongs to the order Kinetoplastida, flagellate protozoa characterised by an organelle known as the kinetoplast, a filamentous structure containing mitochondrial DNA. A phylogeny of this group is shown in Figure 2. *T. brucei* falls into the Trypanosomatida clade, which emerged from within Eubodonida (Deschamps et al., 2011), alongside the other medically important kinetoplastids *Trypanosoma cruzi* and *Leishmania*.

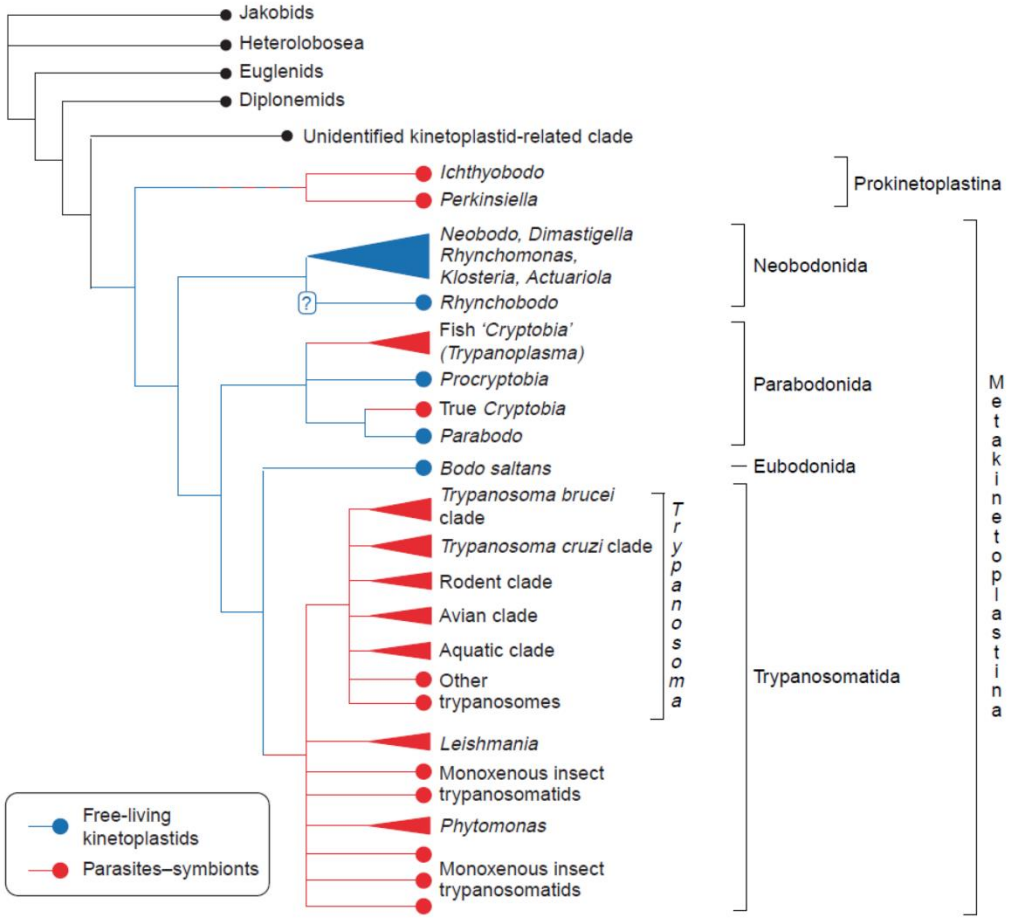


Figure 2. Kinetoplastid evolutionary relationships based on ssu rRNA gene sequences and protein phylogenies. From Simpson et al. (2006), based on the classification of kinetoplastids by Moreira et al. (2004), with the placement of trypanosomatids as a sister group to Eubodonida based on HSP phylogenies (Simpson et al., 2004; Simpson and Roger, 2004). The "unidentified kinetoplastid-related clade" is based on environmental ssu rRNA sequences (López-García et al., 2003). A black line represents a branch outside the kinetoplastids; a red and blue line indicates unknown status; a circle represents a clade with one or very few representatives; a triangle represents a clade with several representatives; a question mark indicates an unstable clade position, based on conflicts between ssu rRNA and HSP data.

The kinetoplastids are highly divergent from traditional model eukaryotes. Representations of the eukaryotic tree of life (see Figure 3 for an example) usually consist of five or six supergroups of organisms, the Opisthokonta, the Amoebozoa, the Excavata, the SAR (Stramenophiles, Alveolata and Rhizaria) group, the Archaeplastida, and the Hacrobia (containing the Haptophyta and Cryptophyta) (Burki, 2014; Keeling et al., 2005; Roger and Simpson, 2009). The kinetoplastids belong to Excavata, a diverse group of heterotrophic protists, whereas the most common models for mitosis, animals and fungi, belong to Opisthokonta. While researchers' ability to resolve the eukaryotic tree is improving, the placing of the root of the tree, or LECA, remains uncertain (Burki, 2014; Eme et al., 2014). Some studies place the root at a divergence between the "Unikonts" (Opisthokonta and Amoebozoa) and the "Bikonts" (everything else), while others position it elsewhere. Most recent studies place the divergence of excavates at or close to the eukaryotic root, meaning that they and the ophisthokonts are highly divergent from one another.

Determining the age of eukaryotic groups is also difficult, because there is no definitive root and the methodology and variables used to produce such estimations can vastly alter the result. The divergence of the excavates can be estimated to have occurred between ~1 and ~1.8 billion years ago, depending on the criteria used, while the root of eukaryotes can be estimated to be between ~1 and ~1.9 billion years old. In all cases, however, all eukaryotic groups appear less than 300 million years after LECA, with Excavata regularly being the earliest appearing group (Eme et al., 2014). Despite the uncertainty surrounding the intricacies of the emergence of the excavates, it is clear that it occurred early in eukaryote evolution. Kinetoplastids are, therefore, very different from organisms most often used to study the mechanisms of mitosis, which are unlikely to be representative of mitosis in trypanosomes, or even eukaryotes as a whole.

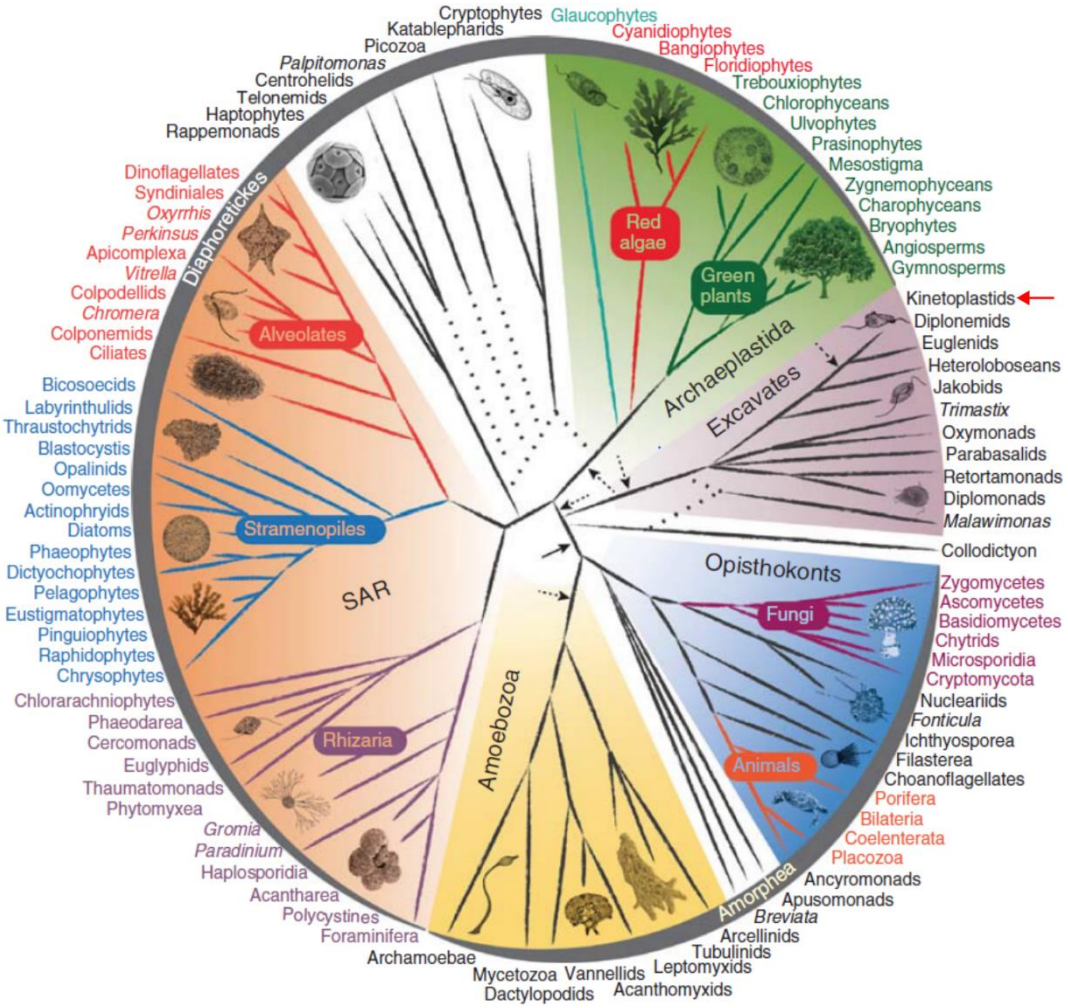


Figure 3. A tree of eukaryotes based on phylogenetics, rare genomic signatures and morphology. A number of groups of eukaryotes are shown from various taxonomic ranks. Dotted lines represent uncertain relationships between groups. Black arrows point to hypothesised roots of the tree. The solid arrow represents a root at the divergence of Unikonts and Bikonts, while broken arrows represent alternative roots. The red arrow marks the location of kinetoplastids. From Burki (2014).

1.1.3. The microtubule cytoskeleton of *Trypanosoma brucei*

Microtubules are a major constituent of the eukaryote cytoskeleton. In models, they are often arranged in an array that is nucleated at a microtubule organising centre (MTOC), and are involved in the transport of cargoes around cells. During mitosis they form the mitotic spindle that separates replicated chromosomes. Microtubules are hollow cylinders formed from dimers of α- and β-tubulin. The tubulin dimers polymerise head-to-tail, to produce protofilaments, 13 of which laterally associate to produce a microtubule. The arrangement of αβ-tubulin polarises the microtubule polymer, producing a "minus-end," at the α-tubulin end, and a "plus-end" at the β-tubulin end. The plus-end displays a property known as "dynamic instability," cycles of slow polymerisation and fast depolymerisation, known as "rescue" and "catastrophe." Whether a microtubule polymerises or depolymerises is dictated by the GTP state of β-tubulin. Polymerisation occurs when both the α- and β-tubulin are bound to GTP. After polymerisation, hydrolysis of the GTP associated with β-tubulin occurs over time, causing curvature of dimers, making microtubules more prone to catastrophe. Growing microtubules, therefore, display a "GTP-cap," a region at the minus-end, in which β-tubulin is GTP bound. Various proteins that bind to the microtubules can regulate the likelihood of rescue and catastrophe events, in turn regulating microtubule length (Alberts et al., 2008a; Desai and Mitchison, 1997; Etienne-Manneville, 2010; Kirschner and Mitchison, 1986a).

The elongate shape of the trypanosome cell is defined by two microtubule structures, a subpellicular array, or "corset," of microtubules and a flagellum (Absalon et al., 2008b; Gull, 1999; Kohl and Gull, 1998; Robinson et al., 1995; Sun et al., 2012; Sunter et al., 2015). Transverse sections of cells show that over 100 microtubules, of variable length, make up the corset. They are arranged helically along the axis of the cell and regularly spaced, in such a way that all microtubule plus-ends are directed towards the posterior of the cell, with the exception of a microtubule quartet associated with flagellum attachment zone. Crosslinking occurs between individual corset microtubules and between corset microtubules and the plasma membrane. Acetylation of α-tubulin and certain proteins, such as

CAP15 and CAP17, may function to stabilise subpellicular microtubules, maintaining cell shape (Gull, 1999; Kohl and Gull, 1998; Sherwin and Gull, 1989; Vedrenne et al., 2002). The length of microtubules and crosslinks formed between them can change, allowing for changes in cell shape. In cell division, extension of subpellicular microtubules and their repositioning under the membrane increases the size of the cell body as the cell divides. Insertion of new microtubules between existing microtubules aids in further increasing cell volume and results in semiconservative inheritance of microtubules by the daughter cells (Sherwin and Gull, 1989; Vaughan and Gull, 2008).

The flagellum is also important in determining the shape of trypanosome cells; flagellar mutants regularly show morphological defects, lacking the normal elongate shape (Absalon et al., 2008b; Bonhivers et al., 2008; Ralston and Hill, 2006). Trypanosomes have a single canonical eukaryote flagellum (Figure 4). Briefly, it is largely made up of an axoneme consisting of microtubules in a "9+2" configuration, a central pair of microtubules surrounded by nine microtubule doublets. Basal bodies function as MTOCs and anchor the flagellum in the cell body. They are formed from a cylinder of nine microtubule triplets. Between the basal body and axoneme lies a transition zone, in which the axonemal central microtubule pair and the third microtubule of microtubule triplet of the basal body terminate. The flagellum of *T. brucei* exits the cell body towards the posterior of the cell, in the majority of life cycle stages, through a gap in the subpellicular microtubule corset, which corresponds with an invagination of the plasma membrane known as the flagellar pocket (FP), the sole site of endo- and exocytosis. In a left-handed spiral, the flagellum then runs along the cell body, towards the anterior of the cell, defining the posterior-anterior axis. The plus-ends of axonemal microtubules are, therefore, at the anterior of the cell, while the minus-ends are at the posterior, the opposite orientation of corset microtubules (reviewed in Langousis and Hill, 2014). Kinetoplastid flagella also contain a structure known as the paraflagellar rod (PFR) that runs parallel to the axoneme. The PFR is a trilaminar structure that is mostly made up of two proteins, paraflagellar rod proteins 1 and 2 (PFR1 and 2), and is attached to the

axoneme by electron dense filaments. The PFR physically supports the flagellum, supplies ATP to the axoneme and interacts with the insect vector. It is also important in flagellar motility and may function in flagellar signalling (Maharana et al., 2015; Portman and Gull, 2010). The attachment of the flagellum to the cell body is mediated by the flagellum attachment zone (FAZ). The FAZ consists of a complex of filaments, junctional complexes and plaques that links the PFR to a specialised FAZ filament and an associated microtubule quartet, within the cell body, and is an important determinant of cell morphology (Sunter et al., 2015; Sunter and Gull, 2015).

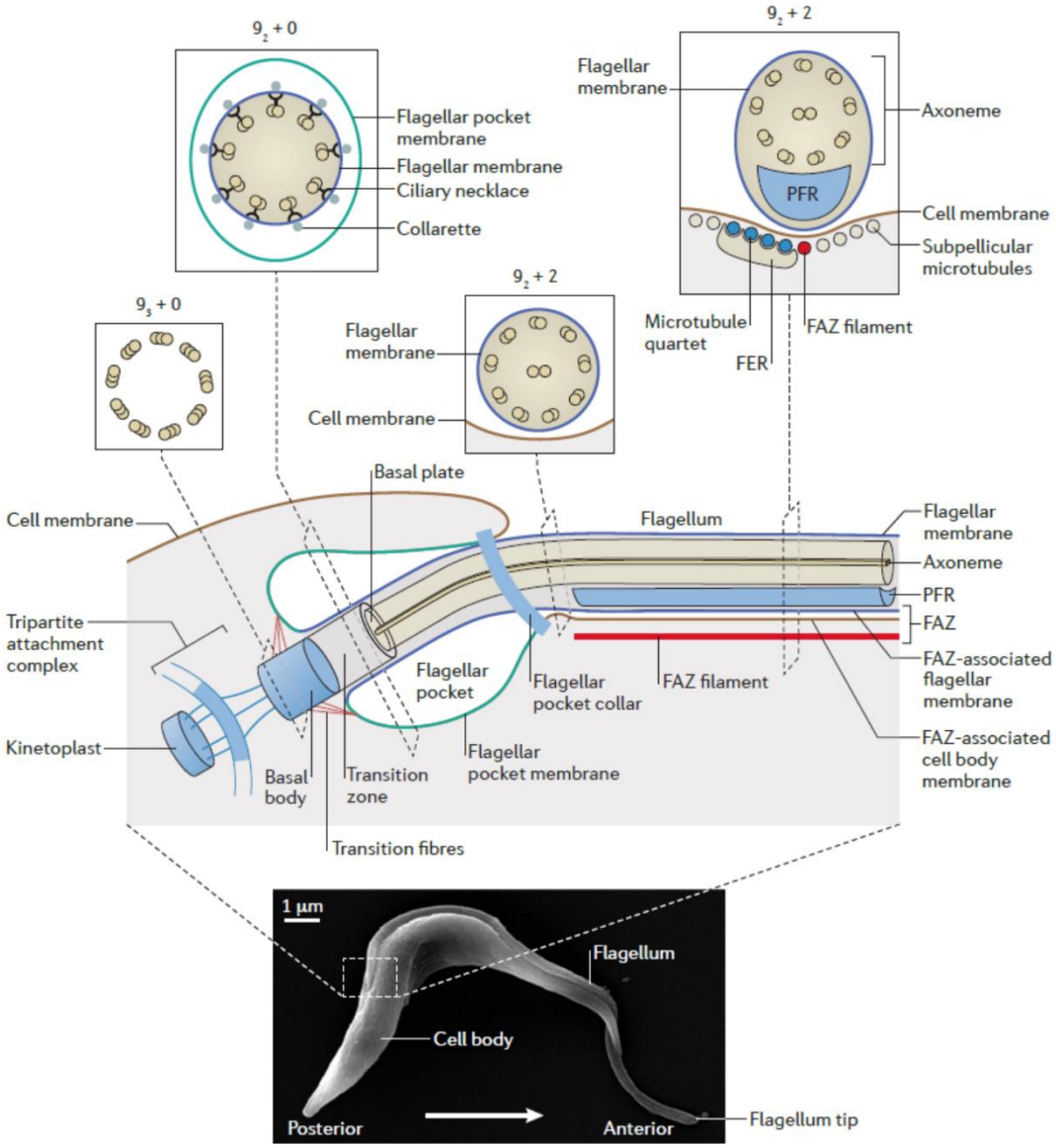


Figure 4. Diagram of the flagellum of *T. brucei*. The lower panel is a scanning electron micrograph of PCF *T. brucei*. The arrow represents the direction of movement. The upper panel is a diagram of the flagellum, showing its structure where it emerges from the cell body. From Langousis and Hill (2014).

The main role of flagella is in motility. In trypanosomes, this is driven by a flagellar wave that moves from the anterior tip of the flagellum to the posterior base (Walker, 1961). Recoil against the surrounding fluid moves the cell in the opposite direction, towards the tip of the flagellum. Occasional reversal of the direction of the wave causes the trypanosome cell to tumble (Baron et al., 2007; Branche et al., 2006; Gadelha et al., 2007). The helical path the flagellum takes around the cell body means that flagellar waves cause the cell to corkscrew, hence the *Trypanosoma* name, which is derived from Greek and means "borer body." This corkscrew motion is effective in propelling the cell through viscous liquids, such as blood (Heddergott et al., 2012). Flagellar motility is required for movement through the insect vector and continuation of the life cycle (Rotureau et al., 2014). It is also hypothesised to aid in evasion of mammalian host immunity, by driving the movement of immunoglobulin bound variant surface glycoprotein (VSG), the major surface protein of BSF cells, into the FP for recycling (Engstler et al., 2007). Flagellar motility is essential for survival of BSF cells, even in culture (Branche et al., 2006; Broadhead et al., 2006; Ralston and Hill, 2006).

Motility mutants also suggest a role for the trypanosome flagellum in cell division, as they show cytokinesis and septation defects. The flagellum and FAZ are important in defining the shape of dividing cells and the cleavage furrow formed during cytokinesis (Robinson et al., 1995; Sun et al., 2012; Sunter et al., 2015). One of the earliest steps in trypanosome cell division is the synthesis of a new flagellum. During this process the developing flagellum follows the path of the old flagellum in an example of structural inheritance, a process in which an existing structure defines the assembly of a new structure in progeny cells (Moreira-Leite et al., 2001). When the new flagellum reaches a certain length, cytokinesis begins at the tip of the flagellum and follows the cleavage furrow formed between the two flagella of the daughter cells (Robinson et al., 1995). The formation of a new flagellum also drives division of other organelles. The kinetoplast is attached to the basal body, via filaments, and as the new flagellum forms, basal bodies move apart in a microtubule dependent process, separating replicated kinetoplasts (Ogbadoyi et al., 2003; Robinson and Gull, 1991). The

majority of this separation occurs after the new flagellum has grown to a point halfway along the old flagellum, where it stops. Further elongation of the new flagellum still occurs at this point, which drives basal body and kinetoplast separation (Absalon et al., 2007; Davidge et al., 2006; Robinson et al., 1995).

The flagellum leaves the cell via an invagination of the surface membrane known as the flagellar pocket (FP), which is the sole site of endo- and exocytosis (reviewed in Field and Carrington, 2009). The FP is believed to hide the invariant receptor proteins from the humoral immune response. It is a complex and highly organised structure that shows very precise localisation in regards to organelles and cytoskeleton elements, as revealed by electron microscopy (Lacomble et al., 2009). This structure requires the presence of the flagellum and displays a distorted shape when the flagellum is absent (Absalon et al., 2008a).

1.1.4. The genome of *Trypanosoma brucei*

T. brucei is a diploid organism, with a genome of ~70Mb. This genome is composed of 11 pairs of megabase chromosomes (MBCs), as well as ~5 intermediate chromosomes (ICs) and ~100 minichromosomes (MCs) (Ersfeld et al., 1999). The MBCs are 1-6Mb in size and are analogous to chromosomes in other diploid organisms. They contain the housekeeping genes in their cores and bloodstream expression sites (BESs) in their subtelomeres, the sites of VSG transcription. The haploid MBC genome is ~26Mb in size and contains 9068 predicted genes, including ~900 pseudogenes and ~1700 genes specific to *T. brucei* (Berriman et al., 2005). The 200-500kb ICs and 50-150kb MCs are aneuploid, as their population varies from cell to cell. Both ICs and MCs exist to carry a portion of the library of VSG genes used in antigenic variation, while ICs also carry BESs and MCs are transcriptionally silent. The VSG genes are contained in the subtelomeres of the chromosomes, while core regions consists of varying numbers of repeats of a 177bp sequence (Alsford et al., 2001; Ersfeld et al., 1999; Wickstead et al., 2003).

Like most eukaryotes, the genes on MBCs are transcribed by the Pol II RNA polymerase. Unusually, however, multiple genes are transcribed into a single unit of RNA, producing polycistronic RNA sequences (Imboden et al., 1987; Muhich and Boothroyd, 1988). ChIP-seq (Siegel et al., 2009) and RNA-seq (Kolev et al., 2010) data suggest there may be ~150 individual polycistrons transcribed from the genome. Polycistrons are separated by strand switch regions (SSRs), which contain sites of transcription initiation and termination (Kolev et al., 2010). SSRs also coincide with origins of replication and interaction between the two processes appears to occur (Tiengwe et al., 2012). The order of genes and polycistrons is well conserved between trypanosomatids, despite divergence of sequences. This synteny suggests that there is strong selective pressure against breaking gene order (El-Sayed et al., 2005; Ghedin et al., 2004), which may be due to the polycistronic nature of transcription and the relatively few transcription start sites within the genome.

Polycistrons are processed into functional messenger RNAs (mRNAs) by two, coupled processes; *trans*-splicing of a capped 35bp spliced leader RNA sequence to the 5' untranslated region (UTR) and polyadenylation of the 3' UTR (LeBowitz et al., 1993; Palenchar and Bellofatto, 2006). Polycistronic transcription means there is very little transcriptional regulation, with little change in RNA levels between life cycle stages (Diehl et al., 2002; Jensen et al., 2009; Siegel et al., 2010; Veitch et al., 2010). The majority of gene regulation in trypanosomes is posttranscriptional, with the 3' UTR dictating stability, translation efficiency and stage specificity (Berberof et al., 1995; Boucher et al., 2002; Clayton, 2002; Furger et al., 1997; Gale et al., 1994; Hotz et al., 1997; Mao et al., 2009; Martínez-Calvillo et al., 2010; Quijada et al., 2002; Vanhamme and Pays, 1995).

Transcription in *T. brucei* is also unusual in its use of the Pol I RNA polymerase. *T. brucei* is the only known eukaryote that uses Pol I to transcribe ribosomal RNA (rRNA), like other eukaryotes, and some protein coding sequences (Günzl et al., 2003). Pol I transcribes VSG, the surface protein of BSF cells used in immune evasion, and procyclin, the surface protein of PCF cells. Procyclin is transcribed from tandem arrays of two or three genes on chromosomes 6 and 10 (Liniger et al., 2001; Roditi et al., 1998). VSG, on the other hand, is transcribed from one of ~15 BESs situated in the subtelomeres of MBCs and ICs. Only one BES is expressed at a time, which is essential for antigenic variation and immune evasion. Antigenic variation occurs through switching of the active BES or recombination of a differing VSG sequence into the active BES (reviewed in Horn, 2014; Taylor and Rudenko, 2006). BESs are up to 60kb in length and contain a VSG coding sequence and a group of expression site associated genes (ESAGs). The number and variety of ESAGs varies from BES to BES (Berriman et al., 2002; Hertz-Fowler et al., 2008; Johnson et al., 1987). In metacyclic cells VSG is transcribed monocistronically from a subtelomeric metacyclic expression site and is the only example of monocistronic transcription of a protein coding sequence and regulation of transcription in *T. brucei* (Ginger et al., 2002; Graham et al., 1999, 1990).

The activity of the eukaryote nucleus is known not be homogenously distributed. Instead processes such as transcription and replication are compartmentalised, allowing the functions of specific regions of nucleoplasm to be specialised (Fraser and Bickmore, 2007; Kosak and Groudine, 2004; Misteli, 2007). Labelling of trypanosome nuclei, through incorporation of BrUTP or BrdUTP, demonstrates that they also display compartmentalisation of transcription (Amiguet-Vercher et al., 2004; Dossin and Schenkman, 2005; Navarro and Gull, 2001) and replication (Elias et al., 2002; Ogbadoyi et al., 2000; Woodward and Gull, 1990), respectively, with specific regions of the nucleus showing stronger labelling.

An important example of compartmentalisation in the nucleus of *T. brucei* is the expression site body (ESB). Pol I transcription is usually restricted to the nucleolus in eukaryotes and for most Pol I transcribed genes in *T. brucei*, including procyclin, this also the case (Landeira and Navarro, 2007). The ESB, however, is an extranucleolar body in which Pol I transcription occurs and is the site of transcription of the active BES (Chaves et al., 1998; Navarro and Gull, 2001). The monoallelic expression of VSG from a single active BES, has been hypothesised to be dependent on the recruitment of the ESB, from which the inactive BESs are excluded (Navarro and Gull, 2001). The ESB recruits RNA transcription and processing machinery, resulting in the high levels of expression of VSG, and its architecture may be involved in maintaining the exclusivity of the active BES (Pays, 2005).

Chromatin in the trypanosome nucleus does not pack as tightly as chromatin in mammalian cells (Belli, 2000) and the 30nm fibres that make up heterochromatin are not formed (Hecker et al., 1994). Furthermore, trypanosome chromosomes do not visibly condense during mitosis (Vickerman and Preston, 1970). It is unclear whether trypanosomes have true heterochromatin and euchromatin, due to the high gene density of the genome, and the lack of transcriptional regulation. Electron microscopy of *T. brucei* and *cruzi* cells has, however, demonstrated that regions of the nucleus show variable electron density (Elias et al., 2001; Ogbadoyi et al., 2000). Electron dense regions,

usually associated with heterochromatin, generally localise to the nuclear periphery, but are excluded from locations proximal to nuclear pores. These electron-dense regions in *T. brucei* also correspond with transcriptionally silent regions, such as the MCs and the subtelomeres of MBCs (Ogbadoyi et al., 2000). Furthermore, nuclear DNA that stains less intensely with DAPI colocalises with TFIIS transcription elongation factors (Uzureau et al., 2008), though it is not known for certain how DAPI staining corresponds to DNA packaging.

Another unusual aspect of the genome of *T. brucei* is the kinetoplast. The single mitochondrion present in all kinetoplastids contains this characteristic structure, which contains the mitochondrial DNA, or kinetoplast DNA (kDNA), which consists of a network interlocking DNA minicircles and maxicircles. In *T. brucei*, the kinetoplast is situated at the base of the flagellum, at the posterior of the mitochondrion and cell. The basal body interacts with a modified region of the mitochondrial membrane through filaments, forming a flagellar attachment complex. This complex is in turn bound to the kinetoplast by a series of filaments referred to as the kineto-flagellar zone. kDNA separation occurs early on in cell division; it is replicated at S phase and segregated during to G2 phase. As previously mentioned the segregation of replicated kDNA is driven by its attachment to the flagellum. As a new flagellum is formed during G2 phase, the basal bodies of the new and old flagella separate, pulling apart kDNA. The kinetoplast and its replication are reviewed in Jensen and Englund, (2012) and Povelones (2014).

1.2. Mitosis in model systems

1.2.1. Open and closed mitosis

In interphase vertebrate and yeast cells chromosomes are relatively uncondensed, with regions of chromatin anchored at the nuclear envelope (NE). The NE is highly organised structure, consisting of two concentric lipid bilayers, that separates the contents of the nucleus from the cytoplasm. Selectively permeable nuclear pores within the NE, occupied by nuclear pore complexes (NPCs), allow for regulated nuclear import and export (reviewed in Hetzer, 2010; Hetzer et al., 2005). Many different proteins within the inner nuclear membrane interact with chromatin and anchor it within the nuclear periphery (reviewed in Simon and Wilson, 2011). This is important for the organisation of chromatin and the resulting regulation of transcription (reviewed in Deniaud and Bickmore, 2009; Steglich et al., 2013). As cells prepare to undergo mitosis, the chromosomes detach from the NE and begin to condense, while the mitotic spindle is assembled. Based on the continuity of the NE, mitotic cells are either categorised as undergoing open mitosis, such as in vertebrate cells, or closed mitosis, which occurs in some yeast. These two categories are extreme examples, however, and a number of examples of mitosis lie between them, in which the NE remains, but is not continuous. These are referred to as semi-open/closed or partially open/closed mitosis (Arnone et al., 2013; Heath, 1980).

In open mitosis in vertebrate cells, NE breakdown (NEBD) occurs during the transition between prophase, in which chromatin condenses, and prometaphase, when spindle assembly occurs. As NEBD is initiated, there is an increase in the permeability of the NE and disassembly of NPCs begins (Lénárt et al., 2003). This disassembly is completed within minutes and is accompanied by a synchronised release of NPC components (Dultz et al., 2008). NEBD continues with the depolymerisation of the nuclear lamina and the detachment of the NE from chromatin, followed by its removal, which is facilitated by dynein motor proteins (Beaudouin et al., 2002; Gerace and Blobel, 1980). NE components are then redistributed into the endoplasmic reticulum (Lu et al., 2009). These events

are triggered by the phosphorylation of NE components by cyclin dependent kinase 1 (Cdk1) complexed with cyclin A2, which regulates the transition between G2 and M phase, or with cyclin B, which is also involved in the early stages of mitosis and inhibition of anaphase (Buendia et al., 2001; Gong et al., 2007; Gong and Ferrell, 2010). Phosphorylation by the Aurora A kinase can also initiate NEBD (Hachet et al., 2007; Portier et al., 2007).

During closed mitoses in yeast the NE remains intact throughout cell division. The mitotic spindle is assembled inside the nucleus and nucleated at spindle pole bodies embedded in the NE. Spindle pole bodies are plaque structures and the MTOCs of yeast spindles. During anaphase, as sister chromatids are separated, the spindle elongates, changing the shape of the nucleus, which eventually divides into two daughter nuclei (Sazer et al., 2014). Though it remains intact, remodelling of the NE and changes in NE dynamics do occur, which is required for the insertion of new spindle pole bodies, the influx of proteins required by the mitotic machinery and expansion of the nuclear envelope. These processes are regulated by Cdk and polo-like kinase (PLK) mitotic kinases (Zhang and Oliferenko, 2013). While yeast appear to import proteins required for mitosis through NPCs, some fungi that perform closed mitoses partially disassemble NPCs, resulting in the equalisation of nucleoplasm and cytoplasm and an influx of required proteins. (Aist, 1969; Aist and Williams, 1972; Robinow, 1969). In *Aspergillus nidulans* the NIMA kinase interacts with NPC proteins and phosphorylates them, resulting in their removal (De Souza et al., 2004; Osmani et al., 2006). The expansion of the NE in yeast mitosis, during anaphase, requires synthesis of phospholipids (Saitoh et al., 1996; Santos-Rosa et al., 2005; Yam et al., 2011). In *Sacchoromyces. cerevisiae* phospholipid synthesis pathways are, therefore, regulated by Cdk1, via phosphorylation of Pah1 (or Smp2), a lipin protein family member (Santos-Rosa et al., 2005).

As mentioned previously, both open and closed mitoses are extreme examples of mitosis and a number of intermediaries exist. The fission yeast *Schizosaccharomyces japonicus*, for example, carries out a largely closed mitosis, with the membrane and NPCs remaining intact. During anaphase, however,

breaks appear in the NE around the spindle equator. In another example, mitosis in *Plasmodiophora brassicae* involves a largely intact NE, with localised NEBD occurring around centrosomes. In embryos of *Caenorhabditis elegans*, the NE contains many perforations, but does not break down. Species of dinoflagellate carry out mitosis with an intact membrane and the spindle is assembled outside the nucleus. Spindle microtubules pass through “cytoplasmic tunnels” and interact with chromosomes through the NE. These examples, reviewed in Drechsler and McAinsh (2012) and Makarova and Oliferenko (2016), and examples of open and closed mitoses demonstrate the varying strategies employed by eukaryotes for mitosis, even by those that are relatively closely related.

1.2.2. The canonical mitotic spindle

The mitotic spindle is a complex, macromolecular machine that functions to separate eukaryotic DNA. The overall structure of the spindle in model eukaryotes is well established, with the canonical spindle belonging to vertebrate cells (Figure 5). It is mainly composed of microtubules, whose dynamic instability allows their plus-ends to seek out chromosomes as the spindle forms. The microtubules are nucleated at the centrosomes, the MTOCs of vertebrate cells, which consist of pair of centrioles, structurally similar to basal bodies, and a pericentriolar matrix, where nucleation takes place. An important constituent of the pericentriolar matrix is γ-tubulin, which form rings of 13 γ-tubulins known as a γ-tubulin ring complex (γ-TURC). Spindle microtubules fall into two classes. Interpolar microtubules form the body of the spindle and give it its structure. Microtubules originating from opposite centrosomes are crosslinked into antiparallel arrays in the spindle midzone. At metaphase, condensed chromosomes lie at the metaphase plate, with sister chromatids bound together at centromeres by the ring-like cohesin complex. They attach to microtubules via multi-protein complexes known as kinetochores, which are assembled at the chromosomes' centromeres. The microtubules are, therefore, known as kinetochore microtubules, the second class of microtubule. The actions of both interpolar and kinetochore microtubules and proteins that act upon them are responsible for the separation of sister chromatids at anaphase. A third class of microtubule, astral microtubules, anchor the spindle at the cell cortex. They emanate outwards from the centrosome and interact with the actin cytoskeleton of the cell cortex via the dynactin protein complex (Alberts et al., 2008b; Petry, 2016; Walczak and Heald, 2008).

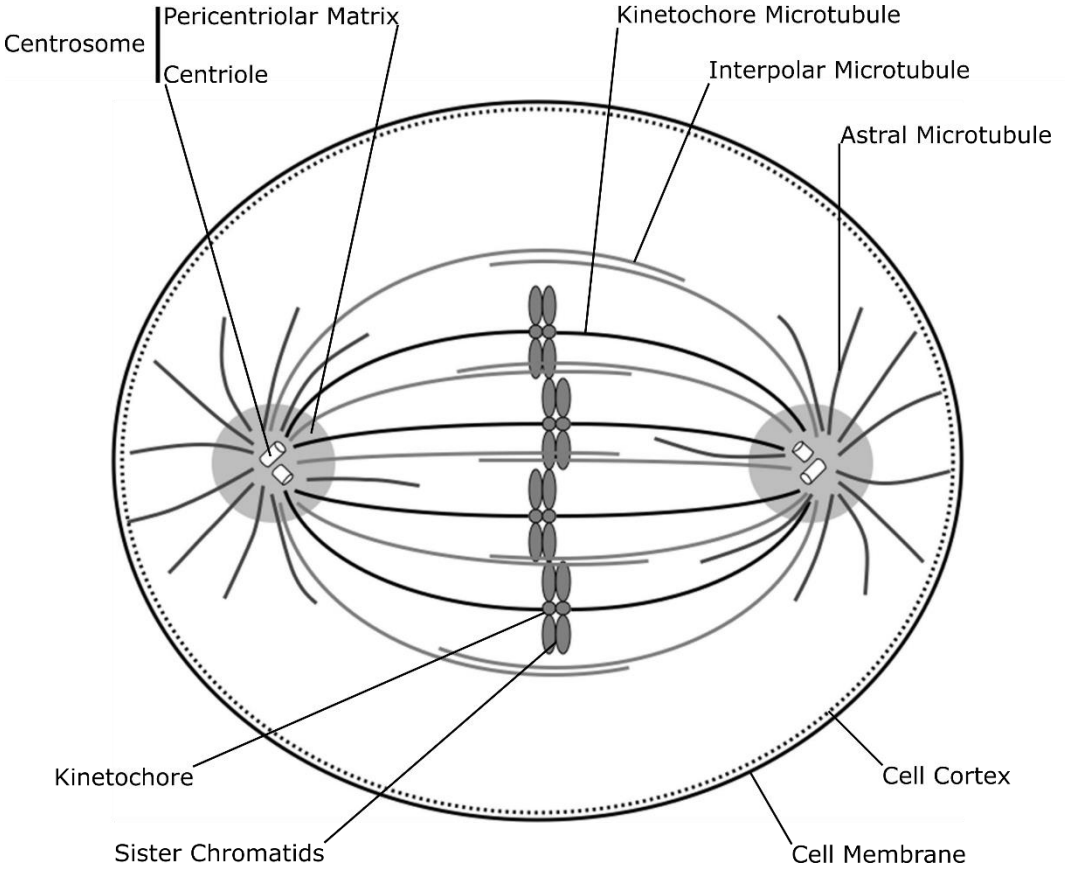


Figure 5. A schematic of the canonical mitotic spindle at metaphase. Two centrosomes, consisting of a centrioles and the pericentriolar matrix serve to nucleate spindle microtubules. Astral microtubules emanate from the centrosome and anchor the spindle at the cell cortex. Interpolar microtubules crosslink in the centre of the spindle, or the spindle midzone, and give the spindle its structure. Kinetochores link kinetochores to the centrosome through kinetochore microtubules. Adapted from Goodman and Zheng (2006).

Spindle assembly largely occurs during prometaphase, but begins in prophase with the duplication of the centrosome (Azimzadeh and Bornens, 2007; Nigg and Stearns, 2011). During S phase the two centrioles within the centrosome are replicated and begin maturing, gathering additional pericentriolar matrix material, increasing their ability to nucleate microtubules. During prophase, the centrosomes separate, a process driven by the formation of microtubules. Continued spindle assembly then occurs through two pathways, a centrosome dependent or independent pathway (Petry, 2016; Walczak and Heald, 2008). In the centrosome dependent pathways growing microtubules are nucleated at the centrosomes, by γ-TURC and other pericentriolar components, an activity that is increased by phosphorylation by mitotic kinases (Albee et al., 2006; Dobbelaere

et al., 2008; Khodjakov and Rieder, 1999; Piehl et al., 2004). These centrosomal microtubules display a high degree of dynamic instability, but become stable when attached to a chromosome, which allows them to quickly sample the volume of the cell for chromosomes (Desai and Mitchison, 1997; Holy and Leibler, 1994; Kirschner and Mitchison, 1986a, 1986b). In a centrosome-independent mechanism, microtubules polymerise in the vicinity of chromosomes. These microtubules are then arranged into an antiparallel array, which is then nucleated at the minus-end of the microtubules (McKim and Hawley, 1995). The polymerisation of microtubules around chromosome is driven by a gradient of RanGTP emanating from chromosomes (Dasso, 2002; Hetzer et al., 2002) and the chromosomal passenger complex (see below) (A. E. Kelly et al., 2007; Sampath et al., 2004), which act to release spindle assembly factors and stabilise microtubules.

During spindle assembly, chromosomes attach to spindle microtubules and move to the metaphase plate, in a process called congression. In classic models, the kinetochores of sister chromatids capture microtubules from opposing spindle poles and track toward the metaphase plate, pulled by the depolymerisation of microtubules (Hayden et al., 1990). As chromosomes congress additional microtubules bind to the kinetochore, creating a bundle of kinetochore microtubules (McEwen et al., 1997). Eventually the chromosomes congress to a point at which the forces acting on the chromatids become equal and they no longer move (Hayden et al., 1990). This process leads to oscillations of chromosomes at the metaphase plate, as individual kinetochores move towards their respective poles. Congression also involves the actions of microtubule motor proteins that pull chromosomes laterally attached to microtubules to the metaphase plate, by acting on the kinetochore and crosslinking chromosome arms and interpolar microtubules (Barisic et al., 2014; Brouhard and Hunt, 2005). This results in a phenomenon known as the “polar ejection force,” in which the chromosome arms point away from the spindle poles (Rieder et al., 1986).

Spindle assembly and function is partly regulated by the actions of the Aurora kinases, a small family of serine–threonine protein kinases (Fu et al., 2007; Vader and Lens, 2008). The mammalian genome encodes three Aurora proteins, Aurora-A, -B and -C. The role of Aurora-C in mitosis remains largely unknown, though it localises to the centrosomes. It is also known to bind to inner centromere proteins and is required for successful meiosis and spermatogenesis (Kimmins et al., 2007; Li et al., 2004; Sasai et al., 2004; Tang et al., 2006). Aurora-A largely localises to the centrosome and is involved in centrosome maturation and separation and centrosome nucleation activity (De Luca et al., 2006; Petretti et al., 2006; Zhao et al., 2005). It is also involved in spindle assembly, through an interaction with a protein complex that localises it to the spindle (Koffa et al., 2006), and in mitotic entry (Hirota et al., 2003; Satinover et al., 2006; Seki et al., 2008). Aurora-B is activated upon binding to the inner centromere protein (INCENP) (Sessa et al., 2005) and interacting with Tousled-like kinase 1 (TLK-1) (Han et al., 2005; Silljé et al., 1999). It is also known to form a chromosomal passenger complex (CPC) with the INCENP, Survivin and Borealin proteins (Vader et al., 2006). The CPC interacts with chromosomes during early mitosis and moves to the spindle during anaphase (Earnshaw and Bernat, 1991). Both chromosome condensation (Giet and Glover, 2001) and sister chromatid cohesion (Dai et al., 2006; Resnick et al., 2006) have been linked to the actions of Aurora-B. It is involved in spindle assembly by inhibiting microtubule destabilising proteins (Gadea and Ruderman, 2006; A. E. Kelly et al., 2007; Sampath et al., 2004). Finally, it ensures correct attachment of chromosomes to kinetochore microtubules, by functioning as part of the spindle assembly checkpoint, and is involved in microtubule reorganisation during anaphase (discussed later).

1.2.3. The kinetochore

Kinetochores are macromolecular complexes that link the centromeres of chromosomes to the plus-ends of microtubules. In vertebrates, they consist of over 100 components and provide the forces necessary for chromosome alignment and tracking of microtubule ends. Based on their localisation and function, kinetochore proteins can be grouped into three groups; inner kinetochore proteins that interact with the centromere, outer kinetochore proteins that connect the kinetochore to microtubules and regulatory proteins that govern and monitor kinetochore activities. The structure of the kinetochore is reviewed in Cheeseman (2014) and in Cheeseman and Desai (2008) and represented in Figure 6, but will be briefly discussed here.

The centromere is defined by a modified histone H3 variant referred to as CENP-A (centromere protein A), which forms specialised nucleosomes and acts as a basis for kinetochore assembly (Liu et al., 2006; Palmer et al., 1991, 1987; Régnier et al., 2005). 16 inner kinetochore proteins associate with CENP-A throughout the cell cycle forming the constitutive centromere-associated network (CCAN) (Foltz et al., 2006; Obuse et al., 2004; Okada et al., 2006). Recently it was demonstrated that seven subunits of the CCAN, the CHIKMLN subcomplex, determined its selectivity for CENP-A (Weir et al., 2016). During mitosis outer kinetochore proteins are added to the CCAN in a rapid process that takes less than 20 minutes (Gascoigne and Cheeseman, 2013). In the fully formed vertebrate cell kinetochore, there are two pathways that connect chromatin and microtubules. In the first, CENP-C binds to CENP-A (Carroll et al., 2010; Kato et al., 2013) and also interacts with the Mis12 complex (Gascoigne et al., 2011; Przewloka et al., 2011; Screpanti et al., 2011). The Mis12 complex interacts with two further protein complexes, the KNL1 and Ndc80 complexes. The Ndc80 complex binds microtubules and is the key microtubule-binding component of the kinetochore. Mis12, KNL1 and Ndc80 form the KMN network and much of the outer kinetochore (Cheeseman et al., 2006, 2004; Obuse et al., 2004; Petrovic et al., 2010). In the second pathway, a complex of CENP-T, -W, -S and -X associates with the DNA of the centromere. CENP-T also interacts with Ndc80, linking

chromatin and microtubules (Gascoigne et al., 2011; Nishino et al., 2013). Both of these pathways are required for proper attachment of chromosomes to microtubules and both are regulated by Cdk1/cyclin B phosphorylation and the exclusion of Ndc80 from the nucleus during interphase (Gascoigne and Cheeseman, 2013). Homologues of vertebrate kinetochore proteins also exist in yeast, though they also use an additional complex of proteins called the Cbf3 complex (reviewed in Biggins, 2013).

Although Ndc80 does interact with microtubules it cannot mediate microtubule tracking. In yeast cells, Ndc80 interacts with the Dam1 complex, which forms a ring around microtubules (Miranda et al., 2005; Westermann et al., 2005). The curvature of microtubules involved in depolymerisation pushes the Dam1 ring towards the microtubules minus-end, causing the kinetochore to follow the shrinking microtubule (Grishchuk et al., 2008; Lampert et al., 2010; Tien et al., 2010). In metazoa, Dam1 is not present, but its role is fulfilled by the Ska complex. The Ska complex allows the kinetochore to track microtubule ends, but differs in its structure and likely its mechanism of action (Daum et al., 2009; Gaitanos et al., 2009; Hanisch et al., 2006; Jeyaprakash et al., 2012; Raaijmakers et al., 2009; Schmidt et al., 2012; Theis et al., 2009; Welburn et al., 2009).

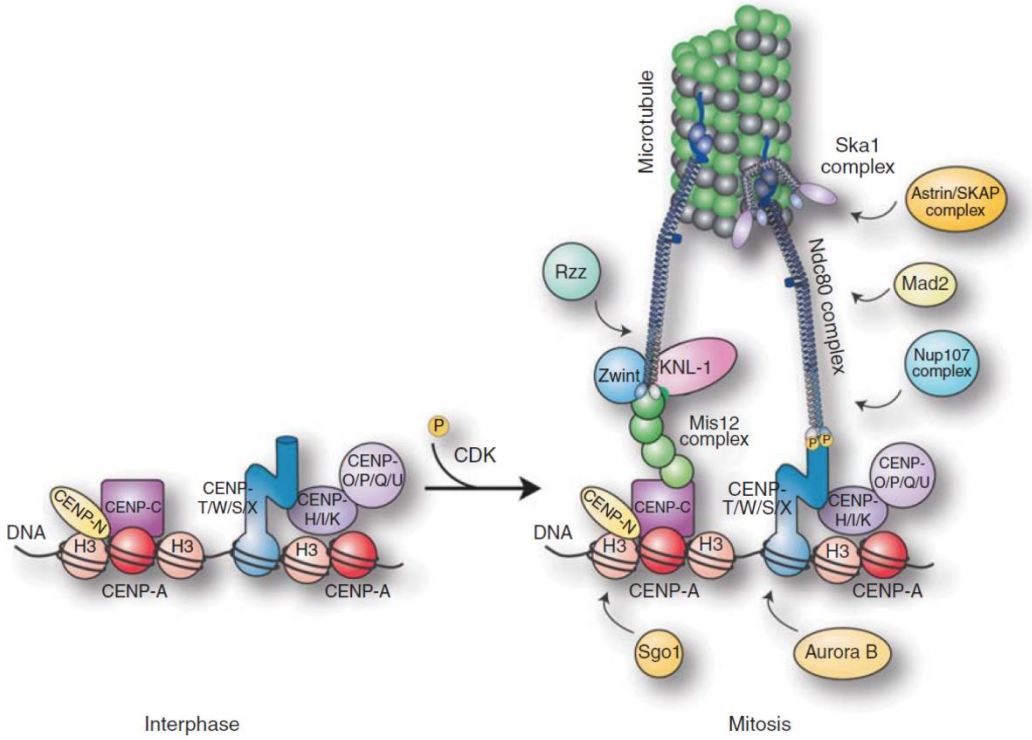


Figure 6. Vertebrate kinetochore structure during interphase and mitosis. During mitosis phosphorylation by Cdk1/cyclin B promotes outer kinetochore assembly upon the CCAN, which is constitutively expressed. From Cheeseman (2014).

1.2.4. Tension sensing at metaphase

Kinetochores are not selective about the microtubules they bind resulting in incorrect attachments that would result in uneven segregation of nuclear DNA. Correct attachment, in which each sister chromatid is bound to kinetochore microtubules from opposing spindle poles, is referred to as amphitely. Incorrect attachments include monotely, in which only a single kinetochore attaches to spindle microtubules, syntely, where both kinetochores bind microtubules emanating from a single pole, and merotely, the binding of a single kinetochore to microtubules emanating from both spindle poles (McIntosh et al., 2012). In the presence of amphitelic attachments the anaphase promoting complex (APC/C), an E3 ubiquitin ligase, triggers the transition from metaphase to anaphase. It does this by tagging inhibitors of mitotic exit, such as cyclin B, and of sister chromatid disjunction, such as securin, which inhibits the activities of separase, an enzyme that hydrolyses the cohesin complex (reviewed in Pines, 2011). When, amphitelic attachments are absent, however, the APC/C is inhibited by the spindle assembly checkpoint (SAC).

In the presence of incorrect attachments, the SAC produces a diffusible inhibitor of the APC/C called the mitotic checkpoint complex (MCC) and also promotes error correction. Generation of the SAC signal begins with the kinase MPS1, which associates with Ndc80, when activated by Aurora-B (Kemmler et al., 2009; Nijenhuis et al., 2013). MPS1 then recruits the SAC proteins BUB1, BUB3, MAD1, MAD2, and BUBR1. MAD2, BUB3, and BUBR1 form the MCC, with MAD1 and BUB1 mediating their assembly (Murray, 2011; Vleugel et al., 2012). The MCC then inhibits the APC/C by preventing its activation by Cdc20 (Hein and Nilsson, 2014). The SAC promotes error correction through regulation of Aurora-B and its substrates. BUB1 phosphorylates histone H2A, which produces a docking site for Borrealin, promoting a centromeric localisation for Aurora-B (Watanabe, 2010). BUBR1 carries a docking site for the B56-PP2A protein phosphatase, localising it to the outer kinetochore (Kruse et al., 2013; Suijkerbuijk et al., 2012). Phosphorylation of proteins by Aurora-B serves to destabilise incorrect kinetochore-microtubule attachments (Alushin et al., 2012; Knowlton et al., 2006;

Umbreit et al., 2012). B56-PP2A, which is in turn regulated by PP1 (protein phosphatase 1) (Grallert et al., 2015), on the other hand, stabilises kinetochore-microtubule attachments by dephosphorylating Aurora-B substrates (Foley et al., 2011; Suijkerbuijk et al., 2012). It is unclear how these effects are balanced to promote correct attachment, though it has been suggested that amphitely creates tension that stabilises kinetochore-microtubule attachments.

It is known that kinetochore-microtubule attachments are stabilised by tension and destabilised by a lack of tension (Nicklas and Ward, 1994). Furthermore, only amphitelic attachments can generate tension across kinetochores, as result of each kinetochore experiencing a pole-directed force. The mechanism by which tension generates microtubule stability is unknown, but a number have been proposed. It has been suggested, for example, that microtubule motors attached to kinetochores pull them towards the minus-end of microtubules, which generates tension. This tension forces the motors to stall, leaving them in a transition state in which they are more stably attached to microtubules (McIntosh et al., 2002). A second proposal suggests that tension across kinetochores physically prevents microtubule filaments from bending and, therefore, reduces the likelihood of catastrophe (Grishchuk, 2009). In a third suggested mechanism (Figure 7) tension separates kinetochore components from the influence of centromeric Aurora-B, allowing the stabilising effects of PP1 and PP2A-B56 phosphatases to dominate (Lampson and Cheeseman, 2011; Tanaka et al., 2002). Regardless of the mechanism, the stabilisation of amphitelic attachments causes them to persist meaning that over time all mitotic chromosomes will eventually display amphitely. Once this state is reached the SAC is silenced and the APC/C can proceed to initiate anaphase.

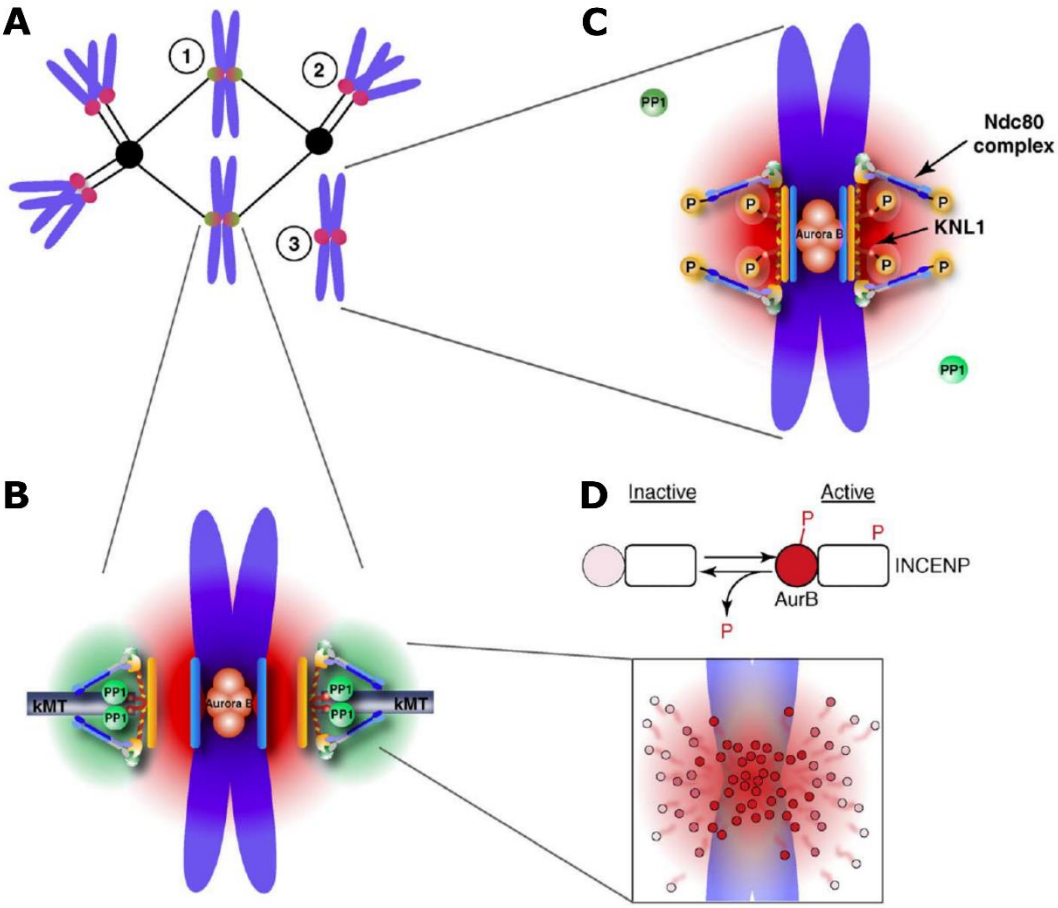


Figure 7. Model of tension sensing by Aurora B kinase. On unattached (3) and incorrectly attached chromosomes (2), a phosphorylation gradient is generated by Aurora B localised at the centromere (red) and phosphorylates sites in the KMN network, which lies within the gradient, destabilising attachment (C). Tension generated by correct attachment (1) separates Aurora B substrates from the phosphorylation gradient, reducing phosphorylation and allowing for recruitment of PP1 to the outer kinetochore, which produces a counteractive dephosphorylation gradient (green) (B). In a model for generation of the phosphorylation gradient (D), recruitment of Aurora B to inner centromere proteins (INCENP) leads to activation of Aurora B by autophosphorylation. This is followed by the release of Aurora B and its eventual inactivation, by dephosphorylation, as it diffuses away from the centromere. From Lampson and Cheeseman (2011).

1.2.5. The separation of sister chromatids at anaphase

Anaphase consists of two phases. Anaphase A involves the depolymerisation of kinetochore microtubules which pull sister chromatids apart and towards the spindle poles. Anaphase B involves separation of spindle poles, through extension of interpolar microtubules, further separating sister chromatids. The relative length of time each phase takes and the amount they contribute to the division of chromosomes varies from organism to organism (Alberts et al., 2008b; Walczak and Heald, 2008).

Depolymerisation of kinetochore microtubules during anaphase A is driven by depolymerising microtubule motors at their plus-ends, which counteracts microtubule stabilising proteins, and at their minus-ends (Gorbsky et al., 1988, 1987). The relative contributions of minus- and plus-end depolymerisation can vary between organisms. In vertebrate cells, ~70% of chromosome movement occurs through plus-ends depolymerisation and ~30% through minus-end depolymerisation (Mitchison and Salmon, 1992). In *Drosophila* embryos and *Xenopus* egg extracts the reverse is true, with depolymerisation of minus-end being the major contributor (Brust-Mascher and Scholey, 2002; Desai et al., 1998; Maddox et al., 2002).

During anaphase B the dynamics of interpolar microtubules change, resulting in spindle elongation. This change relies on two mechanisms, the inhibition of depolymerisation of microtubules and the sliding apart of antiparallel microtubules (Brust-Mascher et al., 2015; Brust-Mascher and Scholey, 2011). In *Drosophila* cells, the Patronin protein mediates the switch to elongation by stabilising microtubule minus-ends, antagonising depolymerising motors (Wang et al., 2013). The action of motor proteins at the spindle midzone then pushes apart growing antiparallel microtubules, elongating the spindle (Brust-Mascher and Scholey, 2011). In some systems, however, these motors act to inhibit and regulate centrosome separation driven by motors' actions on astral microtubules (Collins et al., 2014; Saunders et al., 2007).

1.3. Mitosis in *Trypanosoma brucei*

1.3.1. The mitotic spindle in *Trypanosoma brucei*

Trypanosomes carry out a closed mitosis, with the NE remaining intact and the mitotic spindle assembled within the nucleus (Vickerman and Preston, 1970). Mitosis in *T. brucei* and the mitotic spindle (Figure 8) are unusual in comparison to model systems. At metaphase the spindle microtubules are arranged into a rhomboid shape, nucleated at the poles (Ogbadoyi et al., 2000). Despite this nucleation, the trypanosome spindle lacks clear visible spindle pole bodies. Furthermore, γ-tubulin does not localise to spindle poles in the trypanosome nucleus, instead localising to the nucleolus (Scott et al., 1997). Observations of spindle by transmission electron microscopy, however, have demonstrated a bilaminar structure in the NE in the proximity of nucleated microtubules, which may serve as a pole body (Ogbadoyi et al., 2000). Trypanosomes also lacks the astral microtubules that anchor the spindle to the cell cortex in other organisms. As chromosomes divide during anaphase the spindle rearranges into a linear central microtubule array with peripheral microtubules. In *Leishmania* this consists of ~50 microtubules emanating from opposing poles that overlap in an antiparallel array in the centre of the nucleus, though it may also consist of individual continuous microtubules (Ureña, 1988). After the spindle's transition into its anaphase arrangement, nucleation at the poles becomes less clear, as it becomes bifurcated towards its poles (Ogbadoyi et al., 2000).

In *T. brucei*, certain microtubules terminate in kinetochore-like structures, which can be observed as electron dense plaques by electron microscopy (Ogbadoyi et al., 2000; Schlimme et al., 1993; Solari, 1995). Unusually, only eight such plaques have been observed in trypanosome cells (Solari, 1995), which is far too few for all trypanosome chromosomes, ~125 (~250 when replicated), to associate with individually. Likewise, only 10 kinetochore plaques have been observed in *T. cruzi* (Solari, 1980) and six in *Leishmania* (Ureña, 1986).

Trypanosome chromosomes do not visibly condense during mitosis and, therefore, no clear alignment of chromosomes at the metaphase plate occurs. It is possible that an unusual histone H1A, which binds to chromosomal DNA between nucleosomes, may be partly responsible for this (Burri et al., 1995, 1993; Galanti et al., 1998). The genome of *T. brucei* does, however, code for a homologue of the condensin complex (Gluenz et al., 2008), suggesting some form of condensation does occur. The nuclear DNA of *T. brucei* also behaves curiously during mitosis in that the nucleolus does not break down, as occurs in many eukaryotes. Instead it remains intact and sits within the spindle, with spindle microtubules both surrounding it and passing through it. Early in mitosis, it stretches from its usual spherical form to more bar-shaped form and eventually splits to form the nucleoli of the two daughter cells (Ogbadoyi et al., 2000).

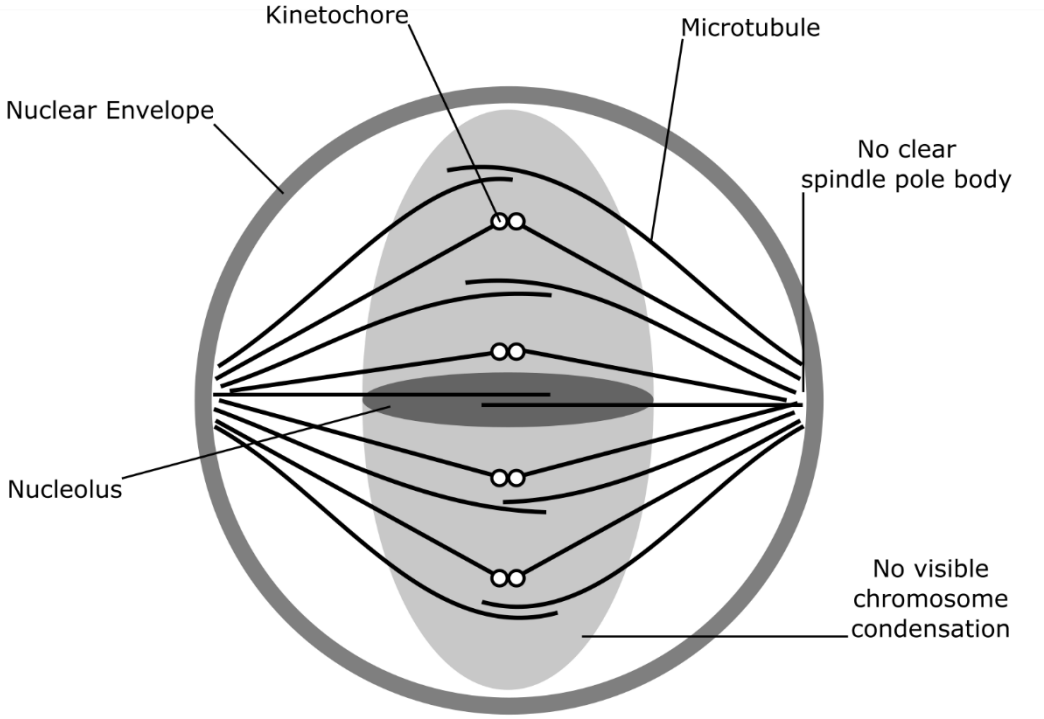


Figure 8. A diagrammatic representation of the mitotic spindle at metaphase in *T. brucei*. The spindle is assembled within the NE, which remains throughout mitosis. The nucleolus also does not break down and sits within the spindle. Spindle microtubules form a rhomboid shape and are nucleated at the spindle poles, though there are no obvious spindle pole bodies. Some spindle microtubules link to kinetochores, of which there are just eight, far fewer than the number of chromosomes, which do not visibly condense.

Spindle assembly in trypanosomes appears to be regulated by Aurora kinases, like other eukaryotes. An Aurora-B homologue, TbAUK1, has been identified in *T. brucei*. Depletion of TbAUK1 in both BSF and PCF cells has demonstrated its requirement for spindle assembly (Li and Wang, 2006; Tu et al., 2006). It forms a CPC with two unique proteins TbCPC1 and TbCPC2, which have little similarity known CPC proteins found in model eukaryotes (Li et al., 2008a, 2008b). Like the CPC in vertebrates, the trypanosome CPC localises to chromosomes in the early stages of mitosis and transfers to the central spindle in the later stages (Figure 9). It also localises to the anterior end of the new FAZ during the transition to cytokinesis and travels along the cleavage furrow as cells divide (Li et al., 2009, 2008a). A homologue of TLK-1, TbTLK1, is also present in *T. brucei*. It is required for spindle assembly and chromosome segregation and interacts with TbAUK1, though it is unclear whether it is involved in the activation of TbAUK1 (Li et al., 2007). The trypanosome CPC also interacts with two kinesin-like proteins, KIN-A and KIN-B, which are concentrated in the nucleus and are required for TbAUK1 localisation, though their function remains unknown (Li et al., 2008a, 2008b).

The role of TbAUK1 in mitosis is unclear. There is no evidence for a SAC in trypanosomes, in which TbAUK1 might function, and perturbation of the spindle does not prevent continued mitosis and cell division (Akiyoshi and Gull, 2013; Ploubidou et al., 1999). Trypanosomatid genomes do code for MAD2 homologues, which can be identified by a HORMA domain present in other MAD2 proteins (Aravind and Koonin, 1998). The trypanosome MAD2, however, lacks a Cdc20 binding domain and localises to the basal body (Akiyoshi and Gull, 2013). It is, therefore, likely that TbMAD2 does not function as a SAC protein.

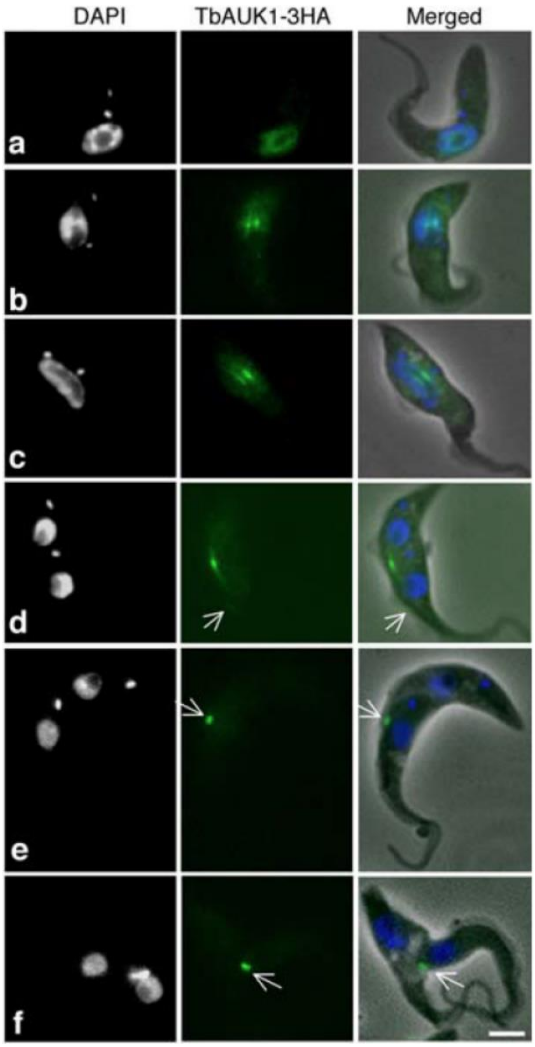


Figure 9. The distribution of TbAUK1 at G2 phase. Images show the location of TbAUK1 labelled with a haemagglutinin tag at G2 phase (a), metaphase (b), early anaphase (c), late anaphase (d) and cytokinesis (e,f). Scale bar = 2μm. From Li et al. (2008a).

1.3.2. Segregation of trypanosome chromosomes

Despite their great number and the small number of kinetochores, chromosomes are separated with fidelity during mitosis. Less than 10^{-3} MC losses occur per cell per generation (Wickstead et al., 2003). It is likely that mechanisms involved in trypanosome chromosome segregation differ from those observed in model systems. In the '90s, Ersfeld and Gull (1997) investigated the division of MBCs and MCs using fluorescence *in situ* hybridisation (FISH). MCs were labelled with probes raised against the 177bp repeat sequences that form their core, while a single MBC was labelled with probes raised against 5S rDNA, which is localised towards the end of chromosome 8 (Berriman et al., 2005). MC and MBC segregation was dependent on the presence of spindle microtubules, demonstrating that both chromosome classes interact with the spindle. During interphase MC signal localised to the nuclear periphery, while 5S rDNA probes produced two foci at the centre of the nucleus. At metaphase MCs aligned at the centre of the nucleus, localising closely with the spindle microtubules. Upon anaphase and the rearrangement of spindle microtubules into the central array, MCs separated into two equally sized groups that migrated along the central spindle to the spindle poles and remained there as the spindle elongated in the later stages of anaphase. 5S rDNA signal displayed a different nuclear distribution during mitosis. It localised to the nuclear periphery at metaphase and, during anaphase, it was found closer to the centre of the spindle, lagging behind the MCs. This apparent lagging of the MBC may in part have been due to the location of 5S rDNA on chromosome 8 and the relative lack of chromosome condensation.

Due to the close association of MCs with the central spindle and their differing localisation to MBCs during mitosis, Gull et al. (1998) proposed the lateral stacking model for MC segregation (Figure 10). They suggested that MBCs interacted with kinetochores, like canonical mitotic chromosomes, while MCs interacted with the mitotic spindle in a very different way. Sister chromatids of replicated MCs were proposed to interact with antiparallel microtubules in the forming central spindle, with one chromatid interacting with a microtubule emanating from one pole and the other interacting with a microtubule emanating

from the other pole. This interaction would be mediated by microtubule motors that would attach the sister chromatids, laterally, to the microtubules. These motor proteins would then drive the separation of MCs, pulling them towards the spindle poles ahead of the dividing MBCs. Apart from the differing localisation of MCs and MBCs described by Ersfeld and Gull (1997), there is, however, little evidence to support this model.

Ogbadoyi et al. (2000) used FISH to track chromosome 1, by producing a probe against the tubulin array, which is located centrally on the chromosome (Hall et al., 2003). The array produced two foci of signal in interphase cells. As DNA began to separate during anaphase, foci were present in the locations proximal to the spindle poles, but were also located distally, separated by relatively large distances. This is perhaps representative of a lack of chromosome condensation. Populations of chromosomes were also localised, with FISH performed against the 177bp repeat cores of MCs and the telomeres of MBCs. MCs showed a similar localisation to that described by Ersfeld and Gull (1997). The telomeres of MBCs colocalised with MCs at interphase and during mitosis. During anaphase, however, a number of telomeres did trail behind the main body of dividing telomeres and MCs. These telomeres may have been those of the larger chromosomes and, again, may be indicative of a lack of chromosome condensation.

As has been described above, trypanosomes separate their chromosomes in processes similar to anaphase in other organisms, with chromosomes moving to poles of the spindle (anaphase A), before the spindle elongates moving the nuclear DNA further apart (anaphase B). In other eukaryotes anaphase is initiated by the APC/C, which tags inhibitors of mitotic exit for degradation. The genome of *T. brucei* encodes homologues of seven core components of the human APC/C, Apc1, Apc2, Apc10, Apc11, Cdc16, CDC23, CDC27 (Kumar and Wang, 2005). Three further components have also been identified and are known as AP1, a homologue of human Apc4, AP2 and AP3 (Bessat et al., 2013). Homologues of cyclin B (CYC6), a key substrate of the APC/C, and Cdk1 (CRK3), the enzyme it interacts with to inhibit mitotic progression, are also present in *T. brucei*

(Hammarton et al., 2003; Li and Wang, 2003; Tu and Wang, 2004). Evidence suggests that the trypanosome APC/C ubiquitinates CYC6 (Bessat et al., 2013). Another substrate of the APC/C, securin, appears to be absent from the trypanosome genome, though the separase enzyme it inhibits is present (Bessat and Ersfeld, 2009). Proteins that form the cohesin complex, which separase hydrolyses, are present (Bessat and Ersfeld, 2009; Gluenz et al., 2008). Four further proteins interact with the APC/C (Bessat, 2014), though their function is unknown.

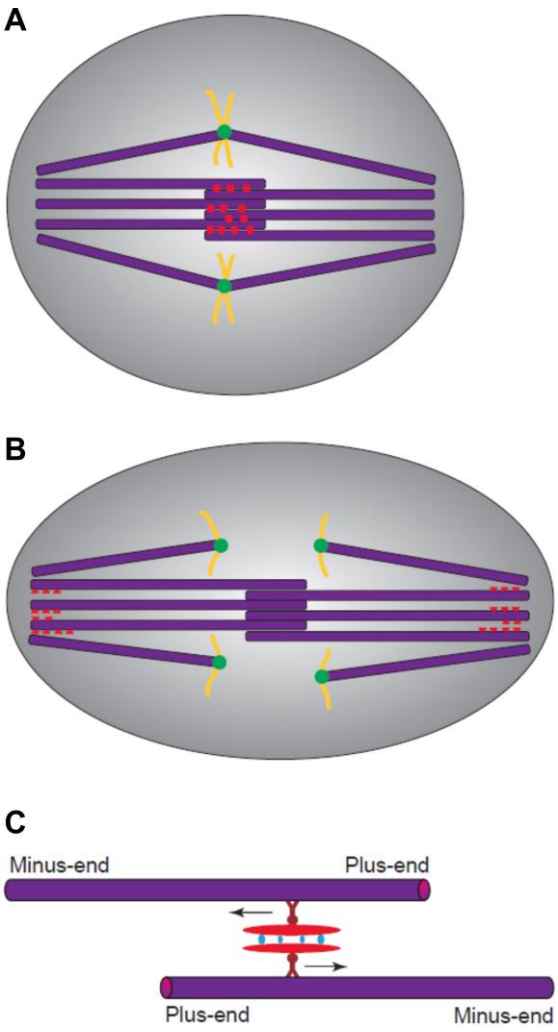


Figure 10. The lateral stacking model for minichromosome segregation in *T. brucei*. MCs (red) associate with the metaphase spindle (purple) laterally, while kinetochores (green) mediate attachment of MBCs (yellow) to microtubules (A). Following metaphase, MCs move quickly to the poles, as MBCs enter anaphase (B). MCs are hypothesised to interact with spindle microtubules through the actions of putative minus-end directed motor proteins (brown) (C). Cohesin-like proteins, which might associate with the chromatid pair, are shown in blue. From Gull et al. (1998).

1.3.3. The trypanosome kinetochore lacks many components present in model systems

The approximately eight kinetochores visible on the trypanosome spindle appear as electron-dense plaques in transmission electron micrographs. These plaques are ~100 × 120nm in size and have a laminate substructure (Figure 11). The substructure at metaphase consists of two electron-dense outer layers (~50nm thick) separated from a thin electron-dense midzone by an electron-transparent intermediate zone. Up to four microtubules terminate in the outer layers of the plaques and link them to the spindle poles. After the initiation of anaphase, these pairs of kinetochores begin to separate altering the substructure of the plaques. This change involves the formation of a 10nm thick electron-dense region proximal to the spindle pole, separated from the rest of the plaque by a 10nm electron-transparent region. The four kinetochore microtubules associate with and terminate in this additional layer. As separation continues the kinetochore pairs separate into individual kinetochores with a trilaminar substructure. This substructure consists of the spindle pole proximal 10nm electron-dense region separated from the main body of the outer kinetochore by a 50nm thick electron-transparent region. The four kinetochore microtubules remain associated with the additional layer. The kinetochores move towards the spindle poles as mitosis progresses in a fashion similar to anaphase A and, during this movement, they are located at the periphery of the nucleolus. After migrating to the poles, the kinetochores remain in their proximity until the culmination of mitosis (Ogbadoyi et al., 2000).

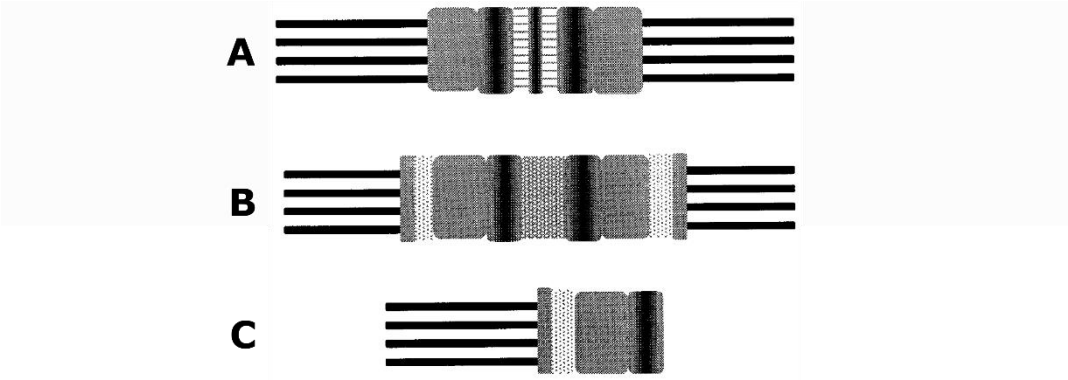


Figure 11. Schematics of *T. brucei* kinetochore plaques. Shown are representations of the plaques at metaphase (A) and the metaphase-anaphase transition, in which they become elongated (B), both consisting of pairs of kinetochores, and a single kinetochore plaque at anaphase (C). Shading represents the electron density, while black lines represent microtubules. From Ogbadoyi et al. (2000).

The trypanosome kinetochore is likely to have a very different protein structure to those described in vertebrate and yeast cells. Trypanosomes have no homologues of the majority of kinetochore proteins or kinetochore interacting proteins that are present in both animals and fungi (Figure 12). Trypanosomes even lack a homologue of CENP-A (Malik and Henikoff, 2003), despite MBCs having well defined centromeres (see below). There are some exceptions to this rule, however. As has been discussed previously, trypanosomes have an Aurora-B homologue, TbAUK1, but they also have a gene coding for a homologue of Skp1p, which forms part of the yeast specific Cbf3 complex, and TOG, a protein that modulates the microtubule binding behaviour of the Ndc80 complex (Berriman et al., 2005).

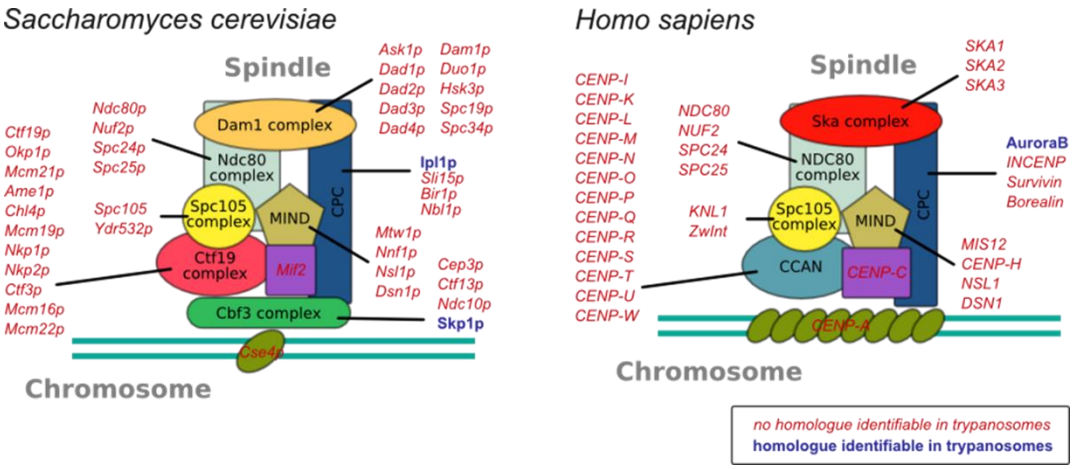


Figure 12. Trypanosomes lack the majority of kinetochore proteins that are conserved between humans and yeast. Complexes that make up the kinetochore are represented by shapes, which are labelled with their constituent proteins. Words in red represent proteins absent from trypanosomes, whereas those in blue are present. Courtesy of Bill Wickstead.

Studies have identified centromeres in trypanosomes by measuring and mapping topoisomerase II activity, which acts as a marker of active centromeres. This analysis has been performed in *T. cruzi* (Obado et al., 2007, 2005) and *T. brucei* (Echeverry et al., 2012; Obado et al., 2007) and identified centromeres consisting of regions of transposable elements. In *T. brucei*, centromeres were only identified on MBCs and topoisomerase II activity was not present on ICs and MCs. The centromeres of the MBCs of *T. brucei* also contained AT rich repeat sequences, which were absent from *T. cruzi* centromeres. Until recently it was unknown what a lack of centromeres means for IC and MC segregation and their interactions with the mitotic spindle and it was unknown if and where kinetochores were assembled in the centromeric regions of MBCs.

A few papers have been published on work that has sought to identify the core components of the trypanosome kinetochore, other than the CPC. Akiyoshi and Gull (2014) identified 19 kinetochore components in *T. brucei*, the majority of which were conserved across kinetoplastids and none of which displayed any homology to conventional kinetochore proteins. The first protein identified, kinetoplastid kinetochore protein 1 (KKT1), displayed a localisation consistent with a kinetochore function (Figure 13). 12 further proteins, KKT2 to 13, were identified, through their interactions with KKT1. Another 6 proteins, KKT14 to 19,

were then found, through their associations with KKT2 to 13. Additionally, KKT4 copurified with constituents of the trypanosome APC/C, suggesting communication between the two. The 19 KKT proteins displayed differing expression profiles over the course of the cell cycle (Figure 14). It was speculated that those proteins that were present until the end of anaphase, namely KKT1, 2, 3, 4, 5, 6, 7, 14, 15, 16, 17, and 18, formed the core kinetochore. ChIP-Seq demonstrated that KKT2 and KKT3, which are constitutively expressed and more likely to interact with centromeres, localised to previously defined centromeric sequences (Echeverry et al., 2012; Obado et al., 2007), suggesting kinetochore assembly does indeed occur at the centromeres of MBCs. Sequences to which KKT2 and KKT3 localised also included the 177bp repeat sequences that form the core of MCs and ICs, suggesting these smaller chromosomes also interact with kinetochores and that sharing of kinetochores might occur between chromosomes. Analysis of the sequences of the KKT2 and 3 suggested protein kinase activity and demonstrated the presence of cysteine rich domains, in which zinc finger motifs were present, and DNA binding motifs. This suggests that these proteins interact with centromeric DNA and modify other proteins, forming the basis for kinetochore assembly. Depletion of KKT2, KKT7, KKT9, KKT11, KKT12, and both KKT10 and KKT19 resulted in the formation of cells with abnormal DNA content and kinetochores that lagged during anaphase. Furthermore, analysis of cells that had been depleted of KKT10 and KKT19 by FISH demonstrated lagging of both MBCs and MCs. Based on affinity purification/mass spectrometry data and localisation patterns the authors suggested potential subcomplexes that might be formed by KKTs. The proposed subcomplexes were the KKT14-KKT15 subcomplex, the KKT16-KKT17-KKT18 subcomplex, and the KKT6-KKT7-KKT8-KKT9-KKT10-KKT11-KKT12-KKT19 subcomplex.

Another KKT, KKT20, was later identified by Nerusheva and Akiyoshi (2016), through its interaction with KKT4. Analysis of the protein's sequence demonstrated that it was similar to those of both KKT2 and 3, particularly in a Cys-rich region, though it was much smaller and lacked a shared kinase domain.

All three proteins were also shown to contain polo box domains, which were involved in the localisation of the proteins to the kinetochore.

More recently, a further set of kinetochore proteins, referred to as the KKT-interacting proteins (KKIPs), were identified by D'Archivio and Wickstead (2016). The first KKIP, KKIP1, was identified through the identification of Ndc80/Nuf2-like sequences in a number of eukaryotes, using hidden Markov models. Fluorescent labelling of the protein demonstrated that it localised to the kinetochore and colocalised with KKT1. Determination of the relative subpixel positions of tagged proteins indicated that KKIP1 functioned in the outer kinetochore, providing further evidence that it fulfils a Ndc90/Nuf2-like role. Knockdown of KKIP1 caused significant a reduction population growth and caused severe spindle and chromosome segregation defects. Finally, identification of proteins that could be copurified with KKIP1, after crosslinking, revealed interaction between KKIP1 and a number of KKTs, including KKT1, as well as six further previously unidentified kinetochore proteins, which were named KKIP2-7.

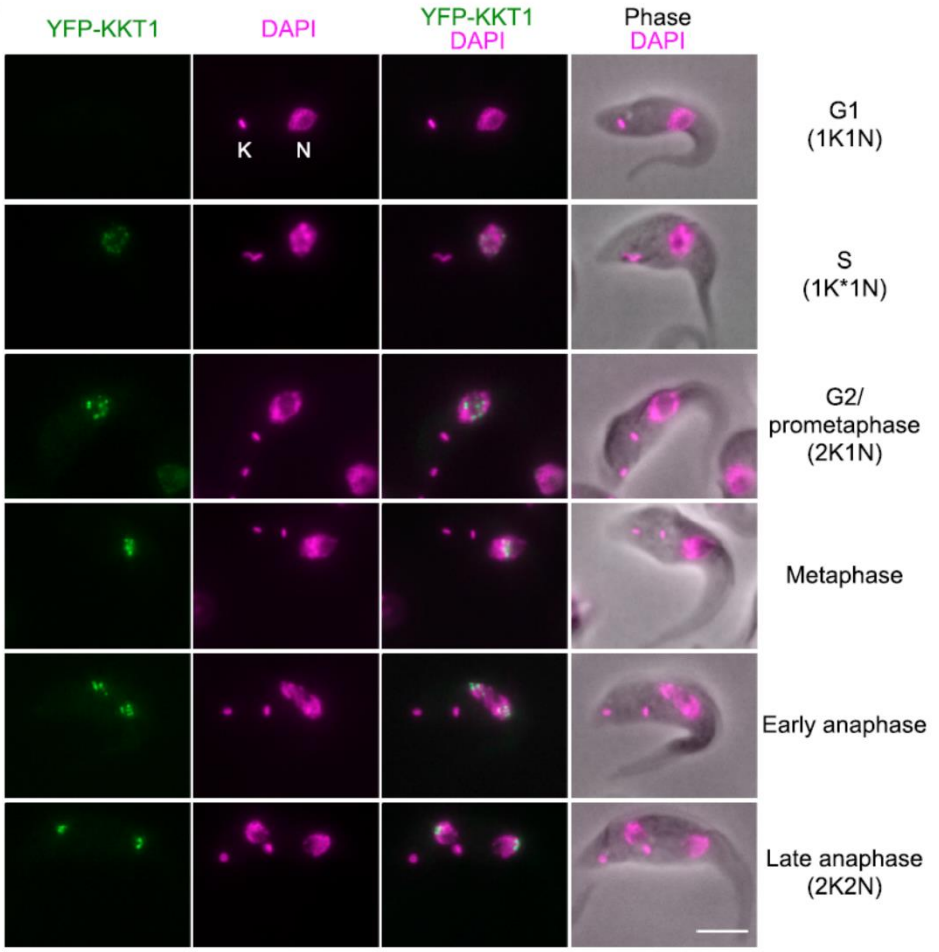


Figure 13. The distribution of KKT1 through the trypanosome cell cycle. Images show the location of YFP labelled KKT1 relative to kinetoplast (K) and nuclear DNA (N). Scale bar = 5μm. From Akiyoshi and Gull (2014).

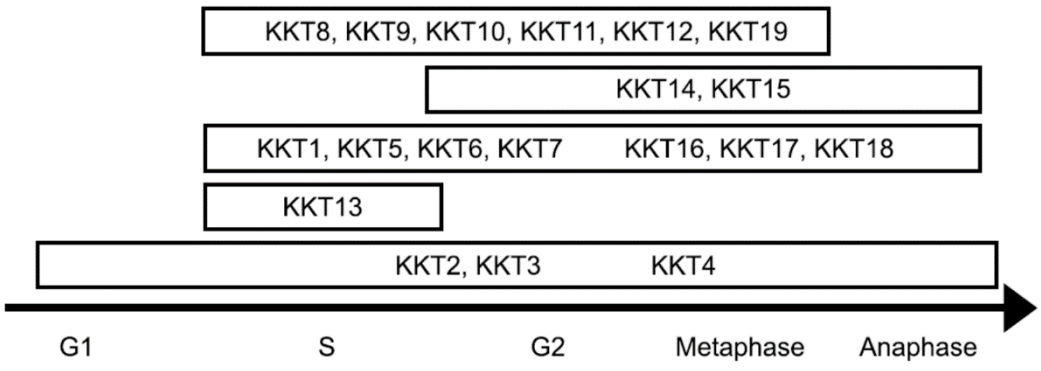


Figure 14. Summary of KKT expression patterns over the course of the cell cycle. From Akiyoshi and Gull (2014).

1.4. Kinesin motors

1.4.1. The kinesin superfamily

The spatiotemporal organisation of molecules and organelles within eukaryotic cells is often the result of the cytoskeleton and the motor proteins that act upon it. Motor proteins are ATPases that convert ATP into mechanical work, allowing them to transport cargo along the cytoskeleton. The actions of certain motor proteins can also regulate and remodel the cytoskeleton. There are three superfamilies of motor protein (Vale, 2003), myosins, dyneins and kinesins (Figure 15).

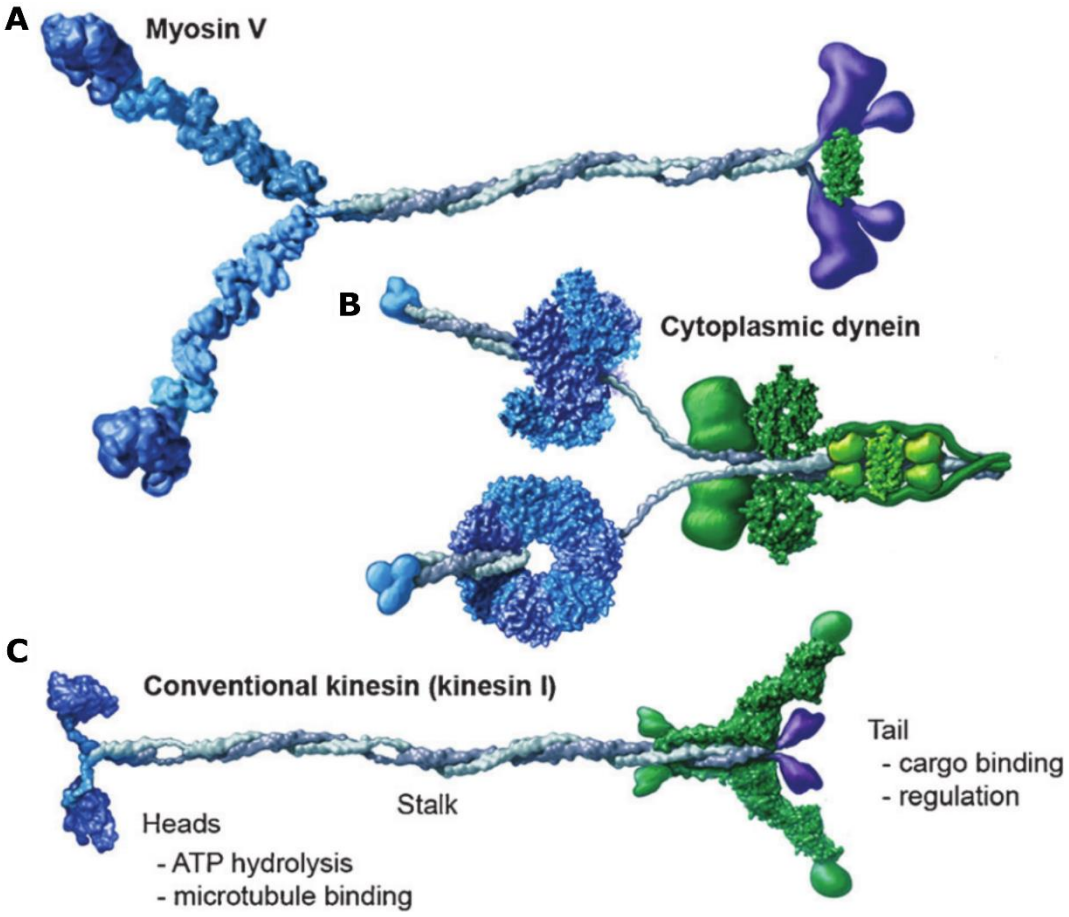


Figure 15. Examples of motor protein superfamily members. Displayed are representations of atomic resolution structures of myosin V (A), cyoplasmic dynein (B) and kinesin-1, or conventional kinesin (C). Motor domains are shown in blue, mechanical amplifiers in light blue, cargo interaction sites in purple and associated polypeptides in green. Adapted from von Delius & Leigh (2011).

Myosin proteins act on the actin cytoskeleton. Both dynein proteins and kinesin proteins act on the microtubule cytoskeletons. They, therefore, perform a number of roles in the mitotic spindle. The functions of dynein are not the focus of work presented in this thesis, so they will not be discussed here, but they are reviewed in Roberts et al. (2013).

The first kinesin discovered was identified in the axoplasm of squid giant axons with a homologue found in bovine brains (Vale et al., 1985). The identification of further homologues, in chick brain (Brady, 1985), sea urchin eggs (Scholey et al., 1985), *Xenopus* and *Drosophila* (Neighbors et al., 1988; Saxton et al., 1988), followed. In later years more kinesins were identified, performing differing roles on the microtubule cytoskeleton, resulting in the creation of the kinesin superfamily (Vale and Goldstein, 1990). The kinesin superfamily was then phylogenetically classified into 14 standardised families (Lawrence et al., 2004), known as kinesin-1 to -14 (Table 1). The kinesin-1 to -12 families generally display plus-end directed motility, while kinesin-14 members are minus-end directed. Kinesin-13 proteins are not motile, moving along microtubules by diffusion, and act as microtubule depolymerising enzymes, a property also shared by kinesin-8 proteins.

Later analysis by Wickstead & Gull (2006) reclassified kinesins into another 14 families and identified two groups of kinesins specific to kinetoplastid organisms. The kinesin-11 family was found to be unsupported, kinesin-4 and kinesin-10 were merged into one kinesin-4/10 family and the kinesin-12 family was split into two families, kinesin-16 and kinesin-17. Work by Wickstead et al., (2010b) then identified three further families (Table 2), as well as 14 paralogue groups, which included the two previously identified kinetoplastid-specific groups. Recent analysis split the kinesin superfamily into 18 families, kinesin-1 to -11, -13 to -16, and -19 to -21 (Richard et al., 2016). These families included 13 of the 14 standardised families and three of the families described by Wickstead et al., (2010b). The kinesin-20 family contained kinesins from the chromista and protozoa, while the kinesin-21 family was a pseudofamily consisting of orphan kinesins from fungi.

Kinesin Family	Representative Members	Structural Features	Functions
Kinesin-1	KIF5, KHC, UNC116, NKin, DdKIF3, DdKIF5		Vesicle transport, Organelle transport, mRNA transport
Kinesin-2	KIF3A/B, KIF17, Krp85/95, Osm3, Fla10	Heterotrimeric or homodimeric	Vesicle transport, Melanosome transport, Intraflagellar transport
Kinesin-3	KIF1A/B, KIF13A, UNC104	Monomeric	Organelle transport
Kinesin-4	KIF4, KIF21A/B, KLP3A, KLP1	C-terminal DNA binding region	Chromosome movement, Organelle transport
Kinesin-5	KIF11, Eg5, BimC, Cin8, Kip1, Cut7, KLP61F	Homotetrameric, Bipolar	Spindle pole separation, Spindle bipolarity
Kinesin-6	KIF20 (MKLP2), KIF23 (MKLP1), Rab6Kinesin, CHO1,		Central spindle assembly and cytokinesis, Spindle polarity
Kinesin-7	KIF10 (CENP-E), CENP-meta, CENP-ana, Kip2		Kinetochore-microtubule attachment
Kinesin-8	KIF18, KIF19, KLP67A, Kip3		Microtubule depolymerising, Nuclear migration, Mitochondrial transport
Kinesin-9	KIF6, KIF9, KRP3, CrKLP1		Unclear
Kinesin-10	KIF22, KID, Nod	C-terminal DNA binding region	Chromosome movement
Kinesin-11	KIF26A/B, VAB8, SMY1	Divergent catalytic core	Signal transduction
Kinesin-12	KIF12, KIF15 (HKLP2), KLP54D, Xklp2	Grouped due to homologous tails	Spindle pole organisation, Organelle transport
Kinesin-13	KIF2, MCAK, KCM1, KLP10A, PfKinI	Central motor	Microtubule depolymerising, Microtubule-kinetochore error correction, Chromosome segregation
Kinesin-14	Subfamily A: KIFC1, CHO2, Ncd, Kar3, KatA Subfamily B: KIFC2, KIFC3, KLP3, a large number of plant-specific isoforms	C-terminal motor	Spindle pole organisation, Organelle transport

Table 1. Standardised kinesin family classification. Reproduced from both Miki et al. (2005) and Verhey & Hammond (2009).

Kinesin Family	Standardised Family Equivalent	Representative Members
Kinesin-1	Kinesin-1	KIF5, KHC, UNC116, DdKIF3, DdKIF5
Kinesin-2	Kinesin-2	KIF3A/B, KIF17, Osm3, Fla10
Kinesin-3	Kinesin-3	KIF1A/B, KIF13A, UNC104
Kinesin-5	Kinesin-5	KIF11, Eg5, BimC, Cin8, Kip1, Cut7, KLP61F
Kinesin-6	Kinesin-6	KIF20 (MKLP2), KIF23 (MKLP1)
Kinesin-7	Kinesin-7	KIF10 (CENP-E), CENP-meta, CENP-ana
Kinesin-8	Kinesin-8	KIF18, KIF19, KLP67A, Kip3
Kinesin-9	Kinesin-9	KIF9, CrKLP1
Kinesin-4/10	Kinesin-4, Kinesin-10	KIF4, KIF21A/B, KLP3A, Nod
Kinesin-13	Kinesin-13	KIF2, MCAK, KCM1, KLP10A
Kinesin-14	Kinesin-14	Subfamily A: KIFC1, CHO2, Ncd, Kar3, KatA Subfamily B: a large number of plant-specific isoforms Other: Kinesin-14: KIFC2, KIFC3
Kinesin-15	Kinesin-12	KIF15 (HKLP2)
Kinesin-16	Kinesin-12	KIF12, KLP54D
Kinesin-17	-	A number of protozoan-specific kinesins
Kinesin-18	-	Kinesins present in a wide range of eukaryotes
Kinesin-19	-	Kinesins present in protozoa, oomycetes and plants
Kinesin-20	-	Kinesins present in protozoa, oomycetes and algae

Table 2. Kinesin family classification after reclassification by Wickstead et al., (2010b).

Each kinesin motor contains one to four heavy chains and a number of light chains, the presence of which varies between families. Kinesin heavy chains consist of a motor domain, which can be N-terminal, C-terminal or central, a stalk domain and a tail domain. Motor and stalk domains are connected by a short neck linker. Kinesin motility is generated by the motor domain and neck. Cycling of the globular motor domain's ATP state is associated with cycles of strong and weak microtubule binding states (Crevel et al., 1996) and this association is largely conserved between kinesins. ATP cycling causes conformational changes in the neck domain that drives a "hand-over-hand" mechanism of action in processive kinesins (Cross, 2016; Kaseda et al., 2003), or a "hold-and-release" mechanism in non-processive kinesins (Cross and McAinsh, 2014; Welburn, 2013).

The stalk domain contains a number of coiled-coils that mediate oligomerisation. Many kinesin superfamily members form dimers, though they can also function as tetramers or monomers. Kinesin-5 family members, for example, form tetramers, producing bipolar structures with two motor domains at each end. This arrangement, mediated by specific regions in the stalk, allows kinesin-5 proteins to crosslink microtubules and slide them relative to one another. (Acar et al., 2013; Kapitein et al., 2005; Kashlna et al., 1996; Weinger et al., 2011). Heterodimerisation also allows for regulation and alteration of function. Kar3, a kinesin-14 protein from *S. cerevisiae*, for example, forms hetrodimers with Cik1 or Vik1, two accessory proteins that lack functional motor domains, which alter Kar3's localisation and activity (Allingham et al., 2007; Sproul et al., 2005).

The tail domain can regulate kinesins by autoinhibition. Kinesin-1 has been observed to take on a folded confirmation that corresponds with an inactive state (Coy et al., 1999; Stock et al., 1999; Vale and Friedman, 1999; Verhey et al., 1998). This property is also shared by kinesin-2, -3 and -7 family members (Espeut et al., 2008; Hammond et al., 2009; Imanishi et al., 2006; Okada et al., 1995). In these folded conformations the tail of the kinesin protein comes into contact with the motor domain and inhibits its microtubule binding and ATPase functions.

Kinesins can then be activated by phosphorylation (Espeut et al., 2008) or by cargo binding (Blasius et al., 2007).

The main role for the tail domain is in binding various substrates. These substrates vary by family and are, therefore, a major determinant of a kinesin's function. They can include cargo, such as vesicles, organelles, protein complexes or RNA, which kinesins transport around the cell. The roles kinesins perform in intracellular transport are reviewed in Hirokawa et al. (2009). The tail domains can also interact with microtubules, proteins that direct the kinesins to certain locations or even chromatin. These properties are important in the functions of various kinesins in mitosis.

1.4.2. Kinesins perform a number of roles in mitosis

Microtubule motors are involved in spindle assembly

Kinesin and dynein motors play important roles in canonical mitotic spindle at all stages of mitosis (Figure 16). The separation of centrosomes early in mitosis is driven by kinesin-5 proteins, such as human KIF11. Kinesin-5 proteins crosslink antiparallel microtubules emanating from centrosomes and the sliding mechanism they generate pushes the centrosomes apart. The separation of centrosomes by kinesin-5 is aided by dynein motors that link microtubules to the NE and to the actin cytoskeleton of the cell cortex (van Heesbeen et al., 2013). The action of the immobile dynein on the microtubules functions to pull the centrosomes apart. In the amoeba *Dictyostelium discoideum*, KIF9, a kinesin-1 protein, also anchors centrosomes to the NE (Leo et al., 2012; Tikhonenko et al., 2013).

Microtubule motors are important in the continued assembly of the spindle and in chromosome congression, during prometaphase. The crosslinking and sliding actions of kinesin-5 continue to function in the developing spindle, acting in self-organisation of microtubules into antiparallel arrays and crosslinking of microtubules emanating from opposing poles. Kinesin-5 proteins are, therefore, important in the formation of a bipolar spindle (Blangy et al., 1995;

Heck et al., 1993; Sawin et al., 1992). The localisation of kinesin-5 proteins is regulated by the Aurora-B kinase. Depletion of the *C. elegans* Aurora-B kinase, AIR-2, greatly reduces the levels of the nematode's kinesin-5, BMK-1, associated with meiotic or mitotic spindles (Bishop et al., 2005). Bidirectionality and microtubule stabilising activities have been demonstrated in kinesin-5 proteins, which may aid in their functions in the spindle. Cin8, a kinesin-5 from *S. cerevisiae*, shows minus-end directed motility when attached to a single microtubule. When crosslinked to antiparallel microtubules it displays slow plus-end directed motility (Düselder et al., 2015; Gerson-Gurwitz et al., 2011; Roostalu et al., 2011; Thiede et al., 2012). This activity has been observed in, the *Schizosaccharomyces pombe* homologue, Cut7 (Edamatsu, 2014). The second kinesin-5 from *S. cerevisiae*, Kip1, which functions in late anaphase, shows bidirectionality and microtubule stabilisation activity (Fridman et al., 2013). Eg5 from *Xenopus* also stabilises microtubules, increasing microtubule growth rate and decreasing the likelihood of catastrophe (Chen and Hancock, 2015).

KIF15, a human kinesin-12 (or kinesin-15), though not required for spindle assembly, cooperates with, the kinesin-5, KIF11 in the arrangement and maintenance of spindle microtubules, even producing functional spindles when KIF11 is partially inhibited (Tanenbaum et al., 2009). KIF15 forms a dimer, with a tail domain capable of binding microtubules, and is a processive plus-end directed kinesin. It can also form a tetramer, which is capable of switching from microtubule to microtubule, allowing it to navigate microtubule networks. On interacting with the microtubule associated protein TPX2, KIF15's processivity is reduced and it functions to crosslink antiparallel microtubules and slide them apart (Drechsler et al., 2014; Sturgill and Ohi, 2013; Tanenbaum et al., 2009). Kinesin-12 protein dimers are also present in rats (Liu et al., 2010), sea urchins (Rogers et al., 2000) and *Xenopus* (Bringmann et al., 2004; Wittmann et al., 1998), where they show similar properties to KIF15. KIF15 also bundles parallel microtubules, focussing their plus-ends, and shows microtubule stabilisation properties. It is also possible that KIF15 specifically targets bundled parallel microtubules (Drechsler and McAinsh, 2016; Sturgill et al., 2014; Sturgill and Ohi,

2013). These behaviours allow KIF15 to function in the formation of stable parallel microtubule bundles, such as kinetochore microtubule bundles.

Kinesin-14 proteins, including human KIFC1, or HSET, also form dimers capable of crosslinking microtubules. Kinesin-14 motors are minus-end directed and often non-processive. They bundle and stabilise microtubules, nucleating them at the spindle pole (Karabay and Walker, 1999; Mountain et al., 1999; Vanneste et al., 2009). It is aided by dynein proteins, in animal cells, which also link nucleated microtubules to the MTOCs, via binding to NuMA (Radulescu and Cleveland, 2010). Klp2, a kinesin-14 from *S. pombe*, selectively traps and bundles parallel microtubules and quickly dissociate from antiparallel microtubules (Braun et al., 2009). This property allows Klp2 to organise microtubules into parallel arrays and nucleate them. This behaviour is also shared by a kinesin-14 in *Drosophila* cells, Ncd (Fink et al., 2009).

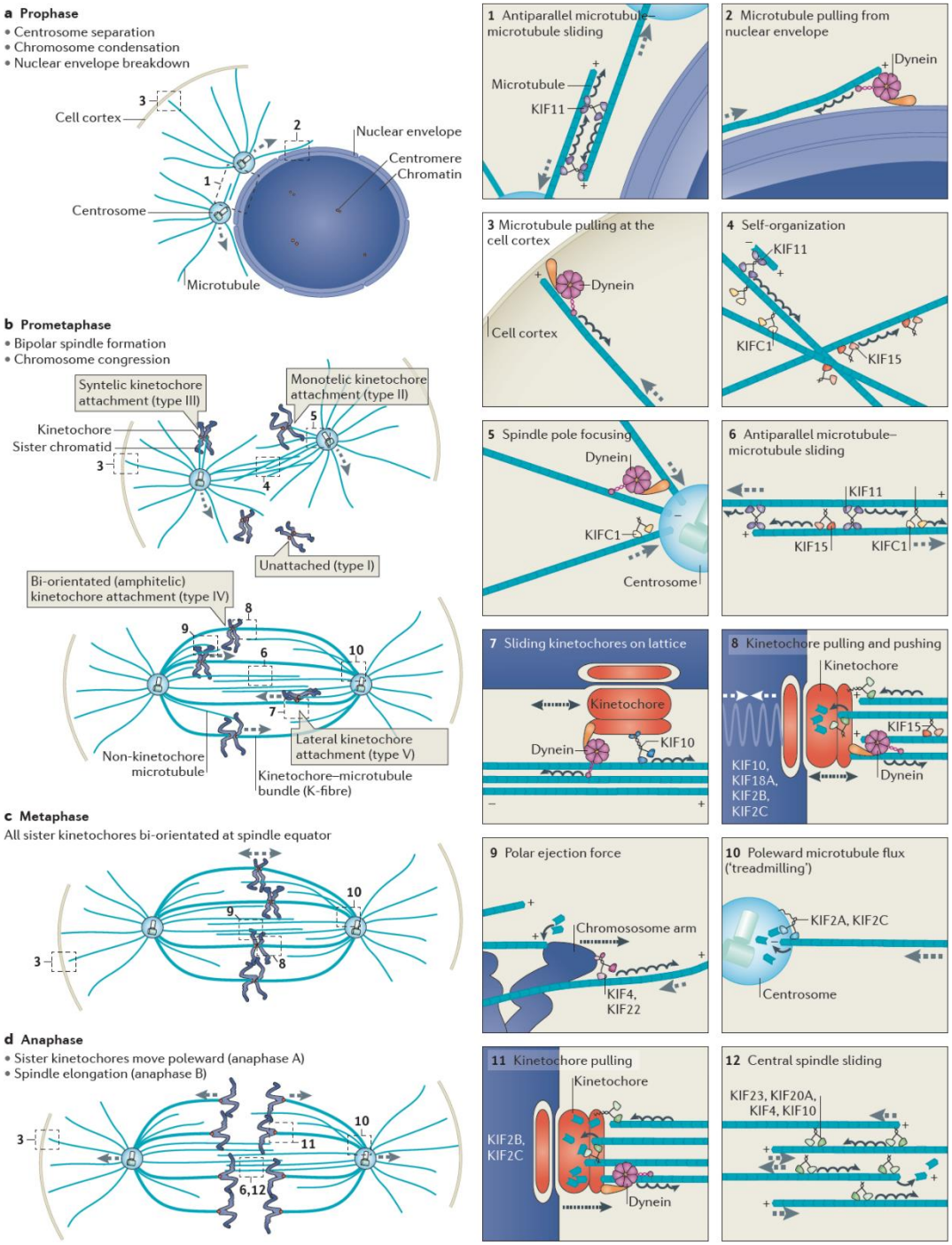


Figure 16. Microtubule motors in the human mitotic spindle. From Cross & McAinsh (2014).

Motor antagonism is required to maintain the spindle

Establishment of bipolar spindles and their maintenance once formed relies on a balance of outward and inward forces generated by the motors that act on spindle microtubules. Work in *S. cerevisiae* has demonstrated the importance of the antagonism of outward directed forces, generated by the actions of dynein on astral mictotubules, by kinesin-5 motors. Knockouts of dynein and kinesin-5 proteins display less severe chromosome segregation defects than cells in which dynein has been knocked out and kinesin-5 is overexpressed (Saunders et al., 1995). In a further example, cells in which both kinesin-5 proteins have been knocked out are not viable, but can be rescued by knockout of kinesin-14 (Hoyt et al., 1993), suggesting restoration of the balance between forces acting on the spindle.

In human cells, in which dyneins generate an inward force by acting on spindle microtubules, depletion of dynein in cells with reduced kinesin-5 activity allowed for bipolar spindle assembly. Bipolar spindles did not form, on the other hand, if dynein was not depleted (Tanenbaum et al., 2008). van Heesbeen et al. (2014) depleted dynein or KIF15 with or without KIF11 inhibition, to investigate the balance of forces between these motors. In cells with established spindles, bias towards an inwards directed force resulted in the formation of monopolar spindles, while greater outward directed forces resulted in the establishment of unstable spindles with reduced polar nucleation. Loss of the activity of all three motors, while preventing spindle assembly, did not affect established spindles. Chromosomes did not align correctly, however, due to a lack of tension on kinetochores and cells did not successfully segregate their chromosomes.

Inhibition of, the *Drosophila* kinesin-5, KLP61F results in the collapse of already assembled bipolar spindles and the convergence of centrosomes (Sharp et al., 1999). Inhibition of KLP61F in an Ncd (kinesin-14) null background results in the assembly of bipolar spindles. These spindles are abnormal, but segregate chromosomes. Alteration of the balance of forces in the spindles of *Drosophila* by overexpression of proteins does not significantly influence spindle length

(Goshima et al., 2005). At the right concentrations, however, KLP61F and Ncd inhibit one another's sliding activity *in vitro* (Tao et al., 2006). Such activity would inhibit spindle pole separation, thereby regulating spindle length. Modelling of KLP61F and Ncd antagonism suggests that randomly positioned motors can imperfectly restrict the relative movement of antiparallel microtubules and thereby regulate spindle length. Varying the concentration of motors alters the control that they exert over spindle length (Deutsch and Lewis, 2015). A balance of forces is, therefore, required for spindle assembly and maintenance in *Drosophila* cells, but its role in length regulation is unclear.

Kinesins in chromosome congression

Mitotic kinesins are important in congression of chromosomes to the metaphase plate. The congression of laterally attached chromosomes is mediated by processive plus-end directed kinesin-7 proteins, such as KIF10 (CENP-E), and dyneins associated with the kinetochore. These motors transport the kinetochore along microtubules, away from and towards the spindle poles (Kapoor et al., 2006; Sardar and Gilbert, 2012; Schaar et al., 1997; Wood et al., 1997; Yang et al., 2007; Yardimci et al., 2008). Aurora kinases and PP1 regulate chromosome congression through regulation of CENP-E; phosphorylated CENP-E drives plus-end directed movement of chromosomes, while dephosphorylated CENP-E does not show affinity for microtubules (Kim et al., 2010). As discussed in section 1.2, congression is also driven by kinetochore microtubules, when chromosomes are biorientated, which generates oscillations of the chromosomes. This behaviour requires kinetochores to track and remain attached to microtubule plus-ends. Work on CENP-E suggests that it can track growing and shrinking microtubule plus-ends. Binding of CENP-E to the microtubule lattice may also act to stabilise kinetochore microtubules (Gudimchuk et al., 2013; Sardar and Gilbert, 2012).

Members of the kinesin-4 and kinesin-10 families (or the kinesin-4/10 family), such as mammalian KIF4A and KIF22, respectively, also contribute to chromosome congression. These plus-end directed kinesins are also known as "chromokinesins," because of their ability to bind to chromatin via DNA binding

elements in their tail domains. While kinetochore motors transport laterally attached chromosomes along kinetochore microtubules, chromokinesins move chromosomes to the metaphase plate by transporting chromosomes along interpolar microtubules, producing the "polar ejection force" (Rieder et al., 1986; Vanneste et al., 2011). Analysis of Nod, a *Drosophila* kinesin-10 (in the standard classification), has shown how these kinesins contribute to congression. Nod is not motile and links chromosomes to microtubule plus-ends, which it tracks, pulling the chromosome arms towards the metaphase plate. This activity is caused by an unusual ATP cycle that stabilises the kinesin's interaction with microtubules, particularly at plus-ends (Cochran et al., 2009). There is no evidence that chromokinesins designated as kinesin-4 members, such as KIF4A, contribute to the polar ejection force (Brouhard and Hunt, 2005; Wandke et al., 2012). It may even act to oppose polar ejection forces by inhibiting microtubule dynamics (Stumpff et al., 2012). Kinesin-4 proteins may also have a role in regulating chromosome condensation, as KIF4A interacts with condensin and its depletion results in hypercondensation of chromosomes (Mazumdar et al., 2004).

The actions of kinetochore motors and chromokinesins cooperate in the congression of chromosomes. Movement of chromosomes towards the spindle poles, driven by dyneins at the kinetochores, counteracts the activities of chromokinesins, destabilising immature or incorrect kinetochore-microtubule attachments. Nearer the poles, CENP-E becomes dominant over dynein and the balance of forces changes, causing chromosomes to move to the metaphase plate (Barisic et al., 2014).

Depolymerising kinesins in the spindle

The actions of depolymerising kinesins are also involved in congression. This includes kinesin-8 proteins, which are processive depolymerases (Roostalu and Surrey, 2013). The human kinesin-8, KIF18A, is required for chromosome congression (Mayr et al., 2007), due to its inhibition of microtubule dynamics, limiting the oscillations of chromosomes. Kinesin-8 proteins depolymerise mictotubules in a length dependent manner, which may aid in keeping

chromosomes at the metaphase plate (Du et al., 2010; Stumpff et al., 2012, 2008; Varga et al., 2006).

Kinesin-13 depolymerases also contribute to congression and the correct alignment of chromosomes, as well as regulating spindle length. Mammalian cells have three kinesin-13 proteins KIF2A, KIF2B and KIF2C, or MCAK. The actions of kinesin-13 proteins at the minus-end of microtubules drive microtubule flux, a translocation of tubulin dimers towards the minus-end that regulates spindle length and drives the mechanism of anaphase A (Ganem et al., 2005; Waters et al., 1996). Anaphase A also involves the actions of plus-end kinesin-13 (Gorbsky et al., 1987; Maney et al., 1998). Plus-end localised kinesin-13 proteins destabilise incorrect kinetochore-microtubule connections, where they are regulated by Aurora-B kinases, and are, therefore, important in error correction and chromosome congression. The absence of MCAK, for example, leads to defects in chromosome congression and segregation defects, due to the presence of incorrect attachments (Andrews et al., 2004; Bakhoum et al., 2009; Kline-Smith et al., 2004; Lan et al., 2004; Maney et al., 1998; Wordeman et al., 2007). The activities of plus-end kinesin-13 proteins also influence oscillations in congression (Jaqaman et al., 2010; Wordeman et al., 2007).

Kinesins in anaphase and cytokinesis

The processes involved in separation of chromosomes at anaphase, which involve the actions of kinesins. The shortening of kinetochore microtubules during anaphase A involves their depolymerisation from their plus-ends and minus-ends (Gorbsky et al., 1987; Mitchison and Salmon, 1992). Both of these processes are driven by the actions of kinesin-13 depolymerases (Rogers et al., 2004). The actions of kinesin-7 proteins at the kinetochore, as well as Dam/Ska complexes, have been also been proposed to aid in its ability to track the shrinking microtubules (McIntosh et al., 2012). The elongation of the spindle in anaphase B, further separating chromosomes, involves kinesin-5 proteins that slide apart growing interpolar microtubules (Brust-Mascher et al., 2009; Brust-Mascher and Scholey, 2011; Straight et al., 1998). Work in *C. elegans* (Saunders et

al., 2007) and mammalian cells (Collins et al., 2014), however, has shown that kinesin-5 proteins can act to limit spindle elongation, inhibiting centrosome separation caused by dyneins acting on astral microtubules.

In late anaphase and cytokinesis, the central spindle forms between dividing chromosomes and consists of bundles of antiparallel microtubules. It is involved in defining the cleavage furrow in cytokinesis and limits spindle elongation, antagonising pulling forces dyneins generate on astral microtubules. The structure and size of the central spindle is determined by kinesins. MKLP1 (KIF23 in Figure 16) kinesin-6 proteins complex with the CYK-4 protein to crosslink antiparallel microtubules, producing and stabilising the microtubule bundles in the central spindle (Matuliene and Kuriyama, 2002; Mishima et al., 2002; Somers and Saint, 2003). The activity of MKLP1 requires phosphorylation by Aurora-B, which is translocated to the central spindle by MKLP2 (KIF20A) proteins (Gruneberg et al., 2004; Kitagawa et al., 2013; Neef et al., 2006). The chromokinesin, KIF4A, also functions in the central spindle, where it limits the length of central spindle microtubules, after activation by Aurora-B (Bieling et al., 2010; Hu et al., 2011; Nunes Bastos et al., 2013). Localised activation of the KIF2A depolymerase by Aurora-B also regulates central spindle microtubule length (Uehara et al., 2013).

1.4.3. Kinesin motor interactions

Kinesins show many interactions with other motors, including cooperation to complete tasks, functional redundancy and antagonism. Kinesin motors can cooperate collectively, with other kinesin family members or with other cytoskeletal motor superfamilies. Microtubule motors often work in teams to collectively generate force (reviewed in Mallik et al., 2013). The effects of cooperation on force generation varies between kinesins. There is a weak relationship, for example, between processive kinesin-1 protein number and force (Furuta et al., 2013) and, therefore, velocity of and distance travelled by cargo (Efremov et al., 2014). The number of non-processive kinesin-14 motors, on the other hand, has a strong relationship with the force generated (Furuta et al.,

2013). The length-dependent regulation of microtubule length by kinesin-8 proteins is also believed to be a function of its collective activity (Varga et al., 2009, 2006). Longer microtubules are thought to accumulate larger numbers of processive kinesin-8 proteins, resulting in greater levels of collective plus-end depolymerisation. In a situation contrary to this, catastrophe of microtubules has an inverse relationship with the concentration of KIF15 motors (Drechsler and McAinsh, 2016).

Interactions between motor superfamilies are required for transport of cargoes and for spindle assembly. Transport of cargoes involves coordination between motors on the microtubule and actin cytoskeletons (reviewed in Brown, 1999; Petrásek and Schwarzerová, 2009). The transport of cargo on the microtubule network requires the actions of plus-end directed kinesins and minus-end directed dynein motors (Millecamps and Julien, 2013). An antagonistic relationship exists between the two motors that is regulated by cells to achieve anterograde or retrograde transport. Recruitment of kinesin-1 motors, for example, reverses minus-end directed transport by dyneins (Rezaul et al., 2016). As discussed previously, cooperation between kinesin-5 and dynein drives centrosome separation. Later cooperation between kinesin-5, -12 (-15), -14 and dynein motors is involved in spindle assembly and their antagonism maintains it. Dynein also acts with kinesin-7 and chromokinesins in the congression of chromosomes to the metaphase plate.

Interactions also occur between kinesin families or differing kinesins from the same family. For example, two kinesin-2 motors cooperate in the intraflagellar transport in *C. elegans* and show differing functions. The first, kinesin-II, transports intraflagellar transport particles through the base and transition zone of cilia. On the axoneme the second kinesin, OSM-3, takes over and transports the cargo to the tips of the cilia (Mijalkovic et al., 2016; Prevo et al., 2015). Many further examples of interactions between kinesins occur in mitosis and have been discussed above. These interactions involve cooperation and antagonism to produce the spindle, regulation of spindle microtubule length

by depolymerases, congression of chromosomes and modification of spindle microtubule dynamics in anaphase and cytokinesis.

Interactions between kinesins can result in functional redundancy upon depletion or inactivation of an individual motor. An example of this is the partial redundancy that exists between KIF11 and KIF15 (Tanenbaum et al., 2009). The two kinesin-5 motors of *S. cerevisiae*, Cin8 and Kip1, show partial redundancy, compensating for one another under certain conditions (Hoyt et al., 1992; Roof et al., 1992; Saunders et al., 1995). Kinesins involved in congression also show some redundancy. Disruption of CENP-E in mammalian cells prevents proper amphitelic kinetochore-microtubule attachment, but does not prevent chromosome congression and initiation of anaphase (McEwen et al., 2001). Furthermore, disruption of kinesin-7 and chromokinesins has an additive effect on the severity of chromosome alignment defects in *Drosophila* (Goshima and Vale, 2003). Kinesin-7 proteins are, therefore, not required for congression, likely through a redundant relationship with chromokinesins. In *Drosophila* cells, the complex interactions between mitotic kinesins can also produce curious phenotypes. Knockdown of depolymerising kinesins, results in the spindle collapsing into a monopolar spindle. The kinesin-5, KLP61F and, the kinesin-14, Ncd, however, can then rearrange the microtubules into a functional monastral bipolar spindle, in which one pole is nucleated at the collapsed centrosomes and the other acentrosomal (Goshima and Vale, 2003).

1.4.4. The phylogenetic distribution of kinesins

Number and variety of kinesins vary greatly among eukaryotes. *S. cerevisiae* has six kinesins from five families (Hildebrandt and Hoyt, 2000), while the human genome encodes 45 kinesins (Hirokawa et al., 2009) and *Arabidopsis* has 61 kinesins (Lee and Liu, 2004; Reddy and Day, 2001), likely compensating for a lack of dyneins (Lawrence et al., 2001). Analysis of the distribution of kinesins across eukaryotes has allowed for some insight to be gained into the evolutionary history of kinesins and the likely kinesin repertoire of LECA.

As part of their kinesin phylogeny and reclassification, Wickstead and Gull (2006) analysed the genomes of 19 eukaryotes, distributed throughout the eukaryotic groups. They showed that no kinesin family was found in every analysed organism, though most kinesin families were distributed throughout eukaryote groups. The newly defined kinesin-17 family, however, was absent from Unikonts. The most common kinesin families were kinesin-5, kinesin-13 and the kinesin-14A subfamily. A number of organisms also had genes encoding orphan kinesins, perhaps compensating for a lack of certain families. The smallest kinesin repertoire belonged to, the apicomplexan, *Theileria annulata*, which had two kinesins, belong to the kinesin-8 and -13 families. *Tetrahymena thermophile*, a chromalveolate, had the largest repertoire, with 77 kinesins, of which 54 could be grouped into families and 23 were ungrouped. The kinesin repertoires containing the most families were those belonging to humans, with 13, and *T. thermophile*, with 12. This analysis of kinesin distribution also revealed that a large number of lineage specific losses of families had occurred, including the loss of the kinesin-14 from the Apicomplexa.

Later work analysed the distribution of kinesin families across the 1624 kinesins of 45 diverse eukaryotes (Wickstead et al., 2010b). As well as the 14 families identified previously, this work identified three additional families, kinesin-18, -19 and -20. 14 additional paralogue groups were also identified, X1-X14, which were not deemed families due to small membership or they belonged to a single eukaryote group. Subfamilies and X groups constituted a total of 51 paralogue groups. The fact that kinesins could be subdivided into 51 paralogue groups, distributed across eukaryote groups, suggested a complex evolutionary diversification of kinesins. It is likely that the majority of these groups were generated by gene duplication events and predated the emergence of the eukaryotic groups. Mapping of paralogue groups to alternative evolutionary trees suggested that LECA likely had a kinesin repertoire containing 11 kinesin families. The kinesin families likely present in LECA were kinesin-1, -2, -3, -4/10, -5, -8, -13, -14, -17 and the kinesin-9A and B subfamilies.

1.4.5. Kinesins in trypanosomes

T. brucei encodes 47 kinesin-like proteins in its genome (Berriman et al., 2005). This includes one kinesin-1, two kinesin-2, one kinesin-3, two kinesin-9, two kinesin-4/10 (neither can be defined as kinesin-4), seven kinesin-13, two kinesin-14, two kinesin-15, three kinesin-16 and one kinesin-17 (Wickstead and Gull, 2006). The *T. brucei* genome also codes for two members of the additional kinesin-19 family defined by Wickstead et al., (2010b) and 16 members of the X paralogue groups, including 13 members of the kinetoplastid-specific X1 and X2 groups. Finally, 6 kinesins are ungrouped. Notable by their absence are the kinesin -4, -5, -6, -7 and -8 families, which all perform important roles in mitosis.

Some work has been performed on the kinesins of *T. brucei*, though little on mitotic kinesins. Kinesins involved in the flagellum and subpellicular array have received some attention. Like in other eukaryotes, the two kinesin-9 proteins of *T. brucei*, one kinesin-9A and one kinesin-9B, function in the flagellum (Demonchy et al., 2009). The kinesin-9A localises to the axoneme of the flagellum and its depletion results in some alteration of motility, but produces no structural changes and does not affect cell viability. The kinesin-9B localises to the basal body and axoneme and is essential for PFR assembly. Its depletion inhibits population growth and cause abnormal flagellar morphology. One of the seven kinesin-13 proteins expressed by *T. brucei*, KIN13-2, localises to the tip of the flagellum, where it is believed to function in flagellar length control (Chan and Ersfeld, 2010; Wickstead et al., 2010a). Deletion of the gene and its overexpression have no significant effect on flagellar length, though knock outs do have longer new flagella during cell division (Chan and Ersfeld, 2010). Overexpression of a homologue in *Leishmania major* results in a significant reduction in flagellar length (Blaineau et al., 2007). In addtition, an X1 group kinesin, Tb927.10.15390 (FAZ7), has been localised to the FAZ, but its function is unknown (Sunter et al., 2015).

Two kinesin proteins have been found to cooperate in regulation of the subpellicular corset of microtubules, forming a complex to do so. They are known

as KIN-C, a X1 group kinesin, and KIN-D, which is ungrouped, and localise to the posterior of the subpellicular microtubule array and throughout it, respectively. Knockdown of KIN-C or KIN-D in PCF cells results in a disorganised subpellicular array (H. Hu et al., 2012; L. Hu et al., 2012; Wei et al., 2013). Knockdown of either kinesin in BSF cells, however, did not disrupt the arrangement of the subpellicular microtubules, but did result in the presence of multinucleated cells, suggesting cytokinesis defects, with flagellar placement defects and enlarged FPs (Wei et al., 2013).

A small number of kinesins have been implicated in mitotis in *T. brucei*. As previously discussed, two kinesin-like proteins, KIN-A and KIN-B, function as part of the CPC with TbAUK1 and CPC1 and 2 (Li et al., 2008a, 2008b). KIN-A belongs to the X9 paralogue group, while KIN-B is not a true kinesin, as it has a divergent and non-functional motor domain (Wickstead et al., 2010b; Wickstead and Gull, 2006). Depletion of these proteins results in defects in the localisation of the CPC and prevents spindle assembly, resulting in failed chromosome segregation and cytokinesis (Li et al., 2008a, 2008b). KIN-C knockdown also results in cytokinesis defects and prevents the trypanosome CPC from translocating from the central spindle to the cleavage furrow, during cytokinesis (L. Hu et al., 2012). This suggests a late mitotic role for KIN-C. One of the seven kinesin-13 proteins present in *T. brucei*, KIN13-1, localises to the mitotic spindle (Chan et al., 2010; Wickstead et al., 2010a). Depletion of KIN13-1 results in extended spindles and chromosome segregation defects, suggesting roles for KIN13-1 in spindle microtubule length regulation and error correction, as well as spindle disassembly defects. This suggests that this kinesin plays a similar role in mitosis to kinesin-13 proteins form other organisms. An X13 group kinesin, referred to has Kinesin^{CaaX}, localises in the proximity of nuclei and kinetoplasts and has been implicated in nuclear and kinetoplast segregation though its function is unknown (Engelson et al., 2011). Interestingly, Kinesin^{CaaX} is farnesylated, a post-transcriptional modification that functions in the mediation of protein-protein or protein-membrane interactions (Novelli and D'Apice, 2012). One other publication has studied a kinesin-14 protein, TbKIFC1 (Dutoya et al., 2001). This protein does not

fall into the kinesin-14A subfamily (Wickstead and Gull, 2006), which contains mitotic kinesins, however, and instead has been implicated in proper acidocalcisome function, calcium rich organelles that may function in osmoregulation in trypanosomes (Rohloff et al., 2004).

Of the 47 kinesins in *T. brucei*, few have been studied and the roles they play remain largely unknown. The lack of important conserved mitotic kinesins in the *T. brucei* and the lack of knowledge regarding mitotic kinesins in *T. brucei* renders the mechanisms by which trypanosomes segregate their trypanosomes mysterious. A large-scale screen of trypanosome kinesins would greatly aid in improving knowledge of their roles and could identify mitotic kinesins for further investigation.

1.5. Trypanosomatid genetic modification technology

Given their divergence from traditional model systems, study of trypanosomatids should provide insight into variation in eukaryote biology. Manipulation of an organism's genetics is a powerful tool in the investigation of its biology. *T. brucei* has emerged as the most genetically tractable trypanosomatid and is often used as a model of these organisms and of kinetoplastids. The range of techniques available to modify the genetics of *T. brucei* and other trypanosomatids is described here.

1.5.1. Established selection markers used for experimentation in trypanosomatids

There are a number of drug resistance markers that can be used in trypanosomes, which has allowed for the development of various genetic techniques. Markers used in *T. brucei* are summarised in Table 3. Four positive selection markers can be used in modifications of *T. brucei*, *T. cruzi* and *Leishmania*: the neomycin (*NEO*) (Cruz and Beverley, 1990; Kelly et al., 1992; ten Asbroek et al., 1990), hygromycin (*HYG*) (Cruz et al., 1991; Lee and van der Ploeg, 1991; Otsu et al., 1995), bleomycin (*BLE*) (Freedman and Beverley, 1993; Jefferies et al., 1993; Taylor et al., 2011), and puromycin (*PUR*) (Freedman and Beverley, 1993; Lorenz et al., 1998; Taylor et al., 2011) selection markers. Nourseothricin (*SAT*) (Joshi et al., 1995; Ruepp et al., 1997) and blasticidin S (BSD) (Brooks et al., 2000) resistance markers can also be used in *T. brucei* and *Leishmania*.

Unlike the previously described markers, Herpes Simplex Virus Thymidine Kinase (HSV-TK) is a negative selection marker. When expressed, it induces sensitivity to acyclovir, a nucleoside analogue, and its derivatives, such as ganciclovir. These analogues are phosphorylated by HSV-TK, producing the monophosphate form, and is subsequently phosphorylated by cellular kinases, to produce the triphosphate form, which inhibits DNA polymerases and causes the cessation of chain elongation. The *HSV-TK* gene has been used to generate ganciclovir sensitivity in mammalian (Mansour et al., 1988) and plant (Czakó and

Márton, 1994) model systems and in, the trypanosomatids, *T. brucei* (Valdés et al., 1996) and *Leishmania* (LeBowitz et al., 1992).

In *T. brucei*, the *URA3* (or *PYR6-5*) gene can also been used as a both a positive and negative selection marker (Scahill et al., 2008), but it differs from the previous markers in that it naturally occurs in the genome. *URA3* codes for orotidine 5'-phosphate decarboxylase (ODCase), an enzyme involved in the pyrimidine ribonucleotide synthesis pathway. Cells carrying the gene are sensitive to fluoroorotic acid (FOA), which produces a toxic metabolite when processed by ODCase. FOA can, therefore, be used to select for replacement of *URA3*. Mutants containing knockouts of both *URA3* and *FUR1*, which codes for an enzyme involved in an alternative pyrimidine ribonucleotide synthesis pathway, require uracil for growth. Including *URA3* in genetic modification of these cells allows for selection of modified cells via absence of uracil. These techniques were developed for use in yeast cells (Pronk, 2002) and have since been modified for use in bacteria (Galvao and de Lorenzo, 2005). Experiments in *T. brucei* have used replacement of *URA3* by a cassette containing a fusion of *HYG* and *HSV-TK* and selection by FOA or ganciclovir to measure rates of gene conversion (Kim and Cross, 2010; Povelones et al., 2012).

Selection Marker	Selection Drug	Drug Target	Mode Of Resistance	Concentrations (μg ml^{-1})	
				BSF	PCF
Neomycin phosphotransferase (NEO)	G418	Ribosomes	Enzymatic inactivation	1-3	15
Hygromycin phosphotransferase (HYG)	Hygromycin	Ribosome translocation	Enzymatic inactivation	4-5	25-50
Bleomycin resistance protein (BLE)	Phleomycin	DNA (creates breaks)	Sequestration	1-2.5	2.5
Puromycin acetyltransferase (PUR)	Puromycin	Ribosomes	Enzymatic inactivation	0.1	1
Streptothricin acetyltransferase (SAT)	Nourseothricin	Ribosomes	Enzymatic inactivation	25	100
Blasticidin S deaminase (BSD)	Blasticidin S	Ribosomes	Enzymatic inactivation	5	10
Herpes simplex virus thymidine kinase (HSV-TK) – negative selection	Ganciclovir	DNA (inhibits replication)	-	5-30	2.5-25
URA3 (PYR6-5) – negative or positive selection	Fluoroorotic acid (FOA)	Pyrimidine ribonucleotide synthesis	-	6	

Table 3. Selection markers available for use in *T. brucei*. Adapted from Clayton (1999) and Cross (2008) with information from Valdés et al. (1996).

1.5.2. The use of episomal constructs for genetic manipulation

Early transformation efforts in trypanosomatids resulted in transient expression of genes from extrachromosomal, episomal sequences. Transient expression of the bacterial chloramphenicol acetyltransferase gene in a number of *Leishmania* species was achieved by generating a construct containing the gene flanked by sequences derived from α-tubulin coding sequences and introducing it into cells by electroporation (Laban and Wirth, 1989). Electroporation of episomal vectors was also used to transiently express chloramphenicol acetyltransferase and a procyclin protein in *T. brucei* and showed that promoters were required to drive their expression (Clayton et al., 1990; Rudenko et al., 1990; Zomerdijk et al., 1990). Transient expression of chloramphenicol acetyltransferase from an episome was soon after achieved in *T. cruzi* (Lu and Buck, 1991).

The first stable transformations of trypanosomatids utilised episomes in *Leishmania*, by introducing plasmids encoding *NEO* flanked by sequences from the dihydrofolate reductase-thymidylate synthase (*dhfr-ts*) coding sequence (Kapler et al., 1990) or α-tubulin genes (Laban et al., 1990). These plasmids were replicated in multiple extrachromosomal copies, frequently forming large circular episomes containing head-to-tail repeats. Later research showed that defined leishmanial origins of replication were not required for maintenance of episomes, episomal gene transcription did not require the presence of defined promoters (Curotto de Lafaille et al., 1992) and that plasmids could be transiently maintained as episomes while lacking sequences derived from *Leishmania* (Papadopoulou et al., 1994). Stable transformation of *T. cruzi* was achieved by introducing a plasmid containing *NEO* flanked by sequences from upstream and downstream of genes coding for GAPDH. This resulted in cells that carried large episomes, containing tandem repeats of the plasmid sequence (Kelly et al., 1992). The generation of stable, single-copy episomes was later achieved in *T. brucei* by introducing plasmids, referred to as pT13-11, containing the *NEO* and a procyclin coding sequence with a procyclin promoter and downstream region. These plasmids were replicated and maintained in PCF cells. A variant, pT11-bs, in which

the procyclin downstream sequences was replaced by a sequence from downstream of the aldolase coding sequence was replicated in BSF cells, but was unstable (Patnaik et al., 1993).

The main use of episomes has been in the complementation of gene knockouts, but they can also be used to determine the minimum requirements for maintenance of DNA elements, as has been described above. In a further example, Espinal et al. (2007) identified a 10bp sequence, from the GPEET promoter, that allowed them to produce a stable episome in PCF cells. Episomes have also been adapted to form artificial chromosomes. The production of stable artificial chromosomes in *T. brucei* essentially involved the linearization of pT13-11 and the addition of telomeric sequences (Lee et al., 1995; Patnaik et al., 1996). An artificial chromosome has also been produced in *Leishmania major* by generating and linearising a plasmid containing *NEO* followed by the sequence downstream of *dhfr-ts* and telomeric sequences with 30kb of random genomic DNA (Casagrande et al., 2005). The production of this chromosome also allowed the researchers to identify a sequence that increased its stability. Another artificial chromosome has also been produced for stable protein expression in *Leishmania tarentolae* (Kushnir et al., 2011). While episomes and artificial chromosomes have their uses, better methods, involving direct modification of genomes, exist for inheritable expression of genes.

1.5.3. Direct modification of trypanosomatid genomes

Methods for modification or disruption of trypanosomatid genomes are important tools to investigate their biology. The introduction of transposons can be performed to randomly disrupt trypanosomatid genomes (reviewed in Damasceno et al., 2010) and specific regions can be modified as well. In 1990, Cruz and Beverley demonstrated homologous gene targeting in *L. major*, showing that *dhfr-ts* could be stably replaced by *NEO*, by introducing a linear construct containing the selection marker flanked by sequences from upstream and downstream of the target gene. At the same time, ten Asbroek et al. (1990) demonstrated insertion of *NEO* into the tubulin array in PCF *T. brucei* using a similar method. These methods take advantage of homologous recombination, which is used by cells to repair double strand breaks that often occur during DNA replication. In dividing cells, linearised constructs containing endogenous sequence, introduced by electroporation, are treated as broken DNA strands and incorporated into the targeted region of the genome. Homologous gene targeting was later shown to be effective in BSF *T. brucei* (Carruthers et al., 1993) and in *T. cruzi* (Hariharan et al., 1993; Otsu et al., 1993). Analysis of recombination in *T. brucei* has demonstrated that the length of the homologous regions and the number of mismatches they contain both influence the efficiency of recombination (Barnes and McCulloch, 2007; Bell and McCulloch, 2003)

In the previous examples, homologous gene targeting was used to replace genes, knocking them out, but it can also be used for endogenous locus tagging (S. Kelly et al., 2007). This involves introducing constructs that are designed in such a way that a sequence coding for a fluorescent protein or epitope tag is inserted adjacent to the target protein coding sequence, so that a labelled protein is produced at endogenous levels. This allows for localisation of proteins in cells for their purification. Use of such techniques is an important step in determining a protein's function and endogenous locus tagging has become a standard technique.

In an adaptation of homologous gene targeting techniques, a gene knockout system using the Cre recombinase and loxP DNA sequences has also been developed in *T. brucei* (Kim et al., 2013; Scahill et al., 2008), so that selection markers can be reused. In this system the targeted gene loci are replaced by a cassettes containing a positive selection marker and *HSV-TK*, flanked by loxP sequences. The Cre recombinase is then expressed in these cells, which recombines loxP sites, deleting the selection markers. Recombination can then be selected for with ganciclovir. This system relies on inducible expression of the Cre recombinase so that it can be expressed at the correct time.

1.5.4. Tetracycline inducible systems

The development of stable homologues gene replacement permitted the later development of inducible expression systems, allowing for controlled expression of proteins. The first of these systems was developed in *T. brucei* by Wirtz and Clayton (1995) for mutational analysis of genes and expression of toxic gene products. A sequence coding for the Tet repressor from *E. coli* was introduced at the tubulin locus and the expressed protein used to control a procyclin promoter in close proximity to a Tet operator. Tetracycline could then be used to activate the promoter. Later work demonstrated that integration of genes, under the control of a T7 promoter, and the coding sequence for T7 RNA polymerase resulted in protein expression at levels greater than endogenous proteins. The T7 promoter could also be regulated by the Tet operator and Tet repressor (Wirtz et al., 1998). Modification of this system resulted in tighter regulation of the promoter and less variability between clones (Wirtz et al., 1999). Further modification streamlined it, so that T7 RNA polymerase and the Tet repressor were expressed from a single construct (Poon et al., 2012). The ribosomal DNA (rDNA) promoter has also been adapted for use in tetracycline inducible gene expression (Alsford et al., 2005). T7 and rDNA promoters have also been used in inducible expression systems in *Leishmania* (Kushnir et al., 2005; Yan et al., 2001; Yao et al., 2007) and in *T. cruzi* (Taylor and Kelly, 2006).

1.5.5. RNA interference

RNA interference (RNAi) was first described by Fire et al. (1998), who demonstrated downregulation of gene expression upon introduction of dsRNA into cells. Before this discovery regulatory antisense RNAs were known to exist in *C. elegans*, suggesting noncoding RNAs may be involved in gene regulation (Lee et al., 1993; Wightman et al., 1993). There are three known pathways in which model animal cells use RNA to regulate gene expression, based on three types of RNA molecule; microRNA (miRNA), small interfering RNA (siRNA) and Piwi-interacting RNA (piRNA) (reviewed in Ipsaro and Joshua-Tor, 2015; Wilson and Doudna, 2013). piRNAs are involved in transcriptional gene silencing, whereas miRNAs and siRNAs molecules are involved in post-transcriptional gene silencing (PTGS). Experimental RNAi takes advantage of siRNA based PTGS mechanisms, to silence protein expression. In this pathway, the Dicer protein cleaves dsRNA into ~20bp fragments, to produce siRNA molecules. Single strands of siRNA then interact with the Argonaute protein to form a RNA-induced silencing complex (RISC). RNA sequences guide the RISC to a complementary mRNA sequence, which it cleaves. siRNAs can also interact with the RNA-induced initiation of transcriptional gene silencing (RITS) complex, directing it complementary genomic DNA sequences, where it induces modification of histones, resulting in downregulated transcription (Verdel et al., 2004; Volpe and Martienssen, 2011).

RNAi is a useful tool for depleting target proteins and is advantageous over gene knockouts, because it ignores ploidy by targeting transcripts and it can be induced or timed, so that functions of essential proteins can be investigated. RNAi does not completely deplete proteins, however, unlike double knockouts. Early attempts at experimental RNAi involved introducing dsRNA into cells or integration of constructs into genomes that transcribed dsRNA (Sharp, 1999). These approaches did, however, produce cytotoxic effects in mammalian cells (Hunter et al., 1975). These effects were avoided by the later development of synthetic siRNA sequences, which could be used to produce strong and specific knockdown of proteins (Elbashir et al., 2001). siRNAs are introduced into cells by transfection with electroporation, viruses or lipids, resulting in transient effects.

To overcome the issue of transience short hairpin RNA (shRNA), which can be expressed from integrated constructs, was developed (Brummelkamp et al., 2002; Paddison et al., 2002). shRNAs are short RNA sequences that form hairpins that act like siRNAs.

RNAi became established in *T. brucei* after it was discovered that dsRNA could mediate protein knockdown (Ngô et al., 1998). Afterwards constructs were generated that produced dsRNA from two opposing inducible promoters, allowing for heritable and inducible RNAi (Alibu et al., 2005; Bastin et al., 2000; LaCount et al., 2000; Shi et al., 2000; Wang et al., 2000). This head-to-head approach and another, involving the production of dsRNA by transcription of hairpin RNA sequences, have become the established methodology for experimental RNAi in *T. brucei* (Tschudi et al., 2003). Hairpins are often used to increase RNAi efficiency, although there is no direct evidence that this is the case in *T. brucei*. It has been demonstrated in yeast, however, that hairpin constructs can have a stronger knockdown effect than head-to-head constructs (Drinnenberg et al., 2009).

T. brucei is the only pathogenic trypanosome in which RNAi is a well-established practice, which contributes greatly to its increased tractability over other trypanosomes. Strains of *T. cruzi* are unresponsive to dsRNA (DaRocha et al., 2004) and both dsRNA and siRNA have no effect on *L. major* and *donovani* (Robinson and Beverley, 2003). A system for generation of dsRNA using inducible T7 promoters has, however, been shown to knockdown proteins in *Trypanosoma congolense*, another African trypanosome (Inoue et al., 2002). More recent work has shown that, although *Leishmania tarentolae*, *mexicana*, *major* and *donovani* lack RNAi pathways, *Leishmania braziliensis* and other members of the *Viannia* subgenus (e.g. *L. guyanensis* and *L. panamensis*) do have functional RNAi pathways (Lye et al., 2010). Successful systems for production of dsRNA and knockdown of proteins have since been demonstrated in *L. braziliensis* (Atayde et al., 2012).

1.5.6. Recent advances in CRISPR technologies in trypanosomes

In recent years the use of clustered regularly interspaced short palindromic repeats (CRISPR) DNA sequences and Cas (CRISPR associated) proteins has emerged as a genome editing technology and been applied in some species of trypanosomatid. CRISPR/Cas systems are used by prokaryotes as adaptable immune mechanisms to defend themselves from foreign nucleic acids, such as viruses and plasmids. Similarly to RNAi, Cas proteins recognise long RNA precursors that are processed into ~40 nucleotide CRISPR RNA (crRNA) sequences and guide the protein to target nucleic acids, which it cleaves (reviewed in Fineran and Charpentier, 2012; Wiedenheft et al., 2012).

In 2012, it was demonstrated that engineered guide RNA (gRNA) sequences, consisting of modified crRNA, could direct the Cas9 protein from *Streptococcus pyogenes* to sequences of interest *in vitro*, creating double strand breaks, and, therefore, had potential as a targeted genome editing tool (Jinek et al., 2012). Cas9 has since been adapted for targeting of endogenous genes and for inducible genome editing in a wide range of organisms (for review, see Sander and Joung, 2014). Work in human cells also showed that an inactivated Cas9 protein tagged with a fluorescent protein could be used to fluorescently label DNA elements (Chen et al., 2013).

CRISPR/Cas systems have also begun to be employed in trypanosome cells. The first example of CRISPR/Cas in trypanosomes involved *T. cruzi* (Peng et al., 2015). Cas9 was expressed from coding sequences integrated into the genome and gRNA sequences later introduced into cells. Later work integrated Cas9 and gRNA coding sequences into the genome (Lander et al., 2015). Around the same time CRISPR/Cas was also shown to be an effective genome editing tool in *L. donavani* (Zhang and Matlashewski, 2015). CRISPR/Cas has yet to see use in *T. brucei*, as RNAi can be used for inducible modification, unlike *T. cruzi* and *Leishmania*. One can foresee a use for the system, however, as a tool for inducible knockout of unexpressed repeat regions, such centromeric repeats or the 177bp repeats of MCs and ICs, as this cannot be achieved using RNAi.

1.5.7. Genome wide genetic modification

Development of RNAi in *T. brucei* as a research tool allowed for the later development of genome-wide screens and systematic studies of gene function. These studies are only possible in *T. brucei*, as experimental RNAi is well-established in this organism. The first such study was performed by Morris et al. (2002), who performed a genome-wide RNAi screen to identify genes involved in glycosylation of procyclin proteins or their expression. An RNAi library was produced by sonicating genomic DNA and introducing the resulting fragments into a head-to-head RNAi constructs. These plasmids were transfected into PCF trypanosome cells generating enough clones to produce ~5× coverage of the genome. Selection of cells lacking glycosylated surfaces, after induction of RNAi, identified a cell line in which a hexokinase gene had been silenced, showing that glycolysis is necessary for the glycosylation of procyclin surface proteins.

Later, Subramaniam et al. (2006) used a RNAi library approach in the first systematic analysis of gene function. 210 of the chromosome 1's 369 genes were knocked down and cells tested for a variety of phenotypes. Knockdown of over 30% of these genes produced a phenotype. RNAi against ~12% of genes was lethal, while an additional 11% produced non-lethal growth defects. The work also demonstrated that essential genes showed no clustering and that they were not widely evolutionarily conserved.

Further genome-wide RNAi screens were performed by Schumann Burkard et al. (2011) and Baker et al. (2011), to identify the mechanisms of action of trypanocidal drugs. Schumann Burkard et al. (2011) performed RNAi using a genome-wide library and selected for cells resistant to melarsoprol or eflornithine. This led to the identification of an adenosine transporter, TbAT1, which is known to be involved in melarsoprol uptake, and an amino acid transporter, AAT6, whose knock down resulted in resistance to eflornithine. Baker et al. (2011) performed similar analyses to research the mechanisms of action of nifurtimox and eflornithine. They also identified AAT6 silencing in

eflornithine resistant cells and found that cells resistant to nifurtimox silenced the nitroreductase enzyme.

The development of next generation sequencing (NGS) techniques has opened up new avenues of research in trypanosomes. For example, NGS can be used for sequencing and analysis of transcriptomes using RNA sequencing (RNA-seq) (reviewed in Kukurba and Montgomery, 2015; Wang et al., 2009). RNA-seq has been used in a number of analyses of trypanosome transcriptomes, including comparisons of transcriptomes between life cycle stages (reviewed in Mani et al., 2012; Siegel et al., 2011). NGS has also been used in analysis of variance in genetics between isolates (for example Downing et al., 2011; Goodhead et al., 2013)

In 2011, a paper describing a technique, for genome-wide analysis of individual gene contributions to fitness, called RNAi target sequencing (RIT-Seq) was published (Alsford et al., 2011). This technique applied NGS to genome-wide RNAi screens. Like previous studies, a RNAi library, containing ~7,500 of the ~10,000 genes in the *T. brucei* genome, was produced by inserting fragments of genomic DNA into RNAi constructs and then integrating constructs into *T. brucei* cells. The resulting population was used in what was essentially a competition assay. This approach involved splitting the population and inducing RNAi or leaving cells uninduced. Genomic DNA was then extracted from induced and uninduced populations and PCR performed to amplify the genomic fragments within RNAi constructs, which were then sequenced with NGS technology. Reads produced by this sequencing were mapped to the genome and the change in the of number of reads per gene, between uninduced and induced cells, used to determine the influence of individual genes on fitness. A reduction in reads representing a certain gene in induced cells, for example, would suggest that RNAi against that gene had reduced cell growth. Significant changes in read number were then used to determine which genes had important roles in trypanosome survival. RIT-Seq was performed in both PCF and BSF cells and in cells differentiating from BSF to PCF. This approach demonstrated that many genes were important for cell survival, including genes coding for proteins

involved in transcription, translation and post-transcriptional regulation and proteins important in flagellar function. It also highlighted genes important to differentiation, including those coding for flagellar proteins, glycolytic proteins and proteins involved in carboxylic acid metabolism and phosphorylation.

A later adaptation of RIT-Seq was used to investigate the contribution of genes to trypanocidal drug sensitivity (Alsford et al., 2012). In this study cells were treated with the drugs eflornithine, suramin, nifurtimox, penatamidine or melarsoprol, after RNAi had been induced. Genomic fragments within RNAi constructs carried by surviving cells were then sequenced by NGS and the resulting reads mapped to the genome. This analysis showed that only AAT6 had been knocked down in eflornithine resistant cells and that knockdown of a number of genes could lead to resistance to the other drugs.

Many aspects of the biology of kinetoplastids remain mysterious. Genome-wide and systematic RNAi screens have proved to be revolutionary tools for probing the biology of many eukaryotes, including trypanosomes, and can be adapted for different purposes. Elaborating and applying such RNAi screens to the investigation of chromosome segregation in trypanosomes should greatly aid in deciphering the process.

2. Aims

Mitosis in animal and yeast model organisms is relatively well understood, as are the roles kinesin motor proteins perform in the process, but they represent a small proportion of the eukaryote domain. *Trypanosoma brucei* is highly divergent from these models and comparatively little is known about how they carry out mitosis. It is known, however, that they perform a mitosis that differs from the canonical process and lack a number of key mitotic kinesins. In work presented in this thesis, I aimed to develop a number of methods, elaborating on previously established techniques, that could be used to investigate trypanosome mitosis, focussing on the mitotic functions of kinesins.

3. Materials and Methods

3.1. Combinatorial library production

3.1.1. Microtubule motor coding sequence PCR

In order to produce DNA for use in the library, PCR was performed. Primers were designed to individually amplify 47 kinesin and 3 cytoplasmic dynein heavy chain coding sequences from TREU927 genomic DNA (Electronic Appendix). If a motor's coding sequence was greater than 3kb, primers were designed to produce 2.5 to 3kb from the 5' end, otherwise the whole sequence was amplified. The amount of DNA produced was determined by spectrophotometry.

3.1.2. Plasmid library production

400ng of each kinesin and dynein coding sequence was mixed in a final solution of 700µl of 1x SSC (150mM NaCl, 15mM sodium citrate pH7.0). The mix was sonicated with a Sonopuls HD2070 ultrasonic homogeniser (Bandelin Electronics) to fragment the DNA, using 30% intensity for 50% of the 5 min pulse time. Isopropanol precipitation was used to concentrate the sonicated DNA, which was then size selected by gel extraction for fragments between 200 and 300bp in size. 3µg of the selected fragments was end-polished and phosphorylated using a NEBNext End Repair Module (NEB). This was followed by blunt-end ligation of linkers. Primers were annealed to produce the "AvrII linker" (TCCTAGGTGCTCGGATTACA and AATGTAATCCGAGCACCTAGGA), the "Sfi vectorette linker" (AGGTAGTCTCCCTTCTCGAATCGTAACCGTTCGGCCAGTGAGGCCT and AGGCCTCACTGGCCTGCAGCCAAGGTATGGAGAAGGGAGAG) and the "Sfi long linker" (ACGACGTGACCACTCTGACGGCCAGTGAGGCCT and AGGCCTCACTGGCCGTCAGAGTGGTCACGTCGTGTACA). 125pmol of the Sfi long linker or 100pmol of the Sfi vectorette linker with 25pmol of the AvrII linker were ligated onto 750ng of library fragments, with 6 units of ligase, at 4°C overnight. The product of this ligation was then size selected to remove any linkers not attached to the ~250bp fragments.

Library fragments were amplified by PCR. Those fragments with Sfi long linkers only, which would go on to form a library of single fragments, or “singles” library, were amplified with a primer complementary to the region within their linkers (CCATACCTTGGCTGCAGG). Fragments with both Sfi vectorette linkers and AvrII linkers, which would go on to form a combinatorial library, or “doubles” library, were amplified using a vectorette PCR methodology, to ensure fragments carried two different linkers. PCR was performed using a primer complementary to a site in the AvrII linker (TGTAATCCGAGCACCTAGGA) and another (CTTCTCGAATCGTAACCGTTC) complementary to the region produced from an incompatible region in the Sfi vectorette linker, after amplification by the first primer. Amplified doubles library product was cut with AvrII, ligated at 15°C for 2 hours and size selected again.

Both singles library fragments and doubles library fragments were then cut with SfiI. 100ng of doubles library fragments was ligated into 400ng of SfiI cut p2T7-177γ, while 100ng of singles library fragments was ligated into 400ng of p2T7-177δ. These plasmids differ from p2T7-177 (Wickstead et al., 2002) in the restriction endonuclease sites present in the multiple cloning site. Ligations were performed for 6 hours at 15°C and inactivated at 30°C for 15 min. Half of the ligations were then made up to 20µl and desalted against 1% agarose/50mM glucose. The recovered DNA was transfected into 100µl high-competency (1-3×10^9cfu/µg) NEB10β *E. coli* cells (NEB) by electroporation with an Eporator (Eppendorf), using a 20kV cm^{-1} voltage gradient. After recovery, cells were transferred to 200ml LB and plasmids purified using a HiSpeed Plasmid Midi Kit (Qiagen), after overnight growth.

3.1.3. Plasmid library analysis

To sequence fragments within the plasmid library by next generation sequencing, fragments were amplified from the singles and doubles libraries using primers CCGGCCGCTCTAGAACTA and CCTCGAGGTCGACGGTAT. 100ng of plasmid template was amplified in 10 cycles of PCR using a 55°C annealing temperature. A second PCR reaction was the performed to add sequencing

adapters to the amplified fragments. PCR was again performed for 10 cycles but with a 62°C annealing temperature. The sequences of primers used for the singles library were AATGATACGGCGACCACCGAGATCTACACCCGGCCGCTCTAGAACTAGG and CAAGCAGAAGACGGCATACGAGATATTGGCCGGTATCGATAAGCTTGGCCTGTGA, while the sequences of those used for the doubles library were AATGATACGGCGACCACCGAGATCTACACAGAACTAGTGGATCCGGCCAGTGA and CAAGCAGAAGACGGCATACGAGATTACAAGCGGTATCGATAAGCTTGGCCTGTGA. The products of these reactions were mixed 9:1, doubles to singles, and sent for sequencing.

Library fragments were sequenced using a MiSeq sequencer (Illumina), using version 3 chemistry and producing 75bp paired end reads. Primers were CCGGCCGCTCTAGAACTAGGA and AGAACTAGTGGATCCGGCCAGTGAGGC, for the forward reads, and CGGTATCGATAAGCTTGGCCTGTGAGGC, for the reverse reads. Index reads were produced with GCCTCACAGGCCAAGCTTATCGATACCG.

The first two bases of reads returned by next generation sequencing, which were from plasmids, were trimmed off and a quality trim was then performed using Sickle (v1.33, paired-end mode with minimum trimmed length of 20 bases and quality threshold of 20 [pe -q 20 -l 20]; Joshi and Fass, 2011). Unpaired reads were mapped to kinesin and dynein coding sequences using Bowtie 2 (Langmead and Salzberg, 2012). A custom script was then used to re-establish links between reads, “re-pairing” them. A subset of these paired reads (every 50th pair) was extracted for analysis in R (R Core Team, 2016). R and the gplots library (Warnes et al., 2016) were used to produce histograms of fragment length, representations of the mapping of fragments to genes and heat maps of frequency of gene combinations in the library.

3.2. Production of plasmids

Unless otherwise stated, all ligations described here were cloned into XL1-Blue *E. coli* cells by heat-shock. These cells were then grown at 37°C.

3.2.1. For the knockdown of kinesin-2 proteins by RNAi

Primers were designed to amplify a ~250bp sequence from the 3' end of the *KIN2A* (Tb11.02.0400) or *KIN2B* (Tb927.5.2090) coding sequences, adding 5' end BamHI and HindIII restriction endonuclease sites and a 3' end XbaI site (TTTGGATCCAAGCTTCCTCGAATCACGTCGC and CTCTAGATTCCTCTTCGAGTGCTGTC and TTTGGATCCAAGCTTACGAGGTCGCCAAGAC and CTCTAGAGCGCCTTGACTTCCTCTT, respectively). *KIN2* fragments were amplified from genomic DNA of the TREU927 strain. Constructs for knock down of individual kinesins by RNA interference (RNAi) were produced by digesting the kinesin-2 fragments with XbaI and HindIII. They were then ligated into the p2T7β plasmid, which had been cut with SpeI and HindIII. The p2T7β plasmid is a modified form of p2T7 (Alibu et al., 2005), containing two SfiI sites in its multiple cloning site. This produced the p2T7β-KIN2A and p2T7β-KIN2B plasmids. Constructs for knockdown of both KIN2 proteins were produced by digesting the *KIN2A* fragment with XbaI and BamHI and the *KIN2B* fragment with XbaI and HindIII. A three-way ligation was then performed to insert the fragments into p2T7β, digested with BamHI and HindIII, producing the p2T7β-KIN2A/B plasmid. Constructs for production of hairpin RNA sequences were produced in two ways. In the first, *KIN2B* fragments were cut with XbaI and BamHI or XbaI and HindIII. The two differently cut fragments were then three-way ligated into BamHI and HindIII cut p2T7β, to create p2T7β-KIN2B/B. In the second, primers were designed that would amplify the *KIN2A* fragment and add a 5' HindIII site and a 3' XhoI site (CCCAAGCTTAATACGAGCTCCTCAAGACA and CCCCCTCGAGTTCCTCTTCGAGTGCTGTC). These *KIN2A* fragments were then digested with XhoI and HindIII and were ligated into p2T7β-KIN2A, itself digested with XhoI and HindIII, forming p2T7β-KIN2A/A.

3.2.2. For the knockdown of other proteins

A plasmid designed for the knockdown of the KKT-interacting protein 1 (KKIP1), p2T7-177-KKIP1, was obtained from Simon D'Archivio. Another for knockdown of the kinesin KIN13-1 was produced from p2T7β. PCR was performed using primers designed to amplify a 431bp fragment from the 5' end of the KIN13-1 coding sequence, while adding SfiI sites to both the 5' and 3' end of the sequence (ATGGCCAGTGAGGCCTGCAGCACGAGCAGTA and ATGGCCAGTGAGGCCAGCACGAGCTCATCACA). PCR product and p2T7β were both cut with SfiI and ligated to produce p2T7β-KIN13-1.

3.2.3. For integration of *HSV-TK* chromosome labels

pMC-T7-HSVTKblast and pMC-rDNA-HSVTKblast were obtained from Simon D'Archivio. These plasmids encode a chimera consisting of *HSV-TK* and the blasticidin resistance marker (*BSD*), which is targeted to the 177bp repeat sequences. pMC-rDNA-HSVTKblast was modified to split the HSV-TK-BSD chimera, by inserting a *PFR2* (paraflagellar rod protein 2) intergenic sequence. Targeting sequences were also changed so that the construct would be directed to to bloodstream expression site 1 (BES1) or to replace the S8 variant surface glycoprotein (VSG) coding sequence. The S8 VSG targeting sequence was extracted from pS8-NeoB (see section 3.2.6.) by digesting with EcoRI and KpnI and ligating it into EcoRI and KpnI cut pMC-T7-HSVTK backbone, generating pS8-HSVTK. The *PFR2* intergenic sequence was amplified from pSiG-BG (courtesy of Dr Catarina Gadelha, University of Nottingham), using primers CCCGGATCCCCGCTGCGCTTAAATGTC and CCCAAGCTTGGTACCTGATGCTT. The pMC-rDNA-HSVTKblast plasmid was also amplified by PCR, with primers adding a HindIII site to the 5' end of *BSD* and maintaining a BamHI site at the 3' end of the HSV-TK coding sequence (CCCAAGCTTATGCCTTTGTCTCAAGAAGAATCC and TTTGGATCCTTAGTTAGCCTCCCCCATCT). The two PCR products were digested with BamHI and HindIII and ligated, producing pS8-HSVTK-PFR. To generate the pBES-HSVTK-PFR plasmid, pS8-HSVTK-PFR and pBES-NeoB (see section 3.2.6.)

were digested with NheI and SalI to remove targeting sequences. The BES1 targeting sequence was then ligated into the backbone from pS8-HSVTK-PFR.

3.2.4. For the creation of a KIN13-1-GFP mitotic spindle tag

To produce a plasmid for labelling of KIN13-1 with green fluorescent protein (GFP), the hygromycin resistance marker (*HYG*) was removed from the pEnG09 plasmid (Wickstead et al., 2010a). It was then replaced with a nourseothricin resistance marker (*SAT*), to produce pEnG09S. PCR was used to produce the plasmid backbone without *HYG* and adding NcoI and MfeI sites (CATCCATGGTAGAGTAGATGCCGACC and CATCAATTGCACTAGAGCTTATTTTATGG, respectively). *SAT* was amplified from pAG25 (Goldstein and McCusker, 1999), using primers that also added EcoRI and NcoI sites (TAGGAATTCATGGGTACCACTCTTGACG and CATCCATGGTTAGGGGCAGGGCATG). The two PCR products were digested with the relevant restriction endonucleases and the two products were ligated.

3.2.5. For the production of fluorescently labelled LacI

To produce Lac repressor protein (LacI) fusion proteins, a construct containing a LacI coding sequence and targeting sequences for replacement of *PUR* in the SmOx cells was synthesised (Integrated DNA Technologies) in a pUC57 backbone. It also contained a number of planned restriction endonuclease sites, for further plasmid synthesis (Figure 17). The construct was moved to pSPR0 (Daniels et al., 2012), by cutting both plasmids with EcoRI and SacI and ligating the LacI sequence into the pSPR0 backbone.

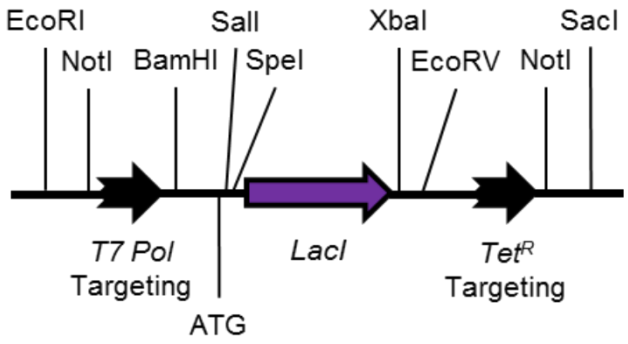


Figure 17. Diagram of synthesised LacI construct. Features are labelled underneath, while restriction endonuclease sites are labelled above. Not to scale.

Genes encoding the fluorescent proteins mStrawberry and yellow fluorescent protein (YFP) were extracted from pEnC0-mS-H and pEnC0-Y-H, respectively, by digesting with XhoI and XbaI and size selecting the relevant fragments. pSPR0-LacI was cut with SalI and SpeI and the fluorescent proteins were ligated into the backbone, to create the plasmids pSPR0-LacI-mSt and pSPR0-LacI–YFP, which were cloned into GM121 *E coli* cells, to avoid methylation of XbaI sites (see below).

To produce a sequence containing the *KIN13-1* intergenic region and *BSD*, pEnG09 and pEnG0B plasmids were cut with SacI and StuI. The backbone fragment from pEnG09 and the fragment containing *BSD* from pEnG0B were ligated, creating pEnG09B. pEnG09B was cut with XbaI and StuI and the pSPR0-LacI-mSt and pSPR0-LacI–YFP plasmids were cut with XbaI and EcoRV. The fragment containing *BSD* and the *KIN13-1* intergenic region, from pEnG09B, and the pSPR0-LacI-mStrawberry and pSPR0-LacI–YFP backbones were ligated. The *KIN13-1* intergenic region was used so that LacI proteins would be expressed at a level similar to KIN13-1. The resulting plasmids were called pLacI-mSt-Bla and pLacI-YFP-Bla.

La protein NLS

For insertion of the La protein nuclear localisation signal (NLS), amplification was performed using primers designed to add a SpeI site to the 5' end of the fluorescent protein coding sequence and a HindIII to the 3' end of the *PFR2* intergenic sequence (GACTCGAGACTAGTGTGAGCAAGGGCGAGGAG and CGAAGCTTGATGCTTTATTGCTTTCTCTTAAATTTG) in pLacI-mSt-Bla and pLacI-YFP-Bla. To generate the NLS, two primers were designed that generated a NLS sequence with HindIII and SpeI compatible ends when annealed (AGCTTATGCGTGGTCACAAGCGCTCTCGTGAGA and CTAGTCTCACGAGAGCGCTTGTGACCACGCATA). pLacI-mSt-Bla and pLacI-YFP-Bla PCR product was then cut with HindIII and SpeI and ligated with the NLS sequence, generating the pLacI-mSt-Bla-La and pLacI-YFP-Bla-La plasmids.

Alternative 3' UTR

To alter the 3' untranslated region (UTR) of the pLacI-mSt-Bla-NLS and pLacI-YFP-Bla-NLS plasmids, they were digested with XbaI and partially digested with SacI, due to the presence of two SacI sites. The *PFR1* intergenic sequence was cut from the pEnG22 plasmid and the *KIF9A* intergenic sequence was cut from the pEnG01 plasmid, using a XbaI and SacI digest. The products of these digests were ligated, producing the pLacI-mSt-Bla-La:*PFR1*, pLacI-YFP-Bla-La:*PFR1*, pLacI-mSt-Bla-La:*KIF9A* and pLacI-YFP-Bla-La:*KIF9A* plasmids.

Alternative NLS

The NLS in pLacI-YFP-Bla-La was altered by digesting the plasmid with HindIII and SpeI and inserting the simian vacuolating virus 40 (SV40) NLS, generated by annealing the primers AGCTTATGCCAAAAAAGAAGAGAAAGGTCA and CTAGTGACCTTTCTCTTCTTTTTTGGCATA. The NLS was changed to a sequence coding for the La protein NLS followed by the TY epitope and YFP by extracting the sequence from pEnT5H-NLSTY-YFP-RPA2Ser2 (Daniels et al., 2012) with HindIII and XbaI and inserting it into the pLacI-YFP-Bla-La backbone.

sfGFP-LacI

To produce plasmids encoding LacI N-terminally labelled with superfolder GFP (sfGFP), a coding sequence was cut from pSiG-HhsfG (courtesy of Dr Catarina Gadelha, University of Nottingham) with XhoI and XbaI and ligated into a pSPR0-LacI backbone that had been cut with SalI and SpeI, generating pSPR0-LacI-sfGFP. Next, the sfGFP-LacI coding sequence was removed from pSPR0-LacI-sfGFP by digesting it with SpeI and XbaI and ligated into pLacI-mSt-Bla-La or pLacI-La-TY-YFP2-Bla cut with SpeI and XbaI, producing pLacI-La-sfGFP-Bla and pLacI-La-TY-sfGFP-Bla, respectively. Plasmids were also created that coded for proteins in which sfGFP and LacI were separated by a short linker consisting of five serine residues. PCR was performed on pSiG-HhsfG template using primers designed to generate a sfGFP coding sequence with a 5' XhoI site and a 3' short linker sequence followed by an XbaI site (CCCCTCGAGACTAGTATGCGTAAAGG and CCTCTAGAAGAACTAGAACTAGA GGTTCCTTTGTACAGTTCATCCA). This PCR product was used as above to produce the pLacI-La-sfGFPL-Bla and pLacI-La-TY-sfGFPL-Bla plasmids.

3.2.6. For the integration of a LacO chromosome tag

A plasmid used for insertion of Lac operator (LacO) repeats into a minichromosome (MC) was built in a number of stages. First, the p2T7-177 plasmid (Wickstead et al., 2002) was cut with ApaI and self-closed, producing p177-Ble. The bleomycin resistance marker (*BLE*) was removed from p177-Ble and replaced with the neomycin resistance marker (*NEO*). PCR was used to produce linear plasmid, without *BLE*, adding XbaI and BamHI sites (CATCTAGACCGACGCCGACCAACA and CAGGATCCGGTGATATAGCTTATTTTATGGCA). The *NEO* gene was then taken from pSPR5, using PCR with primers that added a BamHI and XbaI sites (CAGGATCCATGCGCGAAATCGTCT and CATCTAGATCAGAAGAACTCGTCAAGAAG). Both products were digested with BamHI and XbaI restriction endonucleases and ligated, to produce p177-Neo.

To produce a plasmid that targeted the S8 VSG, the targeting sequence was amplified from pGad8-V8, with primers that amplified the sequence in two halves; a 5' fragment, with SacI and NotI sites (AAAGAGCTCGTCAACAGCATATCTAAAGGGCA and AGCGGCCGCGGTATTTCAATATAGCCGCC), and a 3' fragment, with NotI and KpnI sites (AGCGGCCGCGGTCACACAGACAGGC and TTGGTACCAGCTTGAGTTTGTGTTACAGGG). These targeting fragments were digested with the relevant enzymes, p177-Neo was cut with SacI and KpnI and a three-way ligation was performed.

The aim was to insert LacO repeats by digesting pS8- and pBES-Neo with KpnI and SphI. An extra SphI site exists in the *NEO* sequence, however. To remove this site, PCR was performed to alter a CGC codon to CGT (both of which code for arginine), in position 601-603 of *NEO* (primer sequences were GTATGCCCGACGGCGAG and GCGCCTTGAGCCTGG). The resulting PCR product was blunt-end ligated to produce the pS8-NeoB plasmid.

BES1 targeting sequences were generated by amplifying a sequence from the pBES-H-2 plasmid (courtesy of Dr Catarina Gadelha, University of Nottingham). Again two fragments were produced, a 5' with SacI and NotI sites and a 3' with NotI and KpnI sites (primer sequences were CCCGAGCTCTATGTTTTGTGTATTATTTAGGT and AAGCGGCCGCAAAAGCATCCGAAATA and AAGCGGCCGCTAGATGAGGACATCAA and TTTGGTACCGATATGCACGTCGAT, respectively). After digestion, these fragments were ligated into a backbone produced by digesting pS8-NeoB with SacI and KpnI. This generated the pBES-NeoB plasmid.

256× LacO repeat sequence was cut from pAFS52 (Straight et al., 1996) (a kind gift from Professor Tomo Tanaka, University of Dundee), using KpnI and SphI, and the resulting ~10kb fragment was size selected. LacO repeats were ligated into pBES-NeoB and pS8-NeoB backbones, which themselves had been cut with KpnI and SphI. The product of this ligation was cloned into STBL2 *E. coli* by

electroporation with an Eporator (Eppendorf), using 17kV cm^{-1} and growing cells at 30°C. This resulted the generation of the pBES-LacO and pS8-LacO plasmids.

3.2.7. For the generation of fluorescently labelled kinetochore protein

Plasmids designed for the N-terminal labelling of, the kinetochore proteins, KKT1 (kinetoplastid kinetochore protein 1) and KKIP1 with mStrawberry, pEnNmSt-G2P06Hyg and pEnNYmStP14Hyg, were obtained from Simon D'Archivio and Jennifer McDonald. A further plasmid, for labelling of KKIP5, pEnNmStP14int7Neo, was obtained from Simon D'Archivio. The *NEO* gene in this plasmid was then replaced with the *HYG* gene. pEnNYmStP14Hyg and pEnNmStP14int7Neo were cut with BamHI and NheI, to provide the *HYG* gene and plasmid backbone, and the required fragments size selected. These fragments were ligated, producing pEnNmStP14int7Hyg.

3.3. Cell lines

All bloodstream form (BSF) cell lines were derived from the SmOxB427 cell line (Poon et al., 2012). These cells were cultured in thymidine-free HMI-9 supplemented with 15% foetal bovine serum (Hirumi and Hirumi, 1989) at 37°C with 5% CO_2. All procyclic form (PCF) cell lines were derived from the SmOxP427 cell line (Poon et al., 2012). They were cultured in SDM79 supplemented with 10% foetal bovine serum (Brun and Schönenberger, 1979) at 28°C.

To create BSF cell lines, 10µg of NotI linearised plasmids was transfected into 2.5×10^7 cells resuspended in 120µl Tb-BSF buffer (90mM NaH_2PO_4/Na_2HPO_4 pH7.3, 5mM KCl, 0.15mM $CaCl_2$, 50mM HEPES pH7.3) (Schumann Burkard et al., 2011) using an Amaxa™ Nucleofector™ (Lonza), program Z-001. Transformants were selected for, after cells had recovered for 8 hours, with the relevant drug.

To create PCF cell lines, 6µg of NotI linearised plasmid was transfected into 3×10^7 cells, resuspended in 400µl TEB1 (60mM NaCl, 2.5mM $MgCl_2$, 1mM EDTA, 1mM KH_2PO_4, 4mM K_2HPO_4, 150Mm glucose, 10mM HEPES pH7.4), by capacitance discharge electroporation using an Eporator (Eppendorf) at 4.25 kV cm^{-1}. Again, transformants were selected for, after cells had recovered for 8 hours, with the relevant drug. Alternatively, plasmids were transfected into 3×10^7 cells, as described for BSF cells.

Cell lines, plasmids and drug selection used and the cell line generated are shown in Table 4. Exceptions are the SmOxB427 *HSV-TK-BSD*$_{177bp}$ cell line, which was obtained from Simon D'Archivio, and introduction of pMC-rDNA-HSVTKblast into SmOxP427, which did not produce clones.

Plasmid	Background Cell Line	Resulting Cell Line	Selection (μg ml^{-1}/drug)
p2T7β-KIN2A	SmOxB427	SmOxB427 *KIN2A* RNAi	2.5/phl
P2T7β-KIN2B	SmOxB427	SmOxB427 *KIN2B* RNAi	2.5/phl
p2T7β-KIN2A/B	SmOxB427	SmOxB427 *KIN2A/B* RNAi	2.5/phl
p2T7β-KIN2A/A	SmOxB427	SmOxB427 *KIN2A/A* RNAi	2.5/phl
p2T7β-KIN2B/B	SmOxB427	SmOxB427 *KIN2B/B* RNAi	2.5/phl
Obtained from Simon D'Archivio	SmOxB427	SmOxB427 *HSV-TK-BSD*$_{177bp}$	5/bla
p2T7β-KIN13-1	SmOxB427 *HSV-TK-BSD*$_{177bp}$	SmOxB427 *HSV-TK-BSD*$_{177bp}$ *KIN13-1* RNAi	5/bla 2.5/phl
pMC-T7-HSVTKblast	SmOxP427	No clones produced	10/bla
pMC-rDNA-HSVTKblast	SmOxP427	SmOxP427 *HSV-TK-BSD*$_{177bp}$	10/bla
pBES-HSVTK-PFR	SmOxP427	SmOxP427 *HSV-TK*$_{BES1}$	10/bla
pS8-HSVTK-PFR	SmOxP427	SmOxP427 *HSV-TK*$_{S8\ VSG}$	10/bla
p2T7-177-KKIP1	SmOxP427 *HSV-TK*$_{BES1}$/*HSV-TK*$_{S8\ VSG}$	SmOxP427 *HSV-TK*$_{BES1}$/*HSV-TK*$_{S8\ VSG}$ *KKIP1* RNAi	10/bla 2.5/phl
p2T7β-KIN13-1	SmOxP427 *HSV-TK*$_{BES1}$/*HSV-TK*$_{S8\ VSG}$	SmOxP427 *HSV-TK*$_{BES1}$/*HSV-TK*$_{S8\ VSG}$ *KIN13-1* RNAi	10/bla 2.5/phl
pEnG09S	SmOxP427	SmOxP427 *KIN13-1-GFP*	100/nour
pLacI-mSt-Bla	SmOxP427	mSt-LacI	10/bla
pLacI-YFP-Bla	SmOxP427	Y-LacI	10/bla
pLacI-mSt-Bla-La	SmOxP427	La-mSt-LacI	10/bla
pLacI-YFP-Bla-La	SmOxP427	La-Y-LacI	10/bla
pLacI-mSt-Bla-La:*PFR1*	SmOxP427	La-mSt-LacI:*PFR1*	10/bla
pLacI-YFP-Bla-La:*PFR1*	SmOxP427	La-Y-LacI:*PFR1*	10/bla
pLacI-mSt-Bla-La:*KIF9A*	SmOxP427	La-mSt-LacI:*KIF9A*	10/bla
pLacI-YFP-Bla-La:*KIF9A*	SmOxP427	La-Y-LacI:*KIF9A*	10/bla
pLacI-YFP-Bla-SV40	SmOxP427	SV-Y-LacI	10/bla
pLacI-La-TY-YFP2-Bla	SmOxP427	La-TY-Y$_2$-LacI	10/bla
pLacI-La-sfGFP-Bla	SmOxP427	La-sfG-LacI	10/bla
pLacI-La-sfGFPL-Bla	SmOxP427	La-sfG-link-LacI	10/bla
pLacI-La-TY-sfGFP-Bla	SmOxP427	La-TY-sfG-LacI	10/bla
pLacI-La-TY-sfGFPL-Bla	SmOxP427	La-TY-sfG-link-LacI	10/bla
pBES-LacO	La-TY-sfG-link-LacI	La-TY-sfG-link-LacI LacO$_{BES1}$	10/bla 15/G4
pS8-LacO	La-TY-sfG-link-LacI	La-TY-sfG-link-LacI LacO$_{S8\ VSG}$	10/bla 15/G4
pBES-LacO	La-TY-Y$_2$-LacI	La-TY-Y$_2$-LacI LacO$_{BES1}$	10/bla 15/G4
pS8-LacO	La-TY-Y$_2$-LacI	La-TY-Y$_2$-LacI LacO$_{S8\ VSG}$	10/bla 15/G4

pEnNmSt-G2P06Hyg	La-TY-sfG-link-LacI $LacO_{BES1}$/$LacO_{S8\ VSG}$	La-TY-sfG-link-LacI $LacO_{BES1}$/$LacO_{S8\ VSG}$ *mSt-KKT1*	10/bla 15/G4
pEnNYmStP14Hyg	La-TY-sfG-link-LacI $LacO_{BES1}$/$LacO_{S8\ VSG}$	La-TY-sfG-link-LacI $LacO_{BES1}$/$LacO_{S8\ VSG}$ *mSt KKIP1*	10/bla 15/G4 50/hyg
pEnNmStP14int7Hyg	La-TY-sfG-link-LacI $LacO_{BES1}$/$LacO_{S8\ VSG}$	La-TY-sfG-link-LacI $LacO_{BES1}$/$LacO_{S8\ VSG}$ *mSt KKIP5*	10/bla 15/G4 50/hyg
p2T7-177-KKIP1	La-TY-sfG-link-LacI $LacO_{BES1}$/$LacO_{S8\ VSG}$ *mSt-KKT1*	La-TY-sfG-link-LacI $LacO_{BES1}$/$LacO_{S8\ VSG}$ *mSt-KKT1* *KKIP1* RNAi	10/bla 15/G4 50/hyg 2.5/phl

Table 4. Generation of cell lines used in experimentation. Shown are plasmids, the cells they were introduced into and the cell line produced. The concentration of drugs used to select for successful integration are also shown; phl = phleomycin, bla = blasticidin S, nour = nourseothricin, G4 = G418, hyg = hygromycin.

3.4. Southern blotting

Integration of the HSV-TK coding sequence and LacO repeats into MCs was confirmed by Southern blot. Pulsed field gel electrophoresis (PFGE) was used to separate MCs from megabase chromosomes and intermediate chromosomes. Low melting point agarose plugs (0.8%) were produced at a cell concentration of $4x10^8$ cells ml^{-1}, as described in Wickstead et al. (2004). These plugs were inserted into wells in a 1% agarose gel (SeaKem Gold) for PFGE. PFGE was run for 142 hours using an included angle of 120°, 2V cm^{-1} and a linear switch ramp of 18-42 min, in TB(0.1)E (90mM Tris-borate, 0.2mM EDTA pH 8.2) at 12°C. After PFGE had been completed the gel was stained with 1µg ml^{-1} ethidium bromide for 20 min and imaged.

DNA was transferred from the gel to a positively charged nylon membrane (Boehringer Mannheim), after UV nicking (240nm, 80mJ cm^{-2}), using capillary transfer for 48 hours with buffer consisting of 1.5M NaCl and 0.4M NaOH. After transfer the membrane was neutralised with 0.5M Tris-HCl pH7.0. The DNA was then UV-crosslinked to the membrane (240 nm, 120 mJ cm^{-2}).

Fluorescein-labeled probes were produced from the HSV-TK coding sequence or from the pT1045 plasmid (courtesy of Professor Tomo Tanaka,

University of Dundee) using random primed DNA labelling. 100 ng of template, 2µM random heptamer primers, 100µM dNTP mix, 5 units Klenow and 1x NEBuffer 2 (New England Biolabs) were used and the reaction run at 37°C for 1 hour. The membrane was prehybridised for 1 hour at 60°C with hybridisation buffer (750mM NaCl, 75mM sodium citrate pH7.0, 5% Dextran sulphate, 5% liquid block [Amersham]). 5µl of denatured probes was incubated with the membrane at 60°C overnight in 5ml hybridisation buffer. After hybridisation, stringency washes were performed, which consisted of two washes for 5 min in 1x SSC with 0.1% w/v SDS at 62°C, followed by two washes for 15 min in 0.2x SSC with 0.1% w/v SDS at 62°C. The membrane was then blocked with 10% blocking solution (Roche) in Buffer A (0.3M NaCl, 0.1M Tris-HCl pH7.0), washed four times for 10 min with Buffer A and incubated with anti-fluorescein-AP Fab fragments (Roche), diluted 1:5,000 in Buffer A, for 1 hour. Another set of washes was performed and CDP-Star (Invitrogen) was applied to the membrane, which was then exposed to film.

3.5. Analysis of LacO repeat integration

3.5.1. Diagnostic PCR

Confirmation that LacO repeats had been integrated into the correct location was provided by diagnostic PCRs. Primers were designed to amplify a region of the integrated construct or a region bridging the construct and an area of the genome downstream of the target sequence. GTTGGCCGATTCATTAATGCAG was used as a forward primer in all reactions, while GTGCCTCCAGCTTGAGT was used as the reverse primer in confirmation of replacement of the S8 VSG and CCCTGTGAAAAGTACTAAAGAAGGC in confirmation of integration in BES1. The sequences of reverse primers used to amplify the S8 VSG and BES1 targeting constructs were GTCTGTGTTGCCGAAGC and CAACATTCCTCCCCACAGA, respectively.

3.5.2. G418 sensitivity analysis

To determine whether subpopulations of the La-TY-sfG-link-LacI $LacO_{BES1}$ and La-TY-sfG-link-LacI $LacO_{S8\ VSG}$ cell lines that lacked LacO constructs existed, a test of G418 sensitivity was performed. Cells were diluted and plated on 96 well plates, without drug pressure, so that each cell was predicted to contain, on average, one cell. After ten days the numbers of positive wells were counted. Cells were re-plated, with G418 drug pressure (15µg ml^{-1}), and grown for a week, with dilutions performed when necessary. The number of positive wells were then counted a second time. The number of positive wells was used to estimate the number of independent clones based on the Poisson distribution. Estimations produced from plates with ~40-90 positive wells have relative errors of ≤15% (estimated from 10^6 simulations of plating at densities of 0.001-10 cells per well), and the plate containing wells closest to this range was used to estimate counts of clones.

3.6. Western blotting

RNAi knockdown of KIN13-1 was confirmed by Western blot, following induction for 48 hours with 1µg ml^{-1} tetracycline. Reducing SDS polyacrylamide electrophoresis (SDS-PAGE) was used to separate trypanosome proteins. Cells were harvested by centrifugation and resuspended in boiling Laemmli buffer (2% w/v SDS, 0.4M 2-mercaptoethanol, 10% glycerol, 50mM Tris-HCl pH7.2), to produce whole cell lysates. Lysates from $4.8x10^6$ cells were separated in a 4-20% polyacrylamide TGX gel (Bio-Rad) in buffer consisting of 25mM Tris, 250mM glycine and 0.1% w/v SDS.

Proteins were electrophoretically transferred to a nitrocellulose membrane (Boehringer Mannheim) for 16 hours with a 1.6V cm^{-1} voltage gradient in 25mM Tris, 192mM glycine, 0.02% w/v SDS and 10% methanol. The membrane was blocked with 5% w/v milk powder in TBS-T (20mM Tris-HCl pH7.5, 150mM NaCl, 0.1% Tween-20) for 1 hour. It was then incubated with affinity purified rabbit anti-KIN13-1 polyclonal antibodies (Wickstead et al., 2010a) diluted 1:2,000 in 1% w/v milk in TBS-T, for 1 hour. 1× 1 min and 3× 10 min

washes with TBS-T were performed and the membrane was incubated with goat anti-rabbit IgG peroxidase conjugate (Sigma) secondary antibodies, diluted 1:10,000 in 1% w/v milk in TBS-T. Another set of washes was then performed. To produce an image, Western Lightning ECL (PerkinElmer) was added to the membrane and it was exposed to film.

Expression of KIN13-1-GFP was also confirmed by Western blot as described above, but using a 200ng ml^{-1} mix of monoclonal antibodies 7.1 and 13.1 (Roche), raised against GFP, and goat anti-mouse IgG peroxidase conjugate (Sigma) secondary antibodies. This was followed by application of rabbit anti-KIN13-1 polyclonal antibodies and goat anti-rabbit IgG peroxidase conjugate (Sigma) secondary antibodies.

Expression of mStrawberry protein conjugated LacI was confirmed by blotting with 200ng ml^{-1} 1C51 monoclonal antibody (Abcam), raised against mCherry, and rabbit anti-mouse IgG peroxidase conjugate (Sigma) secondary antibodies. The membrane was washed again and incubated with 200ng ml^{-1} anti-GFP antibodies, as above. A blot performed with IC51 was also used to confirm expression of mStrawberry-KKT1, mStrawberry-KKIP1 or mStrawberry-KKIP5.

3.7. Growth analysis

The influence of knockdown of proteins by RNAi on BSF population growth was determined by performing counts of cells in induced and uninduced populations, with cells diluted to 10^5 cells ml^{-1} every 24 hours. Cells were counted using a Neubauer haemocytometer. The influence of protein knockdown on PCF cells was also determined by performing counts of cells, with cells diluted to 10^5 cells ml^{-1} every 72 hours. Counts of cells were also used to determine effect of 0, 50, 100 or 500 µg ml^{-1} ganciclovir (or penciclovir) on growth of PCF cells, in which *HSV-TK* had been introduced.

3.8. Microscopy

3.8.1. Attachment and mounting of samples

For analysis of both BSF and PCF cells by microscopy, slides were prepared. ~5×10^5 cells were harvested from log-phase cultures by centrifugation, washed with PBS three times and left to adhere to slides. PCF cells were adhered to glass slides, while BSF cells were adhered to derivatised slides. Slides were derivatised by applying a solution of 5% glutaraldehyde and 0.1M $NaHCO_3$ to silane-coated StarFrost® Adhesive slides (Knittel). Samples were fixed with 2% formaldehyde in PBS for 5 min and permeabilised with methanol at −20°C. Cells were then mounted in 5µl mounting medium per slide, containing 200ng ml^{-1} DAPI, 1% 1,4-diazabicyclo[2.2.2]octan, 90% glycerol and 50mM NaH_2PO_4/Na_2HPO_4 (pH8.0).

For cytoskeleton preparations, cells were adhered to slides as above. They were then treated with 1% Nonidet P40 (Roche) in PMEG buffer (40mM PIPES-K pH6.9, 2mM $MgSO_4$, 5mM EGTA, 200mM glucose) for 5 min. Finally, they were washed with PBS and mounted.

3.8.2. Immunofluorescence

So that flagella could be observed, immunofluorescence microscopy was performed. Slides were prepared from BSF cells as described above. After cells were fixed and permeabilised, slides were rehydrated and empty aldehyde groups were blocked in 0.1% w/v glycine in PBS for 5 min. Tissue supernatant containing the L13D6 monoclonal antibody (Kohl et al., 1999), which recognises PRF1 and 2, was diluted 1:50 in PBS and applied. Slides were washed four times for 10 min in PBS and rhodamine (TRITC)-conjugated AffiniPure goat anti-mouse IgG (Jackson ImmunoResearch Laboratories) secondary antibodies applied 1:200 in PBS. Additional washes were then performed and cells mounted as described above.

3.8.3. Imaging

Images of cells were captured from slides, using a 100x oil immersion objective and Photometrics CoolSnap HQ camera or a Retiga R1™ CCD camera (QImaging). Images were then processed using ImageJ (Schneider et al., 2012). Where images were used for comparison, they were processed equally.

3.9. K-N Counts

The effect of RNAi against KIN2 proteins on the cell cycle was ascertained by performing "K-N counts" on cells that had been induced for 0, 8, 16 and 24 hours. The knockdown of KKIP1 was also confirmed by these counts after RNAi was induced for 48 hours. Slides were prepared as described above. The numbers of kinetoplasts and nuclei in individual cells was counted under a 63x or 100x oil immersion objective. During analysis of cells in which RNAi had been performed against KIN2 proteins, the number of cells with abnormal morphology ("round" cells) was also ascertained.

3.10. Minichromosome loss assay

To test for MC loss, following RNAi induction for 48 hours, cells were plated 10, 100 or 1000 cells per well on 96 well plates, in the presence of 100μg ml^{-1} ganciclovir. After a week, for BSF cells, or 10 days, for PCF cells, the number of positive wells was counted, each positive well representing a cell (or cells) that had lost a MC. The number of positive wells was used to estimate the number of independent clones as described in 3.5.2. The number of clones, as well as counts of cells performed before and after RNAi induction, were used to calculate the number of MC loss events that had occurred per cell per generation, during RNAi.

3.11. Analysis of the distribution of fluorescent foci

3.11.1. Counts of LacI/LacO foci

To find the most ideal LacO/LacI cell line for further analysis, a line in which just one chromosome was labelled (no duplication events had occurred) and in which all tagged chromosomes were visible, the number of foci per cell was counted under a 100x oil immersion objective and a Retiga R1™ CCD camera (QImaging). The most suitable clones of La-TY-sfG-link-LacI $LacO_{BES1}$ and La-TY-sfG-link-LacI $LacO_{S8\ VSG}$ were then taken forward for further analysis.

To determine the effects of RNAi on the distribution of LacI foci and, therefore, chromosomes, slides were produced after cells had been induced for 0, 24, 48, 72 and 96 hours. As a control, La-TY-sfG-link-LacI $LacO_{BES1}$ and La-TY-sfG-link-LacI $LacO_{S8\ VSG}$ cells were grown without drug pressure. The number of cells lacking foci or the number interphase cells with two foci was counted as above and calculated as a percentage of the total cells. The number of mitotic cells, in which foci were asymmetrically distributed, suggesting nondisjunction events had occurred, was also determined.

3.11.2. Kinetochore-chromosome distance measurements

To determine the distance between the labelled chromosomes and kinetochore labels, large numbers of images of La-TY-sfG-link-LacI $LacO_{BES1}$ and La-TY-sfG-link-LacI $LacO_{S8\ VSG}$ cells expressing mStrawberry-KKT1, mStrawberry-KKIP1 or mStrawberry-KKIP5 were produced. Using ImageJ, the distance between the centre of chromosome and kinetochore foci (brightest pixel) in cells at different cell cycle stages was manually measured as pixels, which was then converted to µm. The cell cycle stages analysed were G2, metaphase, early anaphase (DAPI stained nuclear DNA continuous), late anaphase (DAPI stained nuclear DNA separated) and cytokinesis.

4. A combinatorial library for assessment of motor function in *Trypanosoma brucei*

4.1. Redundancy of trypanosomal motor proteins

4.1.1. Individual molecular motors do not significantly contribute to the fitness of trypanosomes in high-throughput screens

As has been discussed in section 1.5.5., RNA interference (RNAi) is a well-established technique in *Trypanosoma brucei* for depletion of target proteins. RNAi has been used extensively to investigate the function of individual proteins and more recently has been used for high-throughput investigations. In 2011, a paper describing a technique known as RNAi target sequencing (RIT-Seq) was published by the Horn lab (Alsford et al., 2011). RIT-Seq was developed so that the impact of individual knockdown of proteins on trypanosome fitness could be investigated on a genome-wide scale. The concept of RIT-Seq is based on the use of an inducible RNAi library. Briefly, a library of DNA fragments is introduced into RNAi plasmids, which are then transfected into *T. brucei* cells, to produce a cell line carrying an RNAi library. The population produced is split and either RNAi induced by the addition of tetracycline or the cells left uninduced. Genomic DNA is extracted from induced and uninduced populations, PCR is performed to amplify the genomic fragments within RNAi constructs, which are then sequenced using next generation sequencing technology. The reads produced can be mapped to the library or the whole genome and the number of reads present, for individual fragments or genes, compared between induced and uninduced populations. A reduction in reads suggests RNAi against a certain gene has reduced cell growth. Significant changes in read numbers between induced and uninduced can then be used to infer what proteins might have important roles in trypanosome survival. The data produced by such scalable technologies has been of great interest to a number of fields within trypanosome biology.

Data produced in the original RIT-Seq experiment were replotted and data points representing kinesin coding DNA sequences (CDSs), as defined by Wickstead & Gull (2006) and Wickstead et al. (2010b), labelled (Figure 18). These

data show that knockdown of very few kinesin proteins, significantly reduced cell growth in these experiments. Some kinesins known to produce a significant growth phenotype when knocked down also did not produce a significant phenotype in this RIT-Seq experiment (Table 5). Such kinesins include KIN13-1 (Chan et al., 2010; Wickstead et al., 2010a), TbKIN-D (H. Hu et al., 2012; Wei et al., 2013), Kinesin^{CaaX} (Engelson et al., 2011) and TbKIN-A (Li, Lee, et al. 2008; Li, Umeyama, et al. 2008). Only TbKIN-C caused a significant decrease in growth in RIT-Seq and is also known to produce a growth phenotype when knocked down individually (L. Hu et al., 2012). These discrepancies may be due, in part, to the size of the RIT-Seq data set. The RIT-Seq experiment was performed using fragments mapping to ~7,500 of the ~10,000 genes and hypothetical genes in the *T. brucei* genome. Performing multi-hypothesis tests on such large data sets means more stringent conditions for significance are required for individual changes. In addition to these effects, kinesins in general may not be found to be significant due to their interactions with other kinesin proteins, which were discussed in Chapter 1. Redundancy, in particular, would reduce the likelihood of kinesins displaying significance in RIT-Seq. Reproducing RIT-Seq in a manner that is more sensitive and can also detect redundancy may bring more insight into the importance of kinesins in trypanosome biology.

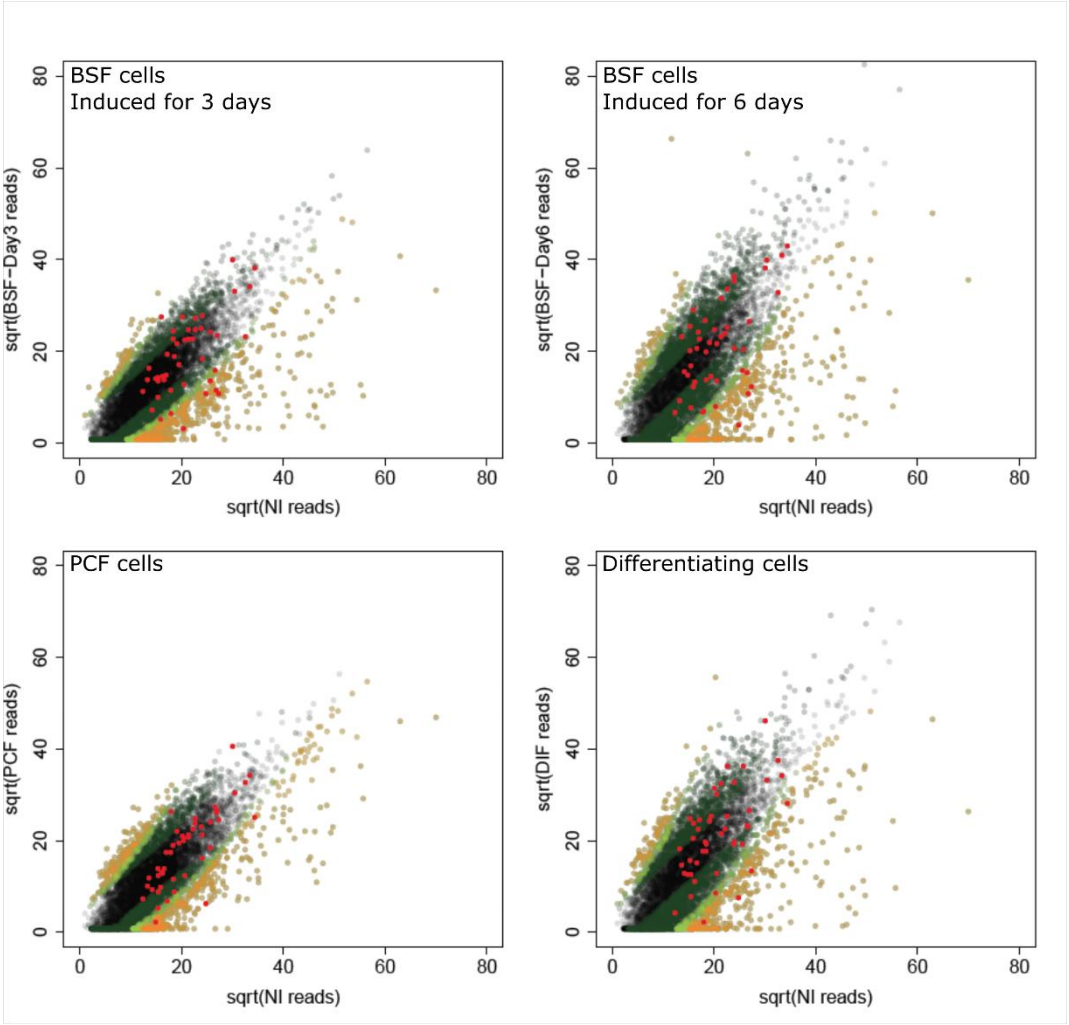


Figure 18. Plots of data from RIT-Seq (Alsford et al., 2011) with kinesins labelled. The number of reads for each gene in induced cells is plotted against the number of reads in uninduced cells (NI-reads). Data points representing kinesins are coloured red. Dark green data points signify a significant difference as defined by the original RIT-Seq study, whereas light green and orange points represent recalculated significances of $p<0.05$ and $p<0.01$, respectively.

Kinesin Gene ID	Synonym	RIT-Seq Data				Growth Phenotype After Previous KD?
		BSF 6 days		PCF		
		Log Fold Change	q-value	Log Fold Change	q-value	
Tb927.1.1350		-0.654	0.840	-0.196	0.423	
Tb927.3.2020		-0.841	0.672	0.004	-0.084	
Tb927.3.2040		0.316	0.319	0.272	-0.167	
Tb927.3.3390		-1.724	0.542	-1.493	0.377	
Tb927.3.3400		-1.042	0.414	-0.751	0.087	
Tb927.3.4960		1.125	-0.211	-0.347	0.445	
Tb927.4.2730		0.390	0.091	0.405	-0.425	
Tb927.4.3910	KIN13-4a	-0.836	0.627	-2.092	0.855	
Tb927.5.2090	KIN2B	-2.293	0.987	-0.291	0.572	
Tb927.5.2410		-1.364	0.935	-0.944	0.815	
Tb927.6.1770		-2.693	0.944	-0.050	0.007	
Tb927.6.2880		-0.445	0.731	-1.134	0.821	
Tb927.6.4390		0.261	0.285	0.010	0.007	
Tb927.7.3000		0.779	0.381	-0.003	0.502	
Tb927.7.3830		0.152	0.313	-1.461	0.797	
Tb927.7.4110		1.135	-0.322	-0.085	0.093	
Tb927.7.4830		1.724	-0.771	-0.579	0.146	
Tb927.7.5650		1.527	-0.717	-0.392	-0.101	
Tb927.7.6290	TbKIF9A	0.282	-0.034	-1.561	0.588	No (Demonchy et al., 2009)
Tb927.7.7120		0.648	-0.188	-0.518	0.145	
Tb927.7.7260	TbKIF9B	-0.762	0.469	-1.387	0.551	Yes (Demonchy et al., 2009)
Tb927.8.2630	TbKIN-C	-5.260	0.997	-3.974	0.998	Yes (L. Hu et al., 2012)
Tb927.8.4840		1.227	-0.300	-0.100	0.241	
Tb927.8.4950		0.592	0.011	0.120	-0.149	
Tb927.8.6830		0.039	0.841	0.015	0.585	
Tb927.8.8350	KIN13-4b	0.801	-0.329	-0.287	-0.082	
Tb927.9.15470		-0.057	0.706	-0.030	0.349	
Tb927.9.3650	KIN13-1	-0.144	0.449	0.674	-0.591	Yes (Chan et al., 2010; Wickstead et al., 2010a)
Tb927.9.9870	KIN13-6	1.473	-0.676	-3.051	0.876	
Tb927.10.1110		0.600	0.632	0.072	0.577	
Tb927.10.12440	Kinesin^{CaaX}	0.256	-0.077	-1.192	0.368	Yes (Engelson et al., 2011)
Tb927.10.12490		1.111	-0.414	0.133	-0.246	
Tb927.10.14570		-1.583	0.960	0.095	0.211	
Tb927.10.14890	TbKIFC1	-2.821	0.908	-0.041	-0.129	
Tb927.10.15390	FAZ7	-1.952	0.739	-0.644	0.152	
Tb927.10.15400		0.698	0.423	0.877	-0.485	
Tb927.10.890		0.646	0.642	-0.896	0.965	
Tb927.11.10760	TbKIN-D	1.025	-0.403	0.098	-0.276	Yes (H. Hu et al., 2012; Wei et al., 2013)
Tb927.11.12180		1.161	-0.297	0.164	-0.067	

Tb927.11.13920	KIN2A	-1.184	0.792	0.021	-0.047	
Tb927.11.2490		-2.628	0.989	-0.058	0.359	
Tb927.11.2880	TbKIN-A	-2.772	0.906	1.104	-0.852	Yes (Li, Lee, et al. 2008; Li, Umeyama, et al. 2008)
Tb927.11.3280	KIN13-5	-0.568	0.415	-0.636	0.194	
Tb927.11.4660	KIN13-2	0.832	-0.281	-2.661	0.889	
Tb927.11.5300	KIN13-3	0.213	0.358	0.055	0.012	
Tb927.11.6400		-0.033	0.104	-5.466	0.967	
Tb927.11.9110		0.233	0.148	-1.341	0.667	

Table 5. RIT-Seq data associated with putative kinesin proteins. Shown is the log fold change in reads after induction, as well as the directional significance of that change, represented by the q-value. Whether or not a growth phenotype was observed after previous attempts at RNAi is also shown.

4.1.2. Kinesin-2 motors are essential for flagellar function in model organisms

Kinesin-2 family proteins are important for the production and maintenance of cilia and flagella in multicellular and unicellular eukaryotes. Kinesin-2s are plus-end directed kinesins, which play an important role in intraflagellar transport (IFT), as well as having roles in vesicle and melanosome transport (Verhey and Hammond, 2009; Wordeman, 2010). Kinesin-2 members perform the anterograde transport of IFT particles, while cytoplasmic dyneins perform the retrograde (Hao and Scholey, 2009). They are, therefore, required for the transport of ciliary or flagellar components. Kinesin-2 proteins are known to be essential for IFT and the production of axonemes in *Caenorhabditis elegans*, *Drosophila*, zebrafish, *Xenopus*, mice and *Chlamydomonas reinhardtii* (Morga and Bastin, 2013; Scholey, 2013). In *C. reinhardtii*, a common model for IFT studies, raising temperature sensitive mutants of *FLA10*, which codes for a kinesin-2 motor, above permissive temperatures halts IFT, preventing assembly of new flagella and maintenance of existing flagella (Cole et al., 1998; Huang et al., 1977; Kozminski et al., 1995; Walther et al., 1994).

The flagellum of *T. brucei* is essential for its survival in its bloodstream form (BSF) stage (Branche et al., 2006; Broadhead et al., 2006; Ralston and Hill, 2006). Cell shape and the cleavage furrow during cytokinesis are defined by the flagellum (Robinson et al., 1995; Sun et al., 2012; Sunter et al., 2015). The flagellum is also important in host-parasite interaction, cell surface recycling and in the movement of nutrients into the flagellar pocket, the sole site of endo- and exocytosis (for reviews see Langousis & Hill 2014; Morga & Bastin 2013). Without IFT and the proteins involved BSF trypanosomes are unable to survive. Knockdown of a number of conventional IFT proteins present in *T. brucei*, for example, produced substantial growth defects and abolished synthesis of new flagella in dividing cells, resulting in the production of round cells, lacking the normal trypanosome cell structure (Absalon et al., 2008b).

T. brucei has two kinesin-2s encoded in its genome (Wickstead and Gull, 2006), KIN2A (Tb927.11.13920) and KIN2B (Tb927.5.2090), and both have been

localised to the flagellum (Bill Wickstead, personal communication). Due to the role these proteins perform in IFT in model systems and the importance of IFT to trypanosome survival, one would expect knockdown of either to significantly reduce growth rates. Only KIN2B had a significant impact on growth in RIT-Seq, after recalculation of significance, and only in BSF cells. A number of possibilities exist that might explain this discrepancy. Firstly, the expected essentiality just might not exist. Secondly, the sensitivity issues with RIT-Seq, as previously discussed, may impact the calculated significance of the effect of kinesin-2 on fitness. Finally, some redundancy might exist between the two kinesin-2 proteins, preventing them from appearing as significant in RIT-Seq. This is an example of the type of redundancy that would be interesting to assess, if a method to do so were available.

4.1.3. Knockdown of both kinesin-2 motors is required to generate a growth phenotype in *Trypanosoma brucei*

To establish whether redundancy exists between the two kinesin-2 proteins in *T. brucei*, three RNAi plasmids were produced. These plasmids were designed so that double stranded RNA (dsRNA) would be produced from a ~250bp fragment of the 3' end of *KIN2A* or *KIN2B* coding sequences, as well as the two fragments in combination. These plasmids were transfected into SmOxB427 cells (Poon et al., 2012) and three clones from each transfection selected. RNAi was induced for 96 hours in these clones, or cells left uninduced, and the number of cells counted every 24 hours. The cumulative cell number was then calculated from the resulting cell counts (Figure 19). RNAi against individual KIN2A and KIN2B proteins had no significant effect on cell number ($p=0.93$ and 0.99, respectively; K-S test). The significance of the effect of KIN2B knockdown differs from that observed in the RIT-Seq experiment. This discrepancy may have been caused by variability in the efficiency of RNAi, based on the sequences used as templates for dsRNA production. When both kinesin-2 proteins were knocked down there was a significant reduction in population growth ($p=0.0025$; K-S test). These data show that there is interaction between the two kinesin-2 genes in *T. brucei*. It should be noted that it is not known how well each individual RNAi worked in these cells, since the endogenous protein was not tagged and we do not have antibodies raised against the proteins in question, so no Western blot was performed. It is, therefore, unknown if or how well the proteins were knocked down in cells. The reproducibility across clones, however, suggests the results are not an artefact of different knockdown efficiencies.

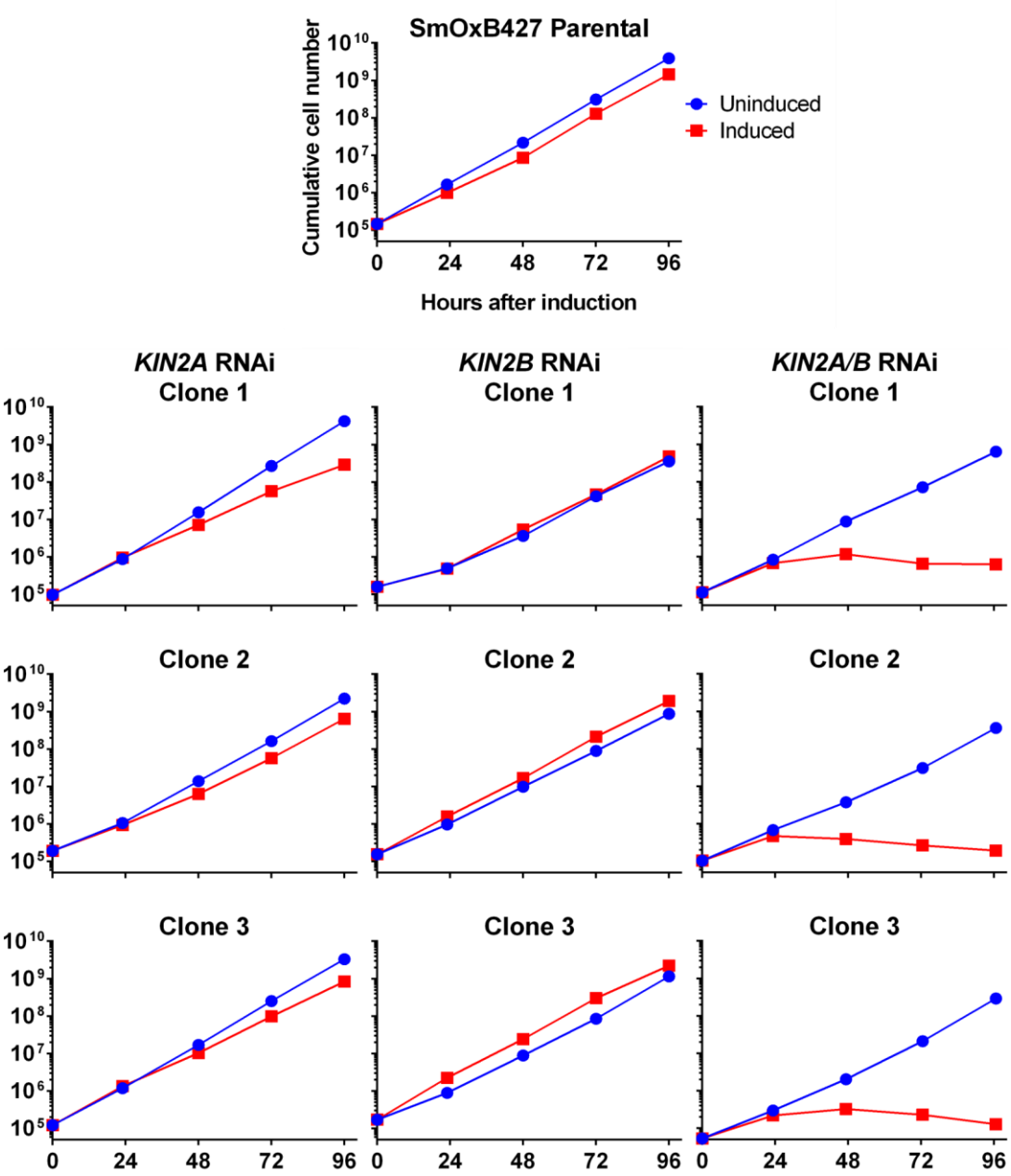


Figure 19. RNAi against KIN2A and KIN2B individually does not affect growth rates, but knockdown of both causes limited population decline. RNAi was induced against KIN2A, KIN2B or a combination of the two for 96 hours. Cells were counted using a haemocytometer every 24 hours and the cumulative cell number calculated.

4.1.4. The *KIN2A/B* knockdown phenotype is not the result of a gross change to the cell cycle

In order to determine whether the cell growth phenotype was due to effects on the cell cycle, “K-N counts” were performed on induced and uninduced cells. K-N counts involve counting the number of kinetoplasts and nuclei in trypanosome cells after staining with DAPI. Cells that have yet to undergo division have one kinetoplast and one nucleus and can be referred to as “1K1N” cells. Kinetoplast DNA is replicated early in nuclear S phase and is segregated during S and G2 phase, creating “2K1N” cells with two kinetoplasts and one nucleus. At anaphase nuclear DNA is separated, producing two nuclei in what are then referred to as “2K2N” cells (Hammarton, 2007; Woodward and Gull, 1990). An overview of this is presented in Figure 20. K-N counts can be utilised to establish the approximate stage of the cell cycle cells are in and can, therefore, be used to determine how treatments affect a population’s movement through the cell cycle.

Cells were induced for 0, 8, 16 or 24 hours and assayed for K-N number (Figure 21). Knockdown of kinesin-2 proteins individually and in combination resulted in time dependent increases in the number of cells with numbers of kinetoplasts and nuclei greater than the normal content (>2K2N). 24 hours of KIN2B knockdown significantly increased the number of >2K2N cells in all three clones ($p=0.037$, 0.012 and 0.027; Z-test). Knockdown of KIN2A resulted in more significant increases in >2K2N cells ($p<0.001$ for all three clones; Z-test), as did knockdown of both KIN2A and KIN2B in combination ($p<0.001$ for all three clones; Z-test). These >2K2N cells were cells that had experienced a cytokinesis failure and then initiated division again. These cytokinesis failures could have influenced population growth, contributing to the growth phenotype observed previously. The increases in aberrant cells were not significantly different between KIN2A and KIN2A/B knockdown ($p=0.12$; paired t-test), however, suggesting that this phenotype was not the root cause of the growth phenotype that occurred when both kinesin-2 proteins were knocked down.

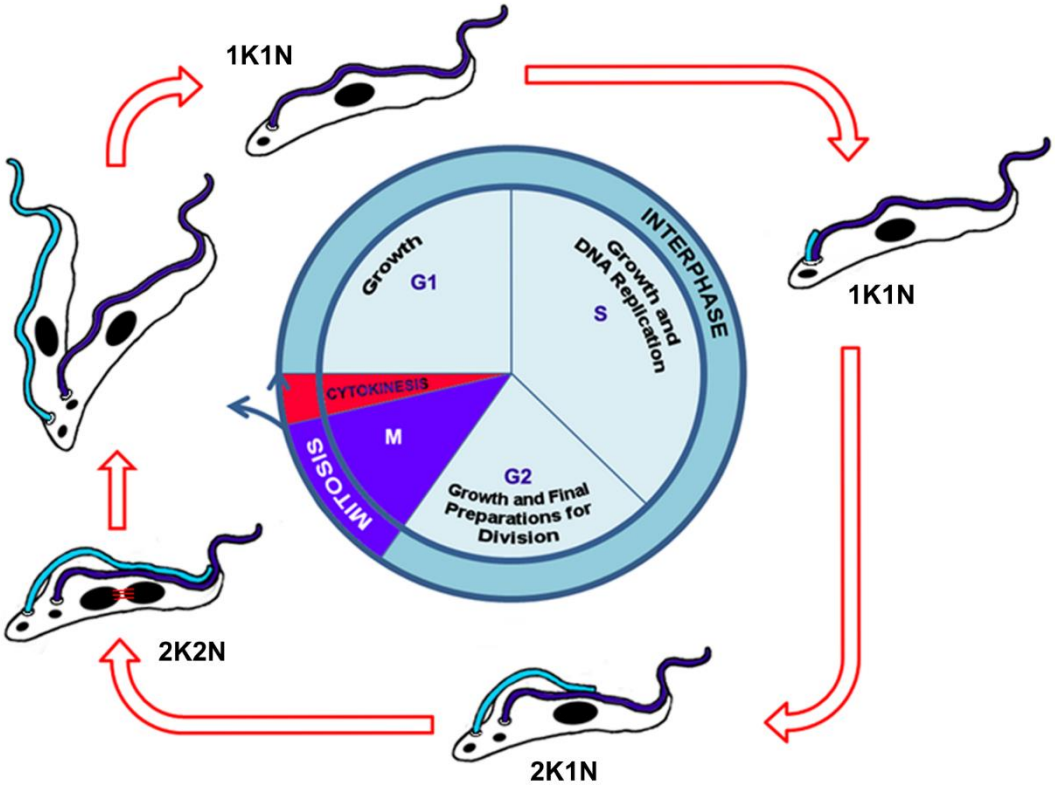


Figure 20. Division of kinetoplasts and nuclei can be used to determine cell cycle stage. Cells not undergoing division have one kinetoplast and one nucleus (1K1N). Early in S phase kinetplast DNA replicated and it is later divided during G2 phase, creating 2K1N cells. As nuclear DNA is separated at anaphase two nuclei are formed and cells are then described as 2K2N. Adapted from Jones et al. (2014).

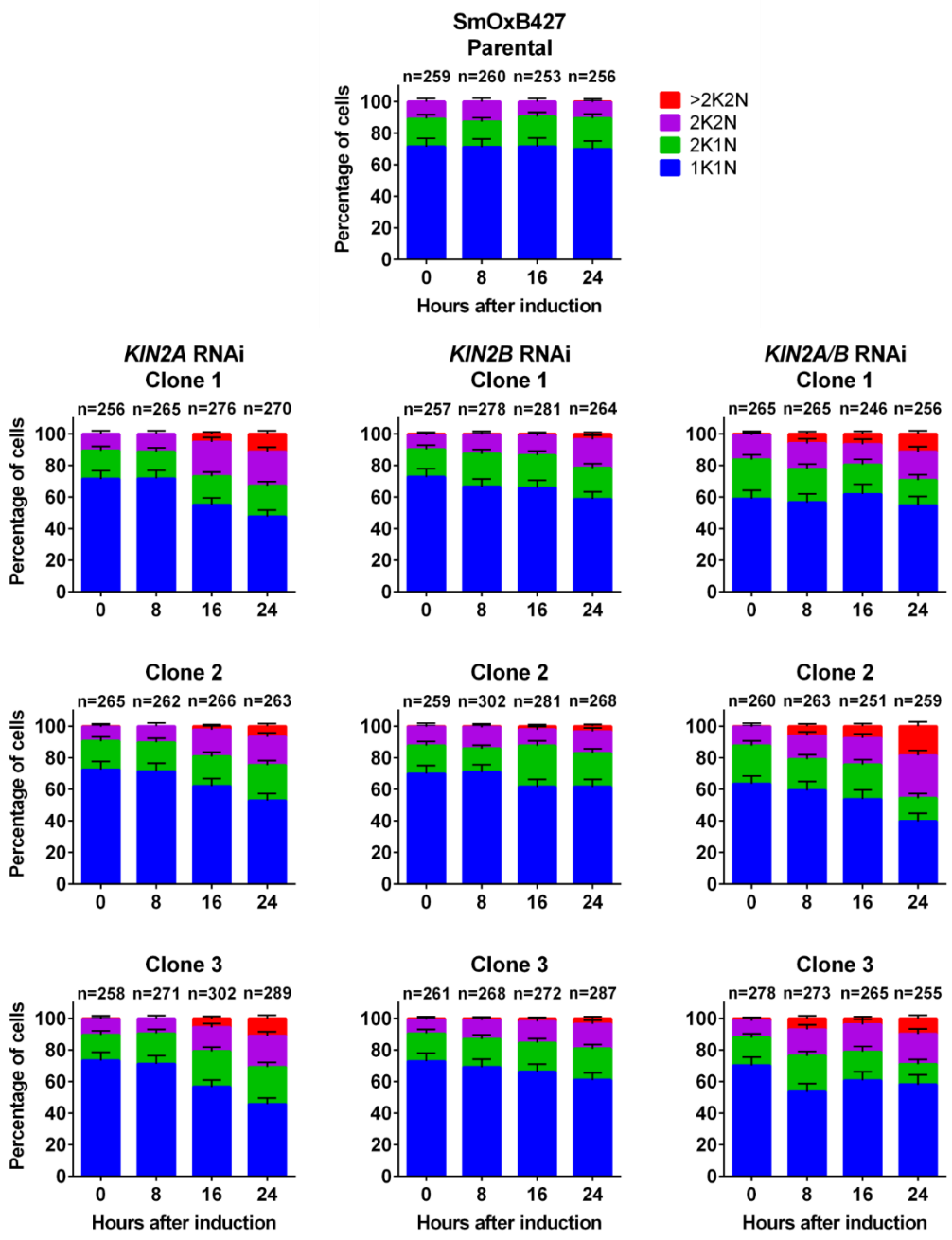


Figure 21. Knockdown of kinesin-2 proteins does not greatly impact the cell cycle. RNAi against KIN2A, KIN2B or KIN2A and B was induced for 0, 8, 16 and 24 hours. Cells were attached to derivatised slides and stained with DAPI. Using fluorescence microscopy, the number of kinetoplasts and nuclei per cell was then counted.

While K-N counts were being performed on populations in which both kinesin-2 proteins had been knocked down I also observed the presence of "round" cells. These cells lacked a normal morphology and obvious flagella, resembling phenotypes of IFT protein knockdown (Absalon et al., 2008b). To determine whether the numbers of these cells increased in a time-dependent manner, they were also counted and percentages calculated (Figure 22). The number of round cells increased in a time-dependent manner over the 24 hour period. All three clones displayed significant increases in these cells after 24 hours (p= 0.0019, 0.0016 and <0.001; Z-test). Microscopy showed that round cells do indeed lack normal trypanosome morphology and appeared to have small or absent flagella (Figure 23). The flagellar pocket of these cells also appears to greatly increase in size, suggesting a defect in endocytosis. Furthermore, round cells were only produced when both kinesin-2 motors were knocked down, further demonstrating interaction between the two proteins.

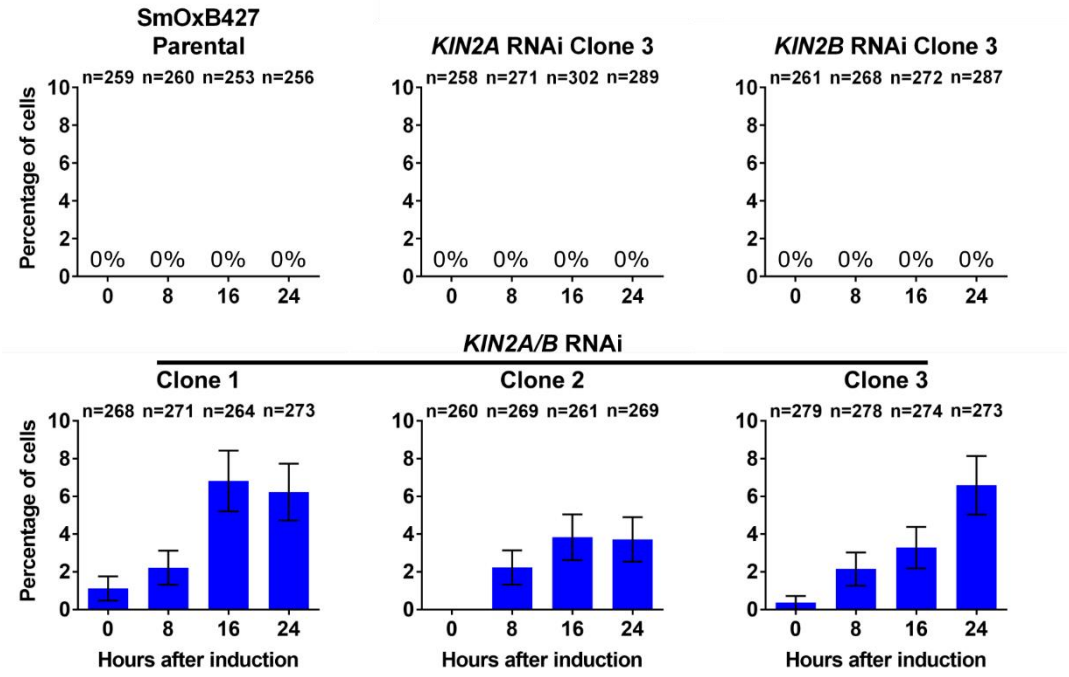


Figure 22. "Round" cells form when both KIN2A and B are knocked down. RNAi against KIN2A, KIN2B or KIN2A/B was induced for 0, 8, 16 and 24 hours. Cells were attached to derivatised slides and stained with DAPI. Using fluorescence microscopy, the number of round cells was counted and percentages calculated. For single kinesin-2 knockdowns only one representative clone is shown.

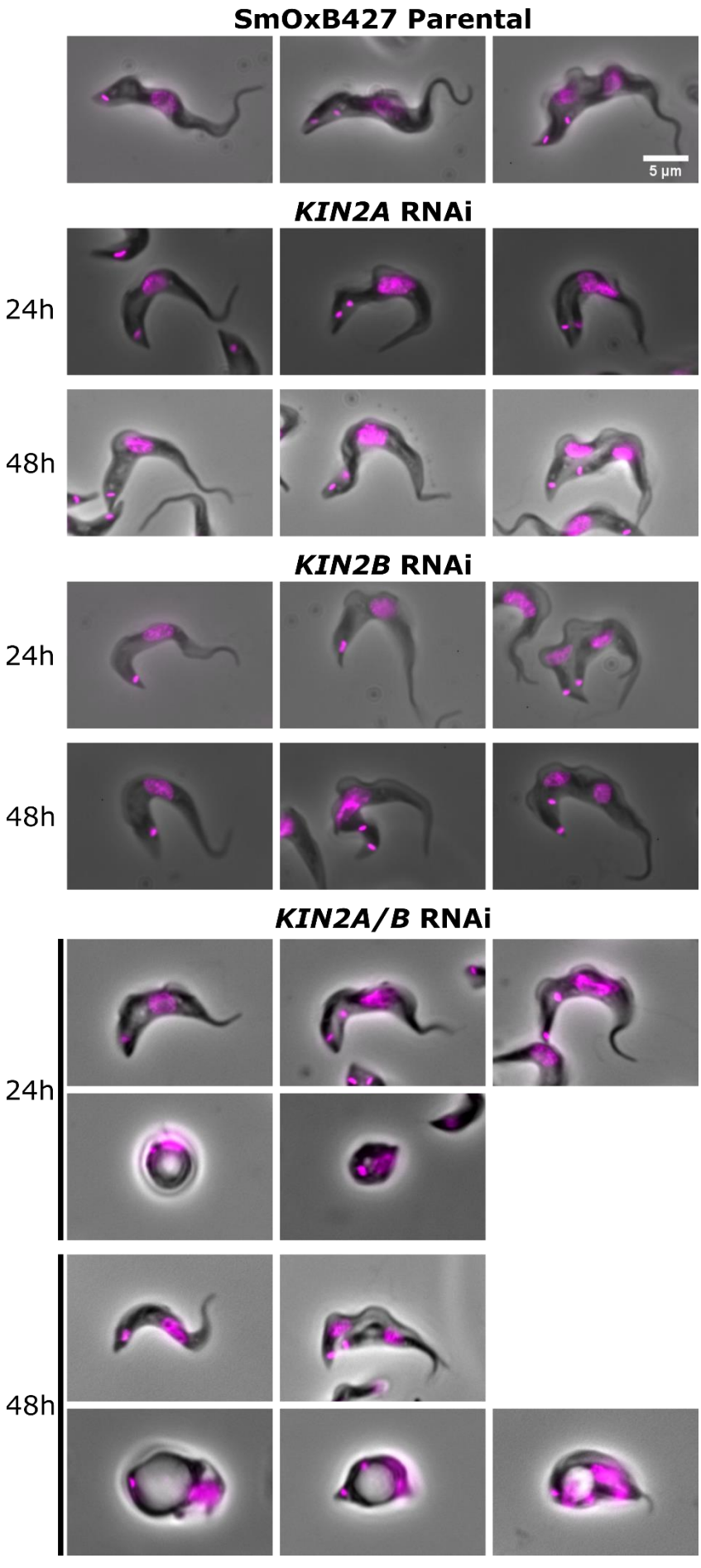

SmOxB427 Parental
5 µm
KIN2A RNAi
24h
48h
KIN2B RNAi
24h
48h
KIN2A/B RNAi
24h
48h

Figure 23. Microscopy of representative cells after induction of RNAi against kinesin-2s. RNAi was induced against, KIN2A, KIN2B and KIN2A/B for 24 or 48 hours. Cells were attached to derivatised slides and stained with DAPI. Images of representative cells were then produced.

4.1.5. *KIN2A/B* knockdown prevents normal flagellum synthesis

Round cells appeared to lack flagella when viewed under a microscope. Furthermore, rounding itself suggests failure of flagellum synthesis, as the flagellum has an important role in determining cell shape in trypanosomes. To determine whether round cells were producing flagella, cells were analysed by immunofluorescence with an antibody recognising the PFR1 and 2 (paraflagellar rod protein 1 and 2) proteins. PFR1 and 2 are a major component of the paraflagellar rod, a structure found in kinetoplastid flagella that interacts with the axoneme and is essential for flagellar function (Bastin et al., 1998; Deflorin et al., 1994; Gadelha et al., 2004). The paraflagellar rod is synthesised in concert with the axoneme (Bastin et al., 1999), so staining of the rod is a good proxy for staining of the whole flagellum. Staining of normal cells produced signal that extended along the length of the flagellum (Figure 24A). Signal from round cells (Figure 24B) suggested that these cells had very small flagella, or lacked flagella altogether. I also observed dividing cells, in which only one flagellum was observed (Figure 24C), indicating that synthesis of a new flagellum had not occurred. These results show that knockdown of both KIN2A and KIN2B in combination prevents synthesis of new flagella. This is expected due to the role of kinesin-2 proteins in IFT, the phenotypes observed having been caused by defects in this process.

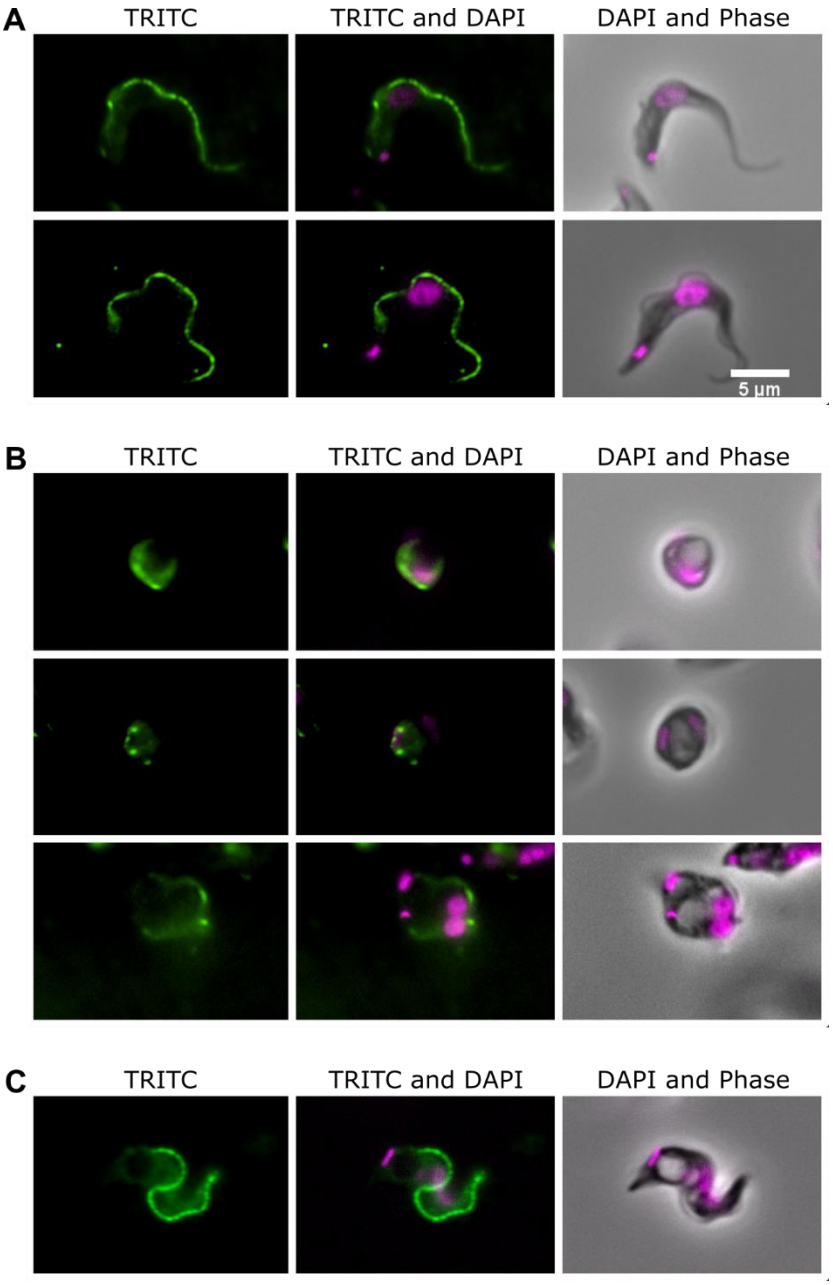


Figure 24. Round cells (B) do not form full length flagella as seen in normal cells (A). Lack of synthesis of new flagella can also be observed in dividing cells (C). Cells were induced for RNAi against KIN2A/B for 24h and attached to derivatised slides. Cells were stained with the L13D6 antibody and a TRITC labelled anti-mouse secondary and DAPI.

4.1.6. Summary

In previous genome-wide RNAi experiments knockdown of kinesins was not found to have a significant impact on cell growth in *T. brucei*. Many of these kinesins, however, have been shown to be important for cell survival in trypanosomes or in model systems in other studies. These discrepancies could be explained by interactions that occur between kinesins, particularly redundancy. By knocking down kinesin-2 proteins in *T. brucei* individually or in combination, I have demonstrated the role these kinesins perform in IFT and that redundancy exists between the two. Adverse phenotypes were only observed when both kinesin-2 proteins were knocked down in combination, providing evidence of this redundancy. It is likely that similar interactions occur between other trypanosomal kinesins and these interactions will, therefore, need to be accounted for when producing an RNAi library for future experimentation.

4.2. Generation of combinatorial libraries

4.2.1. A method for generating libraries of random pairwise combinations for use in RNA interference

I have shown that redundancy exists among kinesin proteins in *T. brucei* and that this can affect the growth phenotypes observed after RNAi. To screen kinesins by RNAi, it would be useful if this redundancy could be accounted for. A solution to this issue would be the production of RNAi libraries containing pairwise combinations of kinesin CDSs.

I designed a strategy for the production of a pairwise combinatorial RNAi library (Figure 25). The CDSs of all 47 kinesin or kinesin-like proteins are produced by PCR and equal masses of PCR product are mixed. The mix is sonicated to produce random ~200bp fragments. Due to having been mixed in equal mass, all kinesin sequences are expected to be represented by an equal number of fragments. The fragments are end-repaired to produce blunt-ends and two different "linker" sequences added. One linker contains a restriction endonuclease site for the purposes of linking fragments, to produce the pairwise combinations. These combinations are expected to contain random combinations of fragments in random orientations, due to the blunt-end ligation of linkers. The second linker contains a second endonuclease site, so that linked fragments can be inserted into an RNAi plasmid, producing the plasmid library.

Though fragments will require two different linkers, in order to be both linked and inserted into plasmids, it is likely that significant proportions of the library will have a single linker at both ends, due to the use of blunt end ligation. The strategy for producing the library will, therefore, include an additional vectorette PCR step, before fragments are linked. Using this approach, in combination with size selection, it is possible to amplify fragments with two different linkers, by PCR, so that the library can be modified to exclusively include fragments that carry both linkers (Figure 26). This methodology, involves the use of a linker that includes an incompatible region and an endonuclease site (linker B) and a linker without this region and a second endonuclease site (linker A). In

the first step of PCR (Figure 26B), DNA strands can only be produced by primers that bind to linker A. This creates a region complementary to the incompatible region in linker B that a second primer binds to, to produce a second strand (Figure 26C). Until the first stage of PCR, the second primer is incapable of binding to anything and dsDNA is not produced. This strategy is not perfect, however. It is possible for PCR product to be produced from template that carries linker A at both ends, because both ends will bind the first primer. To overcome this, linker A and linker B can be ligated to library fragments in a 1:4 ratio, to reduce the number of fragments with two copies of linker A to ~5% of fragments.

It would be helpful to produce combinations of greater than two, to account for interactions that might occur between greater numbers of kinesins. Such combinations are unfortunately unfeasible due to the limited read lengths produced by next generation sequencing. It is likely that in combinations of three sequences, for example, the central fragments would be left unsequenced, as the reads would not extend from the barcoded regions outside the fragments to the centre of the combined fragments.

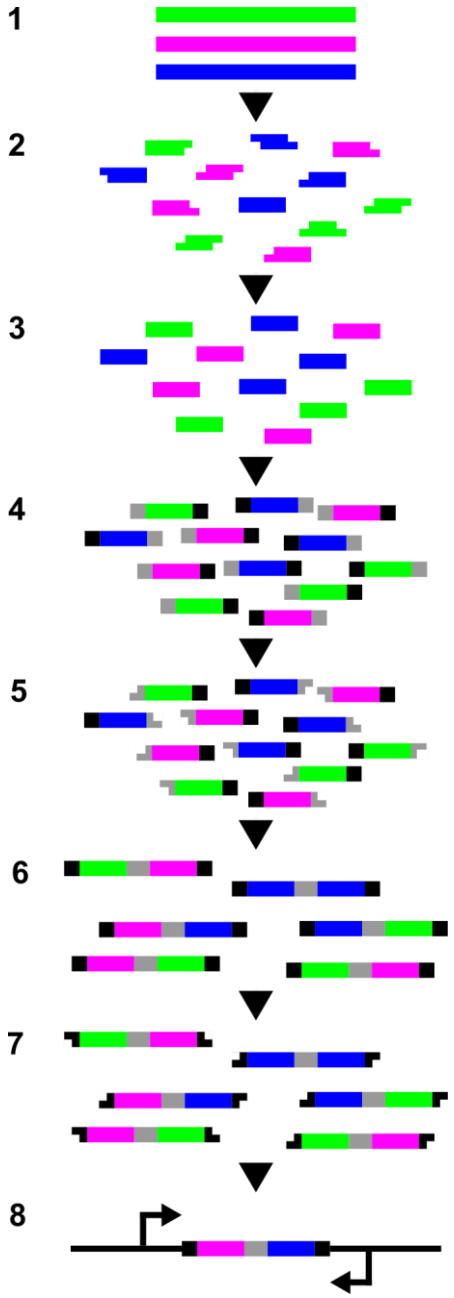


Figure 25. Library assembly schematic (not to scale). CDSs (1) are sheared into 200bp fragments by sonication (2). Ends are repaired (3), so “linker” sequences can be blunt end ligated onto the fragments (4). Linkers are digested with a restriction endonuclease, recognising a site on one linker (5), and fragments ligated together (6). After the digestion with another enzyme (7), the sequence combinations can be inserted into an RNAi vector (8), containing two promoters, for dsRNA production.

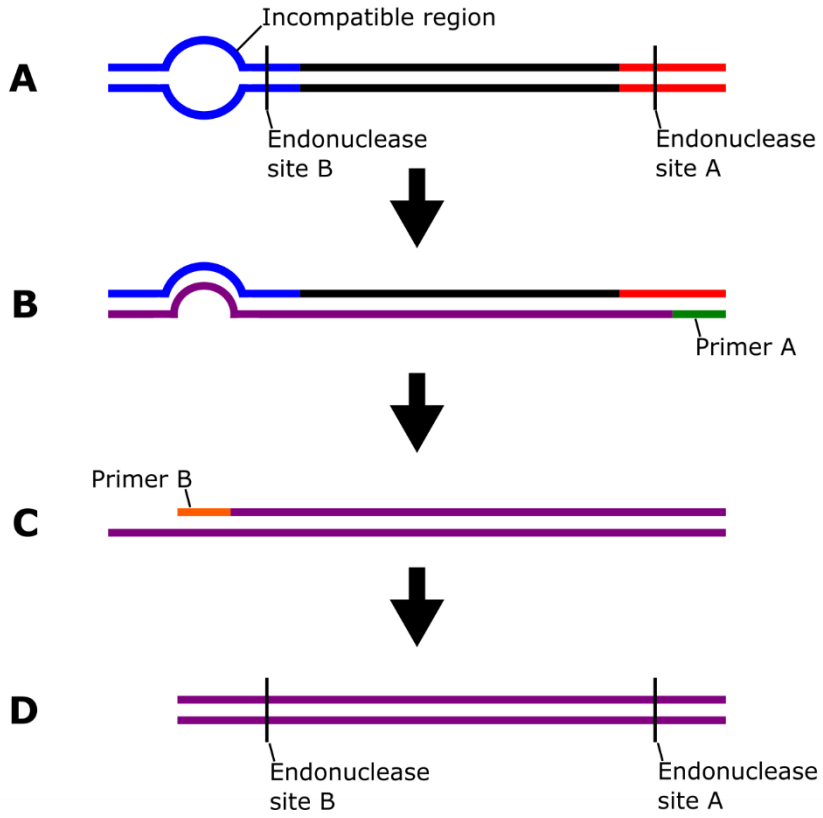


Figure 26. A vectorette PCR strategy for production of library fragments with the desired linkers. A fragment carries two different linkers (A), and linker A and linker B, which carries an incompatible region. When primer A anneals to the linker A in the first round of PCR (B), it produces a strand with a region compatible to the incompatible region in linker B. Primer B can only bind to this new region (C) and, therefore, amplification occurs when both linkers are present.

4.2.2. Producing the kinesin combinatorial library

I aimed to produce a library that would contain the CDSs of all 47 kinesin or kinesin-like proteins in *T. brucei*, as well as the three cytoplasmic dynein heavy chains. Dyneins were included to act as a control and in order to discount them from roles in mitosis. In order to produce CDSs for use in the library, PCR was performed. Primers were designed that would amplify sequences from *T. brucei* TREU927 genomic DNA (Electronic Appendix). If a sequence was greater than 3kb, primers were designed to produce 2.5 to 3kb, otherwise the whole sequence was amplified (Figure 27). The amount of DNA produced was determined by spectrophotometry, so that an equal mass of all sequences could be mixed for random library production.

The PCR product, described above, was sonicated to create fragments of ~200bp (Figure 28A). Fragments were repaired with Klenow and linkers attached by blunt end ligation. The first linker contained the incompatible region and an SfiI site, while the second did not and contained an AvrII site. AvrII was chosen due to its absence in kinesin sequences, while SfiI was chosen due to its non-palindromic cut sites, preventing self-closing. The linkers were also non-phosphorylated to prevent them from ligating to each other. SfII linkers, AvrII linkers and fragments were ligated in a 20:4:1 ratio. The DNA was then gel extracted to remove any linkers that had not ligated and to remove any fragments that had been ligated to each other (Figure 28B). SfiI linkers were also ligated alone so that a single fragment library could be added to the combinatorial library, to ensure full coverage of every single fragment and to provide a comparison for knockdown results later on. Vectorette PCR was then performed to specifically amplify fragments with the correct linkers attached. Fragments with SfiI and AvrII linkers were digested with AvrII and ligated to link fragments and form “double” fragments. The resulting linked fragments were then size selected (Figure 28C) and cut with SfiI. “Single” fragments were ligated into p2T7-177δ and “doubles” into p2T7-177γ. These RNAi plasmids contain two tetracycline inducible T7 promoters for production of dsRNA and integrate into

minichromosomes. The δ and γ forms of the plasmid differ only in their multiple cloning sites.

Ligation of either size-selected “double” or “single” fragments into p2T7-177 derivatives produced libraries consisting of an estimated 1.6×10^7 independent clones 1.5×10^5 independent clones, respectively. This provided a coverage of every possible combination of motor of ~12,000× and coverage of individual motors of ~3,000×. To confirm fragment insertion test digests were performed on plasmids (Figure 28D). A digest was designed using NotI, XhoI and EcoRI, that would drop out the fragments, as well as 508bp of 5’ plasmid DNA and 27bp of 3’ plasmid DNA, which can be seen as a ~750bp or ~1,000bp band on the gel. When AvrII is added to the doubles test digest, the band drops by ~200bp, suggesting a double fragment has been cut in half. These digests, therefore, confirmed that single and double libraries had been produced by the described methodology and that these libraries contained the correct number and size of fragment.

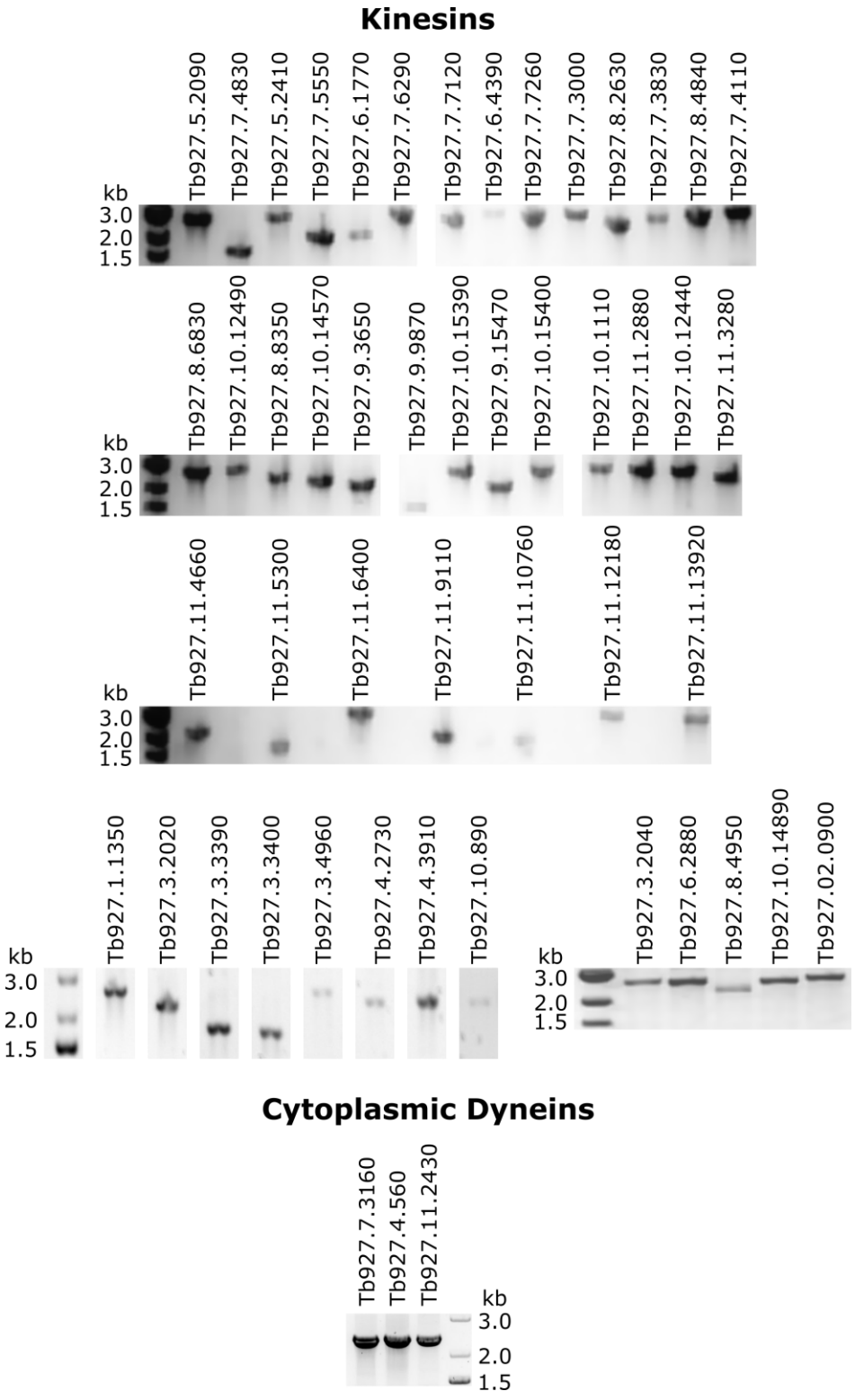
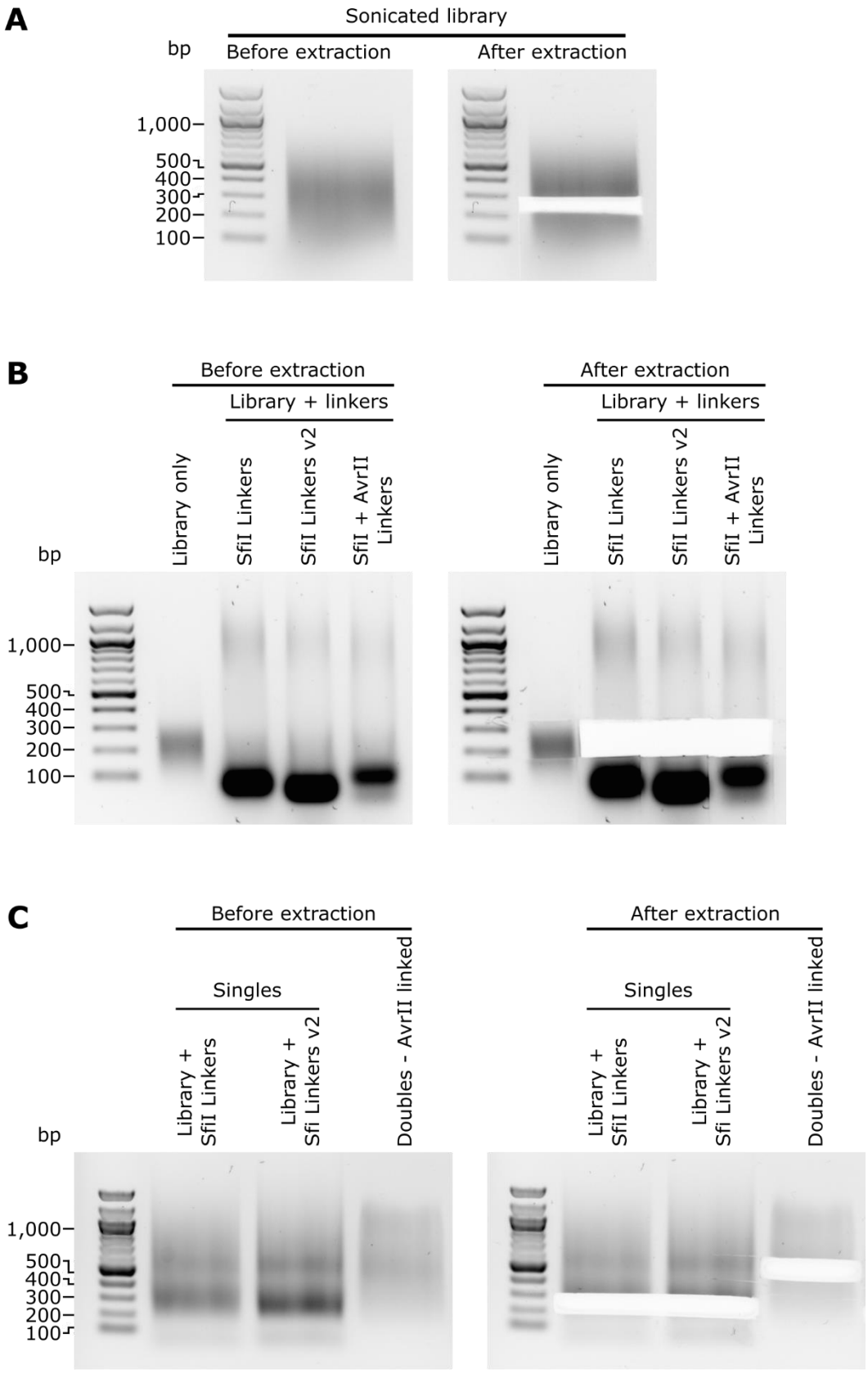


Figure 27. Production of kinesin and dynein heavy chain CDSs. Touchdown PCR was used to produce kinesin and cytoplasmic dynein heavy chain CDSs, or 2,500 to 3,000bp of a CDS if it exceeded 3,000bp. PCR product was run on agarose gels to confirm.


A
Sonicated library
bp
Before extraction
After extraction
1,000
500
400
300
200
100
B
Before extraction
After extraction
Library + linkers
Library + linkers
Library only
SfiI Linkers
SfiI Linkers v2
SfiI + AvrII Linkers
bp
1,000
500
400
300
200
100
C
Before extraction
After extraction
Singles
Singles
Library + SfiI Linkers
Library + Sfi Linkers v2
Doubles - AvrII linked
bp
1,000
500
400
300
200
100

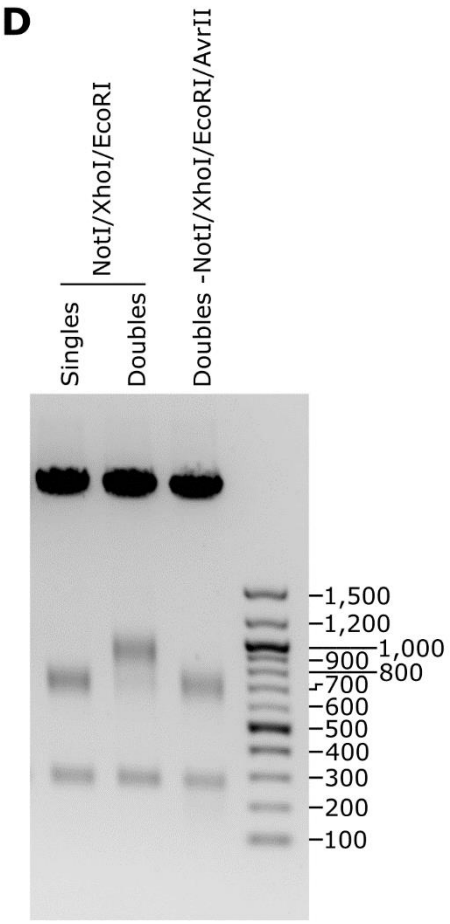


Figure 28. Library production. Kinesin and dynein CDSs were sonicated to fragment them and a 200-300bp band gel extracted (A). Fragments were repaired with Klenow and "linker" sequences blunt-end ligated onto them (B). DNA was extracted to remove linkers that had ligated to themselves and fragments with more than two linkers. Vectorette PCR was performed to produce a library with the correct linkers. Fragments with AvrII linkers were disgested with AvrII and ligated to produce doubles (C). Single and double fragments were then ligated into RNAi plasmids. Test digests were then performed on plasmids to confirm fragment insertion (D).

4.2.3. The pan-kinesin library contains all possible pairwise combinations

To test the effectiveness of the library strategy and overall coverage, microtubule motor CDS fragments from the plasmid library were sequenced. Fragments were amplified from the "doubles" and "singles" libraries using primers that added Illumina adapters. "Doubles" and "singles" PCR products were mixed 9:1 and sent for sequencing by Illumina MiSeq (75bp paired end reads). ~23.2×10^6 read pairs were returned, of which ~22.9×10^6 passed quality control.

89% of the reads could be uniquely mapped to TREU927 kinesin and dynein CDSs (4% mapped to more than one CDS and 7% remained unmapped).

To confirm that libraries were made up of the desired fragment size of ~200bp, analysis of the sizes of insert fragments in the "singles" library was performed (Figure 29). Paired reads were mapped to the genome and the distance between the reads calculated. Reads that were separated by less than 500bp and were orientated so that forward and reverse reads faced each other were identified as single fragments and the distance between them plotted. Insert size ranged between 60 and 320bp and followed a bell-shaped distribution. The most common fragment size was 160-180bp. This is slightly smaller than the expected fragment size of 200bp, showing the difficulties in extracting DNA of specific size, but is still suitable for use in RNAi. Since the "doubles" library was produced from these fragments, it is expected that the distribution of fragment sizes in these plasmids follows a similar profile.

Reads were mapped to kinesin and dynein genes, to determine how they were distributed and whether there were any biases for particular regions of genes (Figure 30). There is some variation in how well represented regions of individual genes are, but good coverage overall. This variation may have been caused by skewed amplification of AT and GC rich regions that can occur in PCR. As Illumina sequencing technologies are based on PCR they can be influenced by this. It is also possible that this variation was caused by how easily regions were sheared. For the majority of genes there is an overrepresentation of reads at the beginning (in the forward orientation) and end (in the reverse orientation) of the sequence. These spikes in frequency are expected of the method used to generate the library. When linear DNA, such as kinesin coding sequence amplified by PCR, is fragmented by sonication, sequences towards the ends will always be adjacent to an end after fragmentation. There is a greater chance that these sequences will be cloned and be present within sequencing reads and they will, therefore, be overrepresented.

Next, mapping of forward and reverse reads was compared. All possible combinations of kinesins and dyneins were present in the library. As expected from the 9:1 ratio of input DNA (expected to give ~1:5 ratio between any one combination and single fragment), Figure 31 demonstrates that “singles” were found more often than any combination. Here reads from “singles” are displayed as combinations of the same kinesin, as the analysis did not differentiate between the two. Considering only pairs for which the forward and reverse read mapped to different kinesins (Figure 32) shows there is some variation in the number of reads for individual combinations. Some combinations are represented by as little as ~15× fewer reads than the most abundant combinations. Although the least well represented combinations appear in small numbers, they suggest a minimum library coverage of ~15-20× exists, within the small portion of the library that was analysed (<2%).

A small number of combinations in the library correspond to a very high number of reads, suggesting they are highly overrepresented in the library. Combinations of Tb927.3.3990 and Tb927.3.3400, both of which are kinesins specific to trypanosomatids (Wickstead and Gull, 2006), are apparently very overrepresented. This can be explained by the two kinesins’ sequence similarity. The CDSs of Tb927.3.3990 or Tb927.3.3400 align very closely and, therefore, a fragment of either CDS in the “singles” library could be assigned as a combination of the two, resulting in this apparent overrepresentation. This also explains the levels of Tb927.4.3910 and Tb927.8.8350 combinations, which are overrepresented to a lesser extent. These sequences code for KIN13-4a and KIN13-4b, respectively, and align well, causing a similar issue with read assignment.

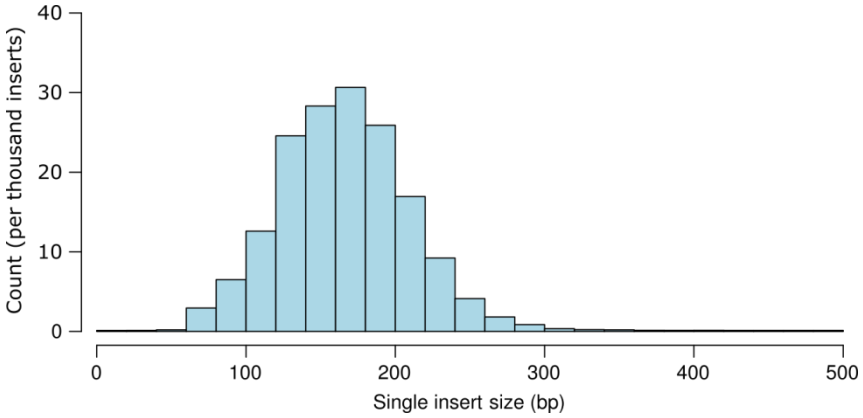


Figure 29. Library fragment size analysis. Read data was used to determine the sizes of single CDS fragments throughout the library.

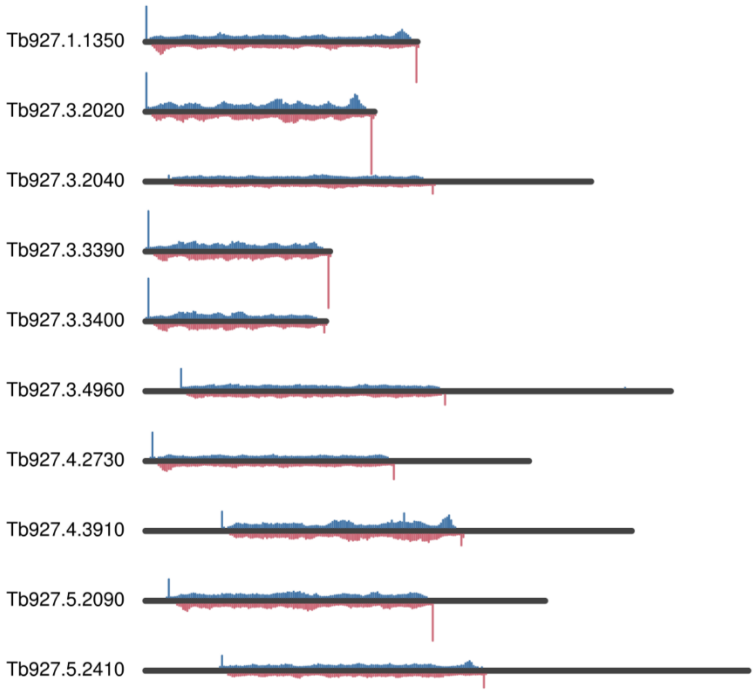


Figure 30. Examples of fragment distribution analysis. 40,000 randomly selected read pairs were mapped to kinesin and dynein CDSs and the numbers of reads corresponding to a specific region of a CDS plotted. Bars representing 10bp of a gene are mapped to representations of that gene, the height of the bar representing the number of reads that map to that region. The colour of the bar represents the direction of the read, with blue representing forward reads and red representing reverse reads.

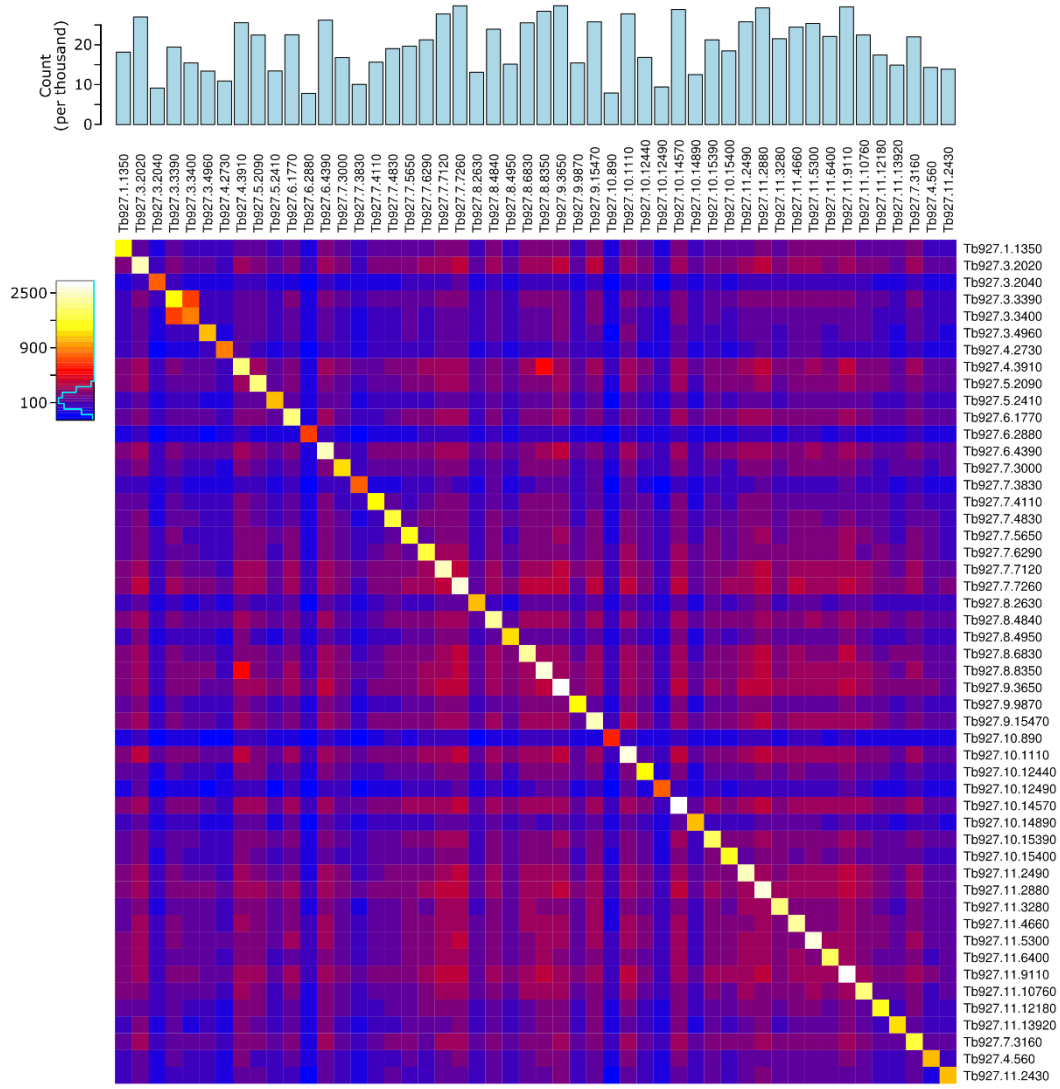


Figure 31. Library coverage analysis. For 40,000 randomly selected read pairs the number of reads representing combinations of fragments and single fragments was determined. The number of reads was used to produce a heat-map of all possible combinations, with blue representing fewer reads produced and white representing a greater number of reads.

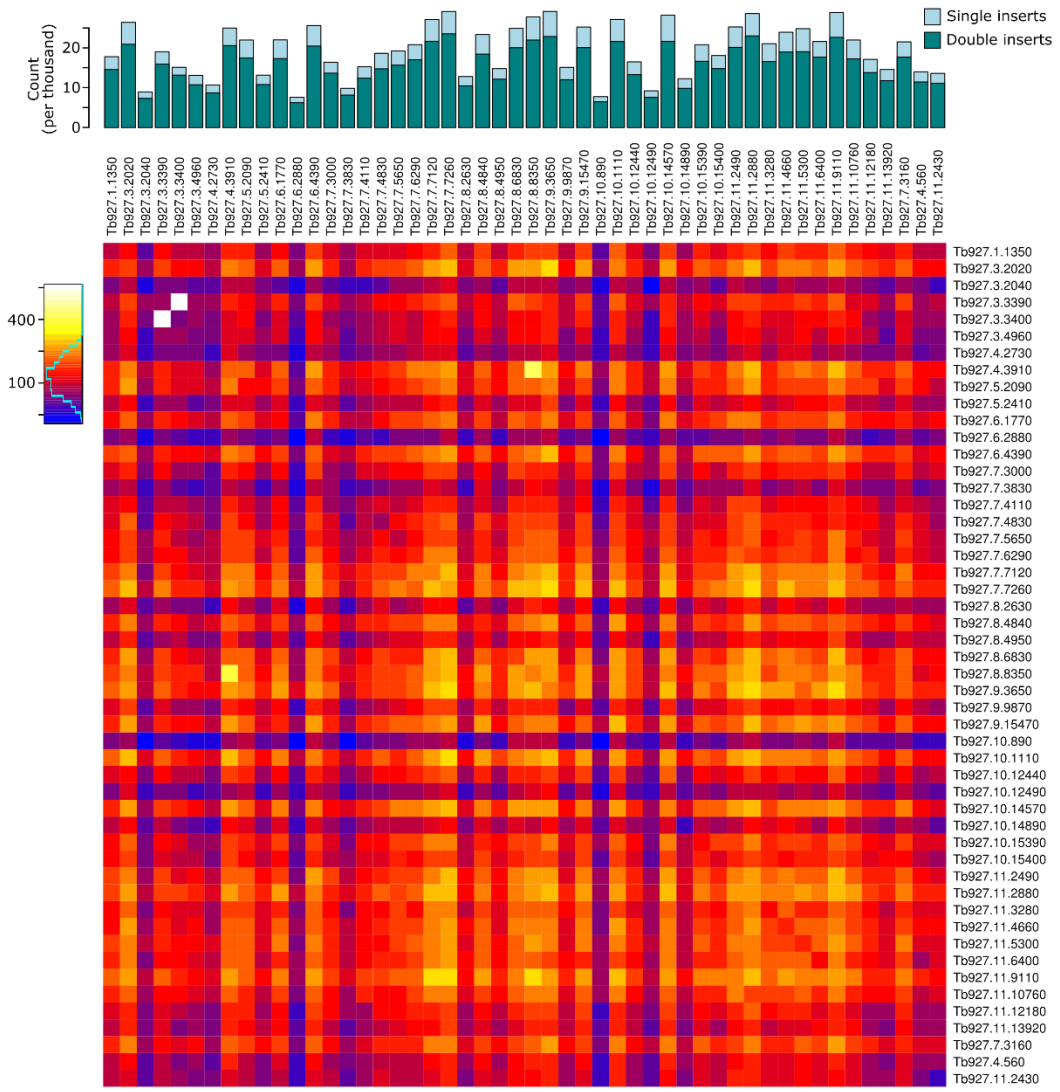


Figure 32. Doubles coverage analysis. The number of reads representing combinations of fragments only was determined. The number of reads was used to produce a heat-map of all possible combinations, with blue representing fewer reads produced and white representing a greater number of reads.

4.2.4. Cells expressing hairpin RNA sequences do not phenocopy individual kinesin knockdown

The strategy for generation of the combinatorial library, presented here, produces random combinations of fragments in varying orientations. This creates the possibility that combinations might be generated that contain the same fragment in the reverse orientation, i.e. hairpins. Hairpin constructs, which form dsRNA by intramolecular folding, are believed to be more effective for knockdown of the targeted mRNA than head-to-head constructs, although there is little experimental data that directly address this. RNAi constructs that produce RNA hairpins when transcribed have been used for RNAi in model systems in the past (Agrawal et al., 2003), but this practice has since been largely superseded by the introduction of siRNAs by various delivery systems. Similar hairpin producing constructs have also been used in *T. brucei* (Kalidas et al., 2011; Shi et al., 2000).

In order to investigate the effects of RNA hairpins on kinesin RNAi in *T. brucei*, two more kinesin-2 RNAi plasmids were produced. They contained a pairwise combination of the *KIN2A* or *KIN2B* fragment, used previously, orientated so that a hairpin would be formed when transcribed. These constructs were transfected into SmOxB427 cells and three clones selected. In the case of *KIN2A*, however, only one survived. Knocking down KIN2B using a hairpin significantly limited cell growth ($p=0.009$; K-S test), although cells began to recover after 72 hours (Figure 33)

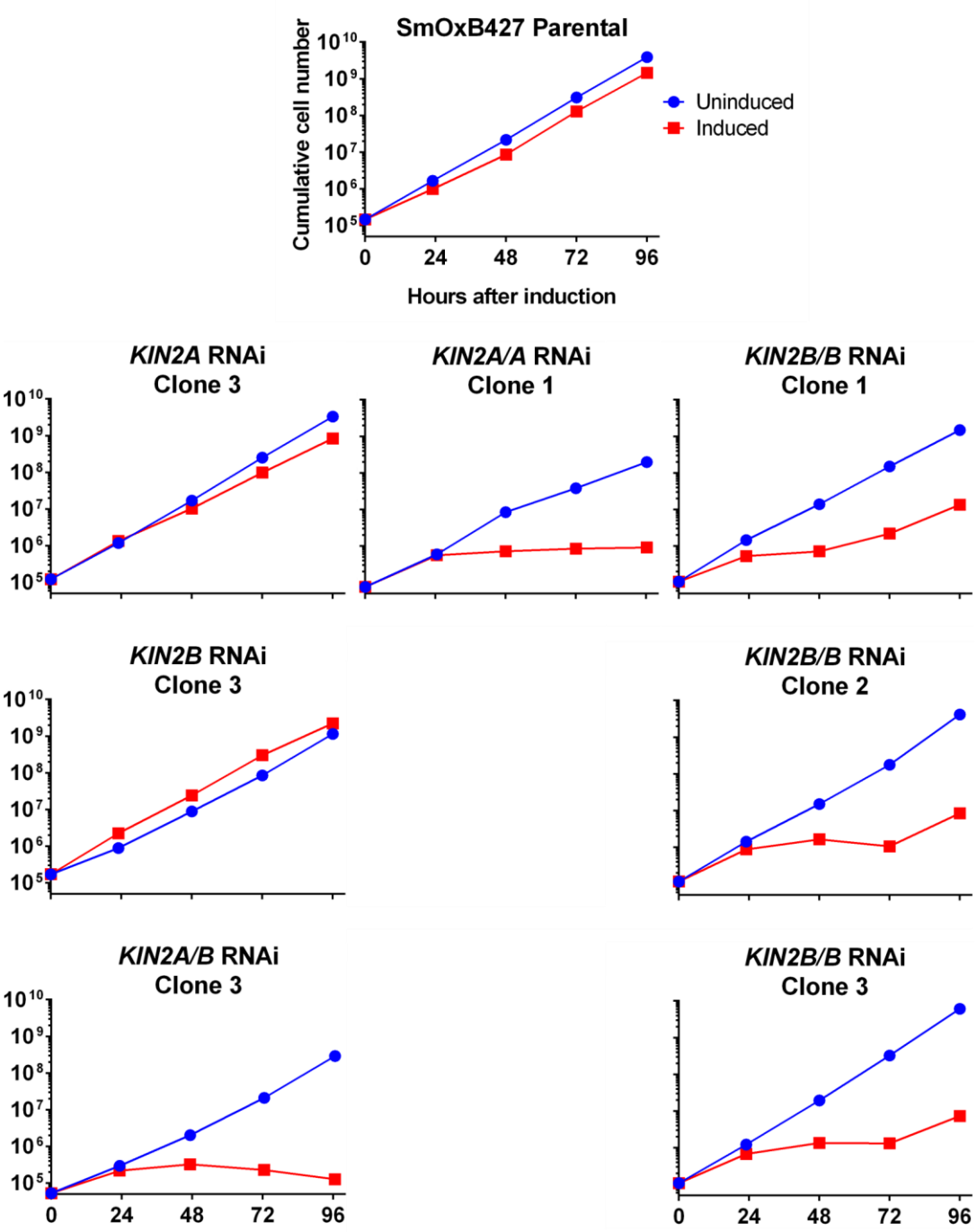


Figure 33. Knockdown of individual kinesin-2s using RNA hairpins temporarily limits cell growth. RNAi was induced against KIN2A and KIN2B, using hairpin constructs, for 96 hours and cells counted every 24 hours. These counts were then used to calculate cumulative cell number. Examples of previous results are included for comparison.

4.2.5. Hairpins have a greater effect on the trypanosome cell cycle

To determine the effect of hairpin RNAi on the trypanosome cell cycle, K-N counts were performed. These counts are presented in Figure 34 and a breakdown of these counts, as bubble plots, in Figure 35. In Figure 34, an increase in the number of 2K2N and >2K2N cells can be observed during *KIN2B/B* RNAi. Over time these >2K2N cells contain increasing numbers of kinetoplasts and nuclei (Figure 35). An increase in 2K2N cells suggests cells have properly segregated replicated kinetoplast and nuclear DNA, but have stalled at cytokinesis. Increases in cells with even greater numbers of kinetoplasts or nuclei suggests further attempts at division in stalled cells. Furthermore, no rounding of cells was observed during *KIN2B/B* RNAi (data not shown). The growth defect ensuing from KIN2B/B knockdown is, therefore, the result of a very different phenotype to that produced by KIN2A/B knockdown.

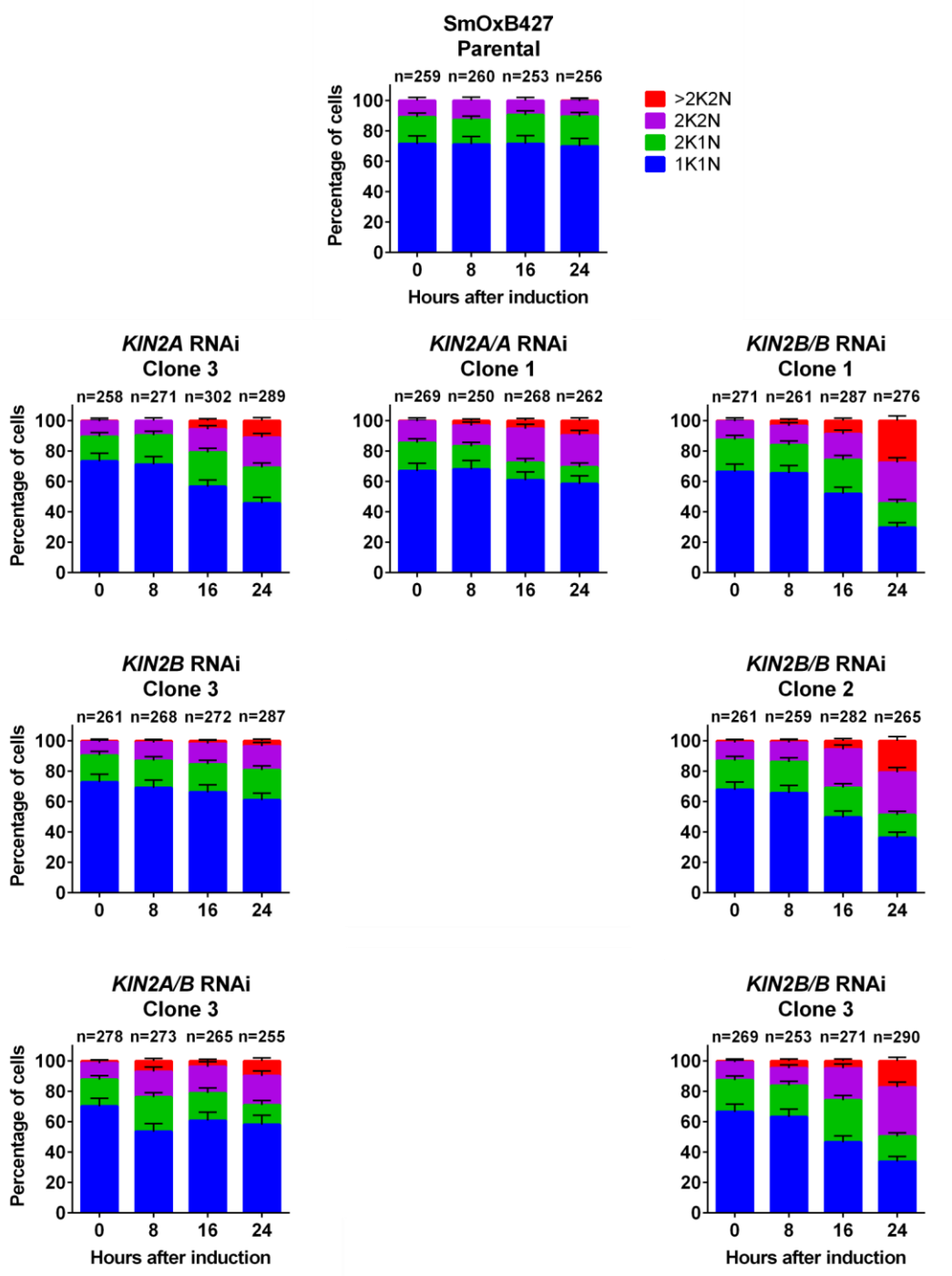
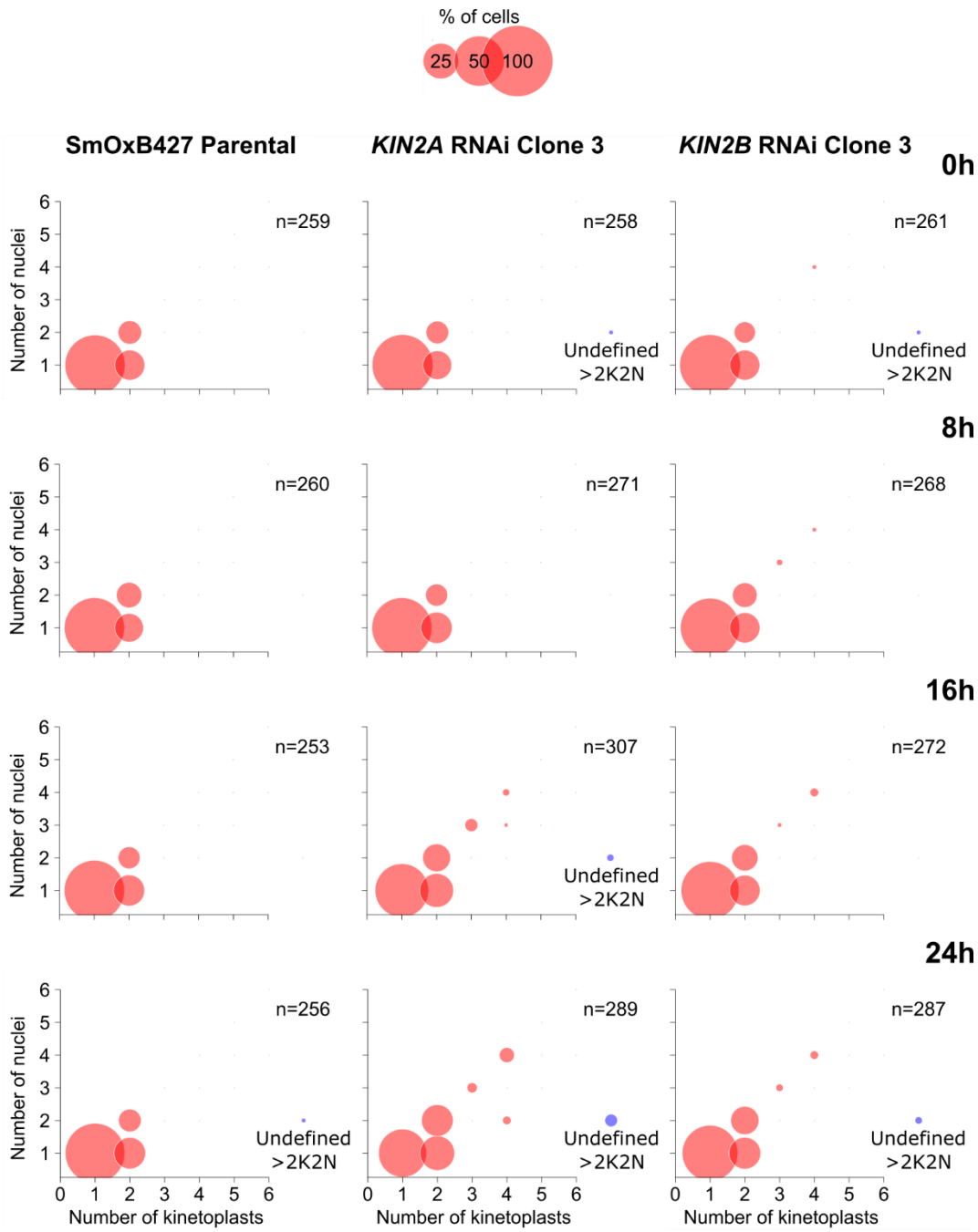


Figure 34. RNAi against single kinesin-2s using hairpins causes cytokinesis defects. RNAi using *KIN2A/A* and *KIN2B/B* template was induced for 0, 8, 16 and 24 hours. Cells were attached to derivatised slides and stained with DAPI. Using fluorescence microscopy, the number of kinetoplasts and nuclei per cell was then counted.


% of cells
25
50
100
SmOxB427 Parental
KIN2A RNAi Clone 3
KIN2B RNAi Clone 3
0h
8h
16h
24h
Number of nuclei
Number of kinetoplasts
n=259
n=258
n=261
n=260
n=271
n=268
n=253
n=307
n=272
n=256
n=289
n=287
Undefined
>2K2N

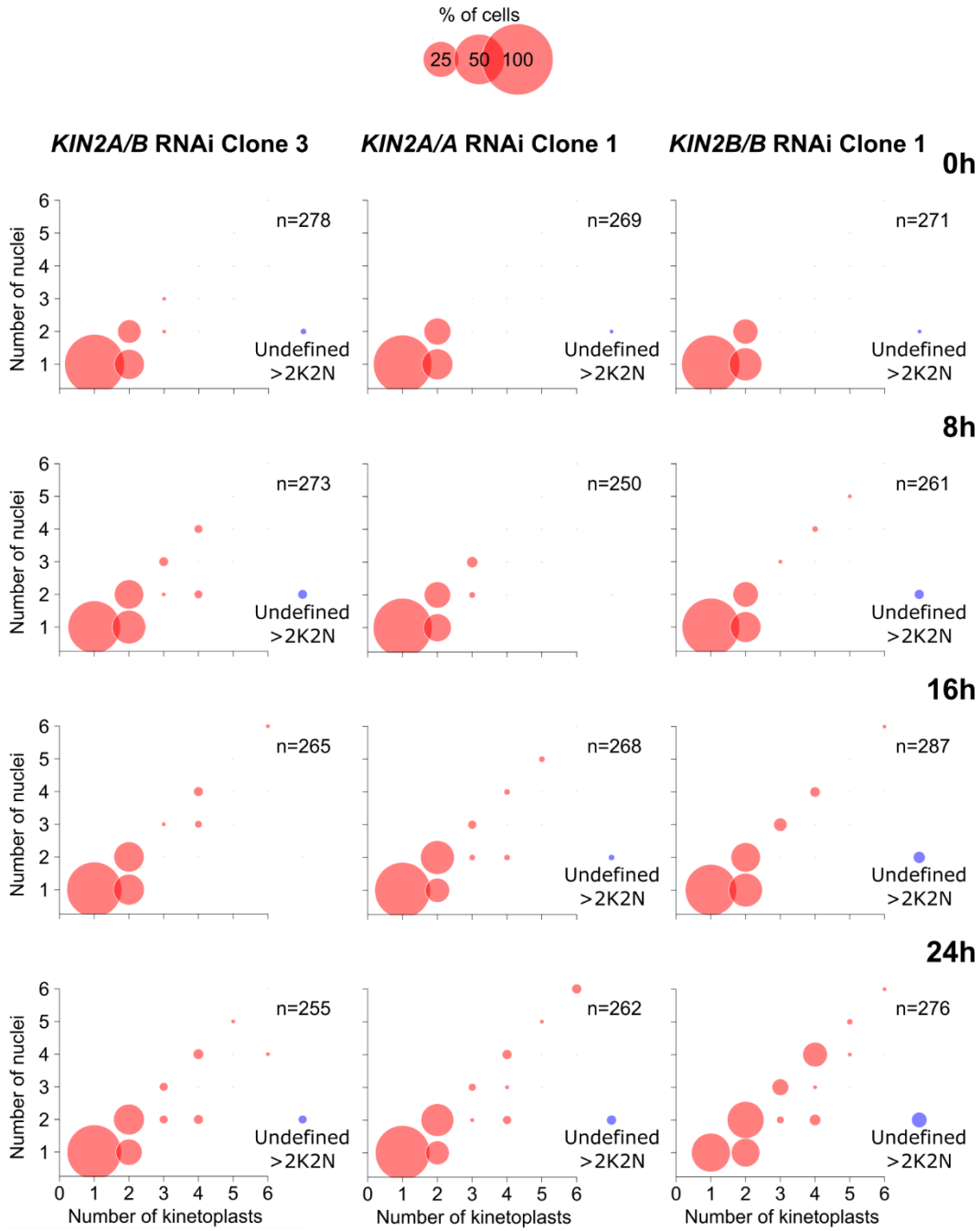


Figure 35. *KIN2B/B* RNAi increases the number of kinetoplasts and nuclei in cells in a time-dependent manner. KN count data was replotted as bubble plots, to demonstrate the distribution of kinetoplasts and nuclei within the cell population and its change during RNAi. The size of the bubble represents the number of cells with a particular number of kinetoplasts and nuclei, which are plotted on the x- and y-axes, respectively.

4.2.6. Hairpins should be excluded from library analysis

The data presented above shows that knockdown of individual kinesin-2 proteins produces a more severe phenotype when hairpin RNA sequences are produced. Hairpins produced a significant growth phenotype, caused by cytokinesis defects, when RNAi using a head-to-head construct, based on the same template, did not. This is likely due to an increase in the efficiency of siRNA generation and, therefore, the efficiency of RNAi.

The fact that hairpins can produce more extreme phenotypes has implications for the combinatorial library experiment. The method by which the library was generated means that there is a possibility that constructs exist within the library that would produce hairpin RNAs when induced. If hairpins are present in the library, they will likely skew induced cell reads produced by next generation sequencing, through increased phenotype effects, impacting the mean change in reads for the kinesin they represent. Due to random nature of fragment production, fragments with identical sequences are unlikely. Sequence similarity between fragments, however, is possible, so, depending on the extent of sequence overlap, hairpins could still be produced. The sheer number of fragments involved in producing the combinatorial library, should limit the number of combinations that can form hairpins. If hairpins are present, however, read data produced by the library screen can be examined for their presence and any related reads eliminated from any further analysis. This can be done by identifying paired end reads that map less than 200-250bp apart with forward and reverse reads orientated in the same direction.

The more severe phenotypes produced by hairpins also have implications for RNAi in trypanosomes. When knocking down proteins in trypanosomes, head-to-head constructs are commonly used to produce dsRNA. Data presented here suggests that use of hairpin constructs has a significantly greater impact on phenotype than head-to-head constructs, when using identical sequences as template and identical RNAi plasmids. It is likely that dsRNA and, therefore, siRNAs were produced with greater efficiency in these cells and led to greater

knockdown of the target mRNA. An increase in off-target effects could also have caused differing phenotypes, though these are uncommon in RNAi in trypanosomes. The effects of the different constructs on protein knockdown, both target and off-target, were not tested, however, due to lack of antibodies or the necessary cell lines. Clearly more research on efficacy of hairpin RNAi constructs in direct comparison to head-to-head constructs is required.

4.2.7. Summary

The data I have presented previously demonstrate that interactions between kinesins in trypanosomes do indeed exist and that these interactions need to be accounted for when producing an RNAi library. A combinatorial RNAi library was produced for this very purpose and was shown to contain all possible combinations of kinesin (and cytoplasmic dynein heavy chain) CDSs, though the relative abundances of each combination did vary. Though the library was designed to produce head-to-head RNAi constructs, the random nature of library production creates the possibility that hairpin constructs might exist. I have also shown that such hairpins could have a significantly different effect on phenotype, when used for RNAi, and so need to be accounted for in any following work.

5. “Reporter” cell lines for library analysis

5.1. A negative selection marker for chromosome loss

To investigate the roles of microtubule motors in trypanosome mitosis, the combinatorial RNAi library developed in Chapter 3 could be used in an experiment designed to determine how knockdown of motors impacts on chromosome segregation, as well as an experiment similar in procedure to the original RIT-Seq experiment. The library will be used in two experiments, one designed to investigate the impact of motor combinations on fitness (Figure 36A) and another designed to detect the loss of chromosomes, using a negative selection marker (Figure 36B).

5.1.1. *HSV-TK* as a negative selection marker in trypanosomes

Knockdown of motor proteins involved in mitosis is likely to cause nondisjunction events and, therefore, the missegregation of chromosomes, resulting in daughter cells that lack the full complement of chromosomes. Chromosome loss could be detected using a “reporter” cell line containing a chromosome tagged with a negative selection marker, so that cells that have lost the tagged chromosome can be selected for. One such selection marker is herpes simplex virus thymidine kinase (HSV-TK). Expression of the HSV-TK enzyme in animal and plant model systems induces sensitivity to nucleoside analogues, such as ganciclovir and other acyclovir derivatives, which act as inhibitors of DNA replication (Czakó and Márton, 1994; Mansour et al., 1988). Phosphorylation by the viral kinase produces the monophosphate form of these analogues and subsequent phosphorylation by cellular kinases produces the triphosphate, which inhibits DNA polymerases and causes cessation of chain elongation. HSV-TK has been applied as a negative selection marker in both *Leishmania major* and *Trypanosoma brucei* (LeBowitz et al., 1992; Valdés et al., 1996). When expressed in procyclic form (PCF) *T. brucei*, HSV-TK causes cell growth to be limited by 10µM ganciclovir and population decline to occur at 100µM (Valdés et al., 1996). The HSV-TK marker has been used to select for *T. brucei* cells that had switched their VSG coat (Cross et al., 1998), for example, and to produce double TOPO3α

knockouts using a single construct, to investigate its role in antigenic variation (Kim and Cross, 2010).

The experiment described in Figure 36B will use a reporter cell line in which a minichromosome (MC) is tagged with HSV-TK. Megabase chromosomes (MBCs) of *T. brucei* contain housekeeping genes and the loss of just one is detrimental to cell survival. Cell death caused by MBC loss will be detected as population decline in the experiment described in Figure 36A, but will be indistinguishable from population decline caused by other defects. The transcriptionally silent MCs, on the other hand, do not contain housekeeping genes and exist to carry a portion of the VSG library. They are, therefore, not essential for cell survival. The expression of HSV-TK from a MC will allow loss of this chromosome to be selected for (Figure 36B), in cells that do not lose MBCs during segregation defects, and for investigation into how motors contribute to chromosome segregation. *HSV-TK*, however, has never been integrated into the silent MCs, all previous work has involved incorporating the gene into MBCs. It was, therefore, necessary to optimise *HSV-TK* constructs for use in MCs, to test sensitivity to ganciclovir in cells expressing HSV-TK from MCs and to test whether HSV-TK could be used for the detection of MC loss.

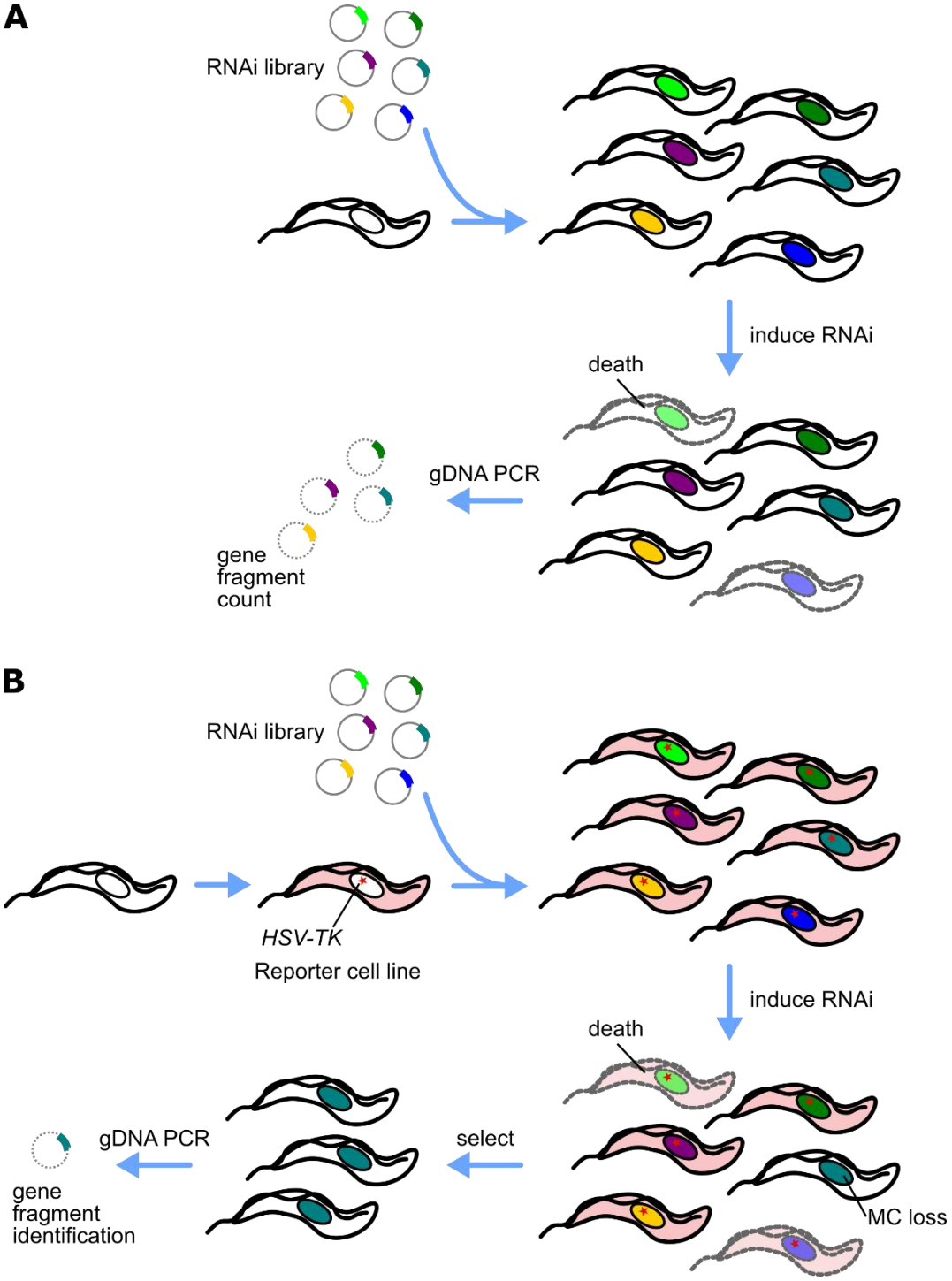


Figure 36. Two strategies for RNAi library investigation. In the first (A), a competition assay, populations of cells containing the library are induced for RNAi, or left uninduced. After RNAi, genomic DNA is purified and library inserts sequenced using next generation sequencing. Changes in the proportions of library fragments, between induced and uninduced populations, can be used to determine how the knockdown of kinesins impacts cell growth. In the second experiment (B), cells are induced and negative selection performed, using *HSV-TK*/ganciclovir, to select for cells that have lost MCs. The library fragments from these cells are then sequenced, to determine knockdown of which kinesins caused chromosome segregation defects. Figures adapted from figures provided by Bill Wickstead.

5.1.2. Transcriptionally active *HSV-TK* can be targeted to minichromosomes in bloodstream form cells

To generate cells that expressed HSV-TK, a construct was designed (Figure 37A) that would produce a chimera consisting of HSV-TK and the blasticidin positive selection marker (HSV-TK-BSD). An HSV-TK-BSD chimera was employed so that cells could not lose the negative selection marker (*HSV-TK*), while retaining the positive selection marker (*BSD*). The construct also contained a T7 promoter to transcribe *HSV-TK-BSD* and was targeted to 177bp repeats. The MCs carry VSG genes in their subtelomeres, while their cores consist of 20-80kb of these repeats, 55% of their total content (Wickstead et al., 2004). By directing constructs to these repeats, *HSV-TK-BSD* can, therefore, be integrated into any of the MCs.

HSV-TK-BSD was introduced into SmOxB427 bloodstream form (BSF) cells, which express the T7 polymerase, creating SmOxB427 *HSV-TK-BSD*$_{177bp}$. To determine how sensitive cells were to ganciclovir, counts of cells treated with 50µg/ml (~200µM) or 100µg/ml (~400µM) ganciclovir were performed, with or without 5µg/ml blasticidin (Figure 37B). The presence of ganciclovir caused population decline in these cells, suggesting they were sensitive to the drug. Populations of cells began to recover after 48-96 hours, though the presence of blasticidin appeared to delay this recovery. These data show that cells are sensitive to ganciclovir and that the presence of blasticidin prevents selection of cells that lose the *HSV-TK-BSD* marker.

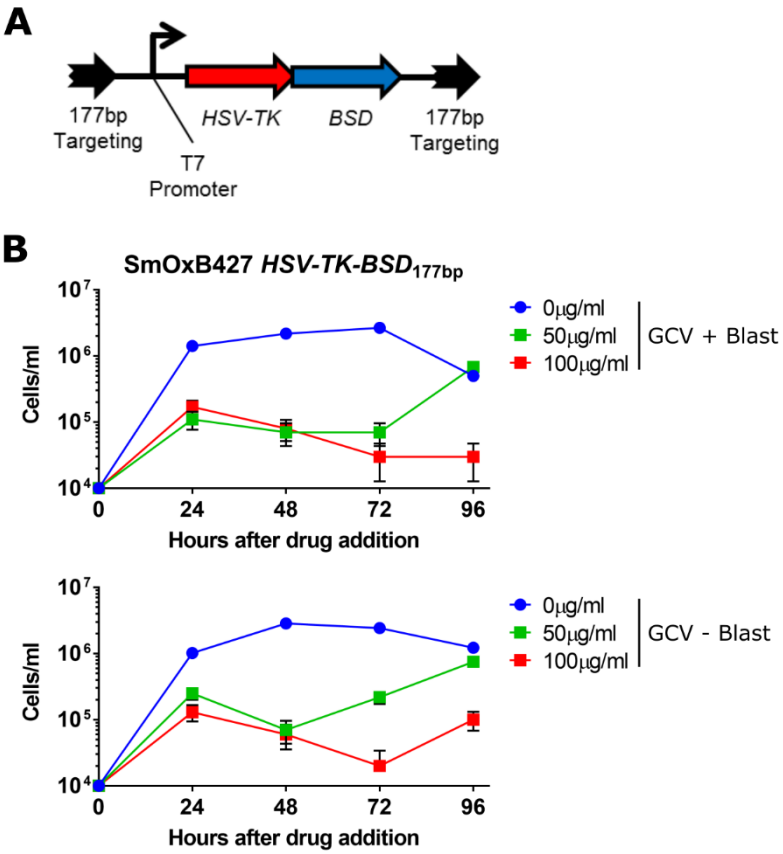


Figure 37. Expression of HSV-TK-BSD chimeras from MCs in BSF trypanosomes induces sensitivity to ganciclovir. A *HSV-TK-BSD* coding plasmid (A) was linearised and transfected into SmOxB427 cells to creating the SmOxB427 *HSV-TK*$_{177bp}$ cell line. Cell counts were then performed every 24 hours for 96 hours, on cells growing in the presence of 0, 50 or 100μg/ml ganciclovir (GCV), with or without 5μg/ml blasticidin (Blast) (B). Unlike previous cell counts, cells were not diluted during the experiment. Instead, the time it took cells to reach maximum density, if at all, was determined. Cell count data were provided by Simon D'Archivio.

5.1.3. Minichromosome loss caused by kinesin knockdown can be detected using negative selection

To determine whether MC loss, caused by kinesin knockdown, could be detected using the HSV-TK negative selection marker, a plasmid designed for knockdown of KIN13-1 (Tb927.9.3650), p2T7β-KIN13-1, was introduced into SmOxB427 *HSV-TK-BSD*$_{177bp}$ cells. KIN13-1 is a kinesin-13 family member, which are depolymerising kinesins in model organisms (Walczak et al., 2013). KIN13-1 is known to be involved in spindle regulation in *T. brucei* and its absence causes chromosome segregation defects (Chan et al., 2010; Wickstead et al., 2010a). The effectiveness of protein knockdown was tested by Western blot (Figure 38A). Knockdown was weak in comparison to uninduced cells, but fairly effective in contrast to the parental cell line, suggesting that there was some "leakiness" associated with the RNAi construct. The phenotype of RNAi clones was also tested by counting cell numbers and by K-N counts (Figure 38B and C). KIN13-1 knockdown had a small impact on population growth and lead to a time dependent increase in aberrant cells. These results are consistent with previous studies (Chan et al., 2010; Wickstead et al., 2010a).

To test for MC loss, RNAi was performed for 48 hours. After 48 hours, cells were plated 10, 100 or 1000 cells to a well on 96 well plates in the presence of 100µg/ml (~400µM) ganciclovir and growth of positive wells counted. Each positive well was representative of a cell (or cells) that had lost its sensitivity to ganciclovir, most likely through the loss of the tagged MC. The number of positive wells was then used to calculate the number of ganciclovir sensitivity loss events that had occurred in each generation, during RNAi. These data are presented in Figure 38D. For comparison, data are also included from an assay that was performed using RNAi against KKIP1 (KKT-interacting protein 1). KKIP1 (Tb427.05.4520) is a kinetochore component identified in the Wickstead lab (D'Archivio and Wickstead, 2016). Knockdown of KKIP1 in BSF cells causes cessation of population growth and gross spindle assembly and chromosome segregation defects.

The sensitivity loss rate in SmOxB427 *HSV-TK-BSD*$_{177bp}$ parental cell line was ~10^{-4} losses per cell per generation, which is consistent with previous work on MC loss (Wickstead et al., 2003). This rate of MC loss is also similar to loss of linear chromosomes in yeast (Dani and Zakian, 1983). Both knockdown of KIN13-1 and KKIP1 caused highly significant increases in losses of ganciclovir sensitivity ($p<0.001$), suggesting knockdown of both caused chromosome segregation defects. In the case of KKIP1, this loss was increased by nearly four orders of magnitude over the baseline seen in the parental line. Even uninduced cells containing KKIP1 RNAi constructs displayed significant increases in loss rate compared to parental cells, suggesting "leakiness" of RNAi in the absence of tetracycline. KIN13-1 RNAi produced a much milder loss phenotype compared to KKIP1, suggesting less severe chromosome segregation defects, which, given each protein's role, is expected. KIN13-1 regulates spindle length, whereas KKIP1's role in the kinetochore means that it is directly involved in linking chromosomes to the spindle. It is, therefore, more likely for KKIP1 knockdown to cause nondisjunction events and the loss of chromosomes.

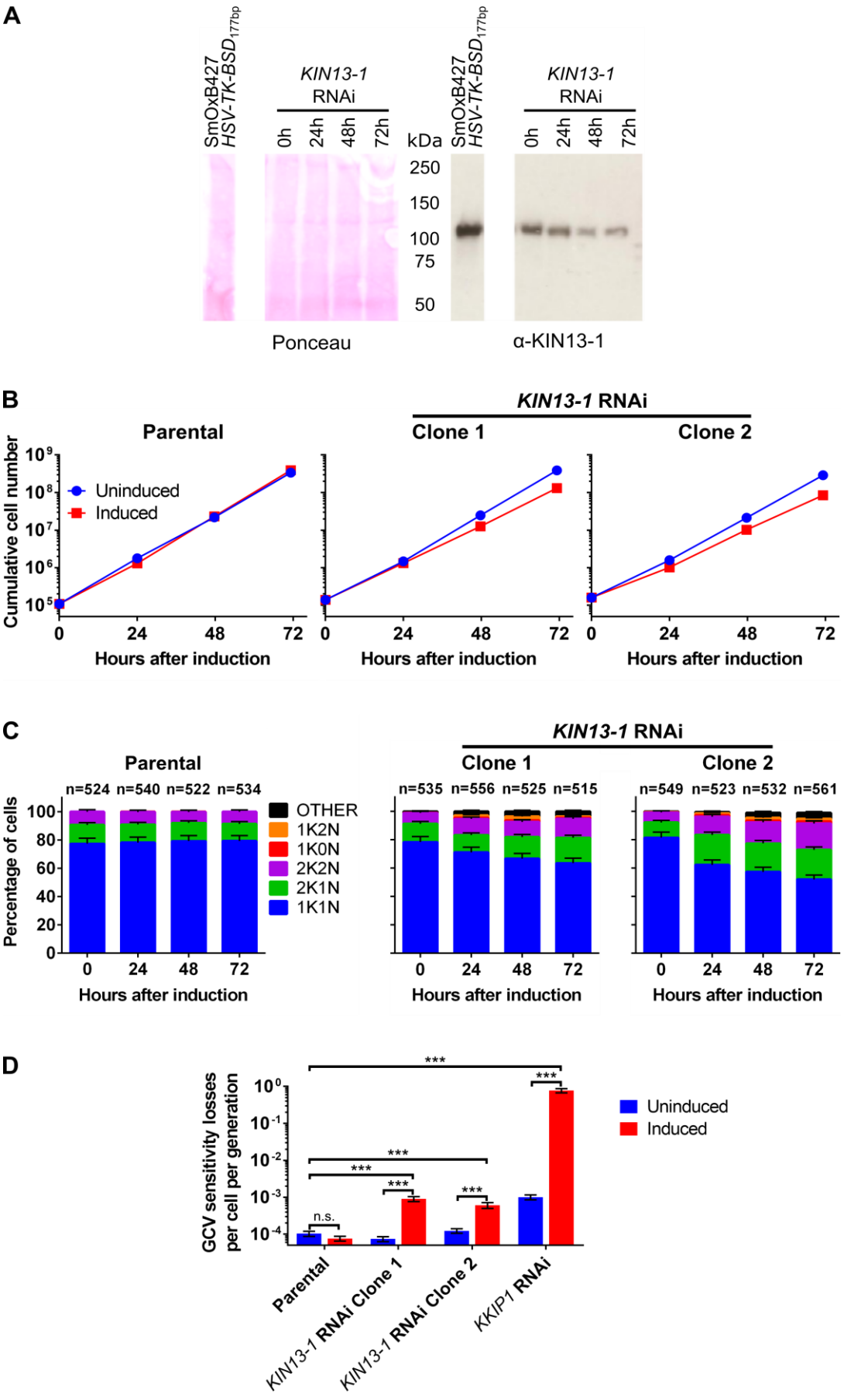

A
SmOxB427
HSV-TK-BSD177bp
KIN13-1
RNAi
0h
24h
48h
72h
kDa
250
150
100
75
50
Ponceau
α-KIN13-1
B
KIN13-1 RNAi
Parental
Clone 1
Clone 2
Cumulative cell number
Uninduced
Induced
Hours after induction
C
Parental
Clone 1
Clone 2
n=524 n=540 n=522 n=534
n=535 n=556 n=525 n=515
n=549 n=523 n=532 n=561
Percentage of cells
OTHER
1K2N
1K0N
2K2N
2K1N
1K1N
Hours after induction
D
GCV sensitivity losses per cell per generation
n.s.
***
Uninduced
Induced
Parental
KIN13-1 RNAi Clone 1
KIN13-1 RNAi Clone 2
KKIP1 RNAi

Figure 38. MC loss caused by KIN13-1 or KKIP1 knockdown can be detected using a negative selection marker in BSF cells. KIN13-1 RNAi plasmids were introduced into SmOxB427 *HSV-TK*$_{177bp}$ cells. A Western blot, using αKIN13-1 polyclonal rabbit antibodies and a goat α-rabbit-HRP secondary, was used to confirm knockdown (A). Cell counts were used to produce cumulative cell numbers (A) and K-N counts performed (B), to confirm the KIN13-1 knockdown phenotype. For MC loss detection, RNAi was induced for 48h and cell numbers counted before and after induction. Cells were then plated on three separate 96 well plates at 10, 100 or 1,000 cells per well. The number of positive wells was counted after a week. Positive well numbers and cell counts were then used to calculate the number of ganciclovir (GCV) sensitivity losses per cell per generation (D). Data from a previous assay using RNAi against KKIP1 are included for comparison. Z-tests were performed to determine the significance of any change in MC loss rate; * = p≤0.05, ** = p≤0.01, *** = p≤0.001. KKIP1 MC loss data was provided by Simon D'Archivio.

5.1.4. Adapting *HSV-TK* constructs for use in procyclic form cells

To determine whether HSV-TK could be used to detect MC loss in PCF cells, constructs used to produce the HSV-TK-BSD chimera in BSF cells were also introduced into SmOxP427 PCF cells. No clones were produced by constructs containing a T7 promoter, on two occasions. Clones were generated when the promoter was switched for the rDNA promoter (Figure 39A), suggesting that the T7 promoter could not be used by PCF cells to sufficiently express the chimera, to induce blasticidin resistance. The SmOxP427 *HSV-TK-BSD*$_{177bp}$ cells produced from constructs containing the rDNA promoter were not sensitive to ganciclovir, however. Population growth was not limited by ganciclovir at 100µg/ml (~400µM) or 500µg/ml (~2mM) (Figure 39B), concentrations much higher than those required to induce cell death in previous studies (Valdés et al., 1996). Cells were also tested against penciclovir, another acyclovir derivative, which can reach greater intracellular concentrations (Kimberlin and Whitley, 2007). Treatment with penciclovir also did not reduce cell growth in comparison to the parental cell line.

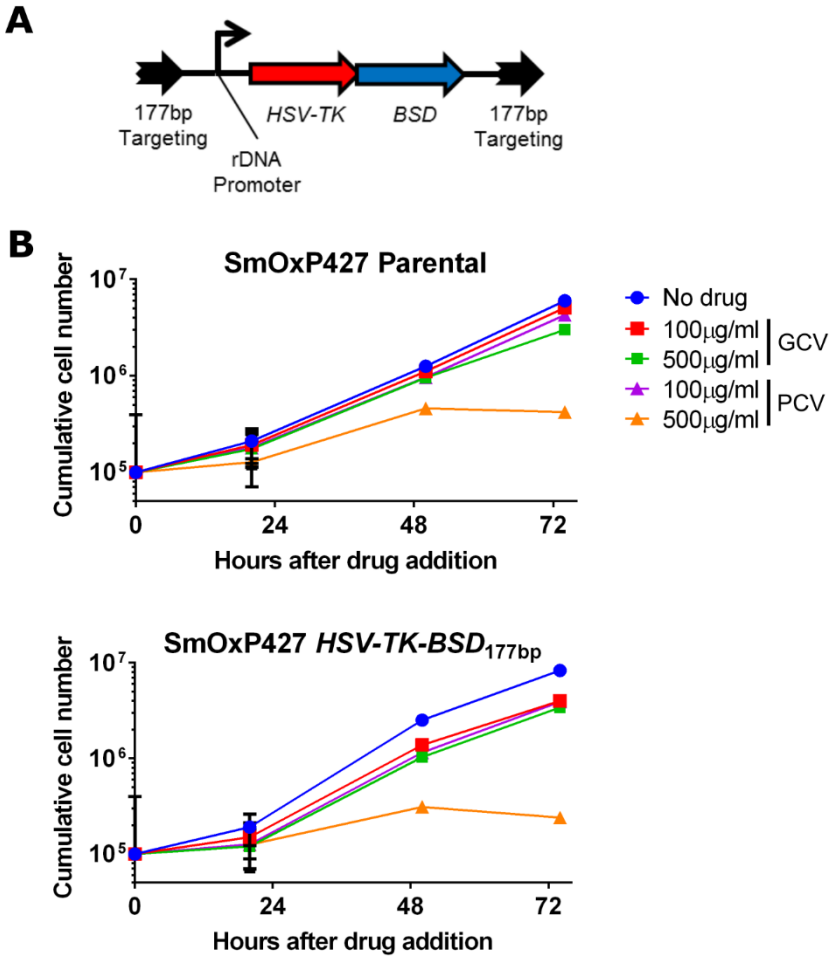


Figure 39. Expression of HSV-TK-BSD chimeras does not induce sensitivity to ganciclovir, or penciclovir, in PCF cells. SmOxP427 cells were transfected with the *HSV-TK-BSD* construct with a rDNA promoter (A), to produce SmOxP427 *HSVTK-BSD*$_{177bp}$ cells. Cells were grown in the presence of 100 or 500µg/ml ganciclovir (GCV) or penciclovir (PCV) for 72h.The number of cells was counted every 24h and used to calculate cumulative cell number (B).

Why are PCF cells not sensitive to ganciclovir, or penciclovir, when expressing the HSV-TK-BSD chimera? PCF cells may not be transcribing enough mRNA from *HSV-TK-BSD* to generate ganciclovir sensitivity, while transcribing enough for blasticidin resistance. This may be due to the promoter used, or because of the gene's location in the MC. The chimera itself may also reduce HSV-TK efficiency below a threshold required for sensitivity in PCF cells.

In an attempt to increase HSV-TK efficiency, the HSV-TK-BSD chimera was split by introducing a *PFR2* intergenic sequence between the two CDSs (Figure 40A). The construct was also retargeted to the S8 VSG CDS, which is known to be

present in a specific MC of a known size, or to Bloodstream Expression Site 1 (BES1), a VSG expression site present on a MBC (Hertz-Fowler et al., 2008), as a positive control. Cells produced by transfecting these new constructs into SmOxP427 were then tested for sensitivity to 100µg ml^{-1} ganciclovir (Figure 40B). In these cells population growth was limited for five or seven days in MC and MBC tagged cells, respectively, before populations began to rise again. Furthermore, K-S tests showed that, for both MC and MBC tags, the differences between numbers of ganciclovir treated and untreated cells were significant (p=0.0037 and 0.0326, respectively). The population recovery that occurred was likely to have been caused by loss of the *HSV-TK* gene or an outgrowth of a resistant subpopulation.

To determine whether the gene had been lost after ganciclovir treatment, a Southern blot was performed (Figure 41). Whole MCs were separated from MBCs using pulsed-field gel electrophoresis (PFGE), transferred to a nylon membrane for blotting and probed with probes derived from *HSV-TK.* This analysis confirmed the presence of *HSV-TK* in MCs, when targeted to the S8 VSG CDS, and in MBCs, when targeted to BES1. No bands were produced by SmOxP427 *HSV-TK*$_{BES1}$ and SmOxP427 *HSV-TK*$_{S8\ VSG}$ genomic DNA after ganciclovir treatment, suggesting that *HSV-TK* had been lost in the populations of all cell lines.

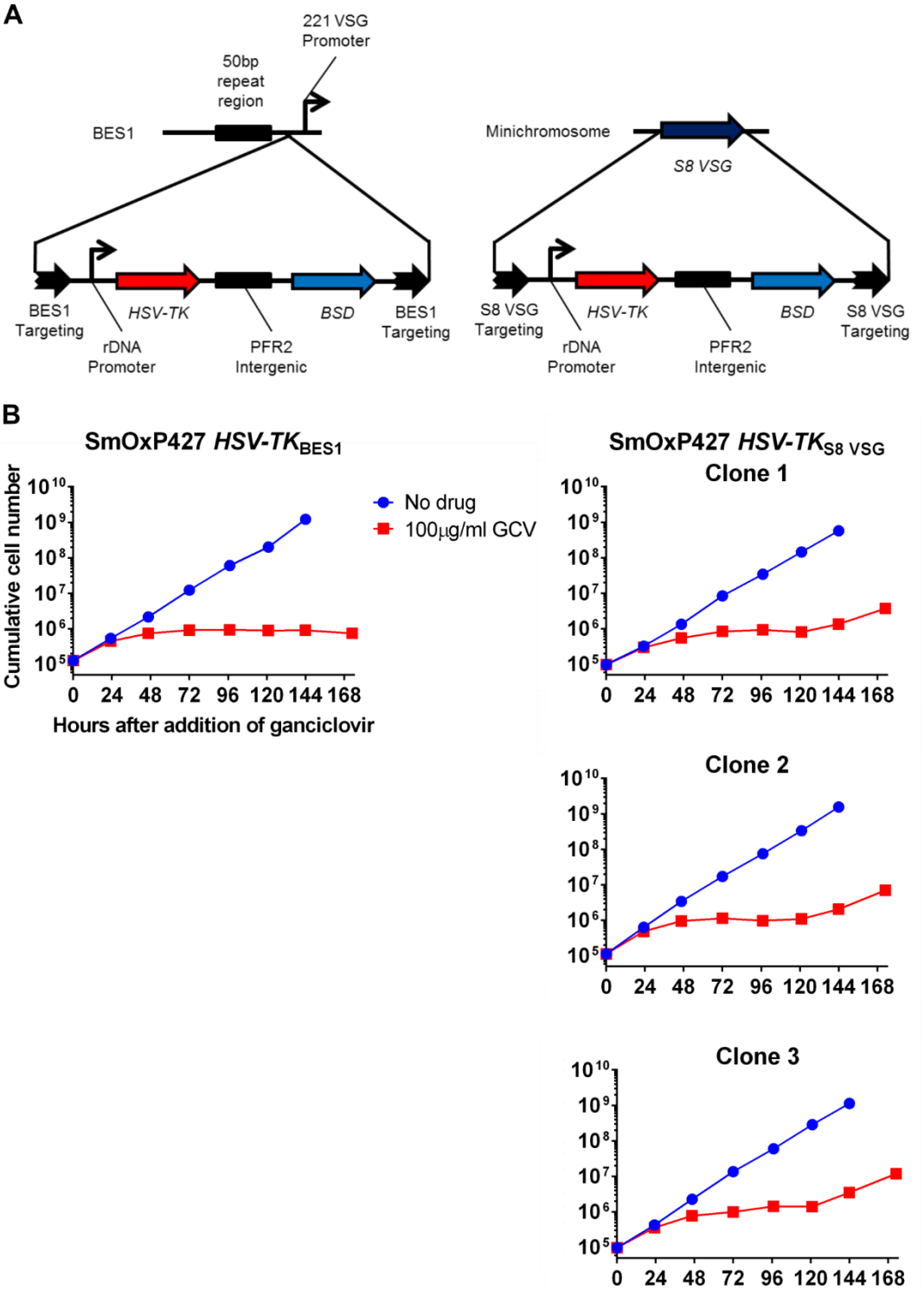


Figure 40. Expression of HSV-TK alone induces sensitivity to ganciclovir in PCF cells. HSV-TK constructs were produced (A) and introduced into SmOxP427 cells to produce the SmOxP427 *HSV-TK*$_{BES1}$ and SmOxP427 *HSV-TK*$_{S8\ VSG}$ cell lines. These cell lines were then grown in the presence of 100µg/ml ganciclovir (GCV) for 168 hours and the number of cells counted every 24 hours. Cell counts were used to calculate cumulative cell number.

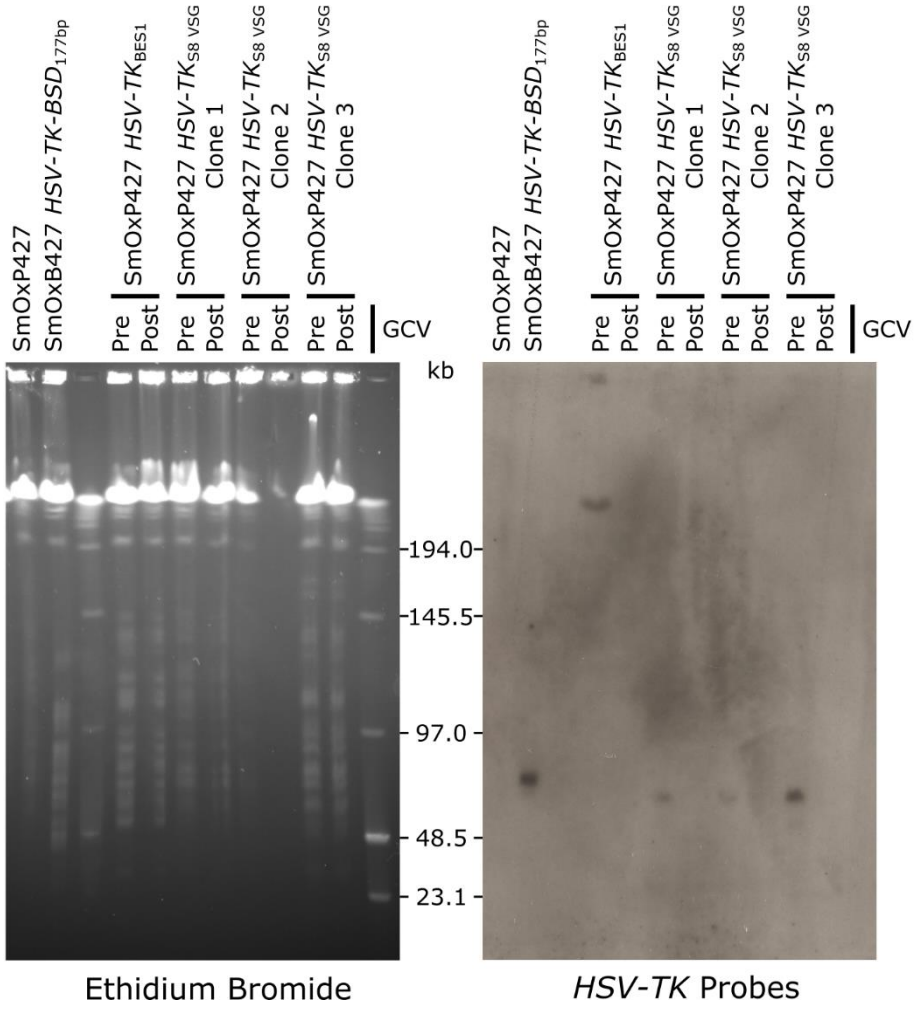


Figure 41. *HSV-TK* integrated into a MC and is lost on ganciclovir selection. PFGE carried out to separate MCs from MBCs. PFGE was performed using agarose plugs prepared from the SmOxP427 *HSV-TK*$_{BES1}$ and SmOxP427 *HSV-TK*$_{S8\ VSG}$ cell lines, from before and after ganciclovir (GCV) treatment for cell counts (Figure 40), as well as relevant controls. After separation chromosomal DNA was transferred to a nylon membrane, by capillary transfer, and probed probes prepared from the HSV-TK CDS.

5.1.5. Minichromosome loss can be detected with less sensitivity in procyclic form cells

To test whether the *HSV-TK* marker could be used to detect MC loss in PCF cells, a second assay for loss of ganciclovir sensitivity was performed. The RNAi plasmids p2T7-177-KKIP1 RNAi and p2T7β-KIN13-1 plasmids were introduced into SmOxP427 *HSV-TK*$_{S8\ VSG}$ cells. RNAi was induced for 48 hours and K-N counts (Figure 42A) and Western blot (Figure 42B) performed to confirm KKIP1 or KIN13-1 knockdown, respectively. A 10-20% proportion of cells displayed aberrant numbers of nuclei and kinetoplasts after KKIP1 knockdown, as expected, and Western blotting showed that the KIN13-1 protein had been knocked down. Cells were then plated in the presence of 100μg ml^{-1} ganciclovir, as described previously, though the number of positive wells was counted after ten days. The results of this assay, displayed as ganciclovir sensitivity losses per cell per generation are shown in Figure 42C. Induction of RNAi increased sensitivity losses in PCF cells, though these increases were considerably smaller than those seen in BSF cells. KKIP1 knockdown only increased losses by less than one order of magnitude, though this increase was still highly significant ($p<0.001$), while no significant change in loss was seen on induction of RNAi against KIN13-1. These results do not correspond with those gathered from BSF cells. A marginally greater baseline loss rate also occurred in parental PCF cells than in BSF cells, which may be a function of a reduced sensitivity to ganciclovir. This reduced sensitivity may also have contributed to the reduced increases in sensitivity losses observed. An increased tolerance to RNAi in PCF cells may also explain these smaller increases. It can be concluded, however, that MC losses can be detected using this HSV-TK based system in PCF cells, but with less sensitivity than can be achieved in BSF cells.

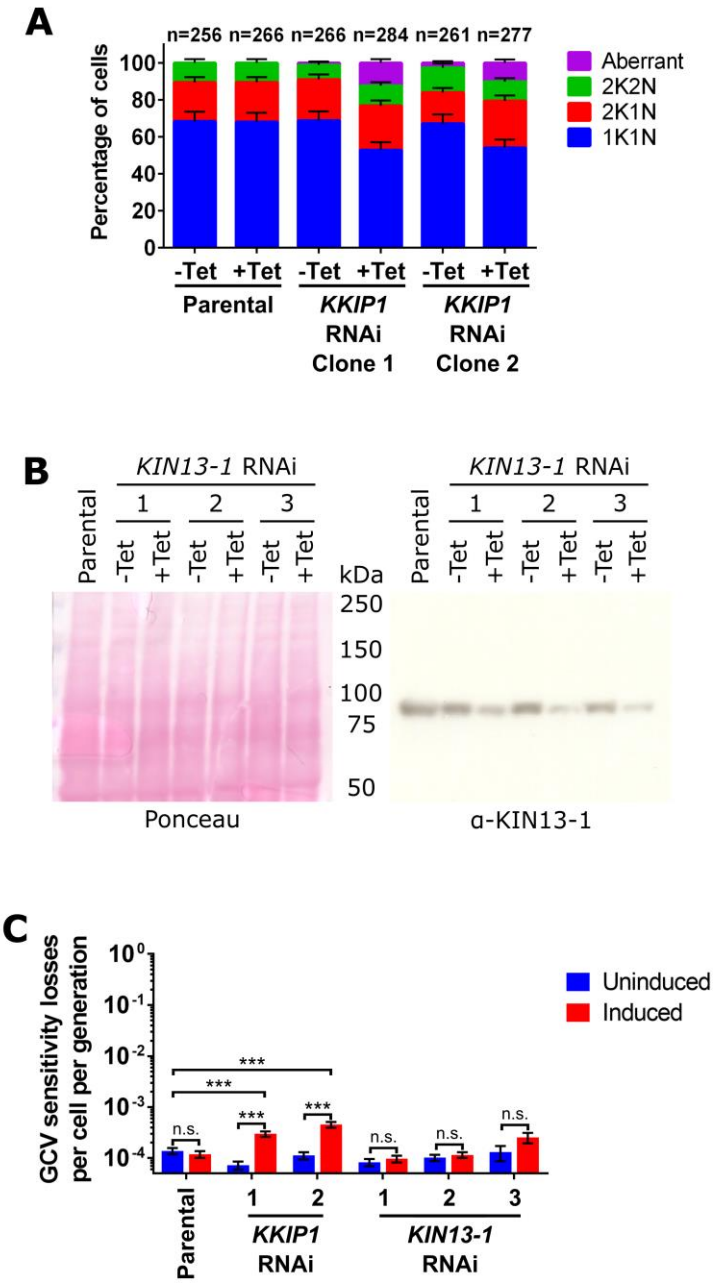


Figure 42. Detection of MC loss using the HSV-TK marker in PCF trypanosome cells. RNAi against KKIP1 or KIN13-1 was induced with tetracycline (Tet) for 48 hours in SmOxP427 *HSV-TK*$_{S8\ VSG}$ cells and confirmed by counts of nuclei and kinetoplasts (A) or Western blotting (B). Cells were then plated on three separate 96 well plates at 10, 100 or 1,000 cells per well. The number of positive wells was counted after ten days and used to calculate the number of ganciclovir (GCV) sensitivity losses per cell per generation (C). Z-tests were performed to determine the significance of any change in MC loss rate; * = p≤0.05, ** = p≤0.01, *** = p≤0.001.

5.1.6. Summary

In the previous chapter a combinatorial RNAi library was produced containing all possible combinations of microtubule motors. An experiment has been designed that will use this combinatorial library to determine how knockdown of microtubule motors affects chromosome segregation. This experiment will use a MC tagged with a negative selection marker, *HSV-TK*, so that chromosome loss can be selected for. *HSV-TK* has been used in *T. brucei* previously, but has only been integrated into MBCs, so it was necessary to optimise *HSV-TK* constructs for use in MCs. A construct was generated that, upon integration into the trypanosome genome, would cause cells to express, from a MC, a chimera containing HSV-TK and the blasticidin positive selection marker. A BSF cell line generated using this construct is demonstrated here to be sensitive to, the nucleoside analogue, ganciclovir. Sensitive PCF cells could not be produced, however. Altering the plasmid to carry the rDNA promoter and splitting the chimera, by inserting the *PFR2* intergenic sequence, yielded a construct that could be used to generate a cell line that is sensitive to ganciclovir, as shown here. I have demonstrated that both the BSF and PCF cell lines expressing HSV-TK can be used to detect MC loss, via the detection of loss of ganciclovir sensitivity, and that this can be done with greater sensitivity in the former.

5.2. Cell lines for validation of mitotic mutants

Once the library experiments, described previously (Figure 36), have been performed, it will be necessary to validate the results. This could be done using a second reporter cell line and microscopy. To validate the role of motor proteins in mitosis, it would be informative for the reporter cell line to contain a spindle label and a chromosome label, so that spindle defects and chromosome segregation defects can be observed. Development of strategies for production of this reporter cell line are described in the following sections.

5.2.1. KIN13-1 can be used as a spindle label

In trypanosomes, it is difficult to label the spindle by directly labelling microtubules with a fluorescent protein and tubulin conjugate. The shape of the trypanosome cell is defined by the flagellum and a subpellicular corset of microtubules (Vickerman 1985; Fenn & Matthews 2007; Ooi & Bastin 2013; Langousis & Hill 2014). This corset is not broken down during mitosis and so labelling tubulin also labels the corset, making the mitotic spindle difficult to observe. As an alternative, KIN13-1 was chosen as an indirect spindle label. KIN13-1 is known to be distributed along the spindle throughout mitosis and its function has been extensively analysed (Chan et al., 2010; Wickstead et al., 2010a).

To produce this spindle tag, KIN13-1 was C-terminally labelled with GFP by endogenous locus tagging at one *KIN13-1* locus. Correct integration and presence of KIN13-1-GFP was verified by Western blot (Figure 43), confirming that one of the two alleles had been labelled. The distribution of KIN13-1-GFP during mitosis was observed by microscopy (Figure 44) and association with microtubules established using cytoskeleton preparations (Figure 45). The rhomboid mitotic spindle became visible at metaphase and, as anaphase occurred, it became more linear and bifurcated, before fading and disappearing by the time cytokinesis occurred. GFP signal remained in cytoskeleton preparations, confirming the tags association with microtubules. These results are consistent with those published in previous studies (Chan et al., 2010; Wickstead et al., 2010a).

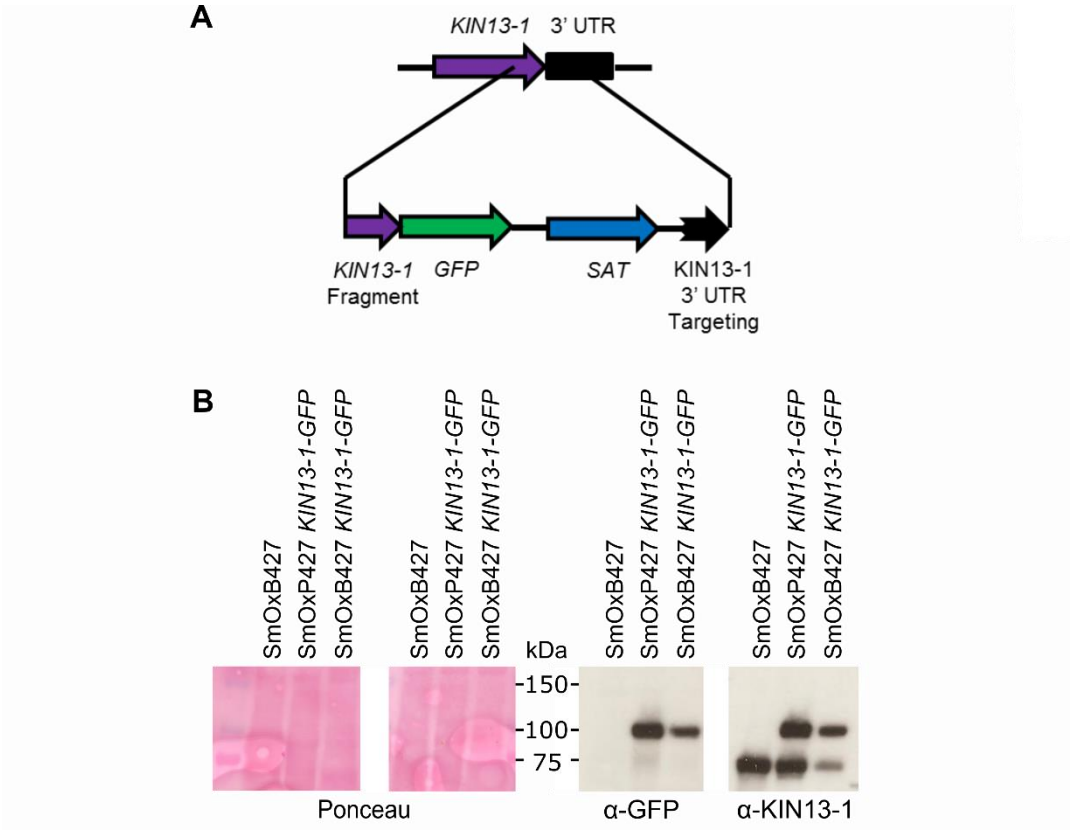


Figure 43. The use of endogenous locus tagging, to produce cells that express KIN13-1-GFP. A sequence coding for GFP was inserted between the 3' end of one the KIN13-1 CDSs and the 3'UTR (A). The production of KIN13-1-GFP was confirmed by Western blot using α-GFP mouse monoclonal antibodies and α-KIN13-1 rabbit polyclonal antibodies (B).

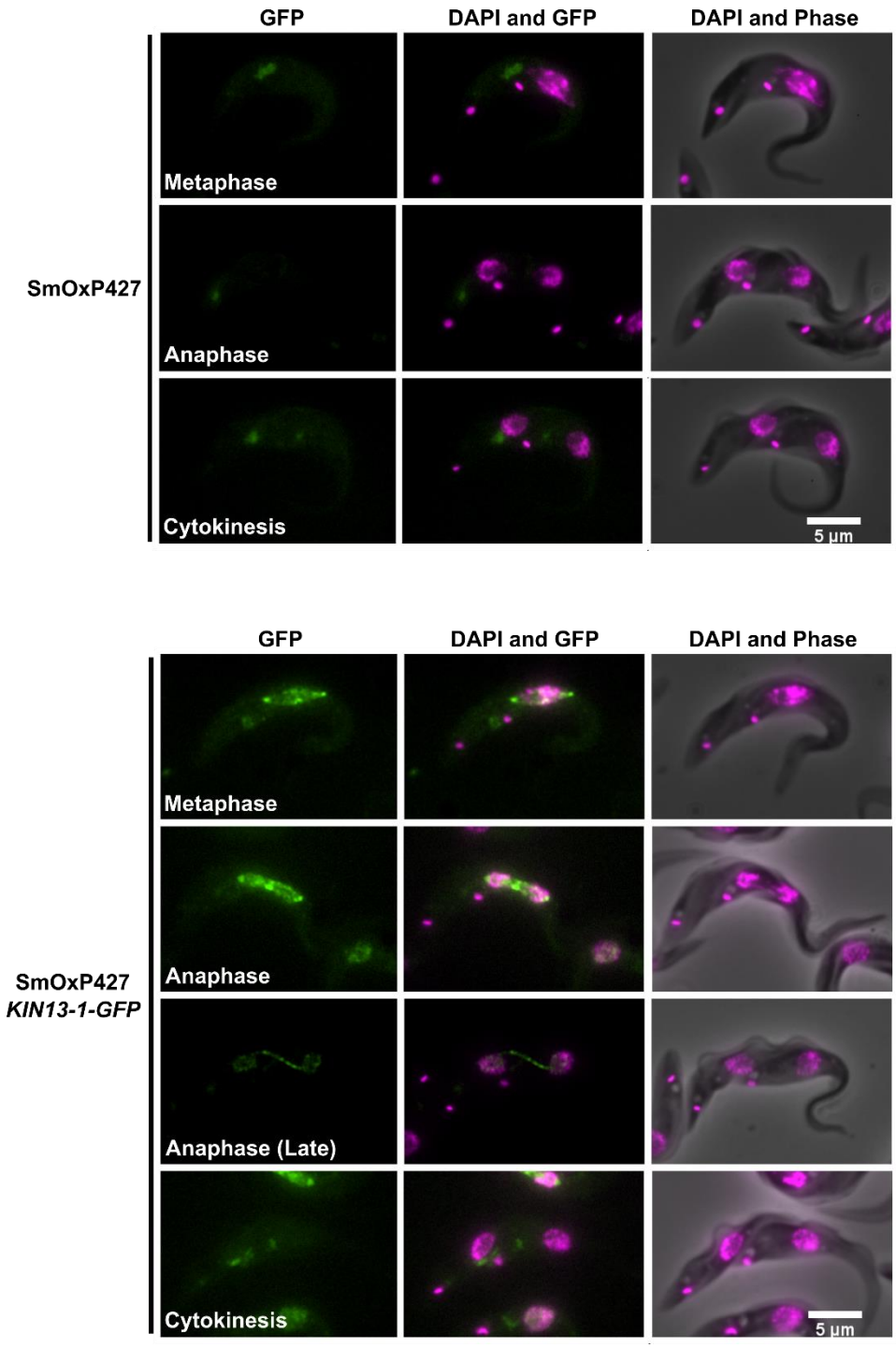


Figure 44. KIN13-1-GFP labels the mitotic spindle. Whole cells were attached to glass slides and stained with DAPI. They were then imaged with fluorescence microscopy to verify nuclear GFP signal at various stages of mitosis.

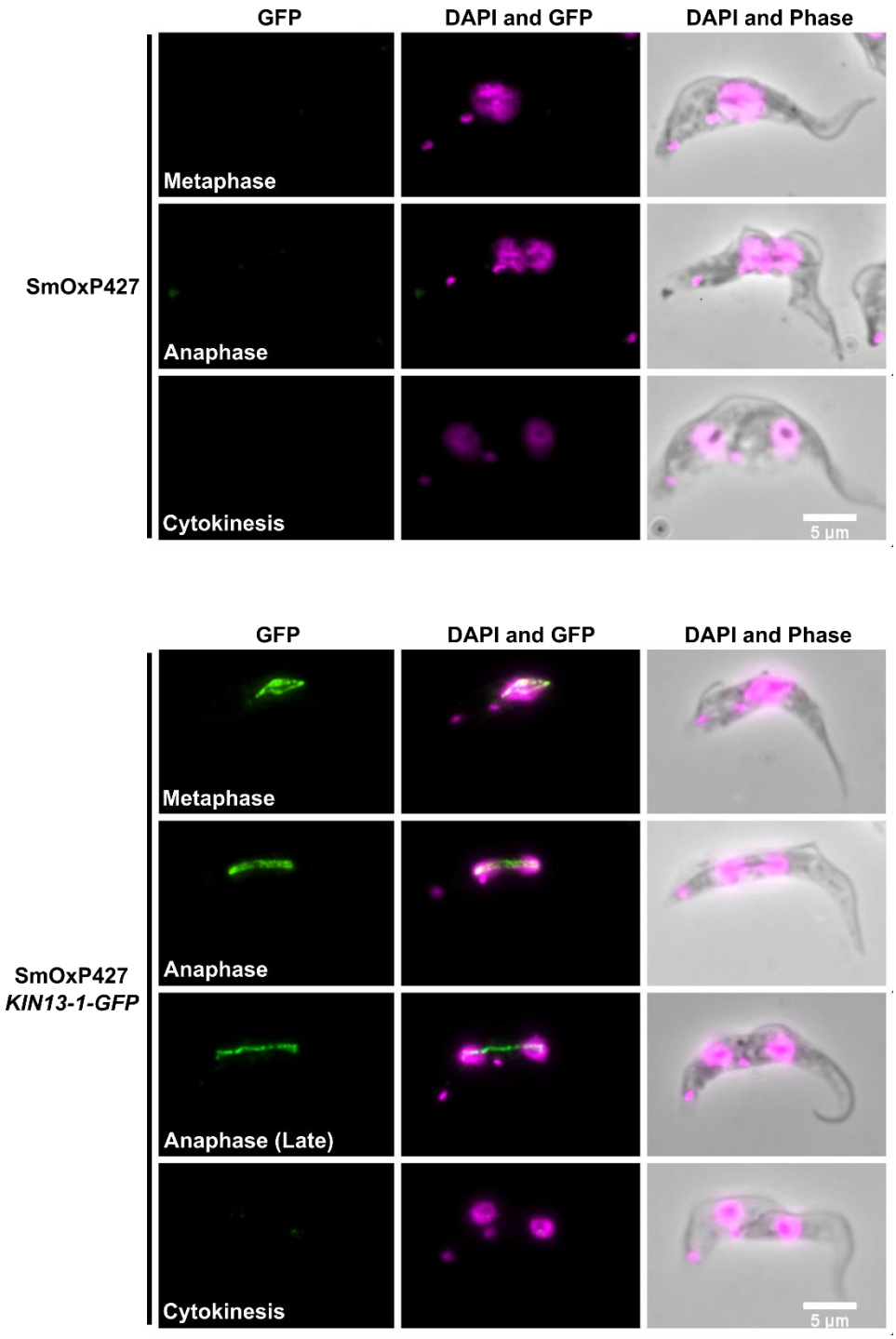


Figure 45. KIN13-1-GFP associates with spindle microtubules. Whole cells were attached to glass slides, cell membranes removed with detergent and DNA stained with DAPI. Cells were then imaged with fluorescence microscopy to verify nuclear GFP signal at various stages of mitosis.

5.2.2. A strategy for the production of a minichromosome label

A reporter cell line containing a visible MC would allow for validation of MC loss library experiments and for observation of nondisjunction events. In order to label MCs, a method for labelling DNA elements is required. One way to achieve this might be to use the binding of the Lac repressor protein (LacI) to Lac operator (LacO) sequences integrated at the site of interest. Such strategies have been used in the past to label DNA elements. Lau et al. (2003), for example, used LacO repeats and fluorescently labelled LacI to label the origin of replication in *E. coli* chromosomes (Figure 46A). Tet operator repeats and Tet repressors were also used to label the replication termination site. These elements could then be observed throughout the *E. coli* cell cycle. LacO repeats have also been used in *T. brucei*, to label the expression site body, the site of VSG mRNA transcription, in the nucleus (Navarro and Gull, 2001). The site was not observed by native fluorescence, however, due to problems with LacI expression levels, caused by the use of an inducible system. The image shown in Figure 46B was, therefore, produced by increasing signal using immunofluorescence.

In order to label a MC, using LacI and LacO, two constructs will be used (Figure 47A), one designed to direct 256 LacO sequences to a MC and another designed to produce fluorescently labelled LacI from a location within a MBC. The labelled LacI should bind to the LacO repeats in the MC, when expressed, thereby labelling the MC (Figure 47B). In the subchapters below I describe how this "LacI/LacO system" was adapted for use in labelling a MC in *T. brucei*, such that these chromosomes could be observed by native fluorescence.

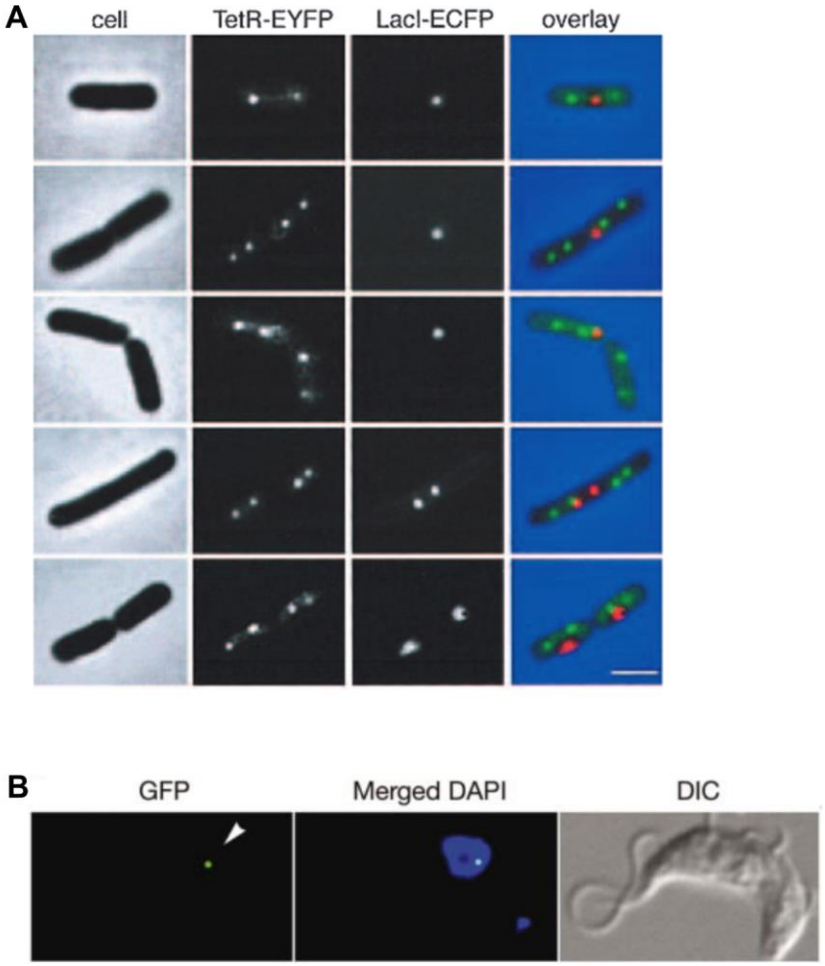


Figure 46. Examples of previous uses of the "LacI/LacO system" for labelling of DNA elements. Shown in A are images from Lau et al. (2003), in which the origin of replication was labelled with LacO repeats and the terminator with TetO repeats, so that these DNA elements could be observed through the cell cycle. Images in B were generated by Navarro & Gull (2001), by labelling the active BES with LacO repeats and using immunofluorescence to visualise GFP-LacI bound to them.

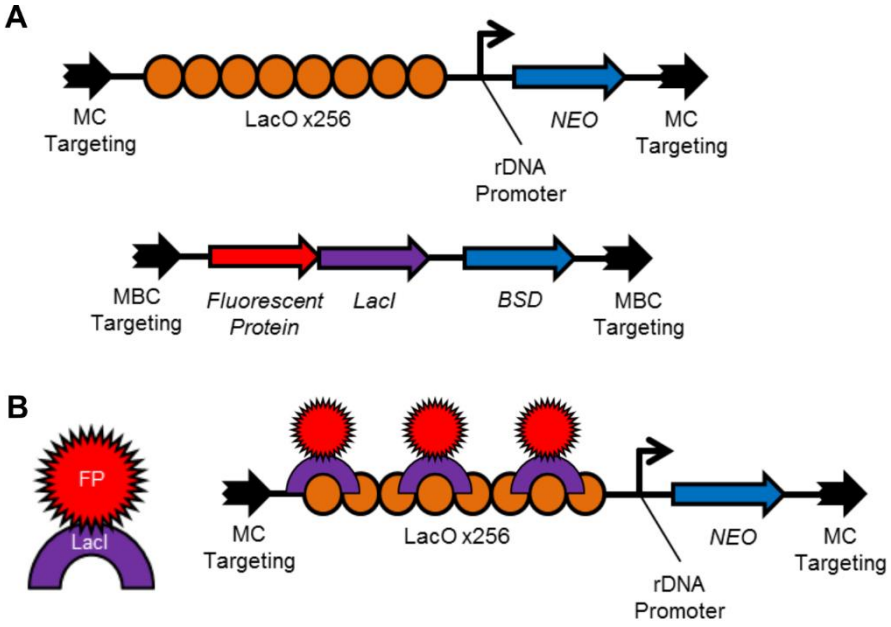


Figure 47. A concept for the labelling of MCs. Constructs are generated that target LacO repeats to a MC and a CDS coding for a fluorescently labelled LacI to a MBC (A). When the labelled LacI is expressed it binds to the LacO repeats (B), thereby labelling the MC.

5.2.3. Directing labelled LacI to the nucleus reduces protein levels

In order to produce cells that expressed fluorescently labelled LacI, constructs were produced that would replace the puromycin resistance marker in the SmOx cell line (Poon et al., 2012) with sequences coding for a mStrawberry or YFP N-terminally tagged LacI (Figure 48A). This site was targeted, because of its location at the start of the highly expressed tubulin array and it made puromycin available as a selection marker for any further work that might be carried out. mStrawberry was chosen as a fluorescent protein, so that the chromosome tag could be paired with KIN13-1-GFP, but it is not commonly used in trypanosomes. YFP was chosen as a backup, in case mStrawberry proved to be unsuitable as a fluorophore. As it was intended for the MC and spindle tags to be used in concert, mStrawberry-LacI coding plasmids were transfected into SmOxP427 *KIN13-1-GFP* cells, creating mSt-LacI *KIN13-1-GFP* cells, whereas YFP-LacI plasmids were transfected into SmOxP427 cells, creating Y-LacI cells. Constructs were also generated that would produce mStrawberry- or YFP-LacI with an N-terminal La protein nuclear localisation signal (NLS) (Figure 49A), which can be used to direct

proteins to the trypanosome nucleus (Marchetti et al., 2000), to produce the La-mSt-LacI and La-Y-LacI cell lines. In addition, all four of the constructs contained a 3' UTR from downstream of the KIN13-1 CDS. Due to polycistronic nature of transcription in *T. brucei*, most regulation of mRNA and protein levels is post-transcriptional. The 3' UTRs of mRNAs play important roles in dictating both mRNA stability and translation rate (Berberof et al., 1995; Boucher et al., 2002; Furger et al., 1997; Hotz et al., 1997; Mao et al., 2009; Quijada et al., 2002). The *KIN13-1* 3' UTR was used in an attempt to produce LacI at numbers equivalent to KIN13-1 (~100-300 proteins per cell). It was predicted that this number of proteins would be enough to occupy as many LacO sites as possible, while limiting the number of free LacI proteins, thereby limiting background fluorescence levels.

When no NLS was present, fluorescently labelled LacI proteins were produced at levels equivalent to KIN13-1-GFP, when determined by Western blot (Figure 48C). Microscopy showed that fluorescent protein signal was distributed throughout the cytoplasm of cells and appeared to be partially excluded from the nucleus (Figure 48B). Placing the La protein NLS at the N-terminus of fluorescently labelled LacI caused the protein to be directed to the nucleus as expected (Figure 49C). Levels were greatly reduced in comparison to protein lacking the NLS, however, when assessed by both microscopy (Figure 49B) and Western blot (Figure 50). Levels were sufficiently low to be below the level of detection by Western blot, suggesting that protein levels were at least ten-fold lower than those of proteins lacking the NLS.

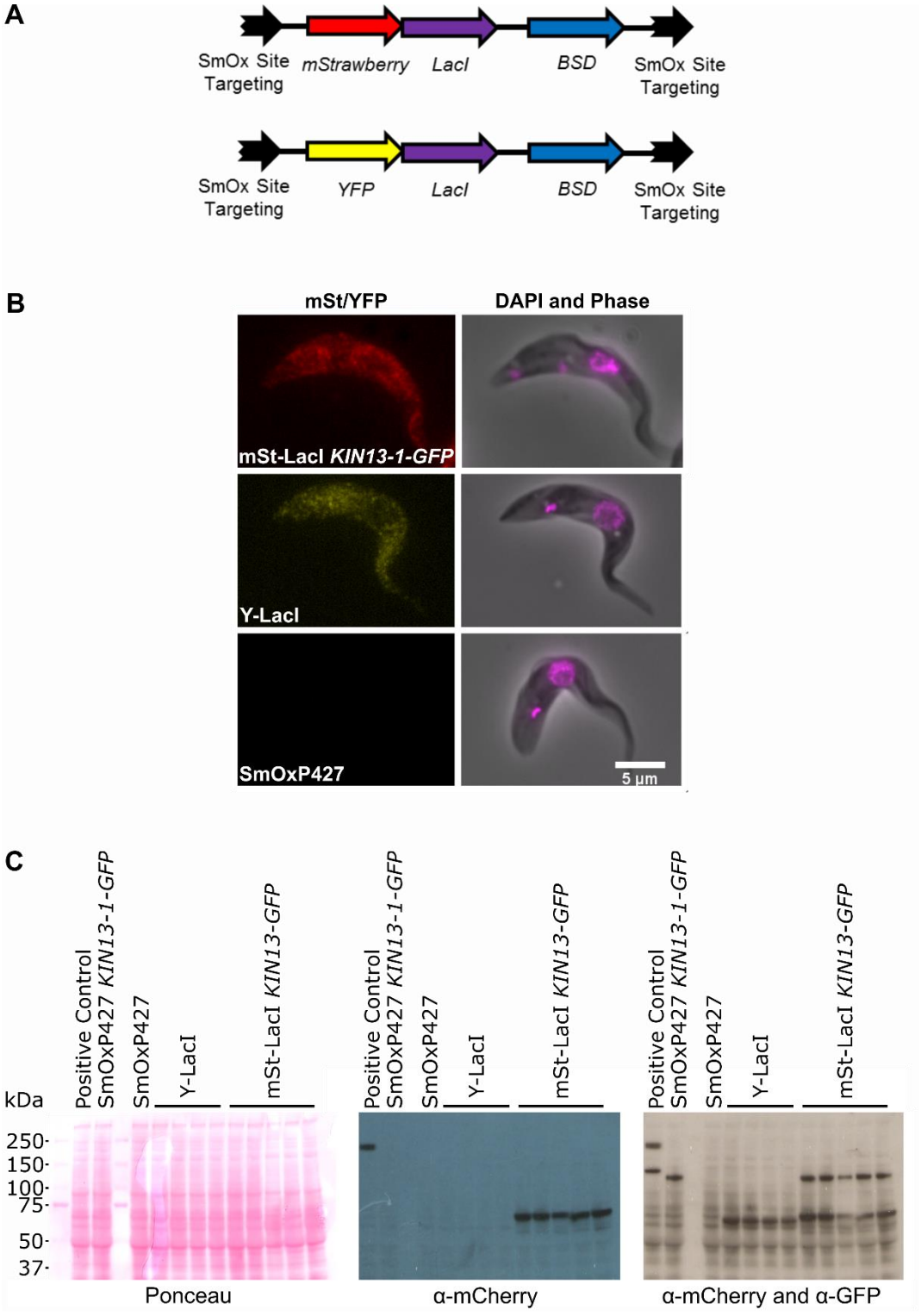


Figure 48. LacI lacking a NLS does not localise to the nucleus. Constructs for the production of fluorescently labelled LacI (A) were transfected into SmOxP427 or SmOxP427 *KIN13-1-GFP* cells. Microscopy was used to determine the distribution of fluorescent signal (B). Production of tagged LacI was confirmed by Western blots (C), using α-mCherry and α-GFP monoclonal antibodies (the epitopes these antibodies bind are present in mStrawberry and YFP). A positive control line containing both mStrawberry and YFP labelled proteins was also included in the blot.

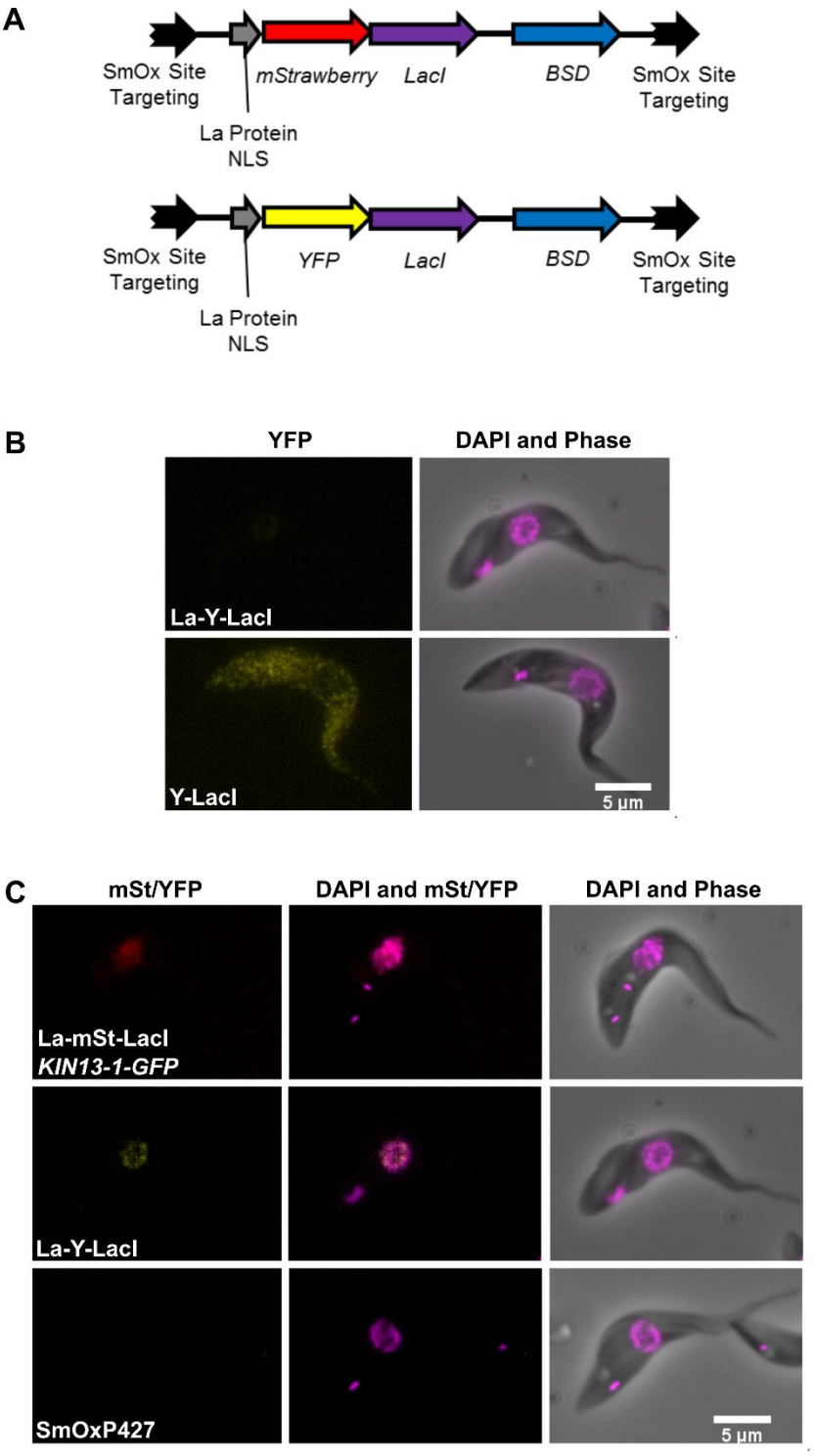


Figure 49. Expressing LacI with an NLS directed the protein to the nucleus, but greatly reduced fluorescent signal levels. Two constructs were produced in order to generate cells expressing mStrawberry-LacI or YFP-LacI with an N-terminal La protein NLS (A). Fluorescence microscopy was used to image cells expressing the proteins and the images processed identically to those found in Figure 48 (B) or so that the localisation of mStrawberry or YFP signal could be determined (C).

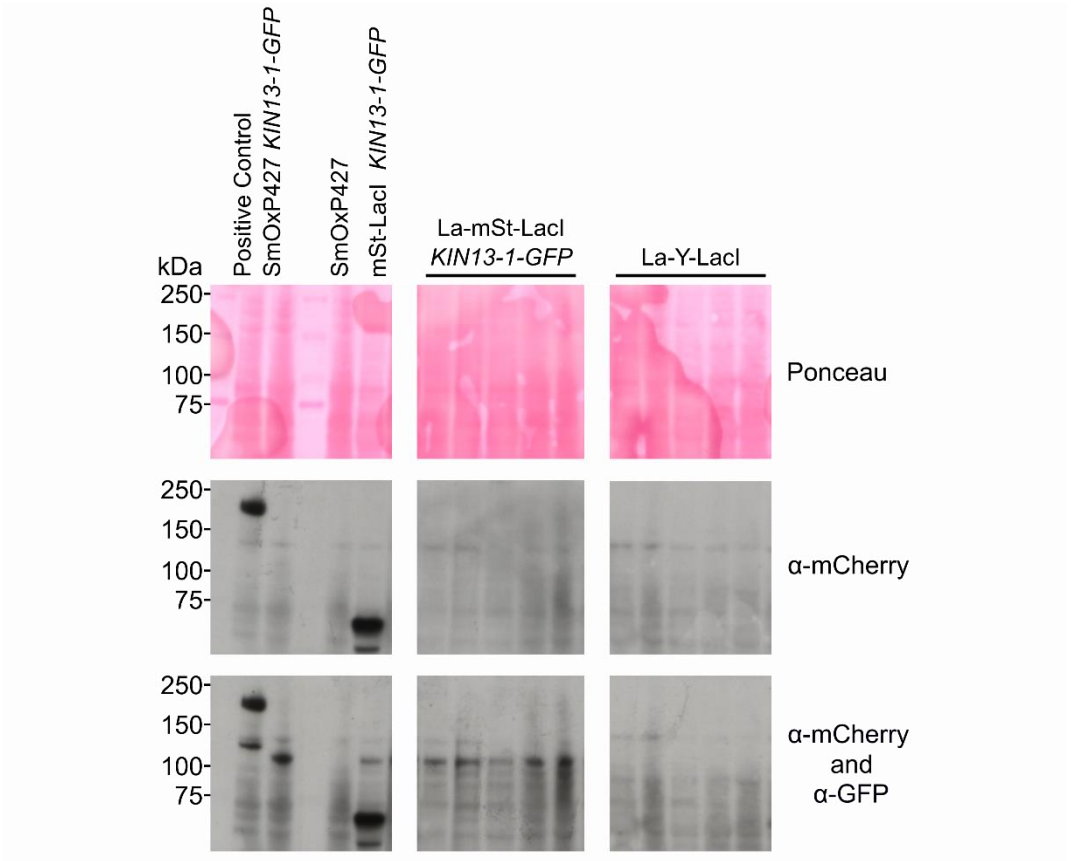


Figure 50. Expressing LacI with an NLS greatly reduces protein levels. LacI protein quantities were determined by Western blot and compared to those of KIN13-1-GFP (SmOxP427 *KIN13-1-GFP*) and mStrawberry-LacI without a NLS.

5.2.4. Altering 3’ untranslated regions does not increase labelled LacI expression

The constructs presented in the previous subchapter contained a 3’ UTR from downstream of the KIN13-1 CDS, in an attempt to produce LacI proteins at concentrations of ~100-300 proteins per cell. Addition of the La NLS, however, greatly reduced LacI levels. In an attempt to restore LacI protein concentrations, the 3’ UTRs in constructs were switched with the 3’ UTRs from *KIF9A* and *PFR1* (Figure 51A). KIF9A and PFR1 proteins are present in trypanosome cells in concentrations 10-fold and 100-fold above that of KIN13-1 (Wickstead, unpublished). The effect of this change in UTRs on LacI protein levels was determined by Western blot (Figure 51B). Neither UTR increased levels of LacI in La-mSt-LacI or La-Y-LacI cells to levels seen when the protein was expressed without an NLS. In the case of both the *KIF9A* and *PFR1* 3’ UTRs, LacI levels remained below the limit of detection.

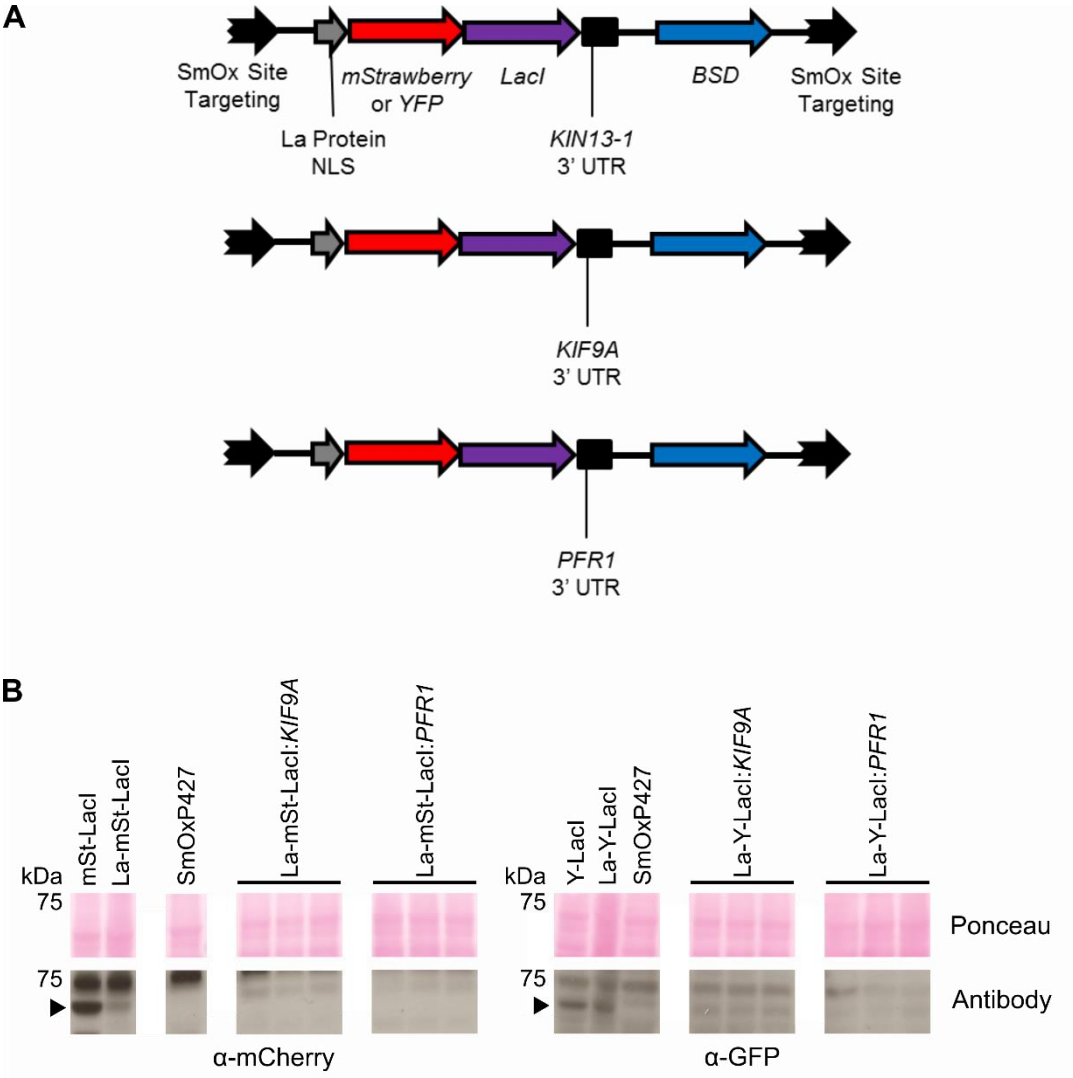


Figure 51. Changing the 3' UTR does not increase LacI expression levels. Constructs were generated, in which the *KIN13-1* 3' UTRs were replaced by 3'UTRs from *KIF9A* or *PFR1* (A). After introduction into cells, Western blots were performed, to determine their impact on LacI levels (B).

5.2.5. Changes to the nuclear localisation signal raise LacI protein levels

As alterations to 3' UTRs did not increase LacI protein concentrations, it is likely that the issues were caused by La protein NLS itself. To raise protein levels to those expected from use of the *KIN13-1* 3' UTR, two new plasmids were devised (Figure 52A). The first was designed to produce YFP-LacI with a SV40 (Simian vacuolating virus 40) NLS at the N-terminus, while the second would generate YFP-LacI with an extra YFP and N-terminal La protein NLS, separated by a TY epitope. Introduction of these two plasmids into SmOxP427 cells generated the SV-Y-LacI and La-TY-Y_2-LacI cell lines. The SV40 NLS strategy was an attempt to increase the protein levels, whereas the production of La-TY-Y_2-LacI was performed in order to increase both protein levels and levels of signal. Furthermore, in previous work by the lab, labelling nuclear proteins with YFP separated from the La NLS by a TY epitope, did not drastically alter protein concentrations, as seen here (Daniels et al., 2012).

Western blotting showed that protein levels were restored in La-TY-Y_2-LacI cells (Figure 53). Chemiluminescent signal produced by LacI from La-TY-Y_2-LacI cells, when half the amount of whole cell lysate was run, was equivalent to that produced by KIN13-1-GFP and to 75pg of GFP, which represents the mass of ~300 proteins per cell from 5×10^6 cells. Microscopy also showed improved levels of YFP signal within the nuclei of La-TY-Y_2-LacI cells (Figure 52B).

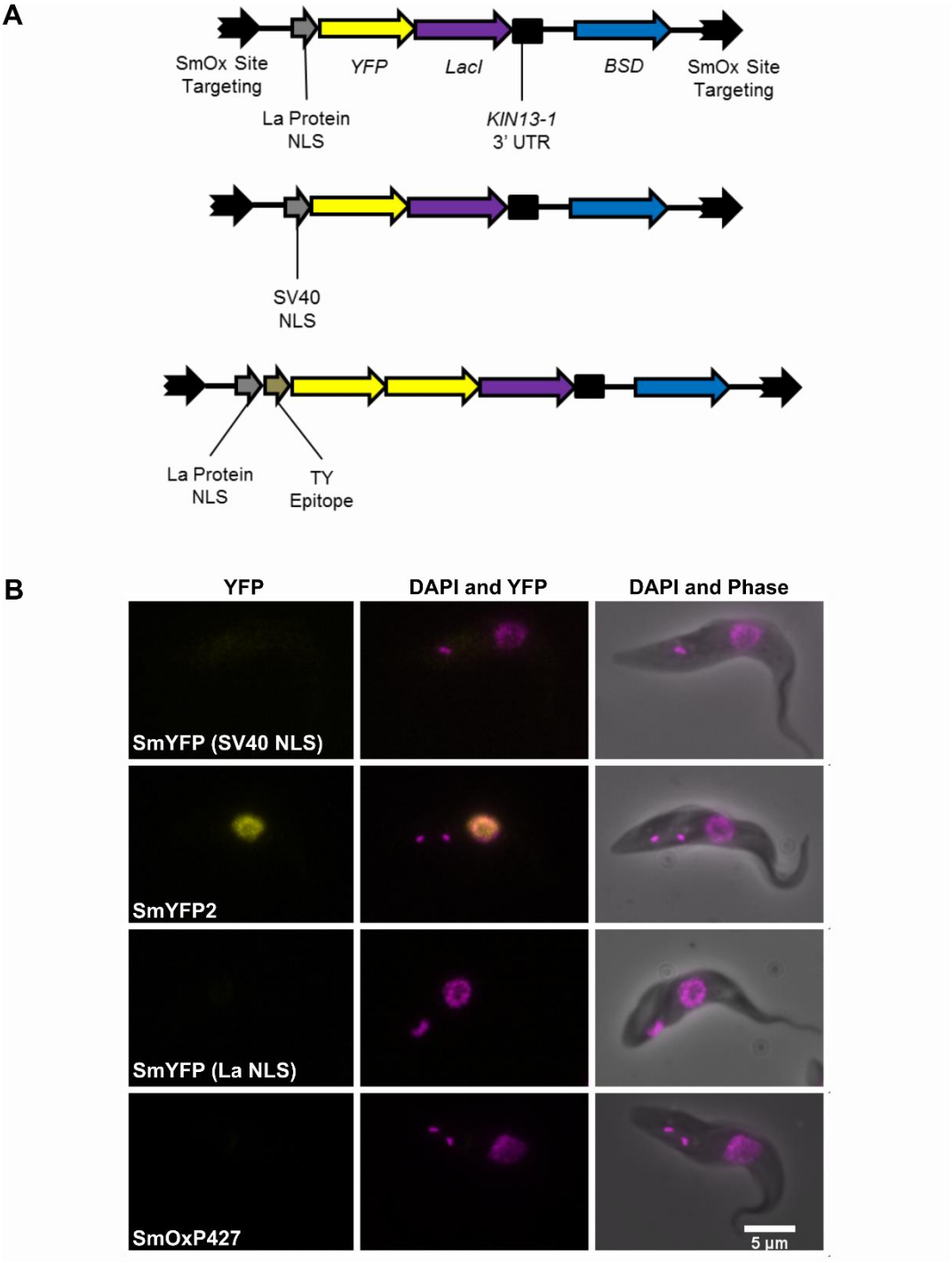


Figure 52. Altering the NLS of YFP-LacI increases fluorescent signal levels. The YFP-LacI coding construct was modified to include the SV40 NLS or the La protein NLS with a TY epitope and an additional YFP (A). Images were taken of representative cells and processed identically to those in Figure 48 (B).

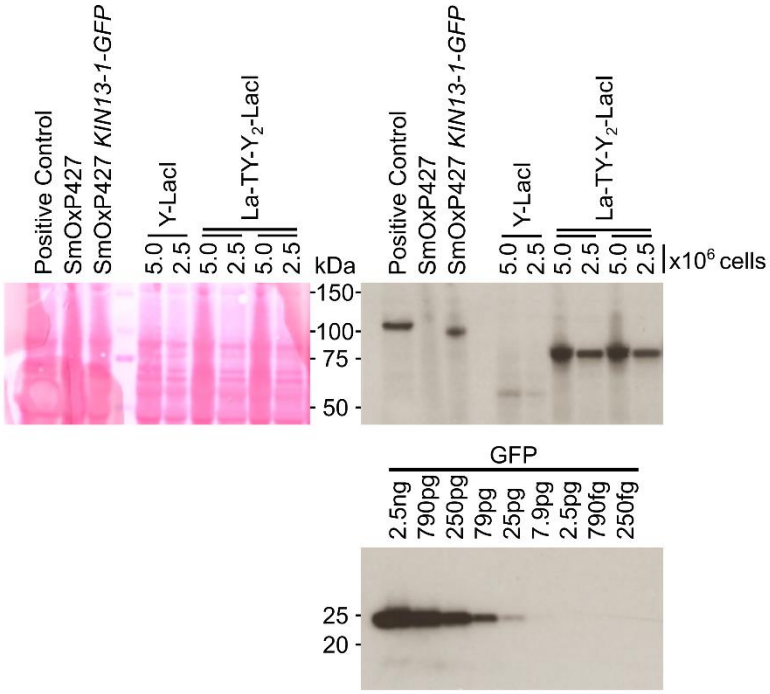


Figure 53. Altering the NLS of YFP- LacI increases protein levels. LacI protein levels were determined by Western blots, using α-GFP antibodies.

5.2.6. The use of sfGFP to label LacI also restores expression levels

The proximity of the various aspects of the mSt/YFP-LacI proteins may have caused issues with protein folding, leading to the reduction in LacI levels seen previously, which was solved by generation of the La-TY-Y_2-LacI cell line. Firstly, it is possible that the TY epitope distanced the NLS from the YFPs allowing the fluorescent proteins to fold correctly. Issues caused by the proximity between YFP and LacI may have been solved by the addition of a second YFP, which, though unable to fold itself, may have provided the distance required for either of the other two proteins to fold correctly. The reduction in LacI levels after addition of an NLS, however, suggests the proximity of this feature to YFP led to issues with protein folding in the fluorescent protein.

To determine how the generation of the La-TY-Y_2-LacI might have increased LacI protein levels and to produce a LacI protein labelled with a single fluorophore, four constructs were produced that coded for LacI fused to superfolder GFP (sfGFP) (Figure 54). All constructs coded for sfGFP-LacI with a

N-terminal La protein NLS, but varied on their inclusion, or lack thereof, of a TY epitope sequence between the NLS and sfGFP and a short linker sequence (coding for five serines) between sfGFP and LacI. These plasmids were used to generate four cell lines; La-sfG-LacI, La-sfG-link-LacI, La-TY-sfG-LacI and La-TY-sfG-link-LacI. A Western blot was then performed on six clones of each, to confirm sfGFP-LacI expression and to compare quantities of the protein between clones (Figure 55). All four strategies gave largely indistinguishable protein levels, which were similar to levels of KIN13-1-GFP. This suggests that the stability of sfGFP had resolved previous folding issues. The cell line that produced the strongest band, La-TY-sfG-link-LacI clone 3, was chosen for future work.

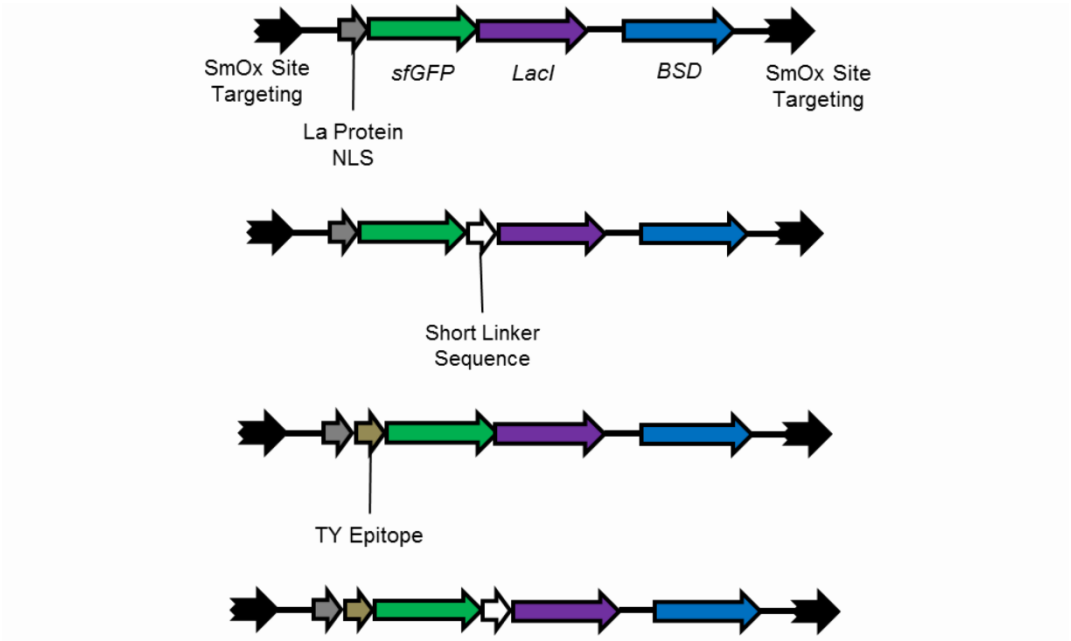


Figure 54. Four constructs for testing LacI expression levels. Four constructs were produced all coding for a various modifications of sfGFP-LacI. The first coded for sfGFP-LacI only (with a La protein NLS). The second separated sfGFP and LacI with a short linker sequence, consisiting of 7 serines. The third contained a TY epitope between the NLS and sfGFP. Finally, the fourth combined the TY epitope and linker sequence, to separate sfGFP from the La protein NLS and LacI.

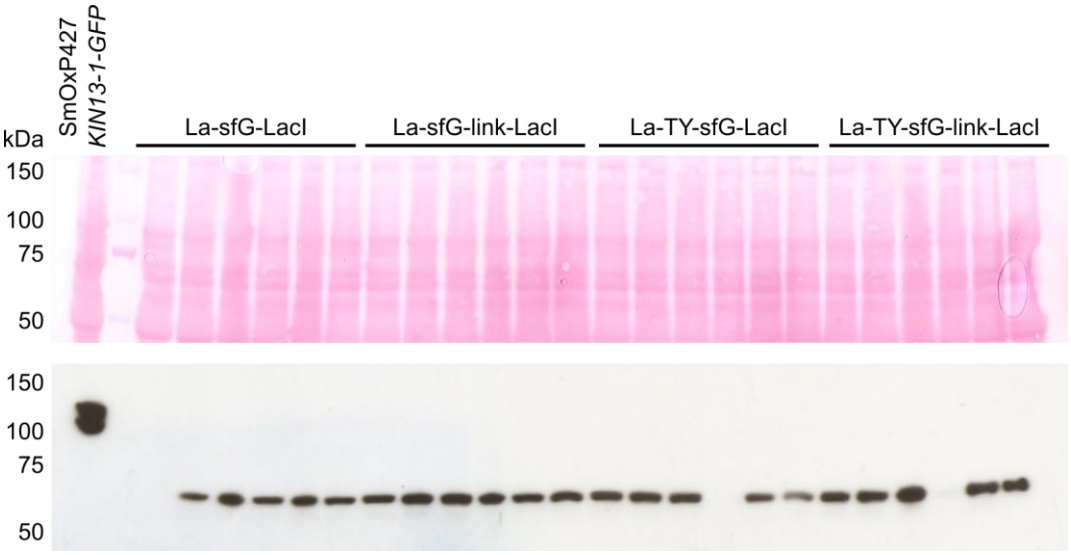


Figure 55. The use sfGFP increases fluorescently labelled LacI levels. A Western blot was performed to determine the quanitities of sfGFP-LacI in whole cell lysates from the four cell lines, La-sfG-LacI, La-sfG-link-LacI, La-TY-sfG-LacI and La-TY-sfG-link-LacI.

5.2.7. A “LacI/LacO system” for observing trypanosome chromosomes

To produce a MBC or MC chromosome label, constructs were generated that would introduce 256 LacO repeats into BES1 or replace the S8 VSG (Figure 56). These LacO repeats would be bound by fluorescently labelled LacI, producing a fluorescent focus at the targeted site. Again, constructs were directed towards the S8 VSG, so that a known MC of a known size would be tagged, and BES1 was targeted as a control. These plasmids were linearised and transfected into La-TY-sfG-link-LacI and La-TY-Y_2-LacI cells, to produce the La-TY-sfG-link-LacI $LacO_{BES1}$, La-TY-sfG-link-LacI $LacO_{S8\ VSG}$, La-TY-Y_2-LacI $LacO_{BES1}$ and La-TY-Y_2-LacI $LacO_{S8\ VSG}$ cell lines. All four of these cell lines produced fluorescent foci that could be observed by native fluorescence (Figure 57). Many of the foci produced by sfGFP-LacI were bright enough to be viewed by eye under blue light and showed little bleaching. These data suggest that integration of LacO repeats in combination with constitutive expression of fluorescently labelled LacI can be used to label DNA elements in *T. brucei*. Furthermore, the visibility of foci by eye, without the use of long exposure times, and their stability opens up more possibilities for future library validation experiments.

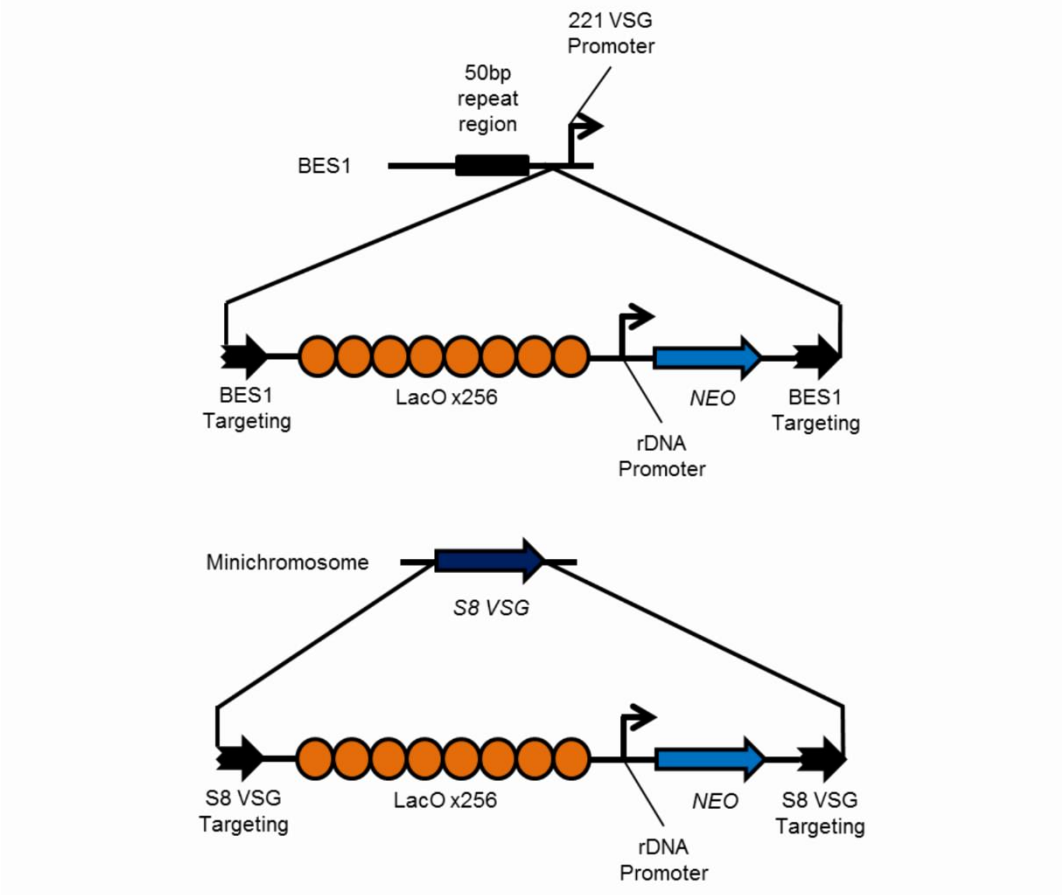


Figure 56. Two strategies for integrating LacO repeats into the trypanosome genome. Two plasmids were produced that would direct LacO repeats to MCs, by replacing the S8 VSG CDS, or to a MBC, by targeting BES1.

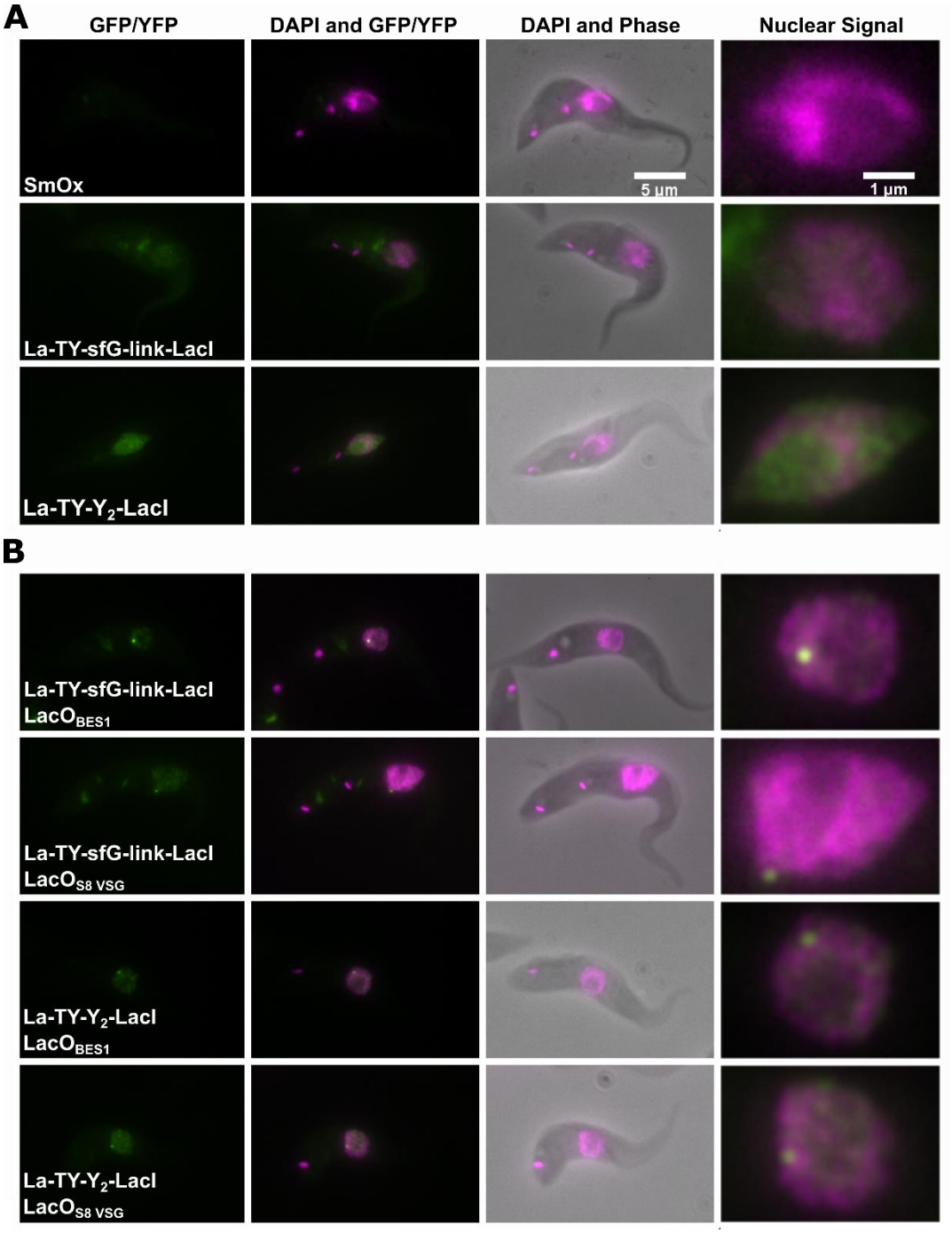


Figure 57. Fluorescent foci are visible when LacO repeats are integrated into the genomes of cells expressing fluorescently labelled LacI. La-TY-sfG-link-LacI and La-TY-Y_2-LacI cells, with (B) or without (A) integrated LacO repeats, were affixed to glass slides and stained with DAPI.

To find the most ideal cell line for future analysis, a line in which just one chromosome was labelled (no duplication events had occurred) and in which all tagged chromosomes were visible, the number of foci per cell was counted. The data from these counts are presented in Figure 58. The smallest proportion of untagged cells was found in La-TY-sfG-link-LacI $LacO_{BES1}$ and La-TY-sfG-link-LacI $LacO_{S8\ VSG}$ cell lines. The higher proportion of untagged cells in La-TY-Y_2-LacI $LacO_{BES1}$ and La-TY-Y_2-LacI $LacO_{S8\ VSG}$ cells may have been due to higher background fluorescence levels masking signal from foci. La-TY-sfG-link-LacI $LacO_{BES1}$ and La-TY-sfG-link-LacI $LacO_{S8\ VSG}$ clones 1 and 2 were selected for further analysis, because they displayed the lowest proportion of untagged cells, as well as displaying very little duplication.

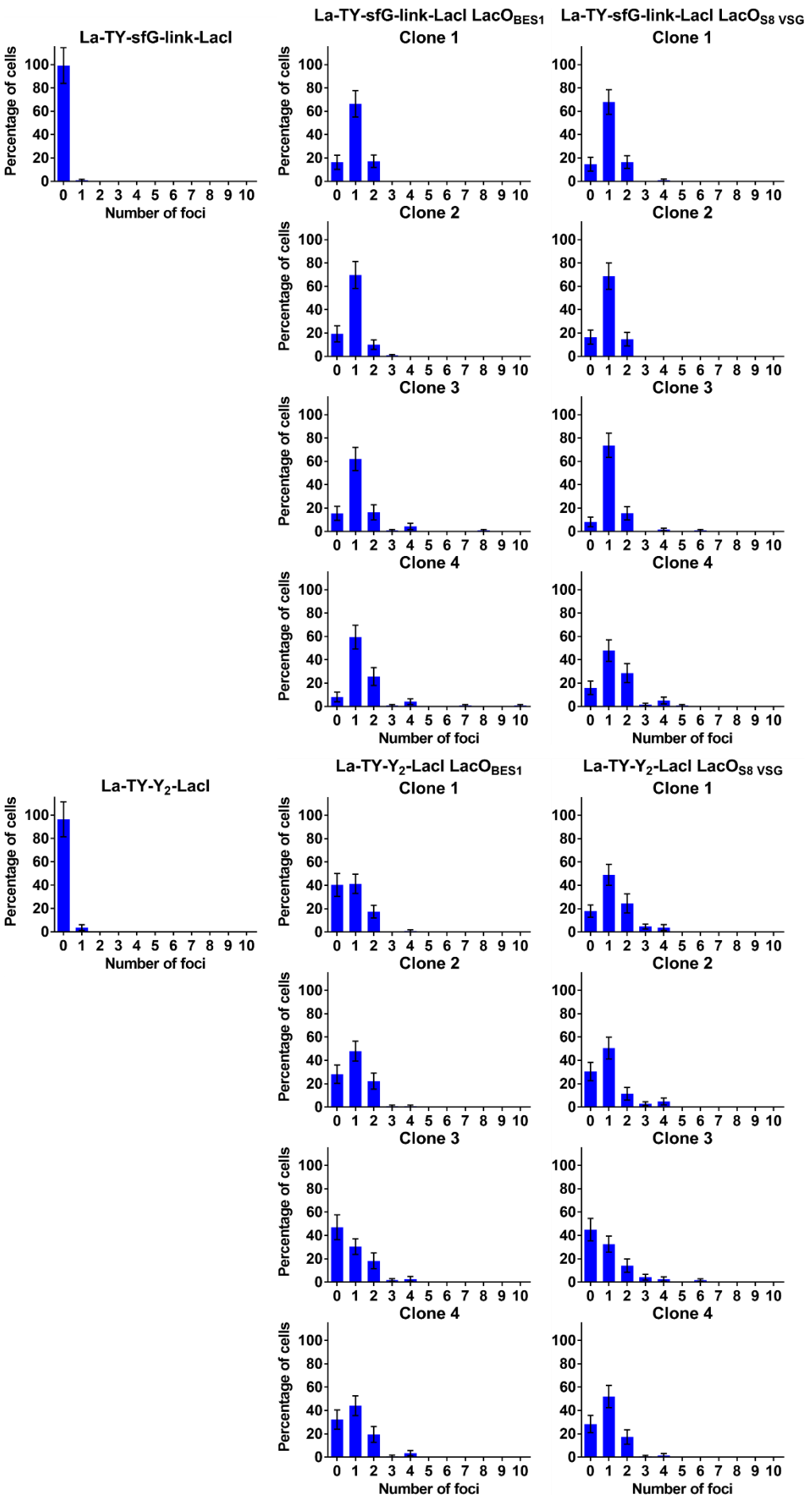

La-TY-sfG-link-LacI
La-TY-sfG-link-LacI LacO$_{BES1}$
La-TY-sfG-link-LacI LacO$_{S8\ VSG}$
La-TY-Y$_2$-LacI
La-TY-Y$_2$-LacI LacO$_{BES1}$
La-TY-Y$_2$-LacI LacO$_{S8\ VSG}$
Clone 1
Clone 2
Clone 3
Clone 4
Percentage of cells
Number of foci

Figure 58. Distribution of foci across multiple LacO cell line clones. The number cells displaying fluorescent foci of various quantities was counted across multiple clones of the La-TY-sfG-link-LacI $LacO_{BES1}$, La-TY-sfG-link-LacI $LacO_{S8\ VSG}$, La-TY-Y_2-LacI $LacO_{BES1}$ and La-TY-Y_2-LacI $LacO_{S8\ VSG}$ cell lines. Percentages were calculated from these counts and plotted.

To determine whether the lack of foci observed in the selected cell lines was due to subpopulations lacking LacO constructs, a G418 sensitivity test was performed (Table 6). Three of the four cell lines produced no clones that were sensitive to G418. These lines, therefore, did not contain cells lacking LacO constructs. Two wells representing an expected seven clones (or 5.4%) of La-TY-sfG-link-LacI $LacO_{S8\ VSG}$ Clone 1 were sensitive to G418. Foci counts showed that ~15% of cells lacked foci in this cell line, so the number of sensitive clones is not representative of all cells lacking foci. These data suggest that the lack of foci observed was not caused by loss of LacO constructs, but was most likely due to foci being outside the focal plane, or LacO repeats may have been inaccessible to LacI in these cells.

Cell Line	Positive Wells		Inferred Clones			
	Before G418	After G418	Before G418		After G418	
La-TY-sfG-link-LacI $LacO_{BES1}$ 1	47	47	64.6	±9.04	64.6	±9.04
La-TY-sfG-link-LacI $LacO_{BES1}$ 2	53	53	77.1	±10.8	77.1	±10.8
La-TY-sfG-link-LacI $LacO_{S8\ VSG}$ 1	71	69	129	±15.5	122	±14.6
La-TY-sfG-link-LacI $LacO_{S8\ VSG}$ 2	45	45	60.7	±9.1	60.7	±9.1

Table 6. Cells lacking foci do not lack LacO repeat constructs. Cells were diluted and plated on 96 well plates, without drug pressure, so that each cell was predicted to contain, on average, one cell. After ten days the numbers of positive wells were counted and number of clones they represented calculated. Cells were re-plated, with G418 drug pressure, and grown for a week, with dilutions performed when necessary. The number of positive wells were then counted and the number of clones calculated a second time.

To confirm that LacO repeats were located in the correct chromosomes in the selected cell lines, a Southern blot was performed on whole chromosomes separated by PFGE (Figure 59). The probes used in the blot were derived from pT1045, a plasmid that contains just the 256 LacO repeats, as well as the genes required for its maintenance in bacteria. The probes, therefore, would also bind bacterial sequences present in the integrated LacO plasmid backbones. These were not introduced by of LacI constructs, due to differing methods employed in plasmid linearisation. Controls in the form of the SmOxP427 Neo_{BES1} and SmOxP427 $Neo_{S8\ VSG}$ cells, as well SmOxP427 Neo_{177bp} cells were, therefore, run. These were cells in which constructs lacking LacO repeats, though otherwise identical to the LacO constructs, had been introduced. Bands representing chromosomes from these cells are less intense than those containing LacO repeats, as expected, indicating they had bound fewer probes. The MC carrying the S8 VSG CDS is ~95kb in size (Wickstead et al., 2004), so the addition of the ~13kb LacO repeats constructs would be expected to create a chromosome of ~108kb. A band of this size was visible in La-TY-sfG-link-LacI $LacO_{S8\ VSG}$ clone 2. A band of ~48.5kb was also visible and was the only band visible in clone 1. This change in size would indicate some change had occurred to the targeted chromosome, which is further indicated by the smaller than expected band in SmOxP427 $Neo_{S8\ VSG}$ cells. The lack of smearing suggests that fragmentation of chromosomes had not occurred and the continued presence of fluorescent foci suggest that the MCs are mitotically stable. It would be interesting to map these chromosomes, as this could provide some insight into the minimum requirements a chromosome requires to be replicated in *T. brucei*.

To confirm that LacO repeats had been integrated into the correct sites, diagnostic PCRs were performed (Figure 60). A forward primer was designed that bound to the BES or S8 construct and a reverse primer that bound downstream of targeting regions, within the trypanosome genome. Another set of primers were designed that would amplify the LacO constructs only. These primers amplified product of expected sizes in all LacO cell lines, showing that LacO repeats had been integrated into the correct sites.

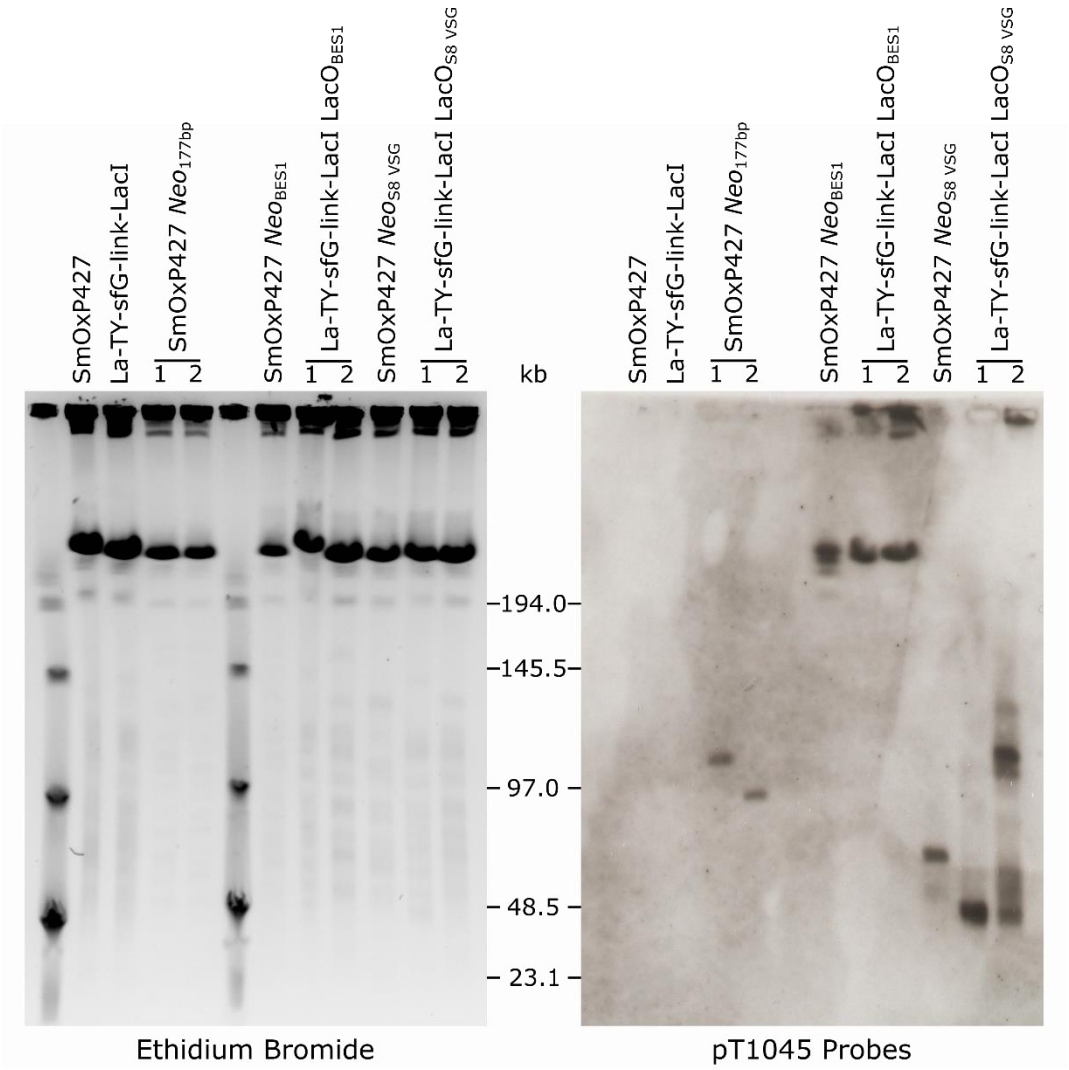


Figure 59. LacO repeats are present in MCs and MBCs. A Southern blot was carried out to confirm the presence of LacO repeats in cell lines. PFGE was performed to separate MCs from MBCs, using agarose plugs prepared from La-TY-sfG-link-LacI $LacO_{BES1}$ and La-TY-sfG-link-LacI $LacO_{S8\ VSG}$. Plugs were also prepared from cells, in which only the *Neo* resistance marker had been introduced into chromosomes (La-TY-sfG-link-LacI Neo_{BES1} and La-TY-sfG-link-LacI $Neo_{S8\ VSG}$), to act as a control.

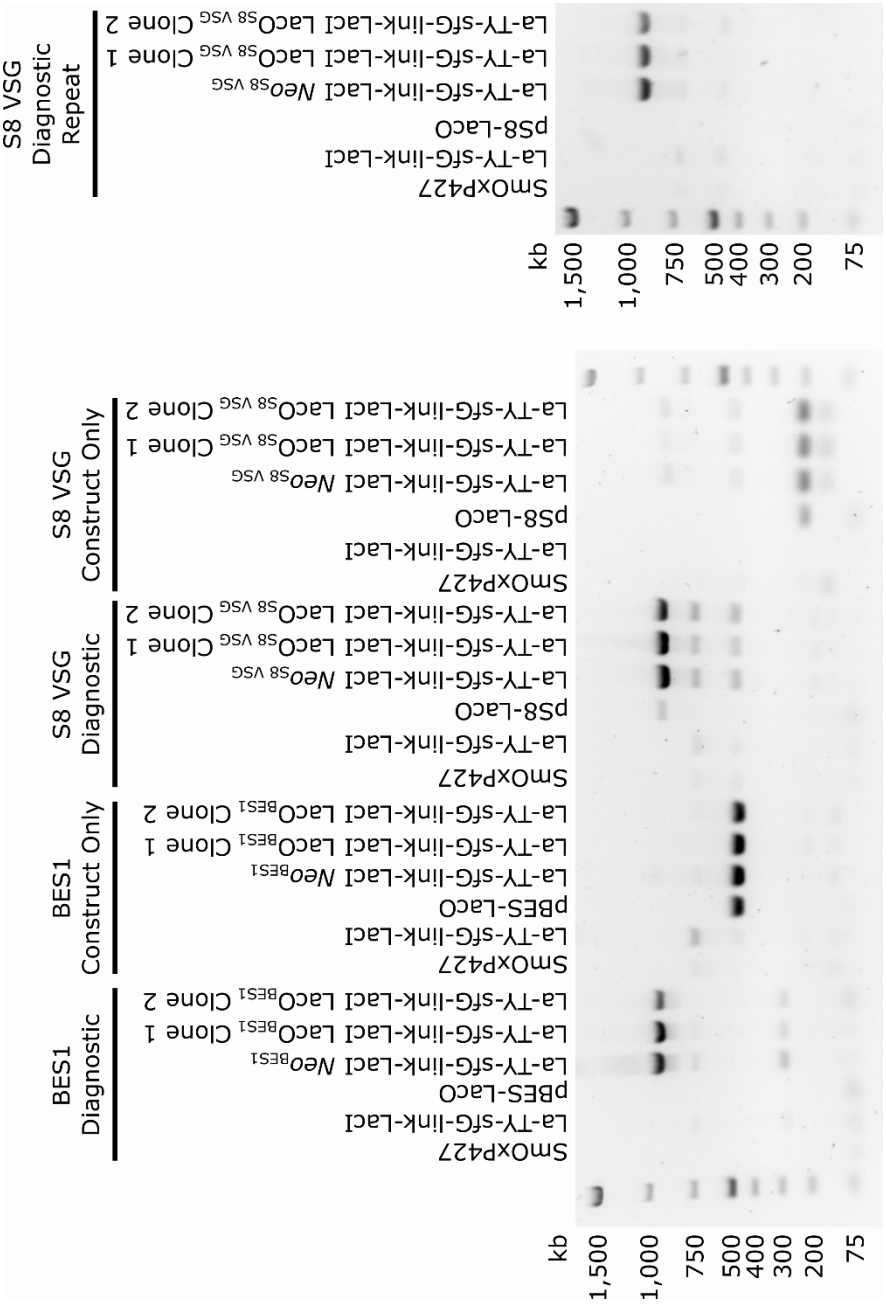


Figure 60. Diagnostic PCRs confirm correct integration of LacO repeats. Primers were designed to amplify a region of the integrated construct (construct only) or a region bridging the construct and the an area of the genome downstream of the target sequence (diagnostic). Touchdown PCRs were performed using these primers. Diagnostic PCR bands were expected to be 929bp and 1,063bp for the La-TY-sfG-link-LacI $LacO_{BES1}$ and La-TY-sfG-link-LacI $LacO_{S8\ VSG}$ cell lines, respectively. “Construct only” PCRs were expected to produce bands of 480bp and 365bp.

5.2.8. Summary

In order to validate the results of the library experiments, it was decided that microscopy would be used, employing “reporter” cell lines, containing a mitotic spindle and/or a MC label. Here, I have demonstrated that KIN13-1-GFP is a valuable spindle label and substitute for tubulin labelling, which could not be used due to the trypanosome’s subpellicular corset of microtubules. A “LacI/LacO system” was developed to label chromosomes. Cells were generated that expressed sfGFP-LacI at levels similar to the KIN13-1 protein (~100-300 proteins per cell), after troubleshooting the reduced protein levels caused by addition of a NLS. sfGFP-LacI proteins bound to LacO repeats that were later integrated into a MC or a MBC, which were shown to produce a bright fluorescent focus representing the location of the chromosome.

6. The movement of individual chromosomes through the *Trypanosoma brucei* cell cycle

In the previous chapter, I described the development of a system for labelling chromosomes using LacO repeats and the LacI protein. This system was developed for the purposes of RNA interference (RNAi) library validation, but it could also be used to investigate movements of chromosomes, interactions between chromosomes and mitotic machinery and the effects of perturbation of these interactions. Below I describe a number of experiments using the chromosome labels for these purposes.

6.1. Observing trypanosomal chromosome movement

6.1.1. Chromosome and minichromosome tags display similar localisations during the cell cycle

In order to demonstrate the changing distributions of chromosomes, images were produced of representative cells containing minichromosome (MC) and megabase chromosome (MBC) tags at different stages of the cell cycle (Figure 61; Figure 62). These images show that fluorescent foci produced by labelled Lac repressor protein (LacI) binding to Lac operator (LacO) repeats can indeed be used to track the movement of MBCs and MCs through the cell cycle. For both the MBC (La-TY-sfG-link-LacI $LacO_{BES1}$) and MC (La-TY-sfG-link-LacI $LacO_{S8\ VSG}$), a single focus can be seen during G1 and G2 phase at the periphery of the nucleus. This positioning of foci is consistent with location of the labelled sites within heterochromatin. Transcriptionally silent genomic DNA, such as BES1 (in PCF cells) and MCs, is associated with the electron-dense heterochromatin, which is located towards the edge of the *T. brucei* nucleus, whereas the active euchromatin is generally found towards the centre (Daniels et al., 2010). At metaphase the focus moves to the metaphase plate, but remains at the nuclear periphery. At anaphase two foci are visible as the sister chromatids are separated and pulled apart. Later in anaphase, the foci are again visible at the leading edge of the DAPI stained DNA. Foci appearing in this position could be due to earlier depolymerisation of kinetochore microtubules, bringing chromosomes into

proximity of the tip of the spindle, similar to anaphase A in model systems (McIntosh et al., 2012). This distribution of MBCs and MCs throughout mitosis is consistent with previous studies (Ersfeld and Gull, 1997; Gull et al., 1998; Ogbadoyi et al., 2000). Furthermore, the locations of foci representing MCs is very similar to that of MBCs, suggesting that similar mechanisms could be involved in separating the two chromosome classes.

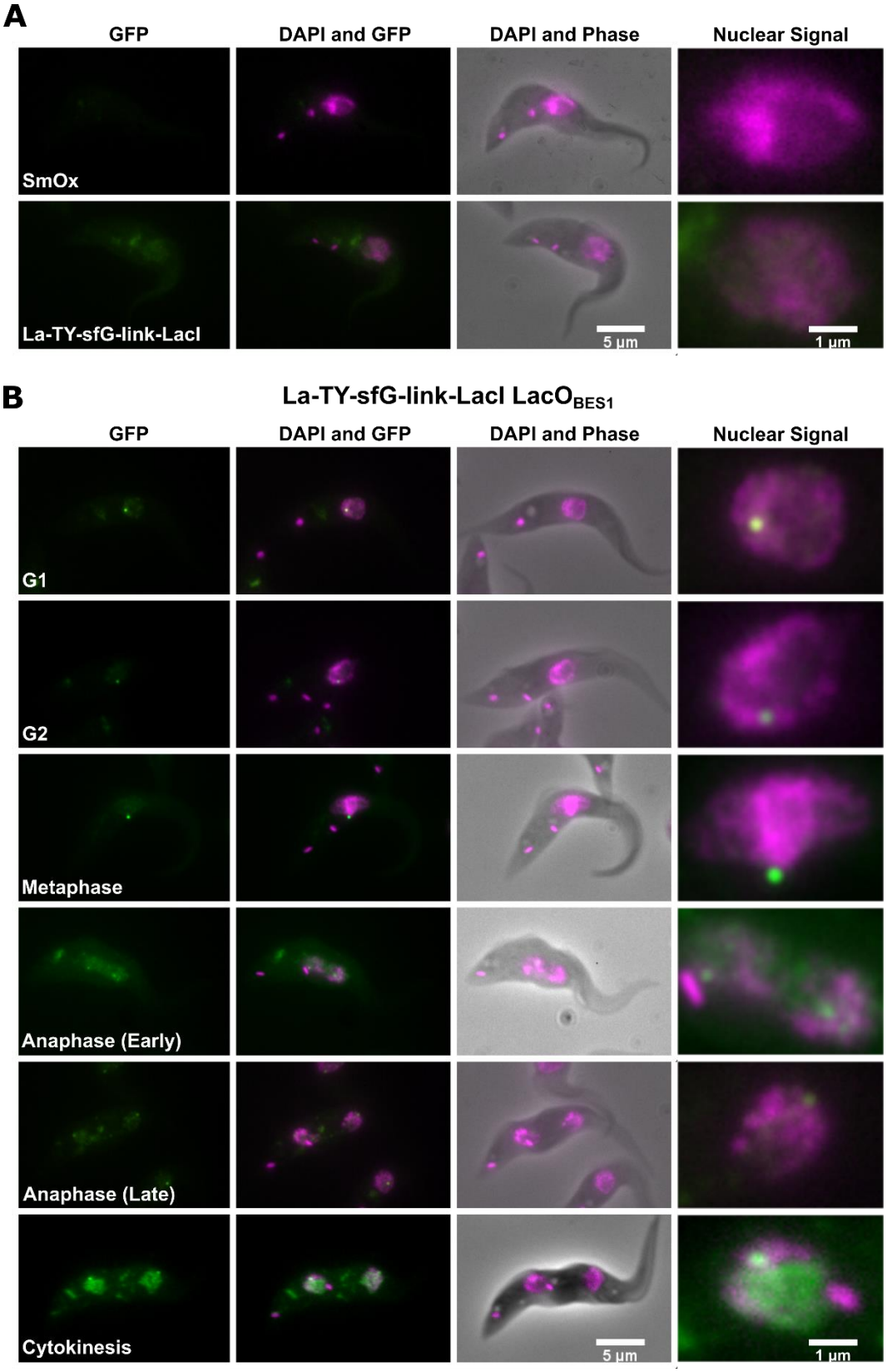


Figure 61. The distribution of MBCs changes through the cell cycle. La-TY-sfG-link-LacI LacO$_{BES1}$ cells (B) and controls (A) were attached to glass slides and stained with DAPI. Images were produced of representative cells at each stage of mitosis.

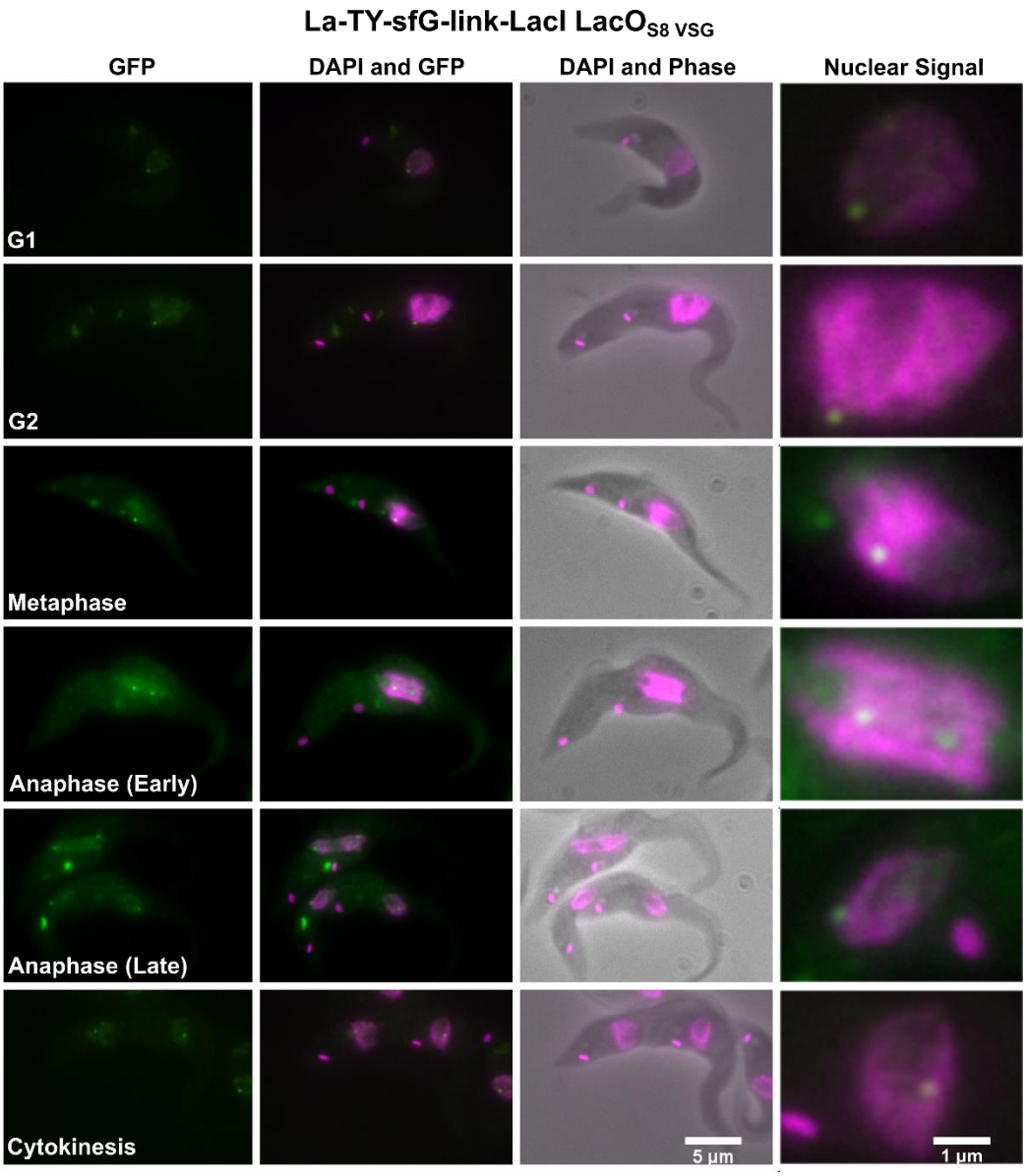


Figure 62. The distribution of MCs changes through the cell cycle. La-TY-sfG-link-LacI $LacO_{S8\ VSG}$ cells were attached to glass slides and stained with DAPI. Images were produced of representative cells at each stage of mitosis

6.1.2. Distribution of fluorescent foci is consistent with kinetochore interaction

In order to determine how MBCs and MCs interacted with kinetochores and whether any differences existed between the two, the relative distributions of kinetochores and chromosomes were investigated. To visualise kinetochores, three different kinetochore proteins were N-terminally labelled with mStrawberry. These proteins were KKT1 (Akiyoshi and Gull, 2014) and KKIP1, which has previously been discussed, as well as KKIP5 (Tb427.07.6630), another kinetochore protein identified by the lab (D'Archivio and Wickstead, 2016). KKT1 is believed to associate close to the centromere, while KKIP1 and 5 may form part of the outer kinetochore. KKIP5 was also of interest, because it is not present at anaphase, so its disappearance could act as a marker for the initiation of chromosome segregation.

The three proteins were labelled with mStrawberry by endogenous locus tagging in both La-TY-sfG-link-LacI $LacO_{BES1}$ and La-TY-sfG-link-LacI $LacO_{S8\ VSG}$ cell lines, creating six cell lines. The production of labelled protein was confirmed by Western blot (Figure 63), which produced the expected bands of 174 and 108kDa for KKT1 and KKIP1, respectively. The size of KKIP5 is predicted to be 89.8kDa, but previous work has demonstrated that it runs at ~150kDa (D'Archivio and Wickstead, 2016), which was also seen in this experiment. The six cell lines were imaged, to determine the distribution of kinetochore proteins and chromosomes, throughout the cell cycle. KKT1 and KKIP1 displayed similar positions at the different stages of mitosis (Figure 64-7). The proteins were not present at G1 phase, but appeared at G2 phase as numerous mStrawberry foci distributed across the nucleus. GFP-LacI signal often colocalised with mStrawberry signal from labelled kinetochore proteins, suggesting interaction between the two and possibly the formation of kinetochores at centromeres. KKT1 and KKIP1 then moved with chromosomes to the metaphase plate. At anaphase, foci representing the two proteins moved to the leading edges of the dividing nuclei, coming into close proximity with one another. Distances between GFP and mStrawberry foci also appeared larger, possibly due to the labelled subtelomeres of MCs and MBCs trailing as centromeres were pulled apart by the spindle. The

distributions of mStrawberry-KKT1 and -KKIP1 were consistent with previously published work (Akiyoshi and Gull, 2014; D'Archivio and Wickstead, 2016). The distribution of mStrawberry and GFP foci did not appear to vary between La-TY-sfG-link-LacI $LacO_{BES1}$ and La-TY-sfG-link-LacI $LacO_{S8\ VSG}$ cell lines, suggesting both MCs and MBCs associate with kinetochores. KKIP5 showed a similar distribution to KKT1 and KKIP1 between G1 and metaphase (Figure 68; Figure 69). Signal associated with the protein quickly disappeared at anaphase, however, and was absent at the very earliest stages of chromosome segregation. This would suggest that KKIP5 can act as a marker for the transition between metaphase and anaphase, though its function in this transition remains to be determined.

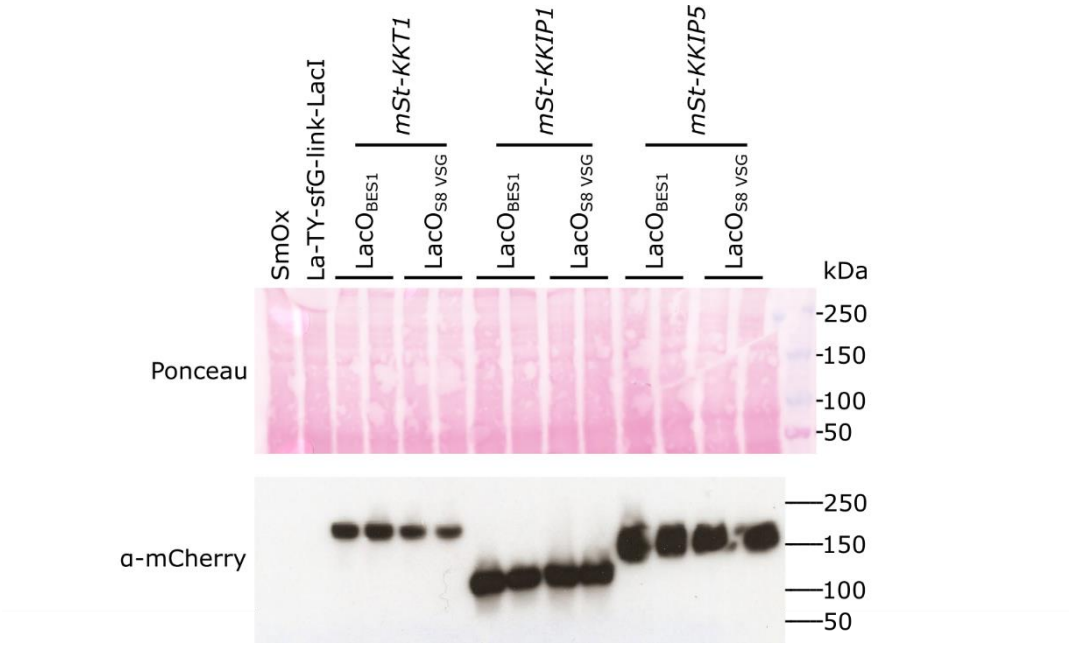


Figure 63. Confirmation of expression of mStrawberry labelled kinetochore proteins. A Western blot was performed using rabbit α-mCherry polyclonal antibodies and a goat α-rabbit-HRP secondary.

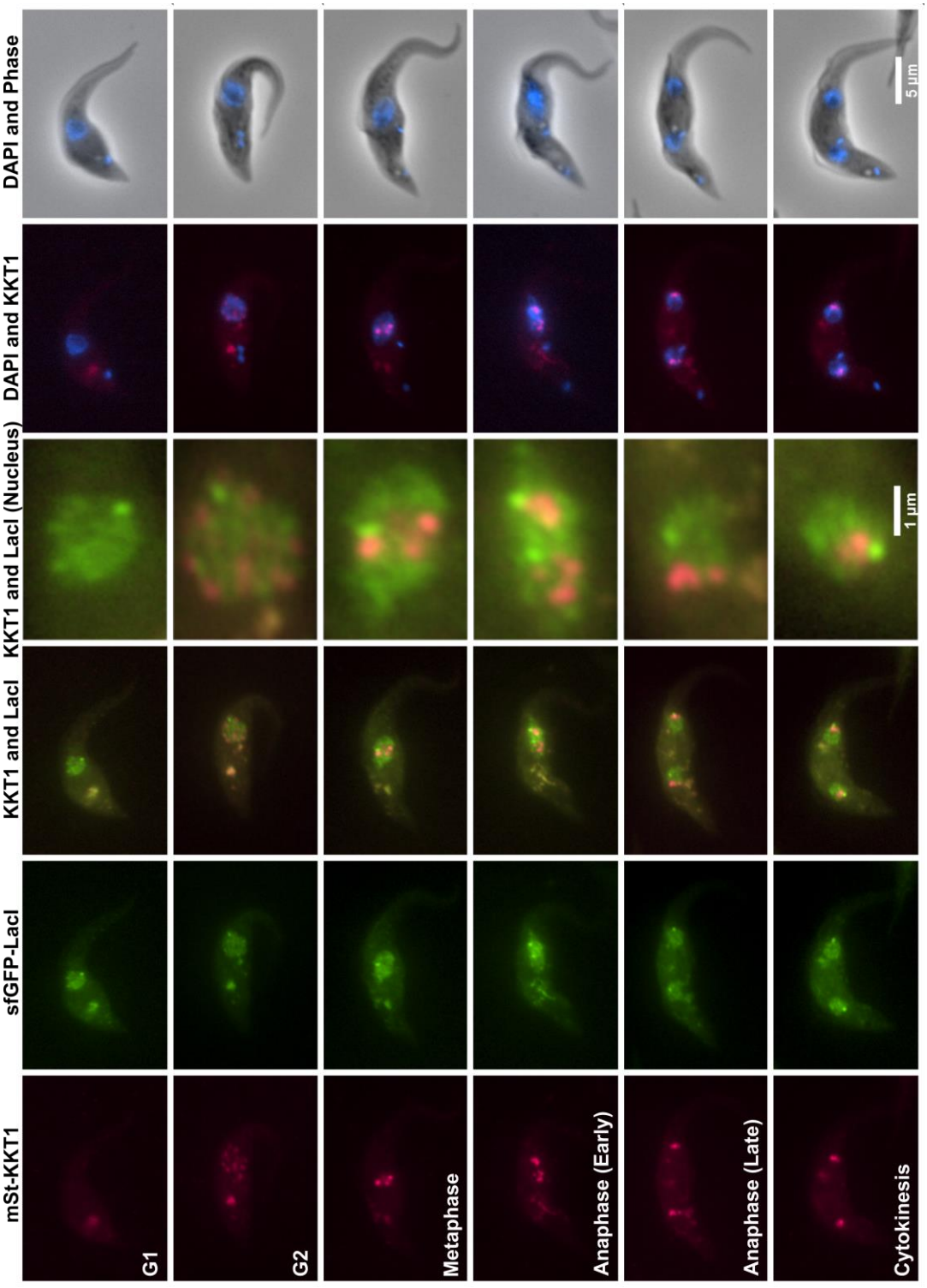


Figure 64. The distribution of LacI/LacO labelled BES1 and mStrawberry-KKT1 throughout the cell cycle. La-TY-sfG-LacI $LacO_{BES1}$ *mSt-KKT1* cells were attached to glass slides and stained with DAPI. Cells were imaged, so that representative images of cell cycle stages could be displayed.

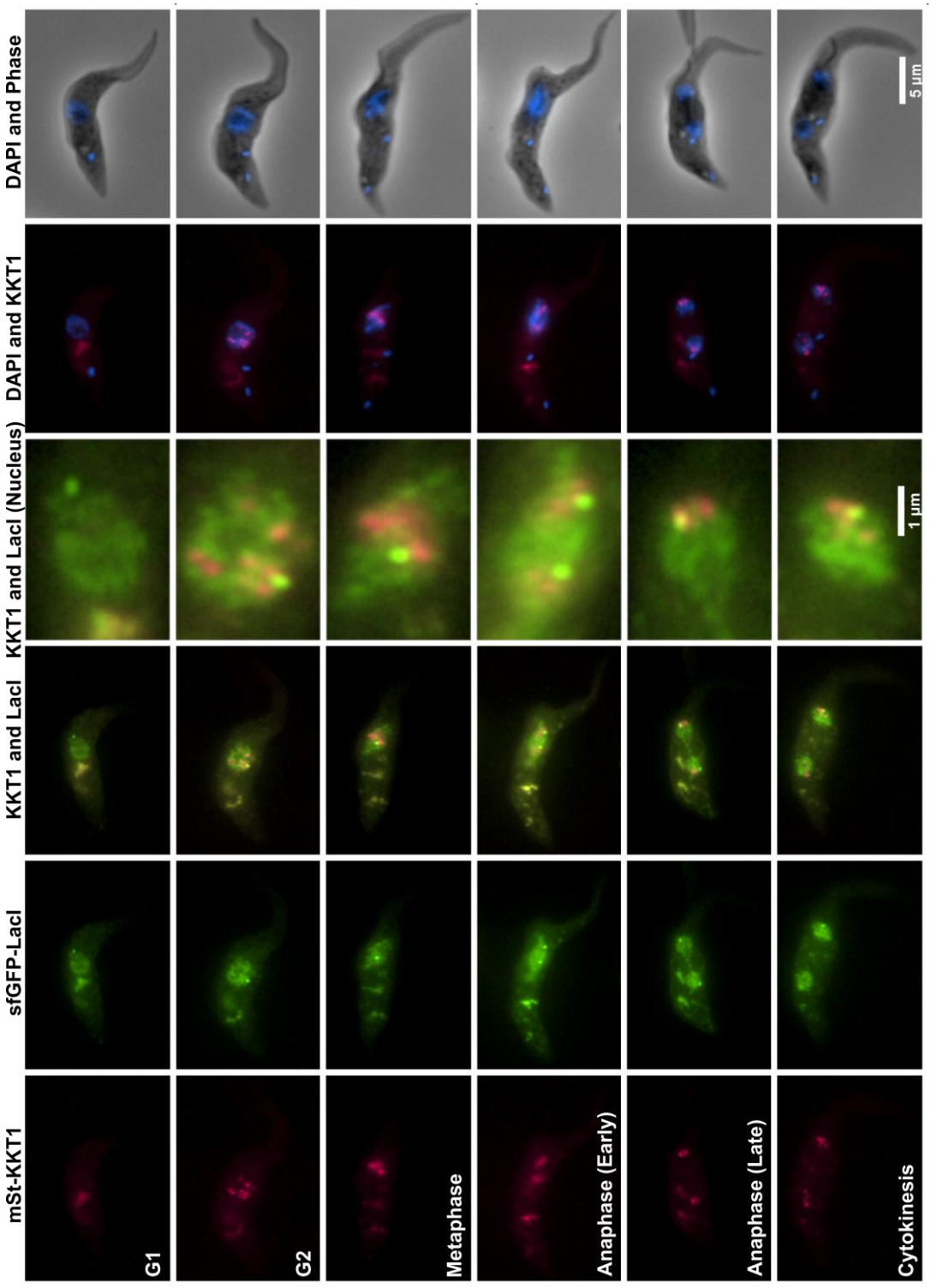


Figure 65. The distribution of the LacI/LacO labelled S8 VSG MC and mStrawberry-KKT1 throughout the cell cycle. La-TY-sfG-link-LacI $LacO_{S8\ VSG}$ *mSt-KKT1* cells were attached to glass slides and stained with DAPI. Cells were imaged, so that representative images of cell cycle stages could be displayed.

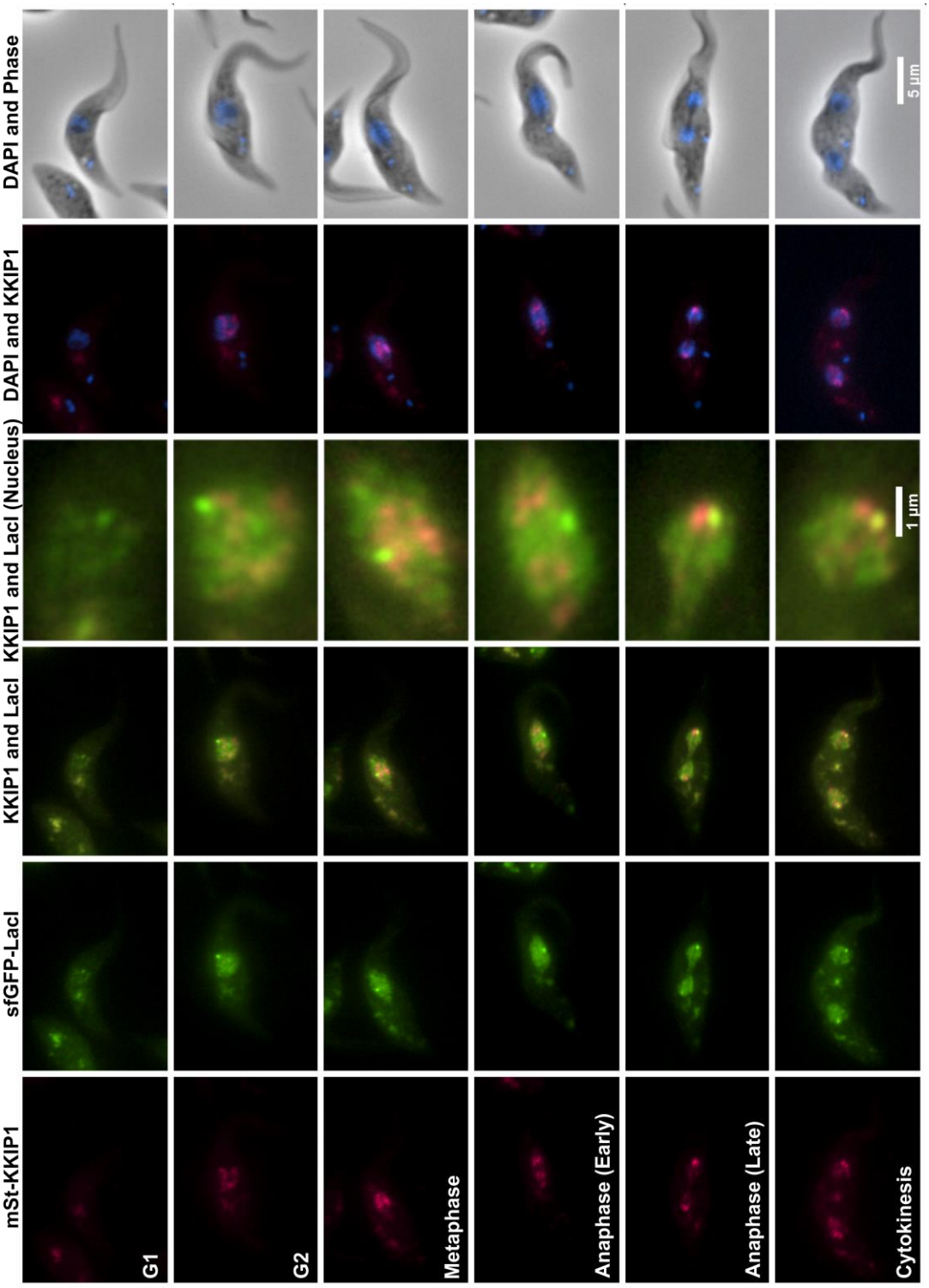


Figure 66. The distribution of LacI/LacO labelled BES1 and mStrawberry-KKIP1 throughout the cell cycle. La-TY-sfG-link-LacI $LacO_{BES1}$ *mSt-KKIP1* cells were attached to glass slides and stained with DAPI. Cells were imaged, so that representative images of cell cycle stages could be displayed.

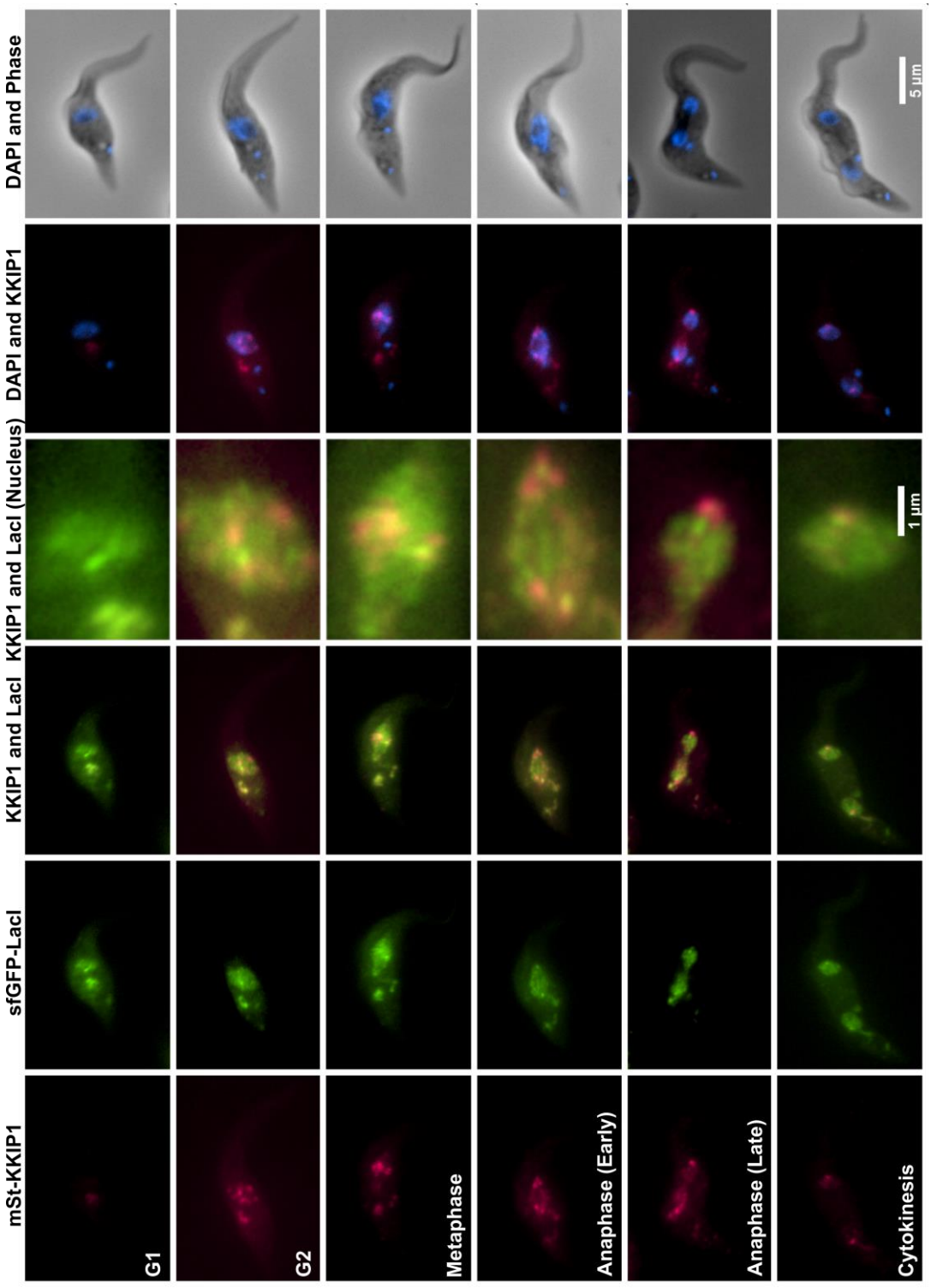


Figure 67. The distribution of the LacI/LacO labelled S8 VSG MC and mStrawberry-KKIP1 throughout the cell cycle. La-TY-sfG-link-LacI $LacO_{S8\ VSG}$ *mSt-KKIP1* cells were attached to glass slides and stained with DAPI. Cells were imaged, so that representative images of cell cycle stages could be displayed.

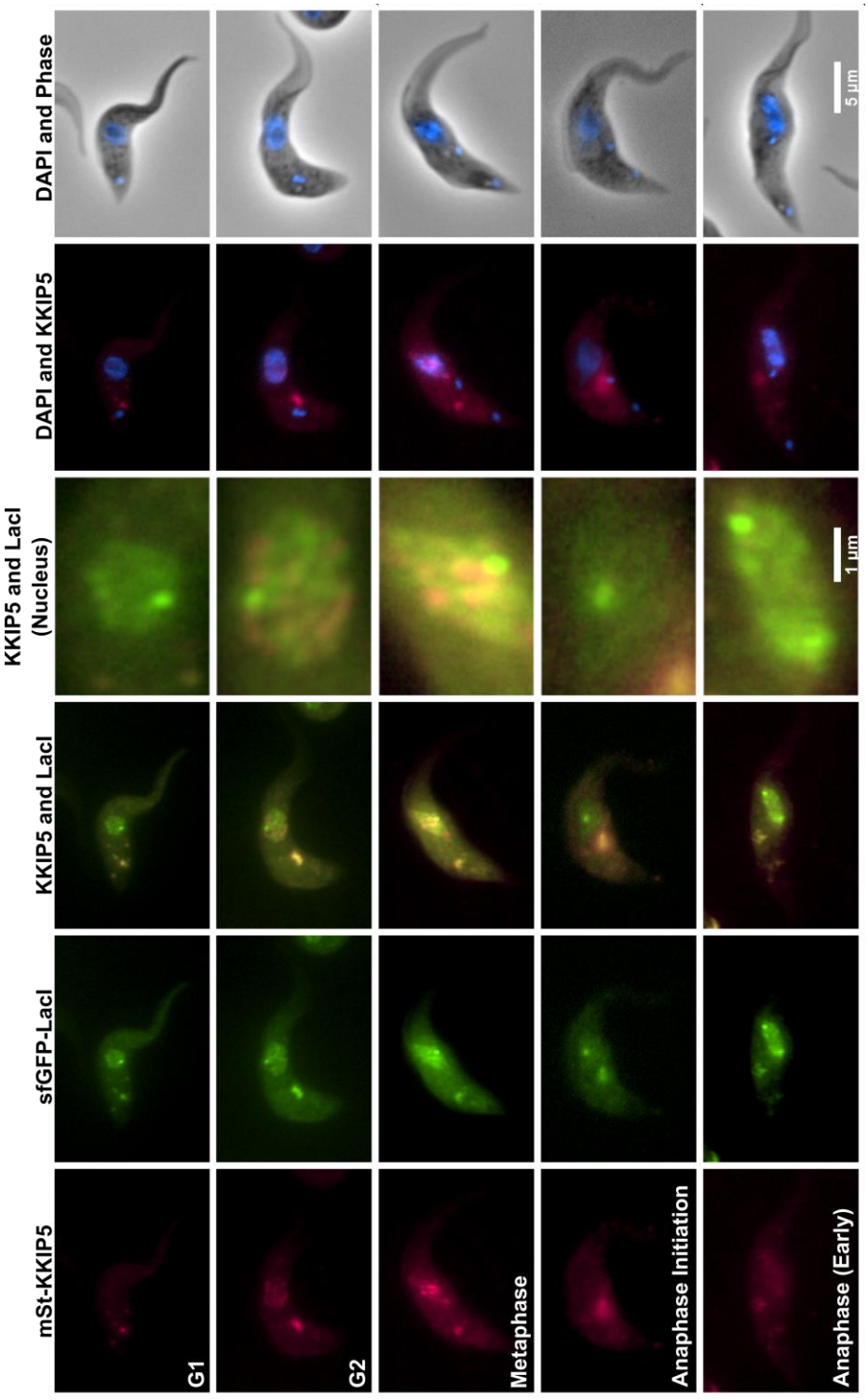


Figure 68. The distribution of LacI/LacO labelled BES1 and mStrawberry-KKIP5 throughout the cell cycle. La-TY-sfG-link-LacI $LacO_{BES1}$ *mSt-KKIP5* cells were attached to glass slides and stained with DAPI. Cells were imaged, so that representative images of cell cycle stages could be displayed.

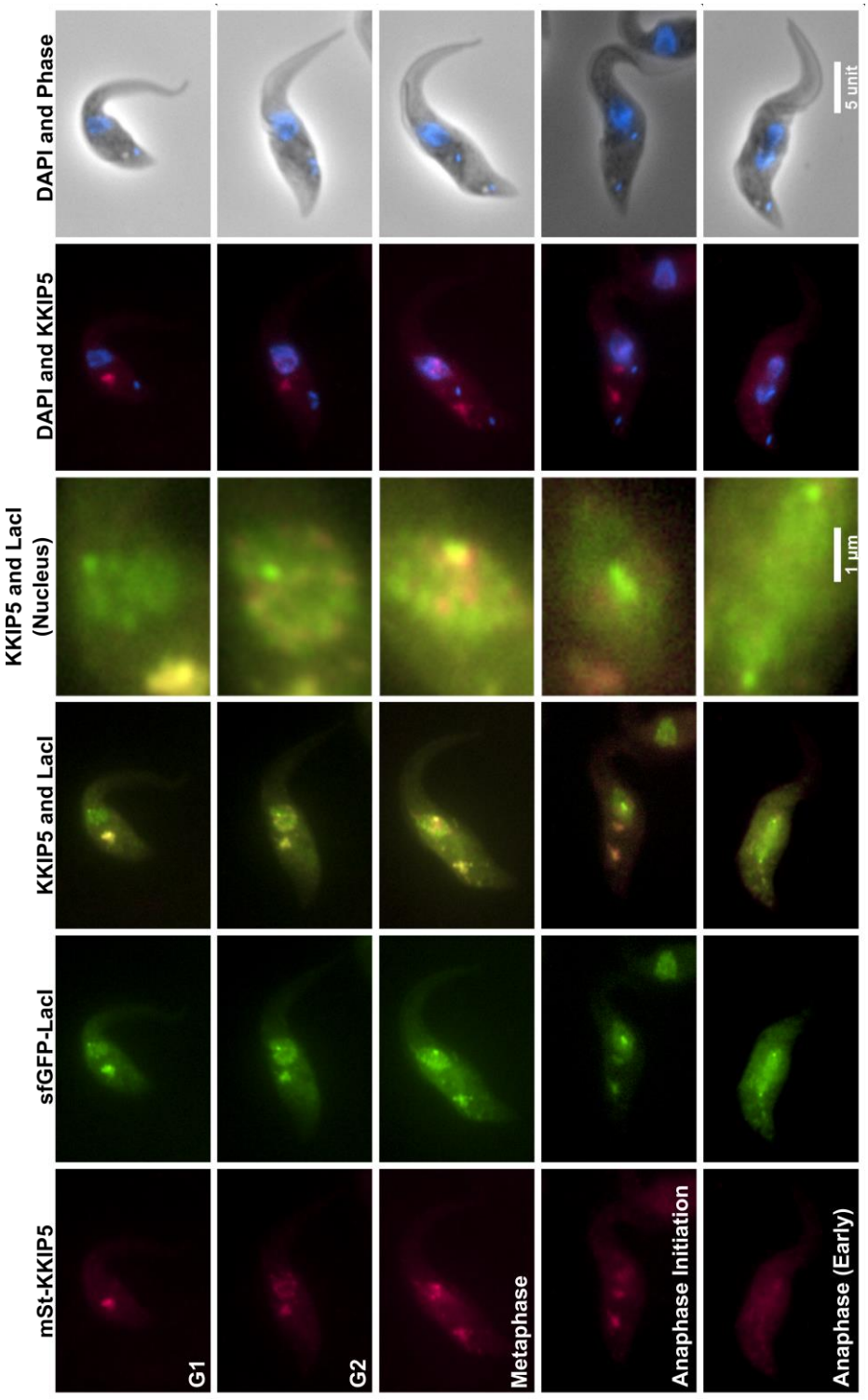


Figure 69. The distribution of the LacI/LacO labelled S8 VSG MC and mStrawberry-KKIP5 throughout the cell cycle. La-TY-sfG-link-LacI $LacO_{S8\ VSG}$ *mSt-KKIP5* cells were attached to glass slides and stained with DAPI. Cells were imaged, so that representative images of cell cycle stages could be displayed.

6.1.3. Distances between chromosomes and kinetochores vary throughout mitosis

To investigate how chromosomes and kinetochores interact, the distances between GFP and mStrawberry foci representing chromosomes and kinetochore proteins were determined. Images were produced of La-TY-sfG-link-LacI $LacO_{BES1}$ and La-TY-sfG-link-LacI $LacO_{S8\ VSG}$ cells expressing mStrawberry-KKT1 or mStrawberry-KKIP1 cells at various stages of mitosis and used for measurement of distances between GFP and mStrawberry fluorescent foci. These measurements were then plotted as Tukey box and whisker plots or as bee swarm plots (Figure 70).

Foci representing MCs were significantly closer to both KKT1 and KKIP1 foci at metaphase than those representing MBCs ($p=<0.001$ and 0.0027, respectively; t-test), which was likely a function of the MC's smaller size, suggesting interaction between MCs and kinetochores. Distances between chromosome labels and both KKT1 and KKIP were also lower at metaphase than at G2 phase. The reduction in separation between KKIP1 and either chromosome class was highly significant ($p<0.001$ in both cases; t-test). The change in distance between KKT1 and MCs was also significant ($p=0.021$; t-test), though to a lesser extent, but between KKT1 and MBCs it was not ($p=0.09$; t-test). Distances between mStrawberry and GFP foci were likely greater during G2 phase, because chromosomes were in the process of condensing and kinetochores were being assembled. In some cases, there may not have been kinetochores assembling on the labelled chromosome, increasing the distance to the nearest mStrawberry focus. At metaphase chromosomes had condensed and kinetochores had formed, reducing the distance between foci. The less significant or insignificant reduction in distance observed between KKT1 and chromosomes may in part be due to its association with centromeres and, therefore, its closer association with the chromosomes. Furthermore, this association means that it is likely to have been laid down earlier in kinetochore assembly, reducing the likelihood of observing chromosomes that had not associated with KKT1 in comparison to KKIP1.

After initiation of anaphase distances between GFP and mStrawberry foci increased. This was likely due spindle changes putting kinetochores under tension and subtelomeres trailing behind as the chromosomes were separated. The increases in distances between KKT1 and KKIP1 and MBCs, however, were insignificant ($p=0.29$ and 0.31; t-test), while distances between the proteins and MCs were significant ($p=0.018$ and 0.0013; t-test). Later on in anaphase distances between KKT1 or KKIP1 and chromosomes fell or rose, respectively, but not significantly, except in the case of MBCs and KKIP1 ($p=0.046$; t-test). While the conservation of patterns in changes in distances between MBCs and MCs suggests similar interactions with kinetochores, the differing significances of these changes may indicate that differing mechanisms may be involved.

These data and the images presented above suggest that MCs do interact with kinetochores. It is, therefore, likely that trypanosome chromosomes share kinetochores, in order to attach to the spindle, and that lateral stacking (Gull et al., 1998) does not occur. It still remains to be determined, however, whether MBCs and MCs differ in the mechanisms by which they interact with the kinetochores.

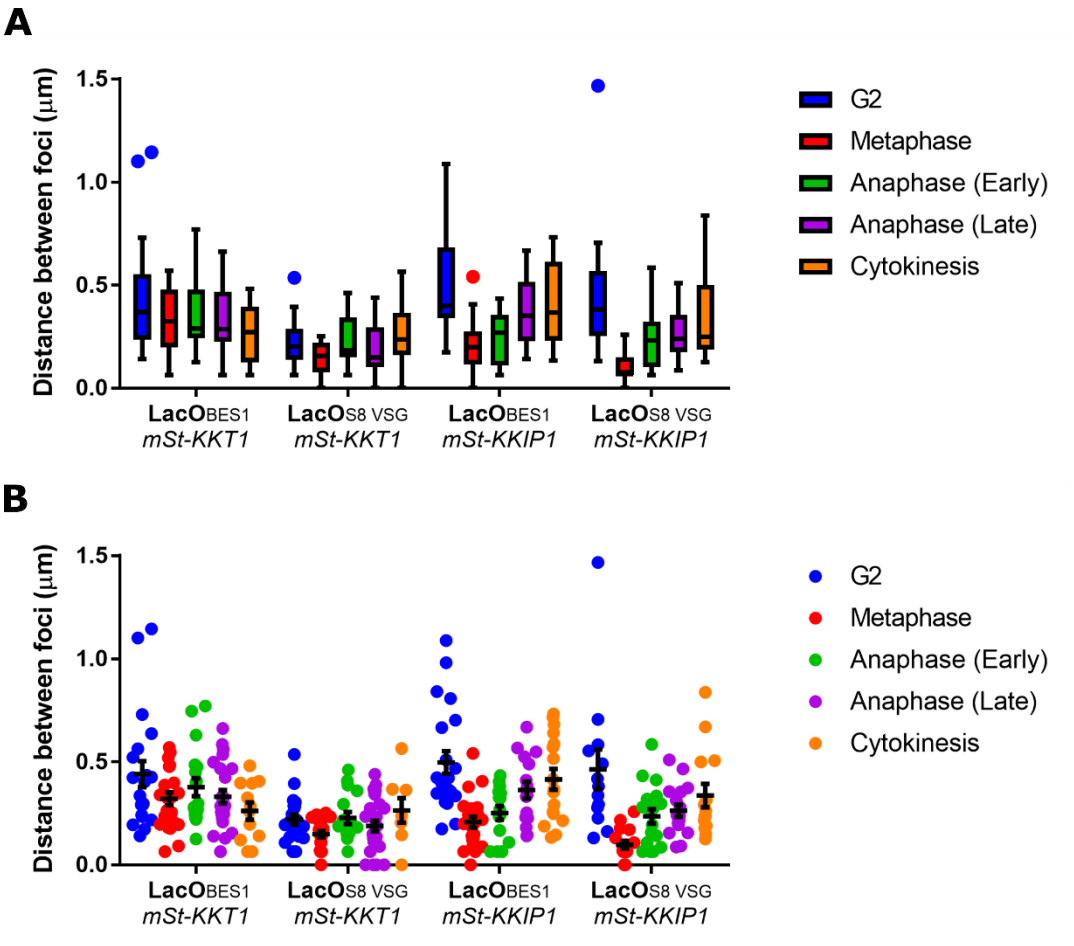


Figure 70. Changes in the distances between chromosome and kinetochore tags occur throughout mitosis. The distance between the chromosomal GFP focus and nearest mStrawberry focus was measured, using ImageJ (Schneider et al., 2012), in images taken of dividing La-TY-sfG-link-LacI $LacO_{BES1}$ and La-TY-sfG-link-LacI $LacO_{S8\ VSG}$ cells expressing mStawberry-KKT1 and mStrawberry-KKIP1 proteins. The minimum possible measurement of overlapping foci was set at 0.0645μm, or 1 pixel. If GFP foci were surrounded by mStrawberry signal the distance was defined as 0μm. Data are presented as a Tukey box and whisker plot with the median distance represented (A) or a bee swarm plot with the mean distance represented (B).

6.1.4. Summary

In the previous chapter a tag for both a MBC and a MC was developed, using a system based on LacO repeats and the LacI protein, as a reporter cell line for validation of library experiments. In this chapter, I have shown that these tags can be used to follow chromosomes through the cell cycle, showing how their position in the nucleus changes as mitosis progresses. It was also possible to use these labelled chromosomes to investigate how chromosomes interact with mitotic machinery. Here, for example, I used these chromosomes to investigate interactions between chromosomes and the kinetochore proteins KKT1, KKIP1 and KKIP5. I demonstrated colocalisation of these proteins with MBCs and MCs and observed changes in these localisations over the course of mitosis, which suggested both chromosome classes do interact with the small number of kinetochores in the trypanosome spindle. Additionally, I showed that the disappearance of KKIP5 occurs very early on chromosome segregation, suggesting it may act as a marker for anaphase initiation.

6.2. Disrupting normal chromosome movement

6.2.1. Fluorescently labelled chromosomes can be used to detect chromosome loss and nondisjunction events

To determine how disruption of normal mitosis affects distribution of chromosome foci among populations of cells, RNAi plasmids targeting KKIP1 and KIN13-1 were introduced into cells with LacI/LacO visualisation of either MBCs or MCs (La-TY-sfG-link-LacI $LacO_{BES1}$ or $LacO_{S8\ VSG}$). To confirm knockdown of proteins, phenotypes were assessed by K-N counts (for KKIP1) or a Western blot (for KIN13-1), after RNAi had been induced for 48 hours (Figure 71). Both demonstrated knock down of the target proteins had occurred. To determine the baseline loss or gain of foci, parental cell lines were grown for 96 hours without drug pressure and cells lacking GFP foci or cells in G1 phase that contained two foci counted (Figure 72A and B). Lack of drug pressure caused no significant change in the number of cells lacking foci and no change in cells possessing two.

The effect of RNAi on the numbers of cells lacking MBC or MC GFP foci was then determined over the course of 96 hours (Figure 72C). Knockdown of both KKIP1 and KIN13-1 produced an increase in numbers of cells lacking foci that represented MCs. In both cases this occurred in a time dependent manner, but only KKIP1 knockdown produced an increase in cells without foci that was significant, tripling the number of these cells after 96 hours. This pattern of apparent chromosome loss agrees with data produced when MC loss was detected using *HSV-TK*. As expected, RNAi targeting either protein did not cause a significant increase in cells lacking BES1 foci, as any cells losing a MBC do not survive in the population, having lost housekeeping genes. Increases in the numbers of G1 phase cells containing two MC foci also occurred over the 96 hours of RNAi against KKIP1 (Figure 72D). Knockdown of KKIP1 significantly increased the amount of these cells, again tripling their numbers. There were also significant increases in cells containing two MBC foci, though they did not appear to be time dependent. These data suggest that the loss of chromosome tags

detected previously, using *HSV-TK*, was caused by nondisjunctions, leading to asymmetric division of chromosomes during mitosis.

In order to determine whether nondisjunctions were the likely cause of chromosome tag loss, the number of cells undergoing mitosis in which foci were asymmetrically distributed between dividing nuclei were counted after ablation of KKIP1 (Figure 73). These were cells that had likely experienced nondisjunction events and were, therefore, not performing chromosome segregation correctly. The numbers of cells with asymmetric distribution of MCs and MBCs significantly increased after RNAi was induced. This increase, however, occurred early on in the experiment before the number of these cells began to fall. As nondisjunction events were the mechanism by which cells lacking foci were produced, this was expected, the fall in cells experiencing nondisjunction events representing increases in cells refractory to RNAi. This is the first direct evidence for nondisjunction events during mitosis in *T. brucei*, after knockdown of a kinetochore component.

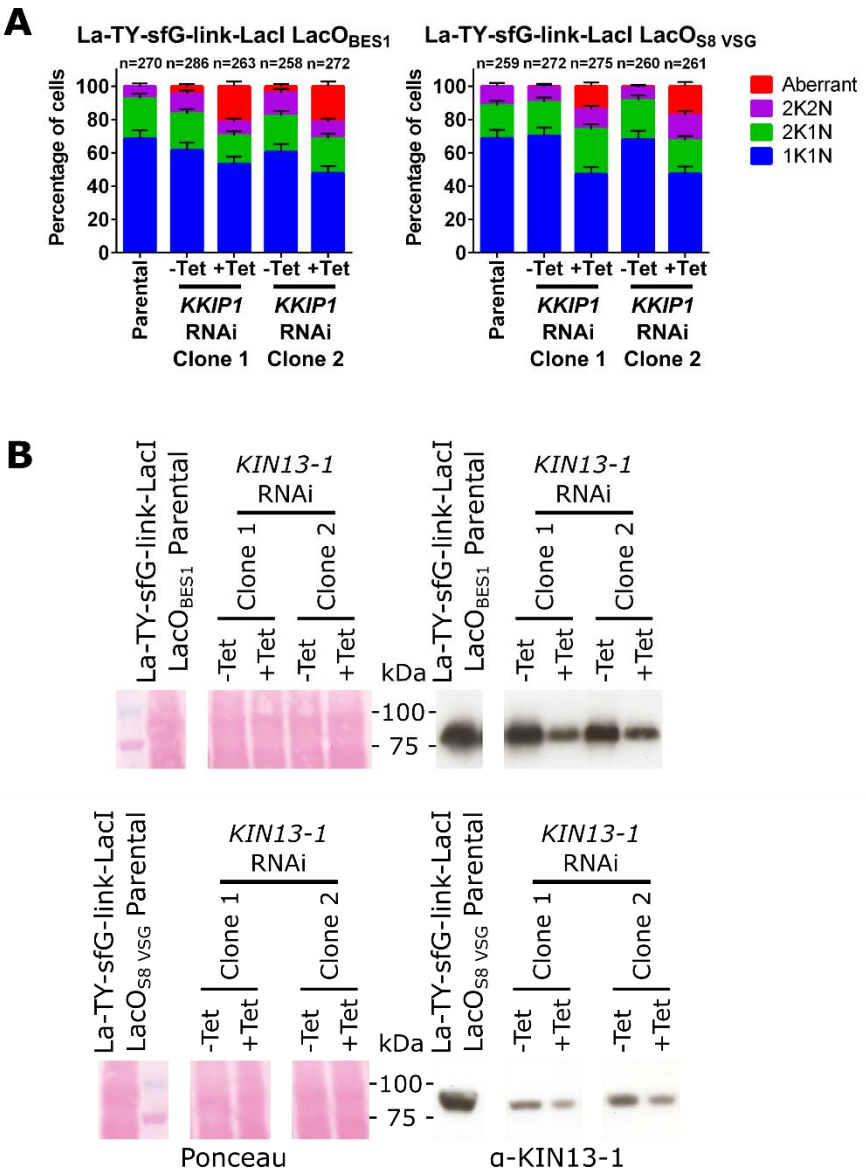


Figure 71. Confirmation of RNAi in LacO labelled cell lines. KKIP1 and KIN13-1 targeting RNAi plasmids were introduced into La-TY-sfG-link-LacI LacO$_{BES1}$ and LacO$_{S8\ VSG}$ cell lines. RNAi was induced with tetracycline (Tet) for 48 hours. KKIP1 knockdown was confirmed by performing counts of nuclei and kinetoplasts (A) and KIN13-1 knockdown was confirmed by means of Western blot, using polyclonal rabbit α-KIN13-1 antibodies and a goat α-rabbit-HRP secondary (B).

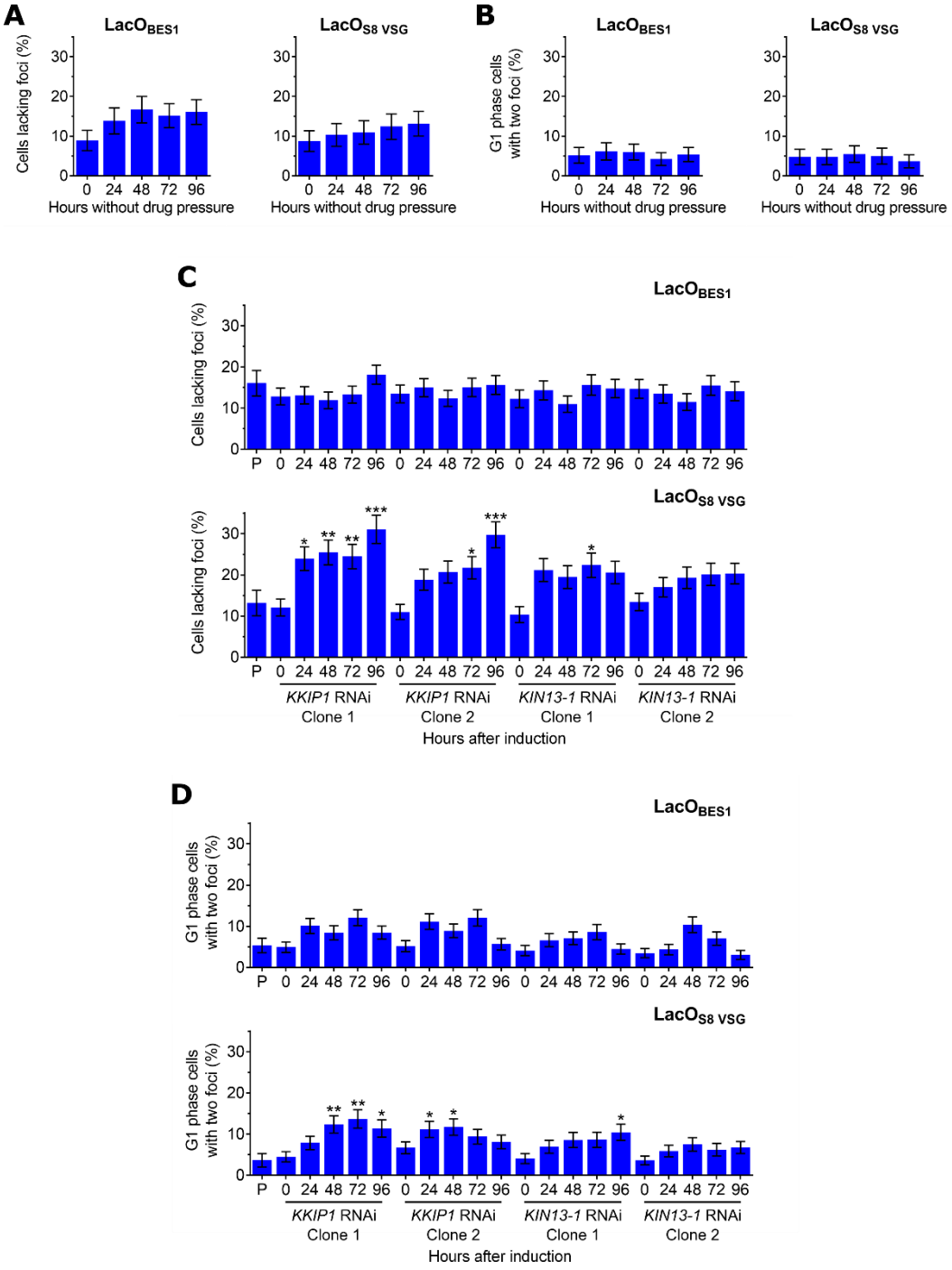


Figure 72. Disruption of mitosis causes MC tags to be lost and produces mitotic cells with asymmetric distribution of foci. La-TY-sfG-link-LacI $LacO_{BES1}$ and La-TY-sfG-link-LacI $LacO_{S8\ VSG}$ cells were grown without drug pressure, for 0, 24, 48, 72 and 96 hours, and the number of cells lacking foci or those in G1 phase containing two foci counted (A and B), to produce a baseline of foci loss or gain. RNAi was then induced against KKIP1 or KIN13-1, in these cell lines, again for 0, 24, 48, 72 and 96 hours. Numbers of cells lacking foci and G1 phase cells with two GFP foci were counted and plotted (C and D). The 96 hour parental baseline was also plotted as a control (P). Z-tests were performed to determine the significance of any changes in the number of these cells compared to P; * = p≤0.05, ** = p≤0.01, *** = p≤0.001.

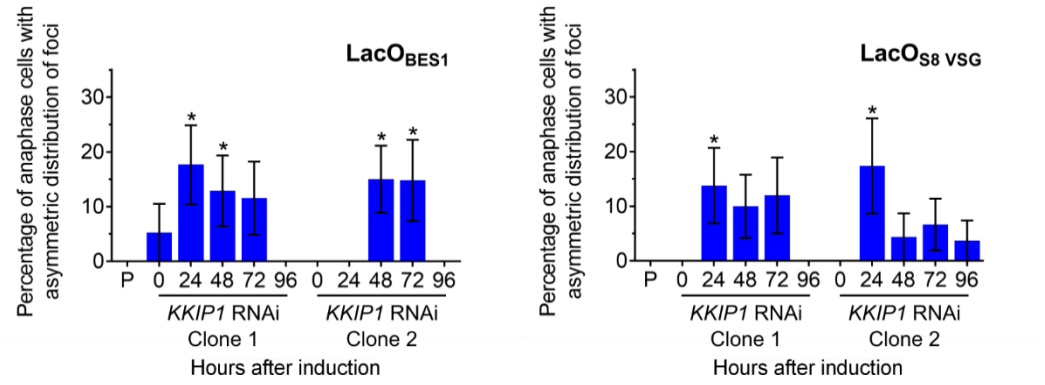


Figure 73. Knock down of KKIP1 causes nondisjunction events to occur. RNAi against KKIP1 was induced for 0, 24, 48, 72 and 96 hours in La-TY-sfG-link-LacI $LacO_{BES1}$ and La-TY-sfG-link-LacI $LacO_{S8\ VSG}$ cells. Anaphase cells in which foci were not equally distributed between nuclei were counted. The 96 hour parental baseline was also plotted as a control (P). Z-tests were performed to determine the significance of any changes in the number of these cells compared to P; * = p≤0.05, ** = p≤0.01, *** = p≤0.001.

6.2.2. KKIP1 knockdown adversely affects kinetochore function

In order to investigate how ablation of KKIP1 might influence kinetochore function, RNAi against KKIP was induced for 24h in cells containing LacI/LacO chromosome tags and expressing mStrawberry-KKT1, to produce cells experiencing nondisjunction events. Images of these cells were then produced, representative examples of which are presented in Figure 74 and Figure 75. Three broad categories of chromosome missegregation could be observed. In the first (Type I), there was no obvious disruption to mitosis, with DNA in the process of being segregated symmetrically, and only the labelled chromosomes appeared to be lagging behind the main body of DNA or was asymmetrically distributed. In the second (Type II), there was symmetric segregation of nuclear DNA with a number of chromosomes, including the labelled chromosomes, lagging or asymmetrically distributed. This was indicated by lagging regions of DAPI stained DNA and abnormal distributions of mStrawberry-KKT1, indicating detached or lagging centromeres. mStrawberry-KKT1 also colocalised with labelled MBC and MBCs suggesting it may have been associated with these chromosomes' centromeres. Finally, in Type III missegregations, there was asymmetric division of nuclear DNA and a number of chromosomes, including labelled chromosomes. In some cases, this asymmetry was so severe, that one daughter cell contained very little, if any, nuclear DNA. In all cases of missegregation, mStrawberry-KKT1 foci continued to colocalise with sfGFP-LacI foci. These images suggest that KKT1 had been laid down at the centromeres even on chromosomes that were not being segregated or had detached from the spindle. This, in turn, indicates that KKIP1 knockdown did not interfere with kinetochore assembly, at least in the early stages, but did adversely affect kinetochore function.

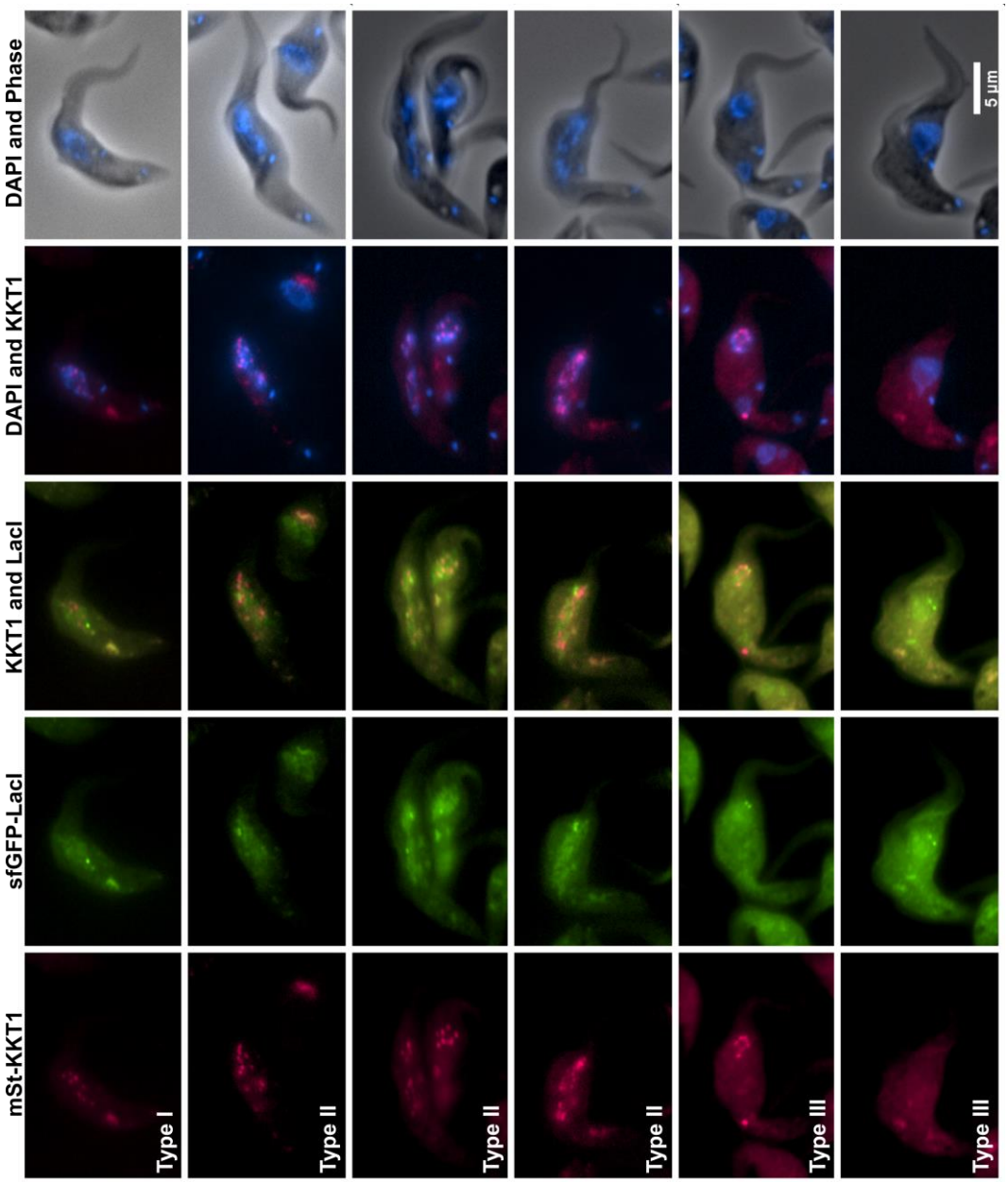


Figure 74. Missegregated MBCs associate with mStrawberry-KKT1. RNAi against KKIP1 was induced for 24 hours in La-TY-sfG-link-LacI $LacO_{BES1}$ *mSt-KKT1*. Cells were attached to glass slides and imaged, to produce representative images of mitotic cells with an asymmetric distribution of foci.

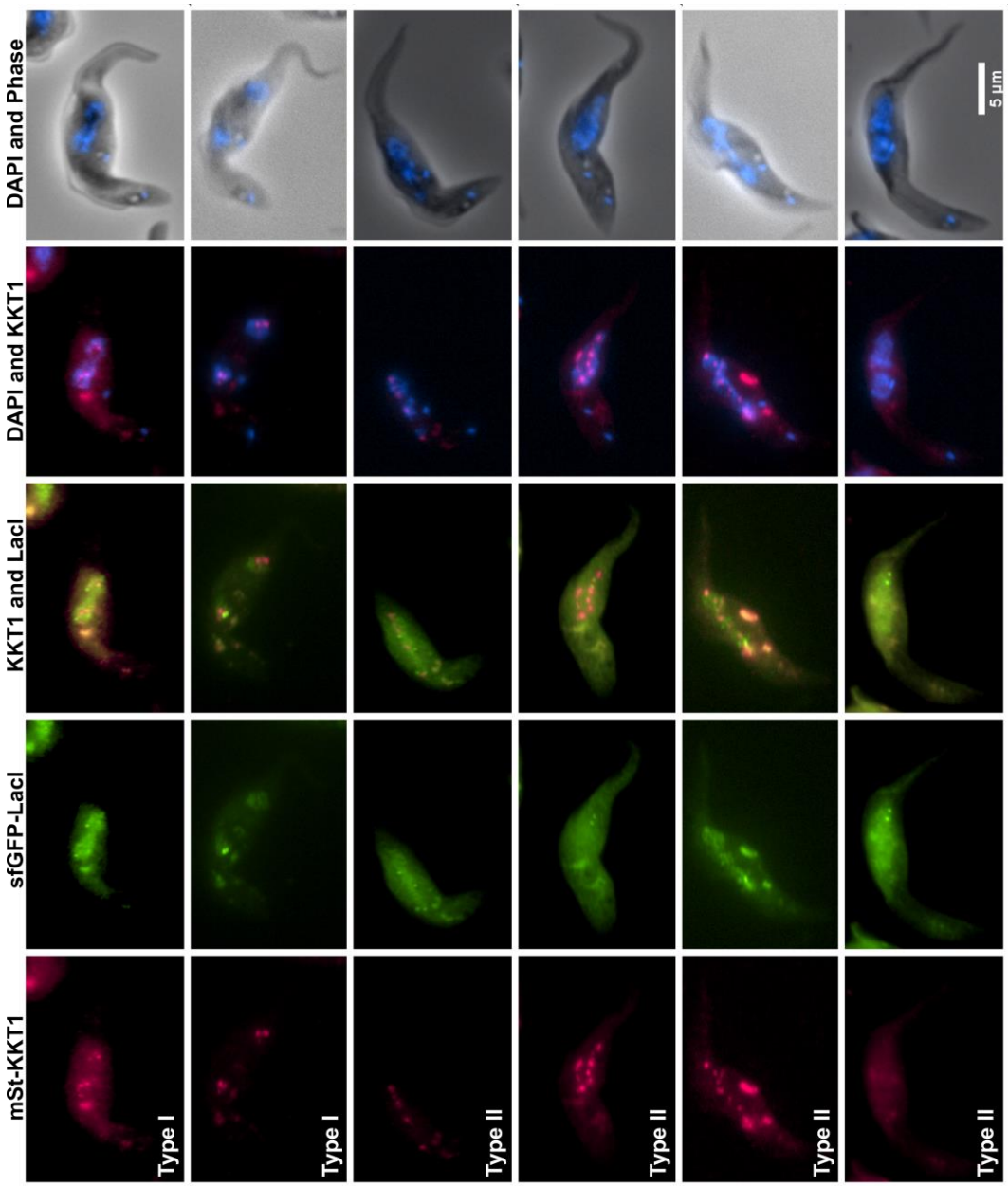


Figure 75. Missegregated MCs associate with mStrawberry-KKT1. RNAi against KKIP1 was induced for 24 hours in La-TY-sfG-link-LacI $LacO_{S8\,VSG}$ *mSt-KKT1*. Cells were attached to glass slides and imaged, to produce representative images of mitotic cells with an asymmetric distribution of foci.

6.2.3. Summary

Earlier I used cell lines containing MBC and MC tags to demonstrate how these chromosomes were distributed through mitosis and how they interacted with the kinetochore proteins KKT1, KKIP1 and KKIP5. Here I used these cell lines to investigate the effects of KKIP1 knockdown on chromosome segregation. This showed that they could be used to corroborate data produced using the *HSV-TK* negative selection marker and to investigate the impact of perturbation of mitotic machinery on individual chromosome division. Furthermore, expressing mStrawberry-KKT1 in these cell lines provided insight into how KKIP1 knockdown impacted on kinetochore function, showing that kinetochore function, but not assembly, was affected by reduced KKIP1 levels.

7. Discussion

7.1. Redundancy in trypanosome kinesins

In this thesis I have reported the consequences of knockdown of kinesin-2 proteins by RNA interference (RNAi) in *Trypanosoma brucei*, individually and in combination. Kinesin-2 proteins play important roles in intraflagellar transport (IFT), as well as performing roles in vesicle and melanosome transport (Verhey and Hammond, 2009; Wordeman, 2010). Due to the flagellum's essentiality to survival in *T. brucei*, at least in bloodstream form (BSF) cells (Branche et al., 2006; Broadhead et al., 2006; Ralston and Hill, 2006), one might expect kinesin-2 proteins to have a substantial influence over fitness. Indeed, the knockdown of a number of conventional IFT proteins in *T. brucei* significantly reduces growth rates and prevents synthesis of flagella (Absalon et al., 2008b). The genome of *T. brucei* encodes two kinesin-2 proteins (Wickstead and Gull, 2006), KIN2A (Tb927.11.13920) and KIN2B (Tb927.5.2090), which both localise to the flagellum (Bill Wickstead, personal communication). In the RNAi target sequencing (RIT-Seq) data, published by Alsford et al. (2011), only KIN2B knockdown caused a significant reduction in the growth, after recalculation of significance.

I have shown that the knockdown of KIN2A or KIN2B individually does not significantly reduce *T. brucei* population growth. Knockdown of the two kinesin-2 proteins in combination, however, does reduce growth, causing limited population decline. This reduction in growth was caused by the inhibition of synthesis of flagella, as demonstrated by fluorescence microscopy, which caused cells to round up and the flagellar pocket (FP) to expand, similar to other IFT knockdown phenotypes. The expansion of the FP is likely due to the lack of a structure provided by the flagellum, leading to defects in endocytosis. These data confirm the role of kinesin-2 proteins in IFT in *T. brucei*. The influence of RNAi against KIN2B on cell growth does not agree with the data provided by Alsford et al. (2011), however. A single fragment was used as template for double stranded RNA (dsRNA) production in the experiments presented here and may have had relatively inefficient knockdown effects. Due to the nature of their experimental

procedure, Alsford et al. (2011) likely induced RNAi against a varied range of fragments covering the KIN2B coding sequence, some of which may have produced a more efficient knockdown. The mean size of genomic fragments used in the RIT-Seq library (~600bp) and lack of size selection of these fragments also mean that off-target effects, due to the presence of another coding sequence, are also a possibility. Differences between RNAi constructs are less likely as both pZJMβ (Wang et al., 2000), used in RIT-Seq, and p2T7β, used here, target tetracycline inducible T7 promoters to the rDNA spacer.

The fact that combinatorial RNAi against the two kinesin-2 sequences resulted in a phenotype, while individual knockdown did not, suggests that redundancy exists between kinesin-2 proteins in *T. brucei*. This is evidence of redundancy between trypanosome kinesins and demonstrates the need to investigate the effects of combinatorial knockdowns. It is likely that the two kinesin proteins form homodimers that perform identical or overlapping functions. Redundancy as a result of overlapping function and of heterotrimerisation (a kinesin-2 heterodimer and the KAP protein; Scholey, 2013) occurs in animal model systems. The redundancy observed between the two trypanosome kinesin-2 proteins is compatible with a situation such as that in *Caenorhabditis elegans*, in which two different kinesin-2 motors, the heterotrimeric kinesin-II and homodimeric OSM-3, perform two differing IFT functions (Mijalkovic et al., 2016; Prevo et al., 2015) with partial redundancy (Evans et al., 2006). In zebrafish, heterotrimeric kinesin-II and homodimeric Kif17 also show some redundancy. Monomers that make up kinesin-II (Kif3b or Kif3c) are also redundant, as either of these proteins can interact with a third monomer (Kif3a) to form kinesin-II (Zhao et al., 2012).

Further analyses of the kinesin-2 proteins in *T. brucei* will be required to determine their roles and relationships, but this was not the focus of this thesis. For instance, the length of flagella under differing RNAi conditions could be measured or the impact of RNAi on IFT particle distribution could be determined. Furthermore, determining whether or not the two proteins heterodimerise, using techniques such as testing for cofractionation after separation of proteins using

sucrose gradients and gel filtration chromatography; co-immunoprecipitation and two-hybrid analyses, would also aid in understanding their relationship.

7.2. The increased efficiency of hairpin RNAi constructs

Data presented in this thesis also provide the first evidence, to my knowledge, that hairpins and head-to-head RNAi constructs, based on identical sequences, have different effects in isogenic *T. brucei*. Knockdown of KIN2B, and KIN2A to some degree, using hairpin constructs resulted in significant limitation of population growth, in contrast to the head-to-head constructs. This appears to have been a function of cell cycle defects rather than flagellar defects, however. This suggests that hairpins may have greater penetrance, which may be due to efficiency of dsRNA production. The likelihood of a hairpin RNA strand annealing to itself is greater than two complementary strands from head-to-head constructs encountering one another and annealing, within the nucleus. In yeast, hairpins have been shown to produce greater levels of the short interfering RNAs (siRNAs) and, as a result, stronger RNAi phenotypes (Drinnenberg et al., 2009). It is also possible that a greater level of short interfering RNA (siRNA) production from hairpins caused off target effects and the phenotype observed was not a true phenotype. In model systems high concentrations of siRNAs can often lead to off target effects (Caffrey et al., 2011).

The impact of hairpins seen here was consistent between independent clones, but is still only a single example of such an effect. Furthermore, only the phenotype was observed and RNA and protein levels were not quantified due to time constraints. It would have been helpful to quantify siRNA or target RNA levels by Northern blot or RT-qPCR (quantitative reverse transcription PCR), or protein levels by Western blot. Further evidence is also required from the application of hairpin constructs to the knockdown of other proteins. If further work confirms the efficiency of the hairpin constructs, this might bring into question past studies that used head-to-head constructs and in which RNAi produced a weaker phenotype or no phenotype at all.

7.3. Combinatorial RNAi libraries

While mitosis and the roles of microtubule motor proteins in this process are relatively well understood in model organisms, little is known about them in trypanosomes. *T. brucei* performs a closed mitosis, in which the nuclear envelope remains intact and the mitotic spindle is assembled within the nucleus (Vickerman and Preston, 1970). Mitosis is unusual *T. brucei*, as the spindle only contains around eight visible kinetochores (Solari, 1995), which is too few for each its ~125 chromosomes to associate with a unique kinetochore, as occurs in model eukaryotes. *T. brucei* has 47 kinesin or kinesin-like genes in its genome, but lacks kinesin-4, -5, -6, -7 and -8 family members (Wickstead and Gull, 2006), all of which have important roles in the canonical spindle. It is, therefore, unclear how the parasite manages to segregate the unusually large number of chromosomes. I have been developing large scale RNAi screens to provide insight into trypanosome mitosis.

I have described a method for generating a combinatorial RNAi library and procedures that use this library, with next generation sequencing techniques, to investigate the roles of kinesin proteins in determining trypanosome fitness and in chromosome segregation. This library contains all possible combinations of kinesins, as well as individual kinesin sequences, to ensure coverage of all sequences and for comparison to the effects of double knockdowns. The library has been transfected into trypanosome cells and is ready for use in the planned experiments. The first, based on RIT-Seq (Alsford et al., 2011), is designed to investigate the impact of motor combinations on fitness, by sequencing the fragments within RNAi constructs in induced and uninduced populations. The second is designed to determine how knockdown of motors impact on chromosome segregation, by selecting for minichromosome (MC) loss and sequencing fragments in the resulting population.

The methodology described here has some limitations. The use of next generation sequencing, to determine the influence of RNAi on populations, limits the library to pairwise combinations. This is due to the read length that these

sequencing technologies can produce versus the length of fragment known to reliably induce RNAi (at least 100bp). In combinations of three ~200bp fragments, for example, the central fragments would likely not be sequenced, as the reads would not extend from the barcoded regions outside the fragments to the centre of the combined fragments. Another issue with the methods used to generate the library is the potential for hairpin constructs to be produced. Though the overall library is head-to-head, the production of random combinations of random fragments will occasionally generate constructs that produce hairpin or partial hairpin RNA sequences, similar to those used in Chapter 3. If hairpin RNAi constructs produce differing phenotypes to head-to-head constructs produced from identical fragments, these hairpins could skew data produced by the planned experiments. Now we know this is the case, it is easy to identify and exclude them from any further analysis.

RNAi screens also come with the limitation of unknown knockdown efficiencies. If the aim is to find candidates for further work, this is not usually considered an issue, particularly with sufficient coverage. The use of a RIT-Seq-like approach, combining large-scale RNAi screens with a competition assay has the potential to produce false negative and false positive results. A false negative, where an expected growth phenotype is not detected, might occur in response to an undetected reduction of knockdown efficiency. A false positive, in which an unexpected growth phenotype occurs, might be caused by off-target effects. These effects should be offset, to some degree, by a library of multiple-fold coverage, due to the generation of a pool of varied siRNAs. Currently a coverage of ~750-1,000× of all possible gene combinations exists in the plasmid library. This was significantly reduced upon introduction into trypanosomes, but still provides, on average, ~10× coverage, assuming no bias in cloning efficiency (~1.2×10^4 clones were produced). Despite its disadvantages, RNAi is still a powerful technique for large scale functional studies of the trypanosome genome. It has the advantages of not being limited by ploidy and allowing for the study of essential genes. Combined with quantitative analysis of

growth, here using techniques involving next generation sequencing, it allows for swift identification of knockdowns that impact cell survivability.

While the kinesin library is designed to investigate the roles of kinesins in mitosis, it could also be applied to analysis of their other roles. Cloning of trypanosome cells containing the library and use of high-throughput microscopy techniques, for example, could be used to determine their roles and interactions in maintaining cell morphology. It could identify roles of kinesins in the flagellum, by identifying cells lacking or displaying shorter flagella or cells with reduced motility, or in the subpellicular corset, by identifying cells with disorganised microtubules. Combining the library with automated kinetoplast and nucleus identification techniques (Obara et al., 2009; Wheeler et al., 2012), could aid in identifying roles for kinesins in nuclear and kinetoplast positioning, as well as their division. A recent study, in *Drosophila* cells, used an RNAi library in conjunction with high-throughput microscopy and a lysosome tag, to track their movement and determine the roles of proteins in organelle transport (Jolly et al., 2016). This would be interesting to perform in trypanosomes with this combinatorial library, but is not so feasible, due the requirement of live, immobile cells.

More generally, the techniques developed here for the production and analysis of the combinatorial library could also be applied to other protein families or groups that might show interaction. For example, they could be used to analyse the relative contributions and synergies between recently identified kinetochore proteins (Akiyoshi and Gull, 2014) to fitness and chromosome segregation, since few components gave significant changes in growth when knocked down individually. Investigations into the expression site associated genes (ESAGs) and genes related to ESAGs (GRESAGs) might also benefit from the use of a combinatorial RNAi library, as these proteins can show redundancy (Salmon et al., 2012). Sequence similarity varies between ESAG and GRESAG family members, however, meaning that RNAi may be less applicable to some.

7.4. An assay for minichromosome loss frequency

The herpes simplex virus thymidine kinase (HSV-TK) coding sequence was introduced into MCs, so that chromosome retention could be selected against using ganciclovir. Introduction of a sequence encoding a chimera consisting of HSV-TK and the blasticidin resistance marker into the 177bp repeat core of MCs produced BSF cells that were sensitive to ganciclovir. Previous work on BSF cells suggests an IC_{50} of ~0.5µg ml^{-1} in the absence of thymidine, which is reduced ten-fold in the presence of 0.16mM thymidine (Scahill et al., 2008). In the work presented here, 50µg ml^{-1} ganciclovir, in thymidine-free medium, limited the cell number by at least one order of magnitude after 24 hours. This is suggestive of a similar level of sensitivity. However, this strategy did not produce sensitive PCF cells, perhaps due to reduced transcription, general insensitivity to the activated drug, reduced HSV-TK activity as a chimera or a combination of these possibilities. SDM-79 medium does contain a small amount of thymine (0.467µM), though this is unlikely to have affected ganciclovir sensitivity. Furthermore, growing cells in thymidine-free medium did not increase sensitivity (data not shown). HSV-TK production was not quantified. However, splitting the chimera and directing it to the subtelomeres of megabase chromosomes (MBCs) or MCs resulted in PCF cells that displayed sensitivity to ganciclovir, suggesting the protein structure had contributed to the reduced sensitivity observed. These PCF cells were less sensitive to ganciclovir than BSF cells. They also displayed less sensitivity to ganciclovir in comparison to previous introductions of HSV-TK into the MBCs of PCF cells (Valdés et al., 1996), suggesting lower levels of transcription may also have contributed. Reduced sensitivity was also detected in cells in which the *HSV-TK* had been integrated into the bloodstream expression site (BES), showing this reduced sensitivity was not limited to expression from MCs. This work suggests that BSF cells will perform better for library experiments.

An assay was designed that used the *HSV-TK* marker to quantify losses of ganciclovir sensitivity and, therefore, MC loss events. Without RNAi this assay allowed for identification of a baseline loss rate. This rate, ~10^{-4} losses per cell per generation, was equivalent to previous studies into the stability of MCs in

trypanosomes (Wickstead et al., 2003) and of chromosomes in yeast (Dani and Zakian, 1983). RNAi against a kinetochore protein previously identified by the lab KKT-interacting protein 1 (KKIP1), increased this loss rate by around four orders of magnitude, in BSF cells. In PCF cells, this increase was less than one order of magnitude, though still highly significant. Knockdown of, the kinesin-13 family member, KIN13-1 also increased MC loss. In BSF cells, there was a highly significant increase to ~10^{-3} losses per cell per generation, quantifying and confirming the chromosome loss observed in previous studies, in which RNAi was induced against KIN13-1 (Chan et al., 2010; Wickstead et al., 2010a). In PCF cells, however, a significant increase was not detected. The lower sensitivity of the assay in PCF cells and may have been due to a continued reduced sensitivity to ganciclovir, perhaps partially caused by reduced transcription, or by a reduced sensitivity to the effects of RNAi.

At least in BSF cells, the *HSV-TK* MC marker can be used in an assay to determine the frequency of MC loss. It has been shown here to be able to detect increased MC loss after RNAi against a kinetochore protein and a mitotic kinesin. The assay could, therefore, be used in validation of library experiments. It could also be used to quantify the effects of other knockdowns, or other genetic manipulations, on segregation fidelity.

7.5. A LacI/LacO system to monitor trypanosome chromosome movement

Lac operator (LacO) repeats and fluorescently labelled Lac repressor (LacI) proteins have been used for the labelling of DNA elements in the past. There are examples of it use for this purpose in bacteria (Lau et al., 2003), in yeast (Robinett et al., 1996; Straight et al., 1996), in mammalian cells (Darzacq et al., 2007; Jacome and Fernandez-Capetillo, 2011; Robinett et al., 1996), where the system has also been used to recruit DNA repair proteins (Soutoglou and Misteli, 2008), and in *T. brucei* (Navarro and Gull, 2001). In *T. brucei*, this system aided in identification of the extranucleolar expression site body, the site of PolI transcription of the active bloodstream expression site (BES). The active BES was labelled with LacO repeats, while a tetracycline inducible construct encoding

GFP-LacI was targeted to the rDNA spacer. This approach resulted in variable levels of GFP-LacI expression and background levels. Cells with lower levels of LacI expression were, therefore, selected, to avoid background, and GFP signal amplified using immunofluorescence techniques.

The major difference in the methodology I have described and developed is in the constitutive expression of fluorescently labelled LacI at levels that allow for observation of DNA elements by native fluorescence. This development involved changes to nuclear localisation signals, untranslated regions (UTRs) and fluorescent proteins used. The eventually successful approach involved the expression of a LacI protein that was N-terminally labelled with superfolder GFP (sfGFP) from the tubulin array, on chromosome 1, under the control of a 3' UTR from *KIN13-1*. The aim of using the *KIN13-1* 3' UTR was to limit the number of LacI proteins to ~100-300 proteins per cell. Use of sfGFP also appeared to solve possible issues with protein folding when other fluorescent proteins were used. When LacO repeats were introduced into subtelomeric locations on MCs and MBCs, bright foci were produced, which were comparable to those from previous work outside trypanosomes, with fluorescence levels far above background levels. They could be viewed by native fluorescence and in some cases were so bright that they could be observed down the eyepiece. The LacI/LacO system described here is the first to be used in *T. brucei*, while employing native fluorescence to view the tag. The foci produced by labelled LacI could be used to track the movement of chromosomes through mitosis, as demonstrated by the production of representative images. Due to the fact that separate cell lines were generated, it was not determined how MBCs and MCs localised relative to one another, as described in experiments performed by Ersfeld and Gull (1997) and Ogbadoyi et al. (2000), so it is unknown which study their distribution corroborates. Their interaction with kinetochore proteins (discussed below), however, suggests their localisation is likely to be similar. This might be something that could be looked into further in the future using the system employed by Lau et al. (2003), which used Tet operator repeats and a labelled Tet repressor, in addition to LacI and LacO repeats.

Integration of RNAi constructs targeting KKIP1 and KIN13-1 into cells containing LacI/LacI chromosome tags allowed for analysis of the effects of knockdown of these proteins on chromosome distribution via microscopy. This showed that RNAi caused a significant increase in cells lacking tagged chromosomes in a time-dependent manner, with a larger effect observed after knockdown of KKIP1 than after knockdown of KIN13-1. A concurrent increase in interphase cells containing two tagged chromosomes also occurred. Mitotic cells with asymmetric distributions of foci were observed in cells in which KKIP1 had been knocked down, suggesting that loss of chromosomes was caused by nondisjunction events. This validated the results obtained biochemically, by MC loss assays using the *HSV-TK* marker and ganciclovir.

The LacI/LacO system developed here can be used for analyses of the effects of disruption of mitosis on chromosome segregation and validation of library experiments. Further analyses could be performed using this tag, including the measurement of distances between sister chromatids or between chromosomes and spindle poles or the nuclear envelope. This could be performed using high-throughput microscopy, to determine the effects of screens on the positioning of chromosomes. The system could also be used for studying how both MCs and MBCs interact with proteins and cellular structures, including the mitotic machinery or to determine how their telomeres interact with nuclear compartments.

7.6. Trypanosome chromosomes share kinetochores

The three kinetochore proteins, KKT1, KKIP1 and KKIP5 were N-terminally labelled with mStrawberry, in order to investigate their interactions with chromosomes, using the LacI/LacO chromosome tags. KKT1 is likely to be closely associated with the centromeres of MBCs, through its interaction with KKT2 and 3, or the 177bp repeats sequences of MCs (Akiyoshi and Gull, 2014), forming the basis of kinetochore assembly. KKIP1 and 5, on the other hand, may form part of the outer kinetochore (D'Archivio and Wickstead, 2016). The distributions of KKT1 and KKIP1 observed in the work presented here are similar to those

observed by Akiyoshi and Gull (2014) and D'Archivio and Wickstead (2016), respectively. All three kinetochore proteins colocalised with both MCs and MBCs during the early stages of mitosis. Both KKT1 and KKIP1 remained in close proximity to the chromosomes during anaphase, but KKIP5 disappeared at the onset of chromosome segregation, suggesting it has a regulatory role. These close associations signify that both MCs and MBCs interact with the large kinetochore foci seen in dividing cells. This supports a model of chromosomes sharing kinetochores, perhaps with multiple chromosomes interacting with an accumulation of protein that forms the kinetochore plaque, and is in disagreement with the lateral stacking model proposed 18 years ago (Gull et al., 1998). This was further supported by measurements of distances between the subtelomeric MC and MBC fluorescent foci and the KKT1 and KKIP1 tags. Both chromosome classes displayed similar patterns of distance changes over mitosis, with the tag on the smaller MC showing a closer association. Knockdown of KKIP1, to produce nondisjunction events and lagging chromosomes, also resulted in lagging mStrawberry-KKT1 foci. The distribution of these foci was similar to those of YFP-KKT2, after knockdown of a number of kinetochore proteins (Akiyoshi and Gull, 2014). Colocalisation of both MBCs and MCs and KKT1 in the background of this KKIP1 knockdown suggests that early stage kinetochore building had occurred on both chromosome classes.

Further work will be required to understand the interactions between chromosomes and kinetochores. The lack of chromosome condensation in trypanosomes likely distanced subtelomeric chromosome tags from kinetochores. Use of LacO/LacI labels of pericentromeric sequences or the 177bp sequences of MC cores would produce a tag in closer proximity to the kinetochore and might prove useful for further analysis of colocalisation. Analysis of kinetochore structure will be required to determine how they interact with chromosomes. The co-purification of kinetochore proteins performed by Akiyoshi and Gull (2014) and by D'Archivio and Wickstead (2016) provide some insight into this. Other conventional analyses of protein interactions would provide further insight. Recent work by Weir et al. (2016) applied biochemical reconstitution techniques

to solving the structure of the mammalian kinetochore and the interactions that occur between proteins within it. As previously mentioned, application of a combinatorial library approach to this problem may also be beneficial.

7.7. Summary

In this thesis, I have presented a number of methodologies for the investigation of mitosis in trypanosomes. I described the development of systems that allow for large scale investigation of proteins' roles in determining fitness and chromosome segregation, which account for redundancy. They will be employed for the study of the roles performed by kinesin motor proteins, though could be adapted to study other groups of proteins. The cell lines developed here can be used to quantify chromosome losses after disruption of mitosis, using negative selection markers, and to study the effects of this disruption on the spindle and on the distribution of chromosomes during mitosis, using fluorescently labelled KIN13-1 and chromosomes. Chromosome labels can also be used to investigate the interactions between chromosomes and mitotic structures, as I have demonstrated here by investigating interactions between chromosomes and kinetochores.

8. References

Absalon, S., Blisnick, T., Bonhivers, M., Kohl, L., Cayet, N., Toutirais, G., Buisson, J., Robinson, D., Bastin, P., 2008a. Flagellum elongation is required for correct structure , orientation and function of the flagellar pocket in *Trypanosoma brucei*. J Cell Sci 121, 3704–3716.

Absalon, S., Blisnick, T., Kohl, L., Toutirais, G., Doré, G., Julkowska, D., Tavenet, A., Bastin, P., 2008b. Intraflagellar transport and functional analysis of genes required for flagellum formation in trypanosomes. Mol Biol Cell 19, 929–944.

Absalon, S., Kohl, L., Branche, C., Blisnick, T., Toutirais, G., Rusconi, F., Cosson, J., Bonhivers, M., Robinson, D., Bastin, P., 2007. Basal body positioning is controlled by flagellum formation in *Trypanosoma brucei*. PLoS One 2, e437.

Acar, S., Carlson, D.B., Budamagunta, M.S., Yarov-Yarovoy, V., Correia, J.J., Niñonuevo, M.R., Jia, W., Tao, L., Leary, J.A., Voss, J.C., Evans, J.E., Scholey, J.M., 2013. The bipolar assembly domain of the mitotic motor kinesin-5. Nat Commun 4, 1343.

Agrawal, N., Dasaradhi, P.V.N., Mohmmed, A., Malhotra, P., Bhatnagar, R.K., Mukherjee, S.K., 2003. RNA interference: biology, mechanism, and applications. Microbiol Mol Biol Rev 67, 657–685.

Aist, J.R., 1969. The mitotic apparatus in fungi, *Ceratocystis fagacearum* and *Fusarium oxysporum*. J Cell Biol 40, 120–135.

Aist, J.R., Williams, P.H., 1972. Ultrastructure and time course of mitosis in the fungus *Fusarium oxysporum*. J Cell Biol 55, 368–389.

Akiyoshi, B., Gull, K., 2013. Evolutionary cell biology of chromosome segregation: insights from trypanosomes. Open Biol 3, 130023.

Akiyoshi, B., Gull, K., 2014. Discovery of unconventional kinetochores in kinetoplastids. Cell 156, 1247–1258.

Albee, A.J., Tao, W., Wiese, C., 2006. Phosphorylation of maskin by Aurora-A is regulated by RanGTP and importin beta. J Biol Chem 281, 38293–38301.

Alberts, B., Johnson, A., Lewis, J., Raff, M., Roberts, K., Walter, P., 2008a. The Cytoskeleton. In: Molecular Biology of the Cell. Garland Science, pp. 965–1052.

Alberts, B., Johnson, A., Lewis, J., Raff, M., Roberts, K., Walter, P., Wilson, J., Hunt, T., 2008b. The Cell Cycle. In: Molecular Biology of the Cell,. Garland Science, pp. 1053–1113.

Alibu, V.P., Storm, L., Haile, S., Clayton, C., Horn, D., 2005. A doubly inducible system for RNA interference and rapid RNAi plasmid construction in *Trypanosoma brucei*. Mol Biochem Parasitol 139, 75–82.

Allingham, J.S., Sproul, L.R., Rayment, I., Gilbert, S.P., 2007. Vik1 modulates microtubule-Kar3 interactions through a motor domain that lacks an active site. Cell 128, 1161–1172.

Alsford, S., Eckert, S., Baker, N., Glover, L., Sanchez-Flores, A., Leung, K.F., Turner, D.J., Field, M.C., Berriman, M., Horn, D., 2012. High-throughput decoding of antitrypanosomal drug efficacy and resistance. Nature 482, 232–236.

Alsford, S., Kawahara, T., Glover, L., Horn, D., 2005. Tagging a *T. brucei* rRNA locus improves stable transfection efficiency and circumvents inducible expression position effects. Mol Biochem Parasitol 144, 142–148.

Alsford, S., Turner, D.J., Obado, S.O., Sanchez-Flores, A., Glover, L., Berriman, M., Hertz-Fowler, C., Horn, D., 2011. High-throughput phenotyping using parallel sequencing of RNA interference targets in the African trypanosome. Genome Res 21, 915–924.

Alsford, S., Wickstead, B., Ersfeld, K., Gull, K., 2001. Diversity and dynamics of the minichromosomal karyotype in *Trypanosoma brucei*. Mol Biochem Parasitol 113, 79–88.

Alushin, G.M., Musinipally, V., Matson, D., Tooley, J., Stukenberg, P.T., Nogales, E., 2012. Multimodal microtubule binding by the Ndc80 kinetochore complex. Nat Struct Mol Biol 19, 1161–1167.

Amiguet-Vercher, A., Pérez-Morga, D., Pays, A., Poelvoorde, P., Van Xong, H., Tebabi, P., Vanhamme, L., Pays, E., 2004. Loss of the mono-allelic control of the VSG expression sites during the development of *Trypanosoma brucei* in the bloodstream. Mol Microbiol 51, 1577–1588.

Andrews, P.D., Ovechkina, Y., Morrice, N., Wagenbach, M., Duncan, K., Wordeman, L., Swedlow, J.R., 2004. Aurora B regulates MCAK at the mitotic centromere. Dev Cell 6, 253–268.

Aravind, L., Koonin, E. V, 1998. The HORMA domain: a common structural denominator in mitotic checkpoints, chromosome synapsis and DNA repair. Trends Biochem Sci 23, 284–286.

Arnone, J.T., Walters, A.D., Cohen-Fix, O., 2013. The dynamic nature of the nuclear envelope: lessons from closed mitosis. Nucleus 4, 261–266.

Atayde, V.D., Ullu, E., Kolev, N.G., 2012. A single-cloning-step procedure for the generation of RNAi plasmids producing long stem–loop RNA. Mol Biochem Parasitol 184, 55–58.

Azimzadeh, J., Bornens, M., 2007. Structure and duplication of the centrosome. J Cell Sci 120, 2139–2142.

Baker, N., Alsford, S., Horn, D., 2011. Genome-wide RNAi screens in African trypanosomes identify the nifurtimox activator NTR and the eflornithine transporter AAT6. Mol Biochem Parasitol 176, 55–57.

Bakhoum, S.F., Thompson, S.L., Manning, A.L., Compton, D.A., 2009. Genome stability is ensured by temporal control of kinetochore-microtubule dynamics. Nat Cell Biol 11, 27–35.

Barisic, M., Aguiar, P., Geley, S., Maiato, H., 2014. Kinetochore motors drive congression of peripheral polar chromosomes by overcoming random arm-ejection forces. Nat Cell Ciology 16, 1249–1256.

Barnes, R.L., McCulloch, R., 2007. *Trypanosoma brucei* homologous recombination is dependent on substrate length and homology, though displays a differential dependence on mismatch repair as substrate length decreases. Nucleic Acids Res 35, 3478–3493.

Baron, D.M., Kabututu, Z.P., Hill, K.L., 2007. Stuck in reverse: loss of LC1 in *Trypanosoma brucei* disrupts outer dynein arms and leads to reverse flagellar beat and backward movement. J Cell Sci 120, 1513–1520.

Bastin, P., Ellis, K., Kohl, L., Gull, K., 2000. Flagellum ontogeny in trypanosomes studied via an inherited and regulated RNA interference system. J Cell Sci 113, 3321–3328.

Bastin, P., MacRae, T.H., Francis, S.B., Matthews, K.R., Gull, K., 1999. Flagellar morphogenesis: protein targeting and assembly in the paraflagellar rod of trypanosomes. Mol Cell Biol 19, 8191–8200.

Bastin, P., Sherwin, T., Gull, K., 1998. Paraflagellar rod is vital for trypanosome motility. Nature 391, 548.

Beaudouin, J., Gerlich, D., Daigle, N., Eils, R., Ellenberg, J., 2002. Nuclear envelope breakdown proceeds by microtubule-induced tearing of the lamina. Cell 108, 83–96.

Bell, J.S., McCulloch, R., 2003. Mismatch repair regulates homologous recombination, but has little influence on antigenic variation, in *Trypanosoma brucei*. J Biol Chem 278, 45182–45188.

Belli, S.I., 2000. Chromatin remodelling during the life cycle of trypanosomatids. Int J Parasitol 30, 679–687.

Berberof, M., Vanhamme, L., Tebabi, P., Pays, A., Jefferies, D., Welburn, S., Pays, E., 1995. The 3'-terminal region of the mRNAs for VSG and procyclin can confer stage specificity to gene expression in *Trypanosoma brucei*. EMBO J 14, 2925–2934.

Berriman, M., Ghedin, E., Hertz-Fowler, C., Blandin, G., Renauld, H., Bartholomeu, D.C., Lennard, N.J., Caler, E., Hamlin, N.E., Haas, B., Bohme, U., Hannick, L., Aslett, M.A., Shallom, J., Marcello, L., Hou, L., Wickstead, B., Alsmark, U.C., Arrowsmith, C., Atkin, R.J., et al., The genome of the African trypanosome *Trypanosoma brucei*. Science 309, 416–422.

Berriman, M., Hall, N., Sheader, K., Bringaud, F., Tiwari, B., Isobe, T., Bowman, S., Corton, C., Clark, L., Cross, G.A.M., Hoek, M., Zanders, T., Berberof, M., Borst, P., Rudenko, G., 2002. The architecture of variant surface glycoprotein gene expression sites in *Trypanosoma brucei*. Mol Biochem Parasitol 122, 131–140.

Bessat, M., 2014. Knockdown of APC/C-associated genes and its effect on viability and cell cycle of protozoan parasite of *Trypanosoma brucei*. Parasitol Res 113, 1555–1562.

Bessat, M., Ersfeld, K., 2009. Functional characterization of cohesin SMC3 and separase and their roles in the segregation of large and minichromosomes in *Trypanosoma brucei*. Mol Microbiol 71, 1371–1385.

Bessat, M., Knudsen, G., Burlingame, A.L., Wang, C.C., 2013. A minimal anaphase promoting complex/cyclosome (APC/C) in *Trypanosoma brucei*. PLoS One 8, e59258.

Bieling, P., Telley, I.A., Surrey, T., 2010. A minimal midzone protein module controls formation and length of antiparallel microtubule overlaps. Cell 142, 420–432.

Biggins, S., 2013. The composition, functions, and regulation of the budding yeast kinetochore. Genetics 194, 817–846.

Bishop, J.D., Han, Z., Schumacher, J.M., 2005. The *Caenorhabditis elegans* Aurora B kinase AIR-2 phosphorylates and is required for the localization of a BimC kinesin to meiotic and mitotic spindles. Mol Biol Cell 16, 742–756.

Blaineau, C., Tessier, M., Dubessay, P., Tasse, L., Crobu, L., Pagès, M., Bastien, P., 2007. A novel microtubule-depolymerizing kinesin involved in length control of a eukaryotic flagellum. Curr Biol 17, 778–782.

Blangy, A., Lane, H.A., D'Hérin, P., Harper, M., Kress, M., Nigg, E.A., 1995. Phosphorylation by p34cdc2 regulates spindle association of human Eg5, a kinesin-related motor essential for bipolar spindle formation in vivo. Cell 83, 1159–1169.

Blasius, T.L., Cai, D., Jih, G.T., Toret, C.P., Verhey, K.J., 2007. Two binding partners cooperate to activate the molecular motor Kinesin-1. J Cell Biol 176, 11–17.

Bonhivers, M., Nowacki, S., Landrein, N., Robinson, D.R., 2008. Biogenesis of the trypanosome endo-exocytotic organelle is cytoskeleton mediated. PLoS Biol 6, e105.

Boucher, N., Wu, Y., Dumas, C., Dubé, M., Sereno, D., Breton, M., Papadopoulou, B., 2002. A common mechanism of stage-regulated gene expression in *Leishmania* mediated by a conserved 3'-untranslated region element. J Biol Chem 277, 19511–19520.

Brady, S.T., 1985. A novel brain ATPase with properties expected for the fast axonal transport motor. Nature 317, 73–75.

Branche, C., Kohl, L., Toutirais, G., Buisson, J., Cosson, J., Bastin, P., 2006. Conserved and specific functions of axoneme components in trypanosome motility. J Cell Sci 119, 3443–3455.

Braun, M., Drummond, D.R., Cross, R.A., McAinsh, A.D., 2009. The kinesin-14 Klp2 organizes microtubules into parallel bundles by an ATP-dependent sorting mechanism. Nat Cell Biol 11, 724–730.

Bringmann, H., Skiniotis, G., Spilker, A., Kandels-Lewis, S., Vernos, I., Surrey, T., 2004. A kinesin-like motor inhibits microtubule dynamic instability. Science 303, 1519–1522.

Broadhead, R., Dawe, H.R., Farr, H., Griffiths, S., Hart, S.R., Portman, N., Shaw, M.K., Ginger, M.L., Gaskell, S.J., McKean, P.G., Gull, K., 2006. Flagellar motility is required for the viability of the bloodstream trypanosome. Nature 440, 224–227.

Brooks, D.R., McCulloch, R., Coombs, G.H., Mottram, J.C., 2000. Stable transformation of trypanosomatids through targeted chromosomal integration of the selectable marker gene encoding blasticidin S deaminase. FEMS Microbiol Lett 186, 287–291.

Brouhard, G.J., Hunt, A.J., 2005. Microtubule movements on the arms of mitotic chromosomes: polar ejection forces quantified in vitro. Proc Natl Acad Sci U S A 102, 13903–13908.

Brown, S.S., 1999. Cooperation between microtubule- and actin-based motor proteins. Annu Rev Cell Dev Biol 15, 63–80.

Brummelkamp, T.R., Bernards, R., Agami, R., 2002. A system for stable expression of short interfering RNAs in mammalian cells. Science 296, 550–553.

Brun, R., Schönenberger, M., 1979. Cultivation and in vitro cloning of procyclic culture forms of *Trypanosoma brucei* in a semi-defined medium. Acta Trop 36, 289–292.

Brust-Mascher, I., Civelekoglu-Scholey, G., Scholey, J.M., 2015. Mechanism for anaphase B: evaluation of “slide-and-cluster” versus “slide-and-flux-or-elongate” models. Biophys J 108, 2007–2018.

Brust-Mascher, I., Scholey, J.M., 2002. Microtubule flux and sliding in mitotic spindles of *Drosophila* embryos. Mol Biol Cell 13, 3967–3975.

Brust-Mascher, I., Scholey, J.M., 2011. Mitotic motors and chromosome segregation: the mechanism of anaphase B. Biochem Soc Trans 39, 1149–1153.

Brust-Mascher, I., Sommi, P., Cheerambathur, D.K., Scholey, J.M., 2009. Kinesin-5-dependent poleward flux and spindle length control in *Drosophila* embryo mitosis. Mol Biol Cell 20, 1749–1762.

Buendia, B., Courvalin, J.C., Collas, P., 2001. Dynamics of the nuclear envelope at mitosis and during apoptosis. Cell Mol Life Sci 58, 1781–1789.

Burki, F., 2014. The eukaryotic tree of life from a global phylogenomic perspective. Cold Spring Harb Perspect Biol 6, a016147.

Burri, M., Schlimme, W., Betschart, B., Kämpfer, U., Schaller, J., Hecker, H., 1993. Biochemical and functional characterization of histone H1-like proteins in procyclic *Trypanosoma brucei brucei*. Parasitol Res 79, 649–659.

Burri, M., Schlimme, W., Betschart, B., Lindner, H., Kämpfer, U., Schaller, J., Hecker, H., 1995. Partial amino acid sequence and functional aspects of histone H1 proteins in *Trypanosoma brucei brucei*. Biol Cell 83, 23–31.

Caffrey, D.R., Zhao, J., Song, Z., Schaffer, M.E., Haney, S.A., Subramanian, R.R., Seymour, A.B., Hughes, J.D., 2011. siRNA off-target effects can be reduced at concentrations that match their individual potency. PLoS One 6, e21503.

Carroll, C.W., Milks, K.J., Straight, A.F., 2010. Dual recognition of CENP-A nucleosomes is required for centromere assembly. J Cell Biol 189, 1143–1155.

Carruthers, V.B., van der Ploeg, L.H., Cross, G.A.M., 1993. DNA-mediated transformation of bloodstream-form *Trypanosoma brucei*. Nucleic Acids Res 21, 2537–2538.

Casagrande, L., Ruiz, J.C., Beverley, S.M., Cruz, A.K., 2005. Identification of a DNA fragment that increases mitotic stability of episomal linear DNAs in *Leishmania major*. Int J Parasitol 35, 973–980.

Chan, K.Y., Ersfeld, K., 2010. The role of the kinesin-13 family protein TbKif13-2 in flagellar length control of *Trypanosoma brucei*. Mol Biochem Parasitol 174, 137–140.

Chan, K.Y., Matthews, K.R., Ersfeld, K., 2010. Functional characterisation and drug target validation of a mitotic kinesin-13 in *Trypanosoma brucei*. PLoS Pathog 6, e1001050.

Chaves, I., Zomerdijk, J., Dirks-Mulder, A., Dirks, R.W., Raap, A.K., Borst, P., 1998. Subnuclear localization of the active variant surface glycoprotein gene expression site in *Trypanosoma brucei*. Proc Natl Acad Sci U S A 95, 12328–33.

Cheeseman, I.M., 2014. The kinetochore. Cold Spring Harb Perspect Biol 6, a015826.

Cheeseman, I.M., Chappie, J.S., Wilson-Kubalek, E.M., Desai, A., 2006. The conserved KMN network constitutes the core microtubule-binding site of the kinetochore. Cell 127, 983–997.

Cheeseman, I.M., Desai, A., 2008. Molecular architecture of the kinetochore-microtubule interface. Nat Rev Mol Cell Biol 9, 33–46.

Cheeseman, I.M., Niessen, S., Anderson, S., Hyndman, F., Yates, J.R., Oegema, K., Desai, A., 2004. A conserved protein network controls assembly of the outer kinetochore and its ability to sustain tension. Genes Dev 18, 2255–2268.

Chen, B., Gilbert, L.A., Cimini, B.A., Schnitzbauer, J., Zhang, W., Li, G.W., Park, J., Blackburn, E.H., Weissman, J.S., Qi, L.S., Huang, B., 2013. Dynamic imaging of genomic loci in living human cells by an optimized CRISPR/Cas system. Cell 155, 1479–1491.

Chen, Y., Hancock, W.O., 2015. Kinesin-5 is a microtubule polymerase. Nat Commun 6, 8160.

Clayton, C.E., 1999. Genetic manipulation of Kinetoplastida. Parasitol Today 15, 372–378.

Clayton, C.E., 2002. Life without transcriptional control? From fly to man and back again. EMBO J 21, 1881–1888.

Clayton, C.E., Fueri, J.P., Itzhaki, J.E., Bellofatto, V., Sherman, D.R., Wisdom, G.S., Vijayasarathy, S., Mowatt, M.R., 1990. Transcription of the procyclic acidic repetitive protein genes of *Trypanosoma brucei*. Mol Cell Biol 10, 3036–3047.

Cochran, J.C., Sindelar, C. V., Mulko, N.K., Collins, K.A., Kong, S.E., Hawley, R.S., Kull, F.J., 2009. ATPase Cycle of the nonmotile kinesin NOD allows microtubule end tracking and drives chromosome movement. Cell 136, 110–122.

Cole, D.G., Diener, D.R., Himelblau, A.L., Beech, P.L., Fuster, J.C., Rosenbaum, J.L., 1998. *Chlamydomonas* kinesin-II-dependent intraflagellar transport (IFT): IFT particles contain proteins required for ciliary assembly in *Caenorhabditis elegans* sensory neurons. J Cell Biol 141, 993–1008.

Collins, E., Mann, B.J., Wadsworth, P., 2014. Eg5 restricts anaphase B spindle elongation in mammalian cells. Cytoskeleton 71, 136–144.

Coy, D.L., Hancock, W.O., Wagenbach, M., Howard, J., 1999. Kinesin's tail domain is an inhibitory regulator of the motor domain. Nat Cell Biol 1, 288–292.

Crevel, I.M., Lockhart, A., Cross, R.A., 1996. Weak and strong states of kinesin and Ncd. J Mol Biol 257, 66–76.

Cross, G., 2008. Tools for genetic analysis in *Trypanosoma brucei* [WWW Document]. http://tryps.rockefeller.edu/trypsru2_genetics.html.

Cross, M., Taylor, M.C., Borst, P., 1998. Frequent loss of the active site during Variant Surface Glycoprotein expression site switching in vitro in *Trypanosoma brucei*. Mol Cell Biol 18, 198–205.

Cross, R.A., 2016. Review: Mechanochemistry of the kinesin-1 ATPase. Biopolymers 105, 476–482.

Cross, R.A., McAinsh, A., 2014. Prime movers: the mechanochemistry of mitotic kinesins. Nat Rev Mol Cell Biol 15, 257–271.

Cruz, A., Beverley, S.M., 1990. Gene replacement in parasitic protozoa. Nature 348, 171–173.

Cruz, A., Coburn, C.M., Beverley, S.M., 1991. Double targeted gene replacement for creating null mutants. Proc Natl Acad Sci U S A 88, 7170–7174.

Curotto de Lafaille, M.A., Laban, A., Wirth, D.F., 1992. Gene expression in *Leishmania*: analysis of essential 5' DNA sequences. Proc Natl Acad Sci U S A 89, 2703–2707.

Czakó, M., Márton, L., 1994. The herpes simplex virus thymidine kinase gene as a conditional negative-selection marker gene in *Arabidopsis thaliana*. Plant Physiol 104, 1067–1071.

D'Archivio, S., Wickstead, B., 2016. Trypanosome outer kinetochore proteins suggest conservation of chromosome segregation machinery across eukaryotes. J Cell Biol.

Dai, J., Sullivan, B.A., Higgins, J.M.G., 2006. Regulation of mitotic chromosome cohesion by Haspin and Aurora B. Dev Cell 11, 741–750.

Damasceno, J.D., Beverley, S.M., Tosi, L.R.O., 2010. A transposon toolkit for gene transfer and mutagenesis in protozoan parasites. Genetica 138, 301–311.

Dani, G.M., Zakian, V.A., 1983. Mitotic and meiotic stability of linear plasmids in yeast. Proc Natl Acad Sci U S A 80, 3406–3410.

Daniels, J.-P., Gull, K., Wickstead, B., 2010. Cell biology of the trypanosome genome. Microbiol Mol Biol Rev 74, 552–569.

Daniels, J.-P., Gull, K., Wickstead, B., 2012. The trypanosomatid-specific N terminus of RPA2 is required for RNA polymerase I assembly, localization, and function. Eukaryot Cell 11, 662–672.

DaRocha, W.D., Otsu, K., Teixeira, S.M.R., Donelson, J.E., 2004. Tests of cytoplasmic RNA interference (RNAi) and construction of a tetracycline-inducible T7 promoter system in *Trypanosoma cruzi*. Mol Biochem Parasitol 133, 175–186.

Darzacq, X., Shav-Tal, Y., de Turris, V., Brody, Y., Shenoy, S.M., Phair, R.D., Singer, R.H., 2007. *In vivo* dynamics of RNA polymerase II transcription. Nat Struct Mol Biol 14, 796–806.

Dasso, M., 2002. The Ran GTPase: Theme and variations. Curr Biol 12, 502–508.

Daum, J.R., Wren, J.D., Daniel, J.J., Sivakumar, S., McAvoy, J.N., Potapova, T.A., Gorbsky, G.J., 2009. Ska3 is required for spindle checkpoint silencing and the maintenance of chromosome cohesion in mitosis. Curr Biol 19, 1467–1472.

Davidge, J.A., Chambers, E., Dickinson, H.A., Towers, K., Ginger, M.L., McKean, P.G., Gull, K., 2006. Trypanosome IFT mutants provide insight into the motor location for mobility of the flagella connector and flagellar membrane formation. J Cell Sci 119, 3935–3943.

De Luca, M., Lavia, P., Guarguaglini, G., 2006. A functional interplay between Aurora-A, Plk1 and TPX2 at spindle poles: Plk1 controls centrosomal localization of Aurora-A and TPX2 spindle association. Cell Cycle 5, 296–303.

De Souza, C.P.C., Osmani, A.H., Hashmi, S.B., Osmani, S.A., 2004. Partial nuclear pore complex disassembly during closed mitosis in *Aspergillus nidulans*. Curr Biol 14, 1973–1984.

Deflorin, J., Rudolf, M., Seebeck, T., 1994. The major components of the paraflagellar rod of *Trypanosoma brucei* are two similar, but distinct proteins which are encoded by two different gene loci. J Biol Chem 269, 28745–28751.

Demonchy, R., Blisnick, T., Deprez, C., Toutirais, G., Loussert, C., Marande, W., Grellier, P., Bastin, P., Kohl, L., 2009. Kinesin 9 family members perform separate functions in the trypanosome flagellum. J Cell Biol 187, 615–622.

Deniaud, E., Bickmore, W.A., 2009. Transcription and the nuclear periphery: edge of darkness? Curr Opin Genet Dev 19, 187–191.

Desai, A., Maddox, P.S., Mitchison, T.J., Salmon, E.D., 1998. Anaphase A chromosome movement and poleward spindle microtubule flux occur at similar rates in *Xenopus* extract spindles. J Cell Biol 141, 703–713.

Desai, A., Mitchison, T.J., 1997. Microtubule polymerization dynamics. Annu Rev Cell Dev Biol 13, 83–117.

Deschamps, P., Lara, E., Marande, W., López-García, P., Ekelund, F., Moreira, D., 2011. Phylogenomic analysis of kinetoplastids supports that trypanosomatids arose from within bodonids. Mol Biol Evol 28, 53–58.

Deutsch, J.M., Lewis, I.P., 2015. Motor function in interpolar microtubules during metaphase. J Theor Biol 370, 1–10.

Diehl, S., Diehl, F., El-Sayed, N.M., Clayton, C., Hoheisel, J.D., 2002. Analysis of stage-specific gene expression in the bloodstream and the procyclic form of *Trypanosoma brucei* using a genomic DNA-microarray. Mol Biochem Parasitol 123, 115–123.

Dobbelaere, J., Josué, F., Suijkerbuijk, S., Baum, B., Tapon, N., Raff, J., 2008. A genome-wide RNAi screen to dissect centriole duplication and centrosome maturation in *Drosophila*. PLoS Biol 6, e224.

Dossin, F.D.M., Schenkman, S., 2005. Actively transcribing RNA polymerase II concentrates on spliced leader genes in the nucleus of *Trypanosoma cruzi*. Eukaryot Cell 4, 960–970.

Downing, T., Imamura, H., Decuypere, S., Clark, T.G., Coombs, G.H., Cotton, J.A., Hilley, J.D., de Doncker, S., Maes, I., Mottram, J.C., Quail, M.A., Rijal, S.,

Sanders, M., Schonian, G., Stark, O., Sundar, S., Vanaerschot, M., Hertz-Fowler, C., Dujardin, J.-C., Berriman, M., 2011. Whole genome sequencing of multiple *Leishmania donovani* clinical isolates provides insights into population structure and mechanisms of drug resistance 2143–2156.

Drechsler, H., McAinsh, A.D., 2012. Exotic mitotic mechanisms. Open Biol 2, 120140.

Drechsler, H., McAinsh, A.D., 2016. Kinesin-12 motors cooperate to suppress microtubule catastrophes and drive the formation of parallel microtubule bundles. Proc Natl Acad Sci U S A 113, E1635-1644.

Drechsler, H., McHugh, T., Singleton, M.R., Carter, N.J., McAinsh, A.D., 2014. The Kinesin-12 Kif15 is a processive track-switching tetramer. Elife 3, e01724.

Drinnenberg, I.A., Weinberg, D.E., Xie, K.T., Mower, J.P., Wolfe, K.H., Fink, G.R., Bartel, D.P., 2009. RNAi in budding yeast. Science 326, 544–550.

Du, Y., English, C.A., Ohi, R., 2010. The kinesin-8 Kif18A dampens microtubule plus-end dynamics. Curr Biol 20, 374–380.

Dultz, E., Zanin, E., Wurzenberger, C., Braun, M., Rabut, G., Sironi, L., Ellenberg, J., 2008. Systematic kinetic analysis of mitotic dis- and reassembly of the nuclear pore in living cells. J Cell Biol 180, 857–865.

Düselder, A., Fridman, V., Thiede, C., Wiesbaum, A., Goldstein, A., Klopfenstein, D.R., Zaitseva, O., Janson, M.E., Gheber, L., Schmidt, C.F., 2015. Deletion of the tail domain of the kinesin-5 Cin8 affects its directionality. J Biol Chem 290, 16841–16850.

Dutoya, S., Gibert, S., Lemercier, G., Santarelli, X., Baltz, D., Baltz, T., Bakalara, N., 2001. A novel C-terminal kinesin is essential for maintaining functional acidocalcisomes in *Trypanosoma brucei*. J Biol Chem 276, 49117–49124.

Earnshaw, W.C., Bernat, R.L., 1991. Chromosomal passengers: toward an integrated view of mitosis. Chromosoma 100, 139–146.

Echeverry, M.C., Bot, C., Obado, S.O., Taylor, M.C., Kelly, J.M., 2012. Centromere-associated repeat arrays on *Trypanosoma brucei* chromosomes are much more extensive than predicted. BMC Genomics 13, 29.

Edamatsu, M., 2014. Bidirectional motility of the fission yeast kinesin-5, Cut7. Biochem Biophys Res Commun 446, 231–234.

Efremov, A.K., Radhakrishnan, A., Tsao, D.S., Bookwalter, C.S., Trybus, K.M., Diehl, M.R., 2014. Delineating cooperative responses of processive motors in living cells. Proc Natl Acad Sci U S A 111, E334-343.

El-Sayed, N.M., Myler, P.J., Blandin, G., Berriman, M., Crabtree, J., Aggarwal, G., Caler, E., Renauld, H., Worthey, E.A., Hertz-Fowler, C., Ghedin, E., Peacock, C., Bartholomeu, D.C., Haas, B.J., Tran, A.-N., Wortman, J.R., Alsmark, U.C.M., Angiuoli, S., Anupama, A., Badger, J., et al., 2005. Comparative genomics of trypanosomatid parasitic protozoa. Science 309, 404–409.

Elbashir, S.M., Harborth, J., Lendeckel, W., Yalcin, A., Weber, K., Tuschl, T., 2001. Duplexes of 21-nucleotide RNAs mediate RNA interference in cultured mammalian cells. Nature 411, 494–498.

Elias, M.C., Marques-Porto, R., Freymüller, E., Schenkman, S., 2001. Transcription rate modulation through the *Trypanosoma cruzi* life cycle occurs in parallel with changes in nuclear organisation. Mol Biochem Parasitol 112, 79–90.

Elias, M.C.Q.B., Faria, M., Mortara, R.A., Motta, M.C.M., De Souza, W., Thiry, M., Schenkman, S., 2002. Chromosome localization changes in the *Trypanosoma cruzi* nucleus. Eukaryot Cell 1, 944–953.

Eme, L., Sharpe, S.C., Brown, M.W., Roger, A.J., 2014. On the age of eukaryotes: evaluating evidence from fossils and molecular clocks. Cold Spring Harb Perspect Biol 6, a016139.

Engelson, E.J., Buckner, F.S., Van Voorhis, W.C., 2011. An essential farnesylated kinesin in *Trypanosoma brucei*. PLoS One 6, e26508.

Engstler, M., Pfohl, T., Herminghaus, S., Boshart, M., Wiegertjes, G., Heddergott, N., Overath, P., 2007. Hydrodynamic flow-mediated protein sorting on the cell surface of trypanosomes. Cell 131, 505–515.

Ersfeld, K., Gull, K., 1997. Partitioning of large and minichromosomes in *Trypanosoma brucei*. Science 276, 611–614.

Ersfeld, K., Melville, S.E., Gull, K., 1999. Nuclear and genome organization of *Trypanosoma brucei*. Parasitol Today 15, 58–63.

Espeut, J., Gaussen, A., Bieling, P., Morin, V., Prieto, S., Fesquet, D., Surrey, T., Abrieu, A., 2008. Phosphorylation relieves autoinhibition of the kinetochore motor CENP-E. Mol Cell 29, 637–643.

Espinal, A., Quijano, J., Hunt, C., Lorenzo, R., Mulligan, C., Sampson, M., Sauchelli, M., Patnaik, P.K., 2007. A 10 base-pair sequence within Domain III of the GPEET procyclin promoter is essential for the autonomous replication of a plasmid in procyclic *Trypanosoma brucei*. Mol Biochem Parasitol 151, 224–228.

Etienne-Manneville, S., 2010. From signaling pathways to microtubule dynamics : the key players. Curr Opin Cell Biol 22, 104–111.

Evans, J.E., Snow, J.J., Gunnarson, A.L., Ou, G., Stahlberg, H., McDonald, K.L., Scholey, J.M., 2006. Functional modulation of IFT kinesins extends the sensory repertoire of ciliated neurons in *Caenorhabditis elegans*. J Cell Biol 172, 663–669.

Fèvre, E.M., Wissmann, B. V, Welburn, S.C., Lutumba, P., 2008. The burden of human African trypanosomiasis. PLoS Negl Trop Dis 2, e333.

Field, M.C., Carrington, M., 2009. The trypanosome flagellar pocket. Nat Rev Microbiol 7, 775–786.

Fineran, P.C., Charpentier, E., 2012. Memory of viral infections by CRISPR-Cas adaptive immune systems: Acquisition of new information. Virology 434, 202–209.

Fink, G., Hajdo, L., Skowronek, K.J., Reuther, C., Kasprzak, A.A., Diez, S., 2009. The mitotic kinesin-14 Ncd drives directional microtubule-microtubule sliding. Nat Cell Biol 11, 717–723.

Fire, A., Xu, S., Montgomery, M.K., Kostas, S.A., Driver, S.E., Mello, C.C., 1998. Potent and specific genetic interference by double-stranded RNA in *Caenorhabditis elegans*. Nature 391, 806–811.

Foley, E.A., Maldonado, M., Kapoor, T.M., 2011. Formation of stable attachments between kinetochores and microtubules depends on the B56-PP2A phosphatase. Nat Cell Biol 13, 1265–1271.

Foltz, D.R., Jansen, L.E.T., Black, B.E., Bailey, A.O., Yates, J.R., Cleveland, D.W., 2006. The human CENP-A centromeric nucleosome-associated complex. Nat Cell Biol 8, 458–469.

Fraser, P., Bickmore, W., 2007. Nuclear organization of the genome and the potential for gene regulation. Nature 447, 413–417.

Freedman, D.J., Beverley, S.M., 1993. Two more independent selectable markers for stable transfection of *Leishmania*. Mol Biochem Parasitol 62, 37–44.

Fridman, V., Gerson-Gurwitz, A., Shapira, O., Movshovich, N., Lakamper, S., Schmidt, C.F., Gheber, L., 2013. Kinesin-5 Kip1 is a bi-directional motor that stabilizes microtubules and tracks their plus-ends *in vivo*. J Cell Sci 126, 4147–4159.

Fu, J., Bian, M., Jiang, Q., Zhang, C., 2007. Roles of Aurora kinases in mitosis and tumorigenesis. Mol Cancer Res 5, 1–10.

Furger, A., Schürch, N., Kurath, U., Roditi, I., 1997. Elements in the 3' untranslated region of procyclin mRNA regulate expression in insect forms of *Trypanosoma brucei* by modulating RNA stability and translation. Mol Cell Biol 17, 4372–4380.

Furuta, K., Furuta, A., Toyoshima, Y.Y., Amino, M., Oiwa, K., Kojima, H., 2013. Measuring collective transport by defined numbers of processive and nonprocessive kinesin motors. Proc Natl Acad Sci U S A 110, 501–506.

Gadea, B.B., Ruderman, J. V, 2006. Aurora B is required for mitotic chromatin-induced phosphorylation of Op18/Stathmin. Proc Natl Acad Sci U S A 103, 4493–4498.

Gadelha, C., LeBowitz, J.H., Manning, J., Seebeck, T., Gull, K., 2004. Relationships between the major kinetoplastid paraflagellar rod proteins: A consolidating nomenclature. Mol Biochem Parasitol 136, 113–115.

Gadelha, C., Wickstead, B., Gull, K., 2007. Flagellar and ciliary beating in trypanosome motility. Cell Motil Cytoskeleton 64, 629–643.

Gaitanos, T.N., Santamaria, A., Jeyaprakash, A.A., Wang, B., Conti, E., Nigg, E.A., 2009. Stable kinetochore-microtubule interactions depend on the Ska complex and its new component Ska3/C13Orf3. EMBO J 28, 1442–1452.

Galanti, N., Galindo, M., Sabaj, V., Espinoza, I., Toro, G.C., 1998. Histone genes in trypanosomatids. Parasitol Today 14, 64–70.

Gale, M., Carter, V., Parsons, M., 1994. Translational control mediates the developmental regulation of the *Trypanosoma brucei* Nrk protein kinase. J Biol Chem 269, 31659–31665.

Galvao, T.C., de Lorenzo, V., 2005. Adaptation of the yeast URA3 selection system to gram-negative bacteria and generation of a Δ*betCDE Pseudomonas putida* strain. Appl Environ Microbiol 71, 883–892.

Ganem, N.J., Upton, K., Compton, D.A., 2005. Efficient mitosis in human cells lacking poleward microtubule flux. Curr Biol 15, 1827–1832.

Gascoigne, K.E., Cheeseman, I.M., 2013. CDK-dependent phosphorylation and nuclear exclusion coordinately control kinetochore assembly state. J Cell Biol 201, 23–32.

Gascoigne, K.E., Takeuchi, K., Suzuki, A., Hori, T., Fukagawa, T., Cheeseman, I.M., 2011. Induced ectopic kinetochore assembly bypasses the requirement for CENP-A nucleosomes. Cell 145, 410–422.

Gerace, L., Blobel, G., 1980. The nuclear envelope lamina is reversibly depolymerized during mitosis. Cell 19, 277–287.

Gerson-Gurwitz, A., Thiede, C., Movshovich, N., Fridman, V., Podolskaya, M., Danieli, T., Lakämper, S., Klopfenstein, D.R., Schmidt, C.F., Gheber, L., 2011. Directionality of individual kinesin-5 Cin8 motors is modulated by loop 8, ionic strength and microtubule geometry. EMBO J 30, 4942–4954.

Ghedin, E., Bringaud, F., Peterson, J., Myler, P., Berriman, M., Ivens, A., Andersson, B., Bontempi, E., Eisen, J., Angiuoli, S., Wanless, D., Von Arx, A., Murphy, L., Lennard, N., Salzberg, S., Adams, M.D., White, O., Hall, N., Stuart, K., Fraser, C.M., El-Sayed, N.M., 2004. Gene synteny and evolution of genome architecture in trypanosomatids. Mol Biochem Parasitol 134, 183–191.

Giet, R., Glover, D.M., 2001. *Drosophila* Aurora B kinase is required for histone H3 phosphorylation and condensin recruitment during chromosome condensation and to organize the central spindle during cytokinesis. J Cell Biol 152, 669–682.

Ginger, M.L., Blundell, P.A., Lewis, A.M., Browitt, A., Günzl, A., Barry, J.D., 2002. *Ex vivo* and *in vitro* identification of a consensus promoter for VSG genes expressed by metacyclic-stage trypanosomes in the tsetse fly. Eukaryot Cell 1, 1000–1009.

Gluenz, E., Sharma, R., Carrington, M., Gull, K., 2008. Functional characterization of cohesin subunit SCC1 in *Trypanosoma brucei* and dissection of mutant phenotypes in two life cycle stages. Mol Microbiol 69, 666–680.

Goldstein, A.L., McCusker, J.H., 1999. Three new dominant drug resistance cassettes for gene disruption in Saccharomyces cerevisiae. Yeast 15, 1541–1553.

Gong, D., Ferrell, J.E., 2010. The roles of cyclin A2, B1, and B2 in early and late mitotic events. Mol Biol Cell 21, 3149–3161.

Gong, D., Pomerening, J.R., Myers, J.W., Gustavsson, C., Jones, J.T., Hahn, A.T., Meyer, T., Ferrell, J.E., 2007. Cyclin A2 regulates nuclear-envelope breakdown and the nuclear accumulation of cyclin B1. Curr Biol 17, 85–91.

Goodhead, I., Capewell, P., Wendi Bailey, J., Beament, T., Chance, M., Kay, S., Forrester, S., MacLeod, A., Taylor, M., Noyes, H., Halla, N., 2013. Whole-genome sequencing of *Trypanosoma brucei* reveals introgression between subspecies that is associated with virulence. MBio 4, 1–8.

Goodman, B., Zheng, Y., 2006. Mitotic spindle morphogenesis: Ran on the microtubule cytoskeleton and beyond. Biochem Soc Trans 34, 716–721.

Gorbsky, G.J., Sammak, P.J., Borisy, G.G., 1987. Chromosomes move poleward in anaphase along stationary microtubules that coordinately diassemble from their kinetochore ends. J Cell Biol 104, 9–18.

Gorbsky, G.J., Sammak, P.J., Borisy, G.G., 1988. Microtubule dynamics and chromosome motion visualized in living anaphase cells. J Cell Biol 106, 1185–1192.

Goshima, G., Vale, R.D., 2003. The roles of microtubule-based motor proteins in mitosis: comprehensive RNAi analysis in the *Drosophila* S2 cell line. J Cell Biol 162, 1003–1016.

Goshima, G., Wollman, R., Stuurman, N., Scholey, J.M., Vale, R.D., 2005. Length control of the metaphase spindle. Curr Biol 15, 1979–1988.

Graham, S.V., Matthews, K.R., Shiels, P.G., Barry, J.D., 1990. Distinct, developmental stage-specific activation mechanisms of trypanosome VSG genes. Parasitology 101 Pt 3, 361–367.

Graham, S.V., Terry, S., Barry, J.D., 1999. A structural and transcription pattern for variant surface glycoprotein gene expression sites used in metacyclic stage *Trypanosoma brucei*. Mol Biochem Parasitol 103, 141–154.

Grallert, A., Boke, E., Hagting, A., Hodgson, B., Connolly, Y., Griffiths, J.R., Smith, D.L., Pines, J., Hagan, I.M., 2015. A PP1-PP2A phosphatase relay controls mitotic progression. Nature 517, 94–98.

Grishchuk, E.L., 2009. Toward a comprehensive and quantitative understanding of intracellular microtubule organization. Mol Syst Biol 5, 251.

Grishchuk, E.L., Efremov, A.K., Volkov, V.A., Spiridonov, I.S., Gudimchuk, N., Westermann, S., Drubin, D., Barnes, G., McIntosh, J.R., Ataullakhanov, F.I., 2008. The Dam1 ring binds microtubules strongly enough to be a processive as well as energy-efficient coupler for chromosome motion. Proc Natl Acad Sci U S A 105, 15423–15428.

Gruneberg, U., Neef, R., Honda, R., Nigg, E.A., Barr, F.A., 2004. Relocation of Aurora B from centromeres to the central spindle at the metaphase to anaphase transition requires MKlp2. J Cell Biol 166, 167–172.

Gudimchuk, N., Vitre, B., Kim, Y., Kiyatkin, A., Cleveland, D.W., Ataullakhanov, F.I., Grishchuk, E.L., 2013. Kinetochore kinesin CENP-E is a processive bi-directional tracker of dynamic microtubule tips. Nat Cell Biol 15, 1–13.

Gull, K., 1999. The cytoskeleton of trypanosomatid parasites. Annu Rev Microbiol 53, 629–655.

Gull, K., Alsford, S., Ersfeld, K., 1998. Segregation of minichromosomes in trypanosomes: implications for mitotic mechanisms. Trends Microbiol 6, 319–323.

Günzl, A., Bruderer, T., Laufer, G., Tu, L., Chung, H., Lee, P., Lee, M.G., 2003. RNA polymerase I transcribes procyclin genes and variant surface glycoprotein gene expression sites in *Trypanosoma brucei*. Eukaryot Cell 2, 542–551.

Hachet, V., Canard, C., Gonczy, P., 2007. Centrosomes promote timely mitotic entry in *C. elegans* Embryos. Dev Cell 12, 531–541.

Hall, N., Berriman, M., Lennard, N.J., Harris, B.R., Hertz-Fowler, C., Bart-Delabesse, E.N., Gerrard, C.S., Atkin, R.J., Barron, A.J., Bowman, S., Bray-Allen, S.P., Bringaud, F., Clark, L.N., Corton, C.H., Cronin, A., Davies, R., Doggett, J., Fraser, A., Grüter, E., Hall, S., et al., 2003. The DNA sequence of chromosome I of an African trypanosome: Gene content, chromosome organisation, recombination and polymorphism. Nucleic Acids Res 31, 4864–4873.

Hammarton, T.C., 2007. Cell cycle regulation in *Trypanosoma brucei*. Mol Biochem Parasitol 153, 1–8.

Hammarton, T.C., Clark, J., Douglas, F., Boshart, M., Mottram, J.C., 2003. Stage-specific differences in cell cycle control in *Trypanosoma brucei* revealed by RNA interference of a mitotic cyclin. J Biol Chem 278, 22877–22886.

Hammond, J.W., Cai, D., Blasius, T.L., Li, Z., Jiang, Y., Jih, G.T., Meyhofer, E., Verhey, K.J., 2009. Mammalian kinesin-3 motors are dimeric *in vivo* and move by processive motility upon release of autoinhibition. PLoS Biol 7, e72.

Han, Z., Riefler, G.M., Saam, J.R., Mango, S.E., Schumacher, J.M., 2005. The *C. elegans* Tousled-like kinase contributes to chromosome segregation as a substrate and regulator of the Aurora B kinase. Curr Biol 15, 894–904.

Hanisch, A., Silljé, H.H.W., Nigg, E.A., 2006. Timely anaphase onset requires a novel spindle and kinetochore complex comprising Ska1 and Ska2. EMBO J 25, 5504–5515.

Hao, L., Scholey, J.M., 2009. Intraflagellar transport at a glance. J Cell Sci 122, 889–892.

Hariharan, S., Ajioka, J., Swindle, J., 1993. Stable transformation of *Trypanosoma cruzi*: inactivation of the PUB12.5 polyubiquitin gene by targeted gene disruption. Mol Biochem Parasitol 57, 15–30.

Hayden, J.H., Bowser, S.S., Rieder, C.L., 1990. Kinetochores capture astral microtubules during chromosome attachment to the mitotic spindle: direct visualization in live newt lung cells. J Cell Biol 111, 1039–1045.

Heath, I.B., 1980. Variant mitoses in lower eukaryotes: Indicators of the evolution of mitosis? In: International Review of Cytology. pp. 1–80.

Heck, M.M., Pereira, A., Pesavento, P., Yannoni, Y., Spradling, A.C., Goldstein, L.S., 1993. The kinesin-like protein KLP61F is essential for mitosis in *Drosophila*. J Cell Biol 123, 665–679.

Hecker, H., Betschart, B., Bender, K., Burri, M., Schlimme, W., 1994. The chromatin of trypanosomes. Int J Parasitol 24, 809–819.

Heddergott, N., Krüger, T., Babu, S.B., Wei, A., Stellamanns, E., Uppaluri, S., Pfohl, T., Stark, H., Engstler, M., 2012. Trypanosome motion represents an adaptation to the crowded environment of the vertebrate bloodstream. PLoS Pathog 8, e1003023.

Hein, J.B., Nilsson, J., 2014. Stable MCC binding to the APC/C is required for a functional spindle assembly checkpoint. EMBO Rep 15, 264–272.

Hertz-Fowler, C., Figueiredo, L.M., Quail, M.A., Becker, M., Jackson, A., Bason, N., Brooks, K., Churcher, C., Fahkro, S., Goodhead, I., Heath, P., Kartvelishvili, M.,

Mungall, K., Harris, D., Hauser, H., Sanders, M., Saunders, D., Seeger, K., Sharp, S., Taylor, J.E., et al., 2008. Telomeric expression sites are highly conserved in *Trypanosoma brucei*. PLoS One 3, e3527.

Hetzer, M., Gruss, O.J., Mattaj, I.W., 2002. The Ran GTPase as a marker of chromosome position in spindle formation and nuclear envelope assembly. Nat Cell Biol 4, E177–184.

Hetzer, M.W., 2010. The nuclear envelope. Cold Spring Harb Perspect Biol 2, 1–16.

Hetzer, M.W., Walther, T.C., Mattaj, I.W., 2005. Pushing the envelope: structure, function, and dynamics of the nuclear periphery. Annu Rev Cell Dev Biol 21, 347–380.

Hildebrandt, E.R., Hoyt, M.A., 2000. Mitotic motors in *Saccharomyces cerevisiae*. Biochim Biophys Acta 1496, 99–116.

Hirokawa, N., Noda, Y., Tanaka, Y., Niwa, S., 2009. Kinesin superfamily motor proteins and intracellular transport. Nat Rev Mol Cell Biol 10, 682–96.

Hirota, T., Kunitoku, N., Sasayama, T., Marumoto, T., Zhang, D., Nitta, M., Hatakeyama, K., Saya, H., 2003. Aurora-A and an interacting activator, the LIM protein Ajuba, are required for mitotic commitment in human cells. Cell 114, 585–598.

Hirumi, H., Hirumi, K., 1989. Continuous cultivation of *Trypanosoma brucei* blood stream forms in a medium containing a low concentration of serum protein without feeder cell layers. J Parasitol 75, 985–989.

Holy, T.E., Leibler, S., 1994. Dynamic instability of microtubules as an efficient way to search in space. Proc Natl Acad Sci U S A 91, 5682–5685.

Horn, D., 2014. Antigenic variation in African trypanosomes. Mol Biochem Parasitol 195, 123–129.

Hotz, H.R., Hartmann, C., Huober, K., Hug, M., Clayton, C., 1997. Mechanisms of developmental regulation in *Trypanosoma brucei*: A polypyrimidine tract in the 3'-untranslated region of a surface protein mRNA affects RNA abundance and translation. Nucleic Acids Res 25, 3017–3025.

Hoyt, M.A., He, L., Loo, K.K., Saunders, W.S., 1992. Two *Saccharomyces cerevisiae* kinesin-related gene products required for mitotic spindle assembly. J Cell Biol 118, 109–120.

Hoyt, M.A., He, L., Totis, L., Saunders, W.S., 1993. Loss of function of *Saccharomyces cerevisiae* kinesin-related CIN8 and KIP1 is suppressed by KAR3 motor domain mutations. Genetics 135, 35–44.

Hu, C.-K., Coughlin, M., Field, C.M., Mitchison, T.J., 2011. KIF4 regulates midzone length during cytokinesis. Curr Biol 21, 815–824.

Hu, H., Hu, L., Yu, Z., Chasse, A.E., Chu, F., Li, Z., 2012. An orphan kinesin in trypanosomes cooperates with a kinetoplastid-specific kinesin to maintain cell morphology by regulating subpellicular microtubules. J Cell Sci 125, 4126–4136.

Hu, L., Hu, H., Li, Z., 2012. A kinetoplastid-specific kinesin is required for cytokinesis and for maintenance of cell morphology in *Trypanosoma brucei*. Mol Microbiol 83, 565–578.

Huang, B., Rifkin, M.R., Luck, D.J.L., 1977. Temperature-sensitive mutations affecting flagellar assembly and function in *Chlamydomonas reinhardtii*. J Cell Biol 72, 67–85.

Hunter, T., Hunt, T., Jackson, R.J., Robertson, H.D., 1975. The characteristics of inhibition of protein synthesis by double-stranded ribonucleic acid in reticulocyte lysates. J Biol Chem 250, 409–417.

Imanishi, M., Endres, N.F., Gennerich, A., Vale, R.D., 2006. Autoinhibition regulates the motility of the *C. elegans* intraflagellar transport motor OSM-3. J Cell Biol 174, 931–937.

Imboden, M.A., Laird, P.W., Affolter, M., Seebeck, T., 1987. Transcription of the intergenic regions of the tubulin gene cluster of *Trypanosoma brucei* : evidence for a polyclstronic transcription unit in a eukaryote. Nucleic Acids Res 15, 7357–7368.

Inoue, N., Otsu, K., Ferraro, D.M., Donelson, J.E., 2002. Tetracycline-regulated RNA interference in *Trypanosoma congolense*. Mol Biochem Parasitol 120, 309–313.

Ipsaro, J.J., Joshua-Tor, L., 2015. From guide to target: molecular insights into eukaryotic RNA-interference machinery. Nat Struct Mol Biol 22, 20–28.

Jacome, A., Fernandez-Capetillo, O., 2011. Lac operator repeats generate a traceable fragile site in mammalian cells. EMBO Rep 12, 1032–1038.

Jaqaman, K., King, E.M., Amaro, A.C., Winter, J.R., Dorn, J.F., Elliott, H.L., Mchedlishvili, N., McClelland, S.E., Porter, I.M., Posch, M., Toso, A., Danuser, G., McAinsh, A.D., Meraldi, P., Swedlow, J.R., 2010. Kinetochore alignment within the metaphase plate is regulated by centromere stiffness and microtubule depolymerases. J Cell Biol 188, 665–679.

Jefferies, D., Tebabi, P., Le Ray, D., Pays, E., 1993. The *ble* resistance gene as a new selectable marker for *Trypanosoma brucei*: fly transmission of stable procyclic transformants to produce antibiotic resistant bloodstream forms. Nucleic Acids Res 21, 191–195.

Jensen, B.C., Sivam, D., Kifer, C.T., Myler, P.J., Parsons, M., 2009. Widespread variation in transcript abundance within and across developmental stages of *Trypanosoma brucei*. BMC Genomics 10, 482.

Jensen, R.E., Englund, P.T., 2012. Network news: the replication of kinetoplast DNA. Annu Rev Microbiol 66, 473–491.

Jeyaprakash, A.A., Santamaria, A., Jayachandran, U., Chan, Y.W., Benda, C., Nigg, E.A., Conti, E., 2012. Structural and functional organization of the Ska complex, a key component of the kinetochore-microtubule interface. Mol Cell 46, 274–286.

Jinek, M., Chylinski, K., Fonfara, I., Hauer, M., Doudna, J.A., Charpentier, E., 2012. A programmable dual-RNA-guided DNA endonuclease in adaptive bacterial immunity. Science 337, 816–822.

Johnson, P.J., Kooter, J.M., Borst, P., 1987. Inactivation of transcription by UV irradiation of *T. brucei* provides evidence for a multicistronic transcription unit including a VSG gene. Cell 51, 273–281.

Jolly, A.L., Luan, C.-H., Dusel, B.E., Dunne, S.F., Winding, M., Dixit, V.J., Robins, C., Saluk, J.L., Logan, D.J., Carpenter, A.E., Sharma, M., Dean, D., Cohen, A.R., Gelfand, V.I., 2016. A genome-wide RNAi Screen for microtubule bundle formation and lysosome motility regulation in *Drosophila* S2 cells. Cell Rep 14, 611–620.

Jones, N.G., Thomas, E.B., Brown, E., Dickens, N.J., Hammarton, T.C., Mottram, J.C., 2014. Regulators of *Trypanosoma brucei* cell cycle progression and differentiation identified using a kinome-wide RNAi screen. PLoS Pathog 10, e1003886.

Joshi, N.A., Fass, J.N., 2011. Sickle: A sliding-window, adaptive, quality-based trimming tool for FastQ files (Version 1.33) [Software] [WWW Document]. https://github.com/najoshi/sickle

Joshi, P.B., Webb, J.R., Davies, J.E., McMaster, W.R., 1995. The gene encoding streptothricin acetyltransferase (sat) as a selectable marker for *Leishmania* expression vectors. Gene 156, 145–149.

Kalidas, S., Li, Q., Phillips, M.A., 2011. A Gateway(R) compatible vector for gene silencing in bloodstream form *Trypanosoma brucei*. Mol Biochem Parasitol 178, 51–55.

Kapitein, L.C., Peterman, E.J.G., Kwok, B.H., Kim, J.H., Kapoor, T.M., Schmidt, C.F., 2005. The bipolar mitotic kinesin Eg5 moves on both microtubules that it crosslinks. Nature 435, 114–118.

Kapler, G.M., Coburn, C.M., Beverley, S.M., 1990. Stable transfection of the human parasite *Leishmania major* delineates a 30-kilobase region sufficient for extrachromosomal replication and expression. Mol Cell Biol 10, 1084–1094.

Kapoor, T.M., Lampson, M.A., Hergert, P., Cameron, L., Cimini, D., Salmon, E.D., McEwen, B.F., Khodjakov, A., 2006. Chromosomes can congress to the metaphase plate before biorientation. Science 311, 388–391.

Karabay, A., Walker, R.A., 1999. The Ncd tail domain promotes microtubule assembly and stability. Biochem Biophys Res Commun 258, 39–43.

Kaseda, K., Higuchi, H., Hirose, K., 2003. Alternate fast and slow stepping of a heterodimeric kinesin molecule. Nat Cell Biol 5, 1079–1082.

Kashlna, A.S., Baskin, R.J., Cole, D.G., Wedaman, K.P., Saxton, W.M., Scholey, J.M., 1996. A bipolar kinesin. Nature 379, 270–272.

Kato, H., Jiang, J., Zhou, B.-R., Rozendaal, M., Feng, H., Ghirlando, R., Xiao, T.S., Straight, A.F., Bai, Y., 2013. A conserved mechanism for centromeric nucleosome recognition by centromere protein CENP-C. Science 340, 1110–1113.

Keeling, P.J., Burger, G., Durnford, D.G., Lang, B.F., Lee, R.W., Pearlman, R.E., Roger, A.J., Gray, M.W., 2005. The tree of eukaryotes. Trends Ecol Evol 20, 670–676.

Kelly, A.E., Sampath, S.C., Maniar, T.A., Woo, E.M., Chait, B.T., Funabiki, H., 2007. Chromosomal enrichment and activation of the Aurora B pathway are coupled to spatially regulate spindle assembly. Dev Cell 12, 31–43.

Kelly, J.M., Ward, H.M., Miles, M.A., Kendall, G., 1992. A shuttle vector which facilitates the expression of transfected genes in *Trypanosoma* cruzi and *Leishmania*. Nucleic Acids Res 20, 3963–3969.

Kelly, S., Reed, J., Kramer, S., Ellis, L., Webb, H., Sunter, J., Salje, J., Marinsek, N., Gull, K., Wickstead, B., Carrington, M., 2007. Functional genomics in *Trypanosoma brucei*: A collection of vectors for the expression of tagged proteins from endogenous and ectopic gene loci. Mol Biochem Parasitol 154, 103–109.

Kemmler, S., Stach, M., Knapp, M., Ortiz, J., Pfannstiel, J., Ruppert, T., Lechner, J., 2009. Mimicking Ndc80 phosphorylation triggers spindle assembly checkpoint signalling. EMBO J 28, 1099–1110.

Khodjakov, A., Rieder, C.L., 1999. The sudden recruitment of gamma-tubulin to the centrosome at the onset of mitosis and its dynamic exchange throughout the cell cycle, do not require microtubules. J Cell Biol 146, 585–596.

Kim, H.-S., Li, Z., Boothroyd, C., Cross, G.A.M., 2013. Strategies to construct null and conditional null *Trypanosoma brucei* mutants using Cre-recombinase and loxP. Mol Biochem Parasitol 191, 16–19.

Kim, H.-S., Cross, G.A.M., 2010. TOPO3α influences antigenic variation by monitoring expression-site-associated VSG switching in *Trypanosoma brucei*. PLoS Pathog 6, e1000992.

Kim, Y., Holland, A.J., Lan, W., Cleveland, D.W., 2010. Aurora kinases and protein phosphatase 1 mediate chromosome congression through regulation of CENP-E. Cell 142, 444–455.

Kimberlin, D.W., Whitley, R.J., 2007. Antiviral therapy of HSV-1 and -2. In: Arvin, A., Campadelli-Fiume, G., Mocarski, E., Moore, P.S., Roizman, B., Whitley, R., Yamanishi, K. (Eds.), Human Herpesviruses: Biology, Therapy, and Immunoprophylaxis. Cambridge University Press, pp. 1153–1174.

Kimmins, S., Crosio, C., Kotaja, N., Hirayama, J., Monaco, L., Höög, C., van Duin, M., Gossen, J.A., Sassone-Corsi, P., 2007. Differential functions of the Aurora-B and Aurora-C kinases in mammalian spermatogenesis. Mol Endocrinol 21, 726–739.

Kirschner, M.W., Mitchison, T., 1986a. Microtubule dynamics. Nature 325, 621.

Kirschner, M.W., Mitchison, T., 1986b. Beyond self-assembly: from microtubules to morphogenesis. Cell 45, 329–342.

Kitagawa, M., Fung, S.Y.S., Onishi, N., Saya, H., Lee, S.H., 2013. Targeting Aurora B to the equatorial cortex by MKlp2 is required for cytokinesis. PLoS One 8, e64826.

Kline-Smith, S.L., Khodjakov, A., Hergert, P., Walczak, C.E., 2004. Depletion of centromeric MCAK leads to chromosome congression and segregation defects due to improper kinetochore attachments. Mol Biol Cell 15, 1146–1159.

Knowlton, A.L., Lan, W., Stukenberg, P.T., 2006. Aurora B is enriched at merotelic attachment sites, where it regulates MCAK. Curr Biol 16, 1705–1710.

Koffa, M.D., Casanova, C.M., Santarella, R., Köcher, T., Wilm, M., Mattaj, I.W., 2006. HURP is part of a Ran-dependent complex involved in spindle formation. Curr Biol 16, 743–754.

Kohl, L., Gull, K., 1998. Molecular architecture of the trypanosome cytoskeleton. Mol Biochem Parasitol 93, 1–9.

Kohl, L., Sherwin, T., Gull, K., 1999. Assembly of the paraflagellar rod and the flagellum attachment zone complex during the *Trypanosoma brucei* cell cycle. J Eukaryot Microbiol 46, 105–109.

Kolev, N.G., Franklin, J.B., Carmi, S., Shi, H., Michaeli, S., Tschudi, C., 2010. The transcriptome of the human pathogen *Trypanosoma brucei* at single-nucleotide resolution. PLoS Pathog 6, 1–15.

Kosak, S.T., Groudine, M., 2004. Form follows function: The genomic organization of cellular differentiation. Genes Dev 18, 1371–1384.

Kozminski, K.G., Beech, P.L., Rosenbaum, J.L., 1995. The *Chlamydomonas* kinesin-like protein FLA10 is involved in motility associated with the flagellar membrane. J Cell Biol 131, 1517–1527.

Kruse, T., Zhang, G., Larsen, M.S.Y., Lischetti, T., Streicher, W., Kragh Nielsen, T., Bjørn, S.P., Nilsson, J., 2013. Direct binding between BubR1 and B56-PP2A phosphatase complexes regulate mitotic progression. J Cell Sci 126, 1086–1092.

Kukurba, K.R., Montgomery, S.B., 2015. RNA sequencing and analysis. Cold Spring Harb Protoc 2015, 951–969.

Kumar, P., Wang, C.C., 2005. Depletion of anaphase-promoting complex or cyclosome (APC/C) subunit homolog APC1 or CDC27 of *Trypanosoma brucei* arrests the procyclic form in metaphase but the bloodstream form in anaphase. J Biol Chem 280, 31783–31791.

Kushnir, S., Cirstea, I.C., Basiliya, L., Lupilova, N., Breitling, R., Alexandrov, K., 2011. Artificial linear episome-based protein expression system for protozoon *Leishmania tarentolae*. Mol Biochem Parasitol 176, 69–79.

Kushnir, S., Gase, K., Breitling, R., Alexandrov, K., 2005. Development of an inducible protein expression system based on the protozoan host *Leishmania tarentolae*. Protein Expr Purif 42, 37–46.

Laban, A., Tobin, J.F., Curotto de Lafaille, M.A., Wirth, D.F., 1990. Stable expression of the bacterial *neo*^{r} gene in *Leishmania enriettii*. Nature 343, 572–574.

Laban, A., Wirth, D.F., 1989. Transfection of *Leishmania enriettii* and expression of chloramphenicol acetyltransferase gene. Proc Natl Acad Sci U S A 86, 9119–9123.

Lacomble, S., Vaughan, S., Gadelha, C., Morphew, M.K., Shaw, M.K., McIntosh, J.R., Gull, K., 2009. Three-dimensional cellular architecture of the flagellar pocket and associated cytoskeleton in trypanosomes revealed by electron microscope tomography. J Cell Sci 122, 1081–1090.

LaCount, D.J., Bruse, S., Hill, K.L., Donelson, J.E., 2000. Double-stranded RNA interference in *Trypanosoma brucei* using head-to-head promoters. Mol Biochem Parasitol 111, 67–76.

Lampert, F., Hornung, P., Westermann, S., 2010. The Dam1 complex confers microtubule plus end-tracking activity to the Ndc80 kinetochore complex. J Cell Biol 189, 641–649.

Lampson, M.A., Cheeseman, I.M., 2011. Sensing centromere tension: Aurora B and the regulation of kinetochore function. Trends Cell Biol 21, 133–140.

Lan, W., Zhang, X., Kline-Smith, S.L., Rosasco, S.E., Barrett-Wilt, G.A., Shabanowitz, J., Hunt, D.F., Walczak, C.E., Stukenberg, P.T., 2004. Aurora B phosphorylates centromeric MCAK and regulates its localization and microtubule depolymerization activity. Curr Biol 14, 273–286.

Landeira, D., Navarro, M., 2007. Nuclear repositioning of the VSG promoter during developmental silencing in *Trypanosoma brucei*. J Cell Biol 176, 133–139.

Lander, N., Li, Z.-H., Niyogi, S., Docampo, R., 2015. CRISPR/Cas9-induced disruption of paraflagellar rod protein 1 and 2 genes in *Trypanosoma cruzi* reveals their role in flagellar attachment. MBio 6, e01012.

Langmead, B., Salzberg, S.L., 2012. Fast gapped-read alignment with Bowtie 2. Nat Methods 9, 357–359.

Langousis, G., Hill, K.L., 2014. Motility and more: the flagellum of *Trypanosoma brucei*. Nat Rev Microbiol 12, 505–518.

Lau, I.F., Filipe, S.R., Søballe, B., Økstad, O.A., Barre, F.X., Sherratt, D.J., 2003. Spatial and temporal organization of replicating *Escherichia coli* chromosomes. Mol Microbiol 49, 731–743.

Lawrence, C.J., Dawe, R.K., Christie, K.R., Cleveland, D.W., Dawson, S.C., Endow, S.A., Goldstein, L.S.B., Goodson, H. V., Hirokawa, N., Howard, J., Malmberg, R.L., McIntosh, J.R., Miki, H., Mitchison, T.J., Okada, Y., Reddy, A.S.N., Saxton, W.M., Schliwa, M., Scholey, J.M., Vale, R.D., Walczak, C.E., Wordeman, L., 2004. A standardized kinesin nomenclature. J Cell Biol 167, 19–22.

Lawrence, C.J., Morris, N.R., Meagher, R.B., Dawe, R.K., 2001. Dyneins have run their course in plant lineage. Traffic 2, 362–363.

LeBowitz, J.H., Cruz, A., Beverley, S.M., 1992. Thymidine kinase as a negative selectable marker in *Leshmania major*. Mol Biochem Parasitol 51, 321–326.

LeBowitz, J.H., Smith, H.Q., Rusche, L., Beverley, S.M., 1993. Coupling of poly(A) site selection and trans-splicing in *Leishmania*. Genes Dev 7, 996–1007.

Lee, M.G., van der Ploeg, L.H., 1991. The hygromycin B-resistance-encoding gene as a selectable marker for stable transformation of *Trypanosoma brucei*. Gene 105, 255–257.

Lee, M.G., Yaping, E., Axelrod, N., 1995. Construction of trypanosome artificial mini-chromosomes. Nucleic Acids Res 23, 4893–4899.

Lee, R.C., Feinbaum, R.L., Ambros, V., 1993. The *C. elegans* heterochronic gene *lin-4* encodes small RNAs with antisense complementarity to *lin-14*. Cell 75, 843–854.

Lee, Y.-R.J., Liu, B., 2004. Cytoskeletal motors in *Arabidopsis*. Sixty-one kinesins and seventeen myosins. Plant Physiol 136, 3877–3883.

Lénárt, P., Rabut, G., Daigle, N., Hand, A.R., Terasaki, M., Ellenberg, J., 2003. Nuclear envelope breakdown in starfish oocytes proceeds by partial NPC disassembly followed by a rapidly spreading fenestration of nuclear membranes. J Cell Biol 160, 1055–1068.

Leo, M., Santino, D., Tikhonenko, I., Magidson, V., Khodjakov, A., Koonce, M.P., 2012. Rules of engagement: centrosome-nuclear connections in a closed mitotic system. Biol Open 1, 1111–1117.

Li, X., Sakashita, G., Matsuzaki, H., Sugimoto, K., Kimura, K., Hanaoka, F., Taniguchi, H., Furukawa, K., Urano, T., 2004. Direct association with inner centromere protein (INCENP) activates the novel chromosomal passenger protein, Aurora-C. J Biol Chem 279, 47201–47211.

Li, Z., Gourguechon, S., Wang, C.C., 2007. Tousled-like kinase in a microbial eukaryote regulates spindle assembly and S-phase progression by interacting with Aurora kinase and chromatin assembly factors. J Cell Sci 120, 3883–3894.

Li, Z., Lee, J.H., Chu, F., Burlingame, A.L., Gunzl, A., Wang, C.C., 2008a. Identification of a novel chromosomal passenger complex and its unique localization during cytokinesis in *Trypanosoma brucei*. PLoS One 3, e2354.

Li, Z., Umeyama, T., Wang, C.C., 2008b. The chromosomal passenger complex and a mitotic kinesin interact with the Tousled-like kinase in trypanosomes to regulate mitosis and cytokinesis. PLoS One 3, e3814.

Li, Z., Umeyama, T., Wang, C.C., 2009. The Aurora kinase in *Trypanosoma brucei* plays distinctive roles in metaphase-anaphase transition and cytokinetic initiation. PLoS Pathog 5, e1000575.

Li, Z., Wang, C.C., 2003. A PHO80-like cyclin and a B-type cyclin control the cell cycle of the procyclic form of *Trypanosoma brucei*. J Biol Chem 278, 20652–20658.

Li, Z., Wang, C.C., 2006. Changing roles of Aurora-B kinase in two life cycle stages of *Trypanosoma brucei*. Eukaryot Cell 5, 1026–1035.

Liniger, M., Bodenmüller, K., Pays, E., Gallati, S., Roditi, I., 2001. Overlapping sense and antisense transcription units in *Trypanosoma brucei*. Mol Microbiol 40, 869–878.

Liu, M., Nadar, V.C., Kozielski, F., Kozlowska, M., Yu, W., Baas, P.W., 2010. Kinesin-12, a mitotic microtubule-associated motor protein, impacts axonal growth, navigation, and branching. J Neurosci 30, 14896–14906.

Liu, S.-T., Rattner, J.B., Jablonski, S.A., Yen, T.J., 2006. Mapping the assembly pathways that specify formation of the trilaminar kinetochore plates in human cells. J Cell Biol 175, 41–53.

López-García, P., Philippe, H., Gail, F., Moreira, D., 2003. Autochthonous eukaryotic diversity in hydrothermal sediment and experimental microcolonizers at the Mid-Atlantic Ridge. Proc Natl Acad Sci U S A 100, 697–702.

Lorenz, P., Maier, A.G., Baumgart, E., Erdmann, R., Clayton, C., 1998. Elongation and clustering of glycosomes in *Trypanosoma brucei* overexpressing the glycosomal Pex11p. EMBO J 17, 3542–3555.

Lu, H.Y., Buck, G.A., 1991. Expression of an exogenous gene in *Trypanosoma cruzi* epimastigotes. Mol Biochem Parasitol 44, 109–114.

Lu, L., Ladinsky, M.S., Kirchhausen, T., 2009. Cisternal organization of the endoplasmic reticulum during mitosis. Mol Biol Cell 20, 3471–3480.

Lye, L.-F., Owens, K., Shi, H., Murta, S.M.F., Vieira, A.C., Turco, S.J., Tschudi, C., Ullu, E., Beverley, S.M., 2010. Retention and loss of RNA interference pathways in trypanosomatid protozoans. PLoS Pathog 6, e1001161.

Maddox, P., Desai, A., Oegema, K., Mitchison, T.J., Salmon, E.D., 2002. Poleward microtubule flux is a major component of spindle dynamics and anaphase a in mitotic *Drosophila* embryos. Curr Biol 12, 1670–1674.

Maharana, B.R., Tewari, A.K., Singh, V., 2015. An overview on kinetoplastid paraflagellar rod. J Parasit Dis 39, 589–595.

Makarova, M., Oliferenko, S., 2016. Mixing and matching nuclear envelope remodeling and spindle assembly strategies in the evolution of mitosis. Curr Opin Cell Biol 41, 43–50.

Malik, H.S., Henikoff, S., 2003. Phylogenomics of the nucleosome. Nat Struct Biol 10, 882–891.

Mallik, R., Rai, A.K., Barak, P., Rai, A., Kunwar, A., 2013. Teamwork in microtubule motors. Trends Cell Biol 23, 575–582.

Maney, T., Hunter, A.W., Wagenbach, M., Wordeman, L., 1998. Mitotic centromere-associated kinesin is important for anaphase chromosome segregation. J Cell Biol 142, 787–801.

Mani, J., Gunasekera, K., Roditi, I., 2012. RNA-Seq Analysis of the transcriptome of *Trypanosoma brucei*. In: RNA Metabolism in Trypanosomes. pp. 237–265.

Mansour, S.L., Thomas, K.R., Capecchi, M.R., 1988. Disruption of the proto-oncogene *int-2* in mouse embryo-derived stem cells: a general strategy for targeting mutations to non-selectable genes. Nature 336, 348–352.

Mao, Y., Najafabadi, H.S., Salavati, R., 2009. Genome-wide computational identification of functional RNA elements in *Trypanosoma brucei*. BMC Genomics 10, 355.

Marchetti, M.A., Tschudi, C., Kwon, H., Wolin, S.L., Ullu, E., 2000. Import of proteins into the trypanosome nucleus and their distribution at karyokinesis. J Cell Sci 113, 899–906.

Martínez-Calvillo, S., Vizuet-de-Rueda, J.C., Florencio-Martínez, L.E., Manning-Cela, R.G., Figueroa-Angulo, E.E., 2010. Gene expression in trypanosomatid parasites. J Biomed Biotechnol 2010, 1–15.

Matthews, K.R., 2005. The developmental cell biology of *Trypanosoma brucei*. J Cell Sci 118, 283–290.

Matuliene, J., Kuriyama, R., 2002. Kinesin-like protein CHO1 is required for the formation of midbody matrix and the completion of cytokinesis in mammalian cells. Mol Biol Cell 13, 1832–1845.

Mayr, M.I., Hümmer, S., Bormann, J., Grüner, T., Adio, S., Woehlke, G., Mayer, T.U., 2007. The human kinesin Kif18A is a motile microtubule depolymerase essential for chromosome congression. Curr Biol 17, 488–498.

Mazumdar, M., Sundareshan, S., Misteli, T., 2004. Human chromokinesin KIF4A functions in chromosome condensation and segregation. J Cell Biol 166, 613–620.

McEwen, B.F., Chan, G.K., Zubrowski, B., Savoian, M.S., Sauer, M.T., Yen, T.J., 2001. CENP-E is essential for reliable bioriented spindle attachment, but chromosome alignment can be achieved via redundant mechanisms in mammalian cells. Mol Biol Cell 12, 2776–2789.

McEwen, B.F., Heagle, A.B., Cassels, G.O., Buttle, K.F., Rieder, C.L., 1997. Kinetochore fiber maturation in PtK1 cells and its implications for the mechanisms of chromosome congression and anaphase onset. J Cell Biol 137, 1567–1580.

McIntosh, J.R., Grishchuk, E.L., West, R.R., 2002. Chromosome-microtubule interactions during mitosis. Annu Rev Cell Dev Biol 18, 193–219.

McIntosh, J.R., Molodtsov, M.I., Ataullakhanov, F.I., 2012. Biophysics of mitosis. Q Rev Biophys 45, 147–207.

McKim, K.S., Hawley, R.S., 1995. Chromosomal control of meiotic cell division. Science 270, 1595–1601.

Mijalkovic, J., Prevo, B., Peterman, E.J.G., 2016. Why motor proteins team up - Intraflagellar transport in *C. elegans* cilia. Worm 5, e1170275.

Miki, H., Okada, Y., Hirokawa, N., 2005. Analysis of the kinesin superfamily: insights into structure and function. Trends Cell Biol 15, 467–476.

Millecamps, S., Julien, J.-P., 2013. Axonal transport deficits and neurodegenerative diseases. Nat Rev Neurosci 14, 161–176.

Miranda, J.J.L., De Wulf, P., Sorger, P.K., Harrison, S.C., 2005. The yeast DASH complex forms closed rings on microtubules. Nat Struct Mol Biol 12, 138–143.

Mishima, M., Kaitna, S., Glotzer, M., 2002. Central spindle assembly and cytokinesis require a kinesin-like protein/RhoGAP complex with microtubule bundling activity. Dev Cell 2, 41–54.

Misteli, T., 2007. Beyond the sequence: Cellular organization of genome function. Cell 128, 787–800.

Mitchison, T.J., Salmon, E.D., 1992. Poleward kinetochore fiber movement occurs during both metaphase and anaphase-A in newt lung cell mitosis. J Cell Biol 119, 569–582.

Moreira-Leite, F.F., Sherwin, T., Kohl, L., Gull, K., 2001. A trypanosome structure involved in transmitting cytoplasmic information during cell division. Science 294, 610–612.

Moreira, D., López-García, P., Vickerman, K., 2004. An updated view of kinetoplastid phylogeny using environmental sequences and a closer outgroup:

Proposal for a new classification of the class Kinetoplastea. Int J Syst Evol Microbiol 54, 1861–1875.

Morga, B., Bastin, P., 2013. Getting to the heart of intraflagellar transport using *Trypanosoma* and *Chlamydomonas* models: the strength is in their differences. Cilia 2, 16.

Morris, J.C., Wang, Z., Drew, M.E., Englund, P.T., 2002. Glycolysis modulates trypanosome glycoprotein expression as revealed by an RNAi library. EMBO J 21, 4429–4438.

Mountain, V., Simerly, C., Howard, L., Ando, A., Schatten, G., Compton, D.A., 1999. The kinesin-related protein, HSET, opposes the activity of Eg5 and cross-links microtubules in the mammalian mitotic spindle. J Cell Biol 147, 351–365.

Muhich, M.L., Boothroyd, J.C., 1988. Polycistronic transcripts in trypanosomes and their accumulation during heat shock: evidence for a precursor role in mRNA synthesis. Mol Cell Biol 8, 3837–3846.

Murray, A.W., 2011. A brief history of error. Nat Cell Biol 13, 1178–1182.

Navarro, M., Gull, K., 2001. A pol I transcriptional body associated with VSG mono-allelic expression in *Trypanosoma brucei*. Nature 414, 759–763.

Neef, R., Klein, U.R., Kopajtich, R., Barr, F.A., 2006. Cooperation between mitotic kinesins controls the late stages of cytokinesis. Curr Biol 16, 301–307.

Neighbors, B.W., Williams, R.C., McIntosh, J.R., 1988. Localization of kinesin in cultured cells. J Cell Biol 106, 1193–1204.

Nerusheva, O.O., Akiyoshi, B., 2016. Divergent polo box domains underpin the unique kinetoplastid kinetochore. Open Biol 6, 150206.

Ngô, H., Tschudi, C., Gull, K., Ullu, E., 1998. Double-stranded RNA induces mRNA degradation in *Trypanosoma brucei*. Proc Natl Acad Sci U S A 95, 14687–14692.

Nicklas, R.B., Ward, S.C., 1994. Elements of error correction in mitosis: microtubule capture, release, and tension. J Cell Biol 126, 1241–1253.

Nigg, E.A., Stearns, T., 2011. The centrosome cycle: Centriole biogenesis, duplication and inherent asymmetries. Nat Cell Biol 13, 1154–1160.

Nijenhuis, W., Von Castelmur, E., Littler, D., De Marco, V., Tromer, E., Vleugel, M., Van Osch, M.H.J., Snel, B., Perrakis, A., Kops, G.J.P.L., 2013. A TPR domain-containing N-terminal module of MPS1 is required for its kinetochore localization by Aurora B. J Cell Biol 201, 217–231.

Nishino, T., Rago, F., Hori, T., Tomii, K., Cheeseman, I.M., Fukagawa, T., 2013. CENP-T provides a structural platform for outer kinetochore assembly. EMBO J 32, 424–436.

Novelli, G., D'Apice, M.R., 2012. Protein farnesylation and disease. J Inherit Metab Dis 35, 917–926.

Nunes Bastos, R., Gandhi, S.R., Baron, R.D., Gruneberg, U., Nigg, E.A., Barr, F.A., 2013. Aurora B suppresses microtubule dynamics and limits central spindle size by locally activating KIF4A. J Cell Biol 2012, 605–621.

Obado, S.O., Bot, C., Nilsson, D., Andersson, B., Kelly, J.M., 2007. Repetitive DNA is associated with centromeric domains in *Trypanosoma brucei* but not *Trypanosoma cruzi*. Genome Biol 8, R37.

Obado, S.O., Taylor, M.C., Wilkinson, S.R., Bromley, E. V., Kelly, J.M., 2005. Functional mapping of a trypanosome centromere by chromosome fragmentation identifies a 16-kb GC-rich transcriptional "strand-switch" domain as a major feature. Genome Res 15, 36–43.

Obara, B., Kelly, S., Wickstead, B., Gull, K., Gavaghan, D., Grau, V., 2009. High-throughput high-resolution image analysis of the trypanosome cell cycle. In: Microscopic Image Analysis with Applications in Biology.

Obuse, C., Yang, H., Nozaki, N., Goto, S., Okazaki, T., Yoda, K., 2004. Proteomics analysis of the centromere complex from HeLa interphase cells: UV-damaged DNA binding protein 1 (DDB-1) is a component of the CEN-complex, while BMI-1 is transiently co-localized with the centromeric region in interphase. Genes to Cells 9, 105–120.

Ogbadoyi, E., Ersfeld, K., Robinson, D., Sherwin, T., Gull, K., 2000. Architecture of the *Trypanosoma brucei* nucleus during interphase and mitosis. Chromosoma 108, 501–513.

Ogbadoyi, E.O., Robinson, D.R., Gull, K., 2003. A high-order trans-membrane structural linkage is responsible for mitochondrial genome positioning and segregation by flagellar basal bodies in trypanosomes. Mol Biol Cell 14, 1769–1779.

Okada, M., Cheeseman, I.M., Hori, T., Okawa, K., McLeod, I.X., Yates, J.R., Desai, A., Fukagawa, T., 2006. The CENP-H-I complex is required for the efficient incorporation of newly synthesized CENP-A into centromeres. Nat Cell Biol 8, 446–457.

Okada, Y., Yamazaki, H., Sekine-Aizawa, Y., Hirokawa, N., 1995. The neuron-specific kinesin superfamily protein KIF1A is a unique monomeric motor for anterograde axonal transport of synaptic vesicle precursors. Cell 81, 769–780.

Ooi, C.-P., Bastin, P., 2013. More than meets the eye: understanding *Trypanosoma brucei* morphology in the tsetse. Front Cell Infect Microbiol 3, Article 71.

Osmani, A.H., Davies, J., Liu, H.-L., Nile, A., Osmani, S.A., 2006. Systematic deletion and mitotic localization of the nuclear pore complex proteins of *Aspergillus nidulans*. Mol Biol Cell 17, 4946–4961.

Otsu, K., Donelson, J.E., Kirchhoff, L.V., 1993. Interruption of a *Trypanosoma cruzi* gene encoding a protein containing 14-amino acid repeats by targeted insertion of the neomycin phosphotransferase gene. Mol Biochem Parasitol 57, 317–330.

Otsu, K., Donelson, J.E., Kirchhoff, L. V, 1995. *Trypanosoma cruzi*: interruption of both alleles of a gene encoding a protein containing 14-amino-acid repeats by targeted insertion of *NEO*^{r} and *HYG*^{r}. Exp Parasitol 81, 529–535.

Paddison, P.J., Caudy, A.A., Bernstein, E., Hannon, G.J., Conklin, D.S., 2002. Short hairpin RNAs (shRNAs) induce sequence-specific silencing in mammalian cells. Genes Dev 16, 948–958.

Palenchar, J.B., Bellofatto, V., 2006. Gene transcription in trypanosomes. Mol Biochem Parasitol 146, 135–141.

Palmer, D.K., O'Day, K., Trong, H.L., Charbonneau, H., Margolis, R.L., 1991. Purification of the centromere-specific protein CENP-A and demonstration that it is a distinctive histone. Proc Natl Acad Sci U S A 88, 3734–3738.

Palmer, D.K., O'Day, K., Wener, M.H., Andrews, B.S., Margolis, R.L., 1987. A 17-kD centromere protein (CENP-A) copurifies with nucleosome core particles and with histones. J Cell Biol 104, 805–815.

Papadopoulou, B., Roy, G., Ouellette, M., 1994. Autonomous replication of bacterial DNA plasmid oligomers in *Leishmania*. Mol Biochem Parasitol 65, 39–49.

Patnaik, P.K., Axelrod, N., Van der Ploeg, L.H.T., Cross, G.A.M., 1996. Artificial linear mini-chromosomes for *Trypanosoma brucei*. Nucleic Acids Res 24, 668–675.

Patnaik, P.K., Kulkarni, S.K., Cross, G.A., 1993. Autonomously replicating single-copy episomes in *Trypanosoma brucei* show unusual stability. EMBO J 12, 2529–2538.

Pays, E., 2005. Regulation of antigen gene expression in *Trypanosoma brucei*. Trends Parasitol 21, 517–520.

Pays, E., Vanhollebeke, B., Vanhamme, L., Paturiaux-Hanocq, F., Nolan, D.P., Pérez-Morga, D., 2006. The trypanolytic factor of human serum. Nat Rev Microbiol 4, 477–486.

Peng, D., Kurup, S.P., Yao, P.Y., Minning, T.A., Tarleton, R.L., 2015. CRISPR-Cas9-mediated single-gene and gene family disruption in *Trypanosoma cruzi*. MBio 6, e02097-14.

Petrásek, J., Schwarzerová, K., 2009. Actin and microtubule cytoskeleton interactions. Curr Opin Plant Biol 12, 728–734.

Petretti, C., Savoian, M., Montembault, E., Glover, D.M., Prigent, C., Giet, R., 2006. The PITSLRE/CDK11p58 protein kinase promotes centrosome maturation and bipolar spindle formation. EMBO Rep 7, 418–424.

Petrovic, A., Pasqualato, S., Dube, P., Krenn, V., Santaguida, S., Cittaro, D., Monzani, S., Massimiliano, L., Keller, J., Tarricone, A., Maiolica, A., Stark, H., Musacchio, A., 2010. The MIS12 complex is a protein interaction hub for outer kinetochore assembly. J Cell Biol 190, 835–852.

Petry, S., 2016. Mechanisms of mitotic spindle assembly. Annu Rev Biochem 85, 659–683.

Piehl, M., Tulu, U.S., Wadsworth, P., Cassimeris, L., 2004. Centrosome maturation: measurement of microtubule nucleation throughout the cell cycle by using GFP-tagged EB1. Proc Natl Acad Sci U S A 101, 1584–1588.

Pines, J., 2011. Cubism and the cell cycle: the many faces of the APC/C. Nat Rev Mol Cell Biol 12, 427–438.

Ploubidou, A., Robinson, D.R., Docherty, R.C., Ogbadoyi, E.O., Gull, K., 1999. Evidence for novel cell cycle checkpoints in trypanosomes: kinetoplast segregation and cytokinesis in the absence of mitosis. J Cell Sci 112, 4641–4650.

Poon, S.K., Peacock, L., Gibson, W., Gull, K., Kelly, S., 2012. A modular and optimized single marker system for generating *Trypanosoma brucei* cell lines expressing T7 RNA polymerase and the tetracycline repressor. Open Biol 2, 110037.

Portier, N., Audhya, A., Maddox, P.S., Green, R.A., Dammermann, A., Desai, A., Oegema, K., 2007. A microtubule-independent role for centrosomes and Aurora A in nuclear envelope breakdown. Dev Cell 12, 515–529.

Portman, N., Gull, K., 2010. The paraflagellar rod of kinetoplastid parasites: From structure to components and function. Int J Parasitol 40, 135–148.

Povelones, M.L., 2014. Beyond replication: Division and segregation of mitochondrial DNA in kinetoplastids. Mol Biochem Parasitol 196, 53–60.

Povelones, M.L., Gluenz, E., Dembek, M., Gull, K., Rudenko, G., 2012. Histone H1 plays a role in heterochromatin formation and VSG expression site silencing in *Trypanosoma brucei*. PLoS Pathog 8, e1003010.

Prevo, B., Mangeol, P., Oswald, F., Scholey, J.M., Peterman, E.J.G., 2015. Functional differentiation of cooperating kinesin-2 motors orchestrates cargo import and transport in *C. elegans* cilia. Nat Cell Biol 17, 1536–1545.

Pronk, J.T., 2002. Auxotrophic yeast strains in fundamental and applied research. Appl Environ Microbiol 68, 2095–2100.

Przewloka, M.R., Venkei, Z., Bolanos-Garcia, V.M., Debski, J., Dadlez, M., Glover, D.M., 2011. CENP-C is a structural platform for kinetochore assembly. Curr Biol 21, 399–405.

Quijada, L., Guerra-Giraldez, C., Drozdz, M., Hartmann, C., Irmer, H., Ben-Dov, C., Cristodero, M., Ding, M., Clayton, C., 2002. Expression of the human RNA-binding protein HuR in *Trypanosoma brucei* increases the abundance of mRNAs containing AU-rich regulatory elements. Nucleic Acids Res 30, 4414–4424.

Raaijmakers, J.A., Tanenbaum, M.E., Maia, A.F., Medema, R.H., 2009. RAMA1 is a novel kinetochore protein involved in kinetochore-microtubule attachment. J Cell Sci 122, 2436–2445.

R Core Team, 2016. R: A language and environment for statistical computing. R Foundation for Statistical Computing, Vienna, Austria [WWW Document]. https://www.r-project.org/

Radulescu, A.E., Cleveland, D.W., 2010. NuMA after 30 years: the matrix revisited. Trends Cell Biol 20, 214–222.

Ralston, K.S., Hill, K.L., 2006. Trypanin, a component of the flagellar dynein regulatory complex, is essential in bloodstream form African trypanosomes. PLoS Pathog 2, e101.

Reddy, A.S., Day, I.S., 2001. Kinesins in the *Arabidopsis* genome: A comparative analysis among eukaryotes. BMC Genomics 2, 2.

Régnier, V., Vagnarelli, P., Fukagawa, T., Zerjal, T., Burns, E., Trouche, D., Earnshaw, W., Brown, W., 2005. CENP-A is required for accurate chromosome segregation and sustained kinetochore association of BubR1. Mol Cell Biol 25, 3967–3981.

Resnick, T.D., Satinover, D.L., MacIsaac, F., Stukenberg, P.T., Earnshaw, W.C., Orr-Weaver, T.L., Carmena, M., 2006. INCENP and Aurora B promote meiotic sister chromatid cohesion through localization of the Shugoshin MEI-S332 in *Drosophila*. Dev Cell 11, 57–68.

Rezaul, K., Gupta, D., Semenova, I., Ikeda, K., Kraikivski, P., Yu, J., Cowan, A., Zaliapin, I., Rodionov, V., 2016. Engineered tug-of-war between kinesin and dynein controls direction of microtubule transport. Traffic 17, 475–486.

Richard, J., Kim, E.D., Nguyen, H., Kim, C.D., Kim, S., 2016. Allostery wiring map for kinesin energy transduction and its evolution. J Biol Chem 40, 20932-20945.

Rieder, C.L., Davison, E.A., Jensen, L.C.W., Cassimeris, L., Salmon, E.D., 1986. Oscillatory movements of monooriented chromosomes and their position relative to the spindle pole result from the ejection properties of the aster and half-spindle. J Cell Biol 103, 581–591.

Roberts, A.J., Kon, T., Knight, P.J., Sutoh, K., Burgess, S.A., 2013. Functions and mechanics of dynein motor proteins. Nat Rev Mol Cell Biol 14, 713–726.

Robinett, C.C., Straight, A., Li, G., Willhelm, C., Sudlow, G., Murray, A., Belmont, A.S., 1996. *In vivo* localization of DNA sequences and visualization of large-scale chromatin organization using lac operator/repressor recognition. J Cell Biol 135, 1685–1700.

Robinow, C.F., 1969. Mitosis in *Aspergillus nidulans*. J Cell Sci 5, 403–431.

Robinson, D.R., Gull, K., 1991. Basal body movements as a mechanism for mitochondrial genome segregation in the trypanosome cell cycle. Nature 352, 731–733.

Robinson, D.R., Sherwin, T., Ploubidou, A., Byard, E.H., Gull, K., 1995. Microtubule polarity and dynamics in the control of organelle positioning, segregation, and cytokinesis in the trypanosome cell cycle. J Cell Biol 128, 1163–1172.

Robinson, K.A., Beverley, S.M., 2003. Improvements in transfection efficiency and tests of RNA interference (RNAi) approaches in the protozoan parasite *Leishmania*. Mol Biochem Parasitol 128, 217–228.

Roditi, I., Furger, A., Ruepp, S., Schürch, N., Bütikofer, P., 1998. Unravelling the procyclin coat of *Trypanosoma brucei*. Mol Biochem Parasitol 91, 117–130.

Roger, A.J., Simpson, A.G.B., 2009. Evolution: Revisiting the root of the eukaryote tree. Curr Biol 19, R165–167.

Rogers, G.C., Chui, K.K., Lee, E.W., Wedaman, K.P., Sharp, D.J., Holland, G., Morris, R.L., Scholey, J.M., 2000. A kinesin-related protein, KRP(180), positions prometaphase spindle poles during early sea urchin embryonic cell division. J Cell Biol 150, 499–512.

Rogers, G.C., Rogers, S.L., Schwimmer, T.A., Ems-McClung, S.C., Walczak, C.E., Vale, R.D., Scholey, J.M., Sharp, D.J., 2004. Two mitotic kinesins cooperate to drive sister chromatid separation during anaphase. Nature 427, 364–370.

Rohloff, P., Montalvetti, A., Docampo, R., 2004. Acidocalcisomes and the contractile vacuole complex are involved in osmoregulation in *Trypanosoma cruzi*. J Biol Chem 279, 52270–52281.

Roof, D.M., Meluh, P.B., Rose, M.D., 1992. Kinesin-related proteins required for assembly of the mitotic spindle. J Cell Biol 118, 95–108.

Roostalu, J., Hentrich, C., Bieling, P., Telley, I.A., Schiebel, E., Surrey, T., 2011. Directional switching of the kinesin Cin8 through motor coupling. Science 332, 94–99.

Roostalu, J., Surrey, T., 2013. The multiple talents of kinesin-8. Nat Cell Biol 15, 889–891.

Rotureau, B., Ooi, C.P., Huet, D., Perrot, S., Bastin, P., 2014. Forward motility is essential for trypanosome infection in the tsetse fly. Cell Microbiol 16, 425–433.

Rudenko, G., Le Blancq, S., Smith, J., Lee, M.G., Rattray, A., Van der Ploeg, L.H., 1990. Procyclic acidic repetitive protein (PARP) genes located in an unusually small alpha-amanitin-resistant transcription unit: PARP promoter activity assayed by transient DNA transfection of *Trypanosoma brucei*. Mol Cell Biol 10, 3492–3504.

Ruepp, S., Furger, A., Kurath, U., Renggli, C.K., Hemphill, A., Brun, R., Roditi, I., 1997. Survival of *Trypanosoma brucei* in the tsetse fly is enhanced by the expression of specific forms of procyclin. J Cell Biol 137, 1369–1379.

Saitoh, S., Takahashi, K., Nabeshima, K., Yamashita, Y., Nakaseko, Y., Hirata, A., Yanagida, M., 1996. Aberrant mitosis in fission yeast mutants defective in fatty acid synthetase and acetyl CoA carboxylase. J Cell Biol 134, 949–961.

Salmon, D., Bachmaier, S., Krumbholz, C., Kador, M., Gossmann, J.A., Uzureau, P., Pays, E., Boshart, M., 2012. Cytokinesis of *Trypanosoma brucei* bloodstream forms depends on expression of adenylyl cyclases of the ESAG4 or ESAG4-like subfamily. Mol Microbiol 84, 225–242.

Sampath, S.C., Ohi, R., Leismann, O., Salic, A., Pozniakovski, A., Funabiki, H., 2004. The chromosomal passenger complex is required for chromatin-induced microtubule stabilization and spindle assembly. Cell 118, 187–202.

Sander, J.D., Joung, J.K., 2014. CRISPR-Cas systems for editing, regulating and targeting genomes. Nat Biotechnol 32, 347–355.

Santos-Rosa, H., Leung, J., Grimsey, N., Peak-Chew, S., Siniossoglou, S., 2005. The yeast lipin Smp2 couples phospholipid biosynthesis to nuclear membrane growth. EMBO J 24, 1931–1941.

Sardar, H.S., Gilbert, S.P., 2012. Microtubule capture by mitotic kinesin centromere protein E (CENP-E). J Biol Chem 287, 24894–24904.

Sasai, K., Katayama, H., Stenoien, D.L., Fujii, S., Honda, R., Kimura, M., Okano, Y., Tatsuka, M., Suzuki, F., Nigg, E.A., Earnshaw, W.C., Brinkley, W.R., Sen, S., 2004. Aurora-C kinase is a novel chromosomal passenger protein that can

complement Aurora-B kinase function in mitotic cells. Cell Motil Cytoskeleton 59, 249–263.

Satinover, D.L., Brautigan, D.L., Stukenberg, P.T., 2006. Aurora-A kinase and inhibitor-2 regulate the cyclin threshold for mitotic entry in *Xenopus* early embryonic cell cycles. Cell Cycle 5, 2268–2274.

Saunders, A.M., Powers, J., Strome, S., Saxton, W.M., 2007. Kinesin-5 acts as a brake in anaphase spindle elongation. Curr Biol 17, 1–5.

Saunders, W.S., Koshland, D., Eshel, D., Gibbons, I.R., Hoyt, M.A., 1995. *Saccharomyces cerevisiae* kinesin- and dynein-related proteins required for anaphase chromosome segregation. J Cell Biol 128, 617–624.

Sawin, K.E., LeGuellec, K., Philippe, M., Mitchison, T.J., 1992. Mitotic spindle organization by a plus-end-directed microtubule motor. Nature 359, 540–543.

Saxton, W.M., Porter, M.E., Cohn, S.A., Scholey, J.M., Raff, E.C., McIntosh, J.R., 1988. *Drosophila* kinesin: characterization of microtubule motility and ATPase. Proc Natl Acad Sci U S A 85, 1109–1113.

Sazer, S., Lynch, M., Needleman, D., 2014. Deciphering the evolutionary history of open and closed mitosis. Curr Biol 24, R1099–1103.

Scahill, M.D., Pastar, I., Cross, G.A.M., 2008. CRE recombinase-based positive-negative selection systems for genetic manipulation in *Trypanosoma brucei*. Mol Biochem Parasitol 157, 73–82.

Schaar, B.T., Chan, G.K., Maddox, P., Salmon, E.D., Yen, T.J., 1997. CENP-E function at kinetochores is essential for chromosome alignment. J Cell Biol 139, 1373–1382.

Schlimme, W., Burri, M., Bender, K., Betschart, B., Hecker, H., 1993. *Trypanosoma brucei* brucei: differences in the nuclear chromatin of bloodstream forms and procyclic culture forms. Parasitology 107, 237–247.

Schmidt, J.C., Arthanari, H., Boeszoermenyi, A., Dashkevich, N.M., Wilson-Kubalek, E.M., Monnier, N., Markus, M., Oberer, M., Milligan, R.A., Bathe, M., Wagner, G., Grishchuk, E.L., Cheeseman, I.M., 2012. The kinetochore-bound Ska1 complex tracks depolymerizing microtubules and binds to curved protofilaments. Dev Cell 23, 968–980.

Schneider, C.A., Rasband, W.S., Eliceiri, K.W., 2012. NIH Image to ImageJ: 25 years of image analysis. Nat Methods 9, 671–675.

Scholey, J.M., 2013. Kinesin-2: a family of heterotrimeric and homodimeric motors with diverse intracellular transport functions. Annu Rev Cell Dev Biol 29, 443–469.

Scholey, J.M., Porter, M.E., Grissom, P.M., McIntosh, J.R., 1985. Identification of kinesin in sea urchin eggs, and evidence for its localization in the mitotic spindle. Nature 318, 483–486.

Schumann Burkard, G., Jutzi, P., Roditi, I., 2011. Genome-wide RNAi screens in bloodstream form trypanosomes identify drug transporters. Mol Biochem Parasitol 175, 91–94.

Scott, V., Sherwin, T., Gull, K., 1997. Gamma-tubulin in trypanosomes: molecular characterisation and localisation to multiple and diverse microtubule organising centres. J Cell Sci 110, 157–168.

Screpanti, E., De Antoni, A., Alushin, G.M., Petrovic, A., Melis, T., Nogales, E., Musacchio, A., 2011. Direct binding of CENP-C to the MIS12 complex joins the inner and outer kinetochore. Curr Biol 21, 391–398.

Seki, A., Coppinger, J.A., Jang, C.-Y., Yates, J.R., Fang, G., 2008. Bora and the kinase Aurora A cooperatively activate the kinase Plk1 and control mitotic entry. Science 320, 1655–1658.

Sessa, F., Mapelli, M., Ciferri, C., Tarricone, C., Areces, L.B., Schneider, T.R., Stukenberg, P.T., Musacchio, A., 2005. Mechanism of Aurora B activation by INCENP and inhibition by hesperadin. Mol Cell 18, 379–391.

Sharp, D.J., Yu, K.R., Sisson, J.C., Sullivan, W., Scholey, J.M., 1999. Antagonistic microtubule-sliding motors position mitotic centrosomes in *Drosophila* early embryos. Nat Cell Biol 1, 51–54.

Sharp, P.A., 1999. RNAi and double-strand RNA. Genes Dev 13, 139–141.

Sherwin, T., Gull, K., 1989. The cell division cycle of *Trypanosoma brucei brucei*: timing of event markers and cytoskeletal modulations. Philos Trans R Soc B 323, 573–588.

Shi, H., Djikeng, A., Mark, T., Wirtz, E., Tschudi, C., Ullu, E., 2000. Genetic interference in *Trypanosoma brucei* by heritable and inducible double-stranded RNA. RNA 6, 1069–1076.

Siegel, T.N., Gunasekera, K., Cross, G.A.M., Ochsenreiter, T., 2011. Gene expression in *Trypanosoma brucei*: lessons from high-throughput RNA sequencing. Trends Parasitol 27, 434–441.

Siegel, T.N., Hekstra, D.R., Kemp, L.E., Figueiredo, L.M., Lowell, J.E., Fenyo, D., Wang, X., Dewell, S., Cross, G.A.M., 2009. Four histone variants mark the boundaries of polycistronic transcription units in *Trypanosoma brucei*. Genes Dev 23, 1063–1076.

Siegel, T.N., Hekstra, D.R., Wang, X., Dewell, S., Cross, G.A.M., 2010. Genome-wide analysis of mRNA abundance in two life-cycle stages of *Trypanosoma brucei* and identification of splicing and polyadenylation sites. Nucleic Acids Res 38, 4946–4957.

Silljé, H.H., Takahashi, K., Tanaka, K., Van Houwe, G., Nigg, E.A., 1999. Mammalian homologues of the plant Tousled gene code for cell-cycle-regulated kinases with maximal activities linked to ongoing DNA replication. EMBO J 18, 5691–5702.

Simon, D.N., Wilson, K.L., 2011. The nucleoskeleton as a genome-associated dynamic “network of networks.” Nat Rev Mol Cell Biol 12, 695–708.

Simpson, A.G.B., Gill, E.E., Callahan, H.A., Litaker, R.W., Roger, A.J., 2004. Early evolution within kinetoplastids (Euglenozoa), and the late emergence of trypanosomatids. Protist 155, 407–422.

Simpson, A.G.B., Roger, A.J., 2004. Protein phylogenies robustly resolve the deep-level relationships within Euglenozoa. Mol Phylogenet Evol 30, 201–212.

Simpson, A.G.B., Stevens, J.R., Lukes, J., 2006. The evolution and diversity of kinetoplastid flagellates. Trends Parasitol 22, 168–174.

Smyth, J.D., 1994. Haemoflagellates. In: Introduction to Animal Parasitology. Cambridge University Press, pp. 57–108.

Solari, A.J., 1980. The 3-dimensional fine structure of the mitotic spindle in Trypanosoma cruzi. Chromosoma 78, 239–255.

Solari, A.J., 1995. Mitosis and genome partition in trypanosomes. Biocell 19, 65–84.

Somers, W.G., Saint, R., 2003. A RhoGEF and Rho family GTPase-activating protein complex links the contractile ring to cortical microtubules at the onset of cytokinesis. Dev Cell 4, 29–39.

Soutoglou, E., Misteli, T., 2008. Activation of the cellular DNA damage response in the absence of DNA lesions. Science 320, 1507–1510.

Sproul, L.R., Anderson, D.J., Mackey, A.T., Saunders, W.S., Gilbert, S.P., 2005. Cik1 targets the minus-end kinesin depolymerase Kar3 to microtubule plus ends. Curr Biol 15, 1420–1427.

Steglich, B., Sazer, S., Ekwall, K., 2013. Transcriptional regulation at the yeast nuclear envelope. Nucleus 4, 379–389.

Stock, M.F., Guerrero, J., Cobb, B., Eggers, C.T., Huang, T.G., Li, X., Hackney, D.D., 1999. Formation of the compact confomer of kinesin requires a COOH-terminal heavy chain domain and inhibits microtubule-stimulated ATPase activity. J Biol Chem 274, 14617–14623.

Straight, A.F., Belmont, A.S., Robinett, C.C., Murray, A.W., 1996. GFP tagging of budding yeast chromosomes reveals that protein-protein interactions can mediate sister chromatid cohesion. Curr Biol 6, 1599–1608.

Straight, A.F., Sedat, J.W., Murray, A.W., 1998. Time-lapse microscopy reveals unique roles for kinesins during anaphase in budding yeast. J Cell Biol 143, 687–694.

Stumpff, J., von Dassow, G., Wagenbach, M., Asbury, C., Wordeman, L., 2008. The kinesin-8 motor Kif18A suppresses kinetochore movements to control mitotic chromosome alignment. Dev Cell 14, 252–262.

Stumpff, J., Wagenbach, M., Franck, A., Asbury, C.L., Wordeman, L., 2012. Kif18A and chromokinesins confine centromere movements via microtubule growth suppression and spatial control of kinetochore tension. Dev Cell 22, 1017–1029.

Sturgill, E.G., Das, D.K., Takizawa, Y., Shin, Y., Collier, S.E., Ohi, M.D., Hwang, W., Lang, M.J., Ohi, R., 2014. Kinesin-12 Kif15 targets kinetochore fibers through an intrinsic two-step mechanism. Curr Biol 24, 2307–2313.

Sturgill, E.G., Ohi, R., 2013. Kinesin-12 differentially affects spindle assembly depending on its microtubule substrate. Curr Biol 1–11.

Subramaniam, C., Veazey, P., Redmond, S., Hayes-Sinclair, J., Chambers, E., Carrington, M., Gull, K., Matthews, K., Horn, D., Field, M.C., 2006. Chromosome-wide analysis of gene function by RNA interference in the african trypanosome. Eukaryot Cell 5, 1539–1549.

Suijkerbuijk, S.J.E., Vleugel, M., Teixeira, A., Kops, G.J.P.L., 2012. Integration of kinase and phosphatase activities by BUBR1 ensures formation of stable kinetochore-microtubule attachments. Dev Cell 23, 745–755.

Sun, Y., Wang, C., Yuan, Y.A., He, C.Y., 2012. An intra-cellular membrane junction mediated by flagellum adhesion glycoproteins links flagellum biogenesis to cell morphogenesis in *Trypanosoma brucei*. J Cell Sci 126, 520–531.

Sunter, J.D., Gull, K., 2015. The flagellum attachment zone: "the cellular ruler" of trypanosome morphology. Trends Parasitol 32, 309–324.

Sunter, J.D., Varga, V., Dean, S., Gull, K., 2015. A dynamic coordination of flagellum and cytoplasmic cytoskeleton assembly specifies cell morphogenesis in trypanosomes. J Cell Sci 128, 1580–1594.

Tanaka, T.U., Rachidi, N., Janke, C., Pereira, G., Galova, M., Schiebel, E., Stark, M.J.R., Nasmyth, K., 2002. Evidence that the Ipl1-Sli15 (Aurora Kinase-INCENP) complex promotes chromosome bi-orientation by altering kinetochore-spindle pole connections. Cell 108, 317–329.

Tanenbaum, M.E., Macůrek, L., Galjart, N., Medema, R.H., 2008. Dynein, Lis1 and CLIP-170 counteract Eg5-dependent centrosome separation during bipolar spindle assembly. EMBO J 27, 3235–3245.

Tanenbaum, M.E., Macůrek, L., Janssen, A., Geers, E.F., Alvarez-Fernández, M., Medema, R.H., 2009. Kif15 cooperates with Eg5 to promote bipolar spindle assembly. Curr Biol 19, 1703–1711.

Tang, C.-J.C., Lin, C.-Y., Tang, T.K., 2006. Dynamic localization and functional implications of Aurora-C kinase during male mouse meiosis. Dev Biol 290, 398–410.

Tao, L., Mogilner, A., Civelekoglu-Scholey, G., Wollman, R., Evans, J., Stahlberg, H., Scholey, J.M., 2006. A homotetrameric kinesin-5, KLP61F, bundles microtubules and antagonizes Ncd in motility assays. Curr Biol 16, 2293–2302.

Taylor, J.E., Rudenko, G., 2006. Switching trypanosome coats: what's in the wardrobe? Trends Genet 22, 614–620.

Taylor, M.C., Huang, H., Kelly, J.M., 2011. Genetic techniques in *Trypanosoma cruzi*. In: Advances in Parasitology. Elsevier Ltd., pp. 231–250.

Taylor, M.C., Kelly, J.M., 2006. pTcINDEX: a stable tetracycline-regulated expression vector for Trypanosoma cruzi. BMC Biotechnol 6, 32.

ten Asbroek, A.L., Ouellette, M., Borst, P., 1990. Targeted insertion of the neomycin phosphotransferase gene into the tubulin gene cluster of *Trypanosoma brucei*. Nature 348, 174–175.

Theis, M., Slabicki, M., Junqueira, M., Paszkowski-Rogacz, M., Sontheimer, J., Kittler, R., Heninger, A.-K., Glatter, T., Kruusmaa, K., Poser, I., Hyman, A.A., Pisabarro, M.T., Gstaiger, M., Aebersold, R., Shevchenko, A., Buchholz, F., 2009.

Comparative profiling identifies C13orf3 as a component of the Ska complex required for mammalian cell division. EMBO J 28, 1453–1465.

Thiede, C., Fridman, V., Gerson-Gurwitz, A., Gheber, L., Schmidt, C.F., 2012. Regulation of bi-directional movement of single kinesin-5 Cin8 molecules. Bioarchitecture 2, 70–74.

Tien, J.F., Umbreit, N.T., Gestaut, D.R., Franck, A.D., Cooper, J., Wordeman, L., Gonen, T., Asbury, C.L., Davis, T.N., 2010. Cooperation of the Dam1 and Ndc80 kinetochore complexes enhances microtubule coupling and is regulated by Aurora B. J Cell Biol 189, 713–723.

Tiengwe, C., Marcello, L., Farr, H., Dickens, N., Kelly, S., Swiderski, M., Vaughan, D., Gull, K., Barry, J.D., Bell, S.D., McCulloch, R., 2012. Genome-wide analysis reveals extensive functional interaction between DNA replication initiation and transcription in the genome of *Trypanosoma brucei*. Cell Rep 2, 185–197.

Tikhonenko, I., Magidson, V., Gräf, R., Khodjakov, A., Koonce, M.P., 2013. A kinesin-mediated mechanism that couples centrosomes to nuclei. Cell Mol Life Sci 70, 1285–1296.

Tschudi, C., Djikeng, A., Shi, H., Ullu, E., 2003. *In vivo* analysis of the RNA interference mechanism in *Trypanosoma brucei*. Methods 30, 304–312.

Tu, X., Kumar, P., Li, Z., Wang, C.C., 2006. An Aurora kinase homologue is involved in regulating both mitosis and cytokinesis in *Trypanosoma brucei*. J Biol Chem 281, 9677–9687.

Tu, X., Wang, C.C., 2004. The involvement of two cdc2-related kinases (CRKs) in *Trypanosoma brucei* cell cycle regulation and the distinctive stage-specific phenotypes caused by CRK3 depletion. J Biol Chem 279, 20519–20528.

Uehara, R., Tsukada, Y., Kamasaki, T., Poser, I., Yoda, K., Gerlich, D.W., Goshima, G., 2013. Aurora B and Kif2A control microtubule length for assembly of a functional central spindle during anaphase. J Cell Biol 202, 623–636.

Umbreit, N.T., Gestaut, D.R., Tien, J.F., Vollmar, B.S., Gonen, T., Asbury, C.L., Davis, T.N., 2012. The Ndc80 kinetochore complex directly modulates microtubule dynamics. Proc Natl Acad Sci U S A 109, 16113–16118.

Ureña, F., 1986. Three-dimensional reconstructions of the mitotic spindle and dense plaques in three species of *Leishmania*. Zeitschrift für Parasitenkd 72, 299–306.

Ureña, F., 1988. [Ultrastructure of the mitotic nuclei in *Leishmania mexicana* ssp. Tridimensional reconstruction of the mitotic spindle and dense plaques]. Rev Biol Trop 36, 129–137.

Uzureau, P., Daniels, J.-P., Walgraffe, D., Wickstead, B., Pays, E., Gull, K., Vanhamme, L., 2008. Identification and characterization of two trypanosome TFIIS proteins exhibiting particular domain architectures and differential nuclear localizations. Mol Microbiol 69, 1121–1136.

Vader, G., Lens, S.M.A., 2008. The Aurora kinase family in cell division and cancer. Biochim Biophys Acta - Rev Cancer 1786, 60–72.

Vader, G., Medema, R.H., Lens, S.M.A., 2006. The chromosomal passenger complex: guiding Aurora-B through mitosis. J Cell Biol 173, 833–837.

Valdés, J., Taylor, M.C., Cross, M.A., Ligtenberg, M.J., Rudenko, G., Borst, P., 1996. The viral thymidine kinase gene as a tool for the study of mutagenesis in *Trypanosoma brucei*. Nucleic Acids Res 24, 1809–1815.

Vale, R.D., 2003. The molecular motor toolbox for intracellular transport. Cell 112, 467–480.

Vale, R.D., Friedman, D.S., 1999. Single-molecule analysis of kinesin motility reveals regulation by the cargo-binding tail domain. Nat Cell Biol 1, 293–297.

Vale, R.D., Goldstein, L.S.B., 1990. One motor, many tails: An expanding repertoire of force-generating enzymes. Cell 60, 883–885.

Vale, R.D., Reese, T.S., Sheetz, M.P., 1985. Identification of a novel force-generating protein, kinesin, involved in microtubule-based motility. Cell 42, 39–50.

van Heesbeen, R.G.H.P., Raaijmakers, J.A., Tanenbaum, M.E., Medema, R.H., 2013. Nuclear envelope-associated dynein cooperates with Eg5 to drive prophase centrosome separation. Commun Integr Biol 6, e23841.

van Heesbeen, R.G.H.P., Tanenbaum, M.E., Medema, R.H., 2014. Balanced activity of three mitotic motors is required for bipolar spindle assembly and chromosome segregation. Cell Rep 8, 948–956.

Vanhamme, L., Pays, E., 1995. Control of gene expression in trypanosomes. Microbiol Rev 59, 223–240.

Vanneste, D., Ferreira, V., Vernos, I., 2011. Chromokinesins: localization-dependent functions and regulation during cell division. Biochem Soc Trans 39, 1154–1160.

Vanneste, D., Takagi, M., Imamoto, N., Vernos, I., 2009. The role of Hklp2 in the stabilization and maintenance of spindle bipolarity. Curr Biol 19, 1712–1717.

Varga, V., Helenius, J., Tanaka, K., Hyman, A.A., Tanaka, T.U., Howard, J., 2006. Yeast kinesin-8 depolymerizes microtubules in a length-dependent manner. Nat Cell Biol 8, 957–962.

Varga, V., Leduc, C., Bormuth, V., Diez, S., Howard, J., 2009. Kinesin-8 motors act cooperatively to mediate length-dependent microtubule depolymerization. Cell 138, 1174–1183.

Vaughan, S., Gull, K., 2008. The structural mechanics of cell division in *Trypanosoma brucei*. Biochem Soc Trans 36, 421–424.

Vedrenne, C., Giroud, C., Robinson, D.R., Besteiro, S., Bosc, C., Bringaud, F., Baltz, T., 2002. Two related subpellicular cytoskeleton-associated proteins in *Trypanosoma brucei* stabilize microtubules. Mol Biol Cell 13, 1058–1070.

Veitch, N.J., Johnson, P.C.D., Trivedi, U., Terry, S., Wildridge, D., MacLeod, A., 2010. Digital gene expression analysis of two life cycle stages of the human-infective parasite, *Trypanosoma brucei gambiense* reveals differentially expressed clusters of co-regulated genes. BMC Genomics 11, 124.

Verdel, A., Jia, S., Gerber, S., Sugiyama, T., Gygi, S., Grewal, S.I.S., Moazed, D., 2004. RNAi-mediated targeting of heterochromatin by the RITS complex. Science 303, 672–676.

Verhey, K.J., Hammond, J.W., 2009. Traffic control: regulation of kinesin motors. Nat Rev Mol Cell Biol 10, 765–777.

Verhey, K.J., Lizotte, D.L., Abramson, T., Barenboim, L., Schnapp, B.J., Rapoport, T.A., 1998. Light chain-dependent regulation of kinesin's interaction with microtubules. J Cell Biol 143, 1053–1066.

Vickerman, K., 1985. Developmental cycles and biology of pathogenic trypanosomes. Br Med Bull 41, 105–114.

Vickerman, K., Preston, T.M., 1970. Spindle microtubules in the dividing nuclei of trypanosomes. J Cell Sci 6, 365–383.

Vleugel, M., Hoogendoorn, E., Snel, B., Kops, G.J.P.L., 2012. Evolution and function of the mitotic checkpoint. Dev Cell 23, 239–250.

Volpe, T., Martienssen, R.A., 2011. RNA interference and heterochromatin assembly. Cold Spring Harb Perspect Biol 3, a003731.

von Delius, M., Leigh, D.A., 2011. Walking molecules. Chem Soc Rev 40, 3656–3676.

Walczak, C.E., Gayek, S., Ohi, R., 2013. Microtubule-depolymerizing kinesins. Annu Rev Cell Dev Biol 29, 417–441.

Walczak, C.E., Heald, R., 2008. Mechanisms of mitotic spindle assembly and function. Int Rev Cytol 265, 111–158.

Walker, P.J., 1961. Organization of function in trypanosome flagella. Nature 189, 1017–1018.

Walther, Z., Vashishtha, M., Hall, J.L., 1994. The *Chlamydomonas* FLA10 gene encodes a novel kinesin-homologous protein. J Cell Biol 126, 175–188.

Wandke, C., Barisic, M., Sigl, R., Rauch, V., Wolf, F., Amaro, A.C., Tan, C.H., Pereira, A.J., Kutay, U., Maiato, H., Meraldi, P., Geley, S., 2012. Human chromokinesins promote chromosome congression and spindle microtubule dynamics during mitosis. J Cell Biol 198, 847–863.

Wang, H., Brust-Mascher, I., Civelekoglu-Scholey, G., Scholey, J.M., 2013. Patronin mediates a switch from kinesin-13-dependent poleward flux to anaphase B spindle elongation. J Cell Biol 203, 35–46.

Wang, Z., Gerstein, M., Snyder, M., 2009. RNA-Seq: a revolutionary tool for transcriptomics. Nat Rev Genet 10, 57–63.

Wang, Z., Morris, J.C., Drew, M.E., Englund, P.T., 2000. Inhibition of *Trypanosoma brucei* gene expression by RNA interference using an integratable vector with opposing T7 promoters. J Biol Chem 275, 40174–40179.

Warnes, A.G.R., Bolker, B., Bonebakker, L., Huber, W., Liaw, A., Lumley, T., Magnusson, A., Moeller, S., Schwartz, M., 2016. Package "gplots."

Watanabe, Y., 2010. Temporal and spatial regulation of targeting Aurora B to the inner centromere. Cold Spring Harb Symp Quant Biol 75, 419–423.

Waters, J.C., Mitchison, T.J., Rieder, C.L., Salmon, E.D., 1996. The kinetochore microtubule minus-end disassembly associated with poleward flux produces a force that can do work. Mol Biol Cell 7, 1547–1558.

Wei, Y., Hu, H., Lun, Z.-R., Li, Z., 2013. The cooperative roles of two kinetoplastid-specific kinesins in cytokinesis and in maintaining cell morphology in bloodstream trypanosomes. PLoS One 8, e73869.

Weinger, J.S., Qiu, M., Yang, G., Kapoor, T.M., 2011. A nonmotor microtubule binding site in kinesin-5 is required for filament crosslinking and sliding. Curr Biol 21, 154–160.

Weir, J.R., Faesen, A.C., Klare, K., Petrovic, A., Basilico, F., Fischböck, J., Pentakota, S., Keller, J., Pesenti, M.E., Pan, D., Vogt, D., Wohlgemuth, S., Herzog, F., Musacchio, A., 2016. Insights from biochemical reconstitution into the architecture of human kinetochores. Nature 537, 249–253.

Welburn, J.P.I., 2013. The molecular basis for kinesin functional specificity during mitosis. Cytoskeleton 70, 476–493.

Welburn, J.P.I., Grishchuk, E.L., Backer, C.B., Wilson-Kubalek, E.M., Yates, J.R., Cheeseman, I.M., 2009. The human kinetochore Ska1 complex facilitates microtubule depolymerization-coupled motility. Dev Cell 16, 374–385.

Westermann, S., Avila-Sakar, A., Wang, H.-W., Niederstrasser, H., Wong, J., Drubin, D.G., Nogales, E., Barnes, G., 2005. Formation of a dynamic kinetochore-microtubule interface through assembly of the Dam1 ring complex. Mol Cell 17, 277–290.

Wheeler, R.J., Gull, K., Gluenz, E., 2012. Detailed interrogation of trypanosome cell biology via differential organelle staining and automated image analysis. BMC Biol 10, 1.

WHO, 2012. Research priorities for Chagas disease, human African trypanosomiasis and leishmaniasis. World Health Organ Tech Rep Ser.

Wickstead, B., Carrington, J.T., Gluenz, E., Gull, K., 2010a. The expanded kinesin-13 repertoire of trypanosomes contains only one mitotic kinesin indicating multiple extra-nuclear roles. PLoS One 5, e15020.

Wickstead, B., Ersfeld, K., Gull, K., 2002. Targeting of a tetracycline-inducible expression system to the transcriptionally silent minichromosomes of *Trypanosoma brucei*. Mol Biochem Parasitol 125, 211–216.

Wickstead, B., Ersfeld, K., Gull, K., 2003. The mitotic stability of the minichromosomes of *Trypanosoma brucei*. Mol Biochem Parasitol 132, 97–100.

Wickstead, B., Ersfeld, K., Gull, K., 2004. The small chromosomes of *Trypanosoma brucei* involved in antigenic variation are constructed around repetitive palindromes. Genome Res 14, 1014–1024.

Wickstead, B., Gull, K., 2006. A “holistic” kinesin phylogeny reveals new kinesin families and predicts protein functions. Mol Biol Cell 17, 1734–1743.

Wickstead, B., Gull, K., Richards, T.A., 2010b. Patterns of kinesin evolution reveal a complex ancestral eukaryote with a multifunctional cytoskeleton. BMC Evol Biol 10, 110.

Wiedenheft, B., Sternberg, S.H., Doudna, J.A., 2012. RNA-guided genetic silencing systems in bacteria and archaea. Nature 482, 331–338.

Wightman, B., Ha, I., Ruvkun, G., 1993. Posttranscriptional regulation of the heterochronic gene *lin-14* by *lin-4* mediates temporal pattern formation in *C. elegans*. Cell 75, 855–862.

Wilson, R.C., Doudna, J.A., 2013. Molecular mechanisms of RNA interference. Annu Rev Biophys 42, 217–239.

Wirtz, E., Clayton, C., 1995. Inducible gene expression in trypanosomes mediated by a prokaryotic repressor. Science 268, 1179–1183.

Wirtz, E., Hoek, M., Cross, G.A.M., 1998. Regulated processive transcription of chromatin by T7 RNA polymerase in *Trypanosoma brucei*. Nucleic Acids Res 26, 4626–4634.

Wirtz, E., Leal, S., Ochatt, C., Cross, G.A.M., 1999. A tightly regulated inducible expression system for conditional gene knock-outs and dominant-negative genetics in *Trypanosoma brucei*. Mol Biochem Parasitol 99, 89–101.

Wittmann, T., Boleti, H., Antony, C., Karsenti, E., Vernos, I., 1998. Localization of the kinesin-like protein Xklp2 to spindle poles requires a leucine zipper, a microtubule-associated protein, and dynein. J Cell Biol 143, 673–685.

Wood, K.W., Sakowicz, R., Goldstein, L.S., Cleveland, D.W., 1997. CENP-E is a plus end-directed kinetochore motor required for metaphase chromosome alignment. Cell 91, 357–66.

Woodward, R., Gull, K., 1990. Timing of nuclear and kinetoplast DNA replication and early morphological events in the cell cycle of *Trypanosoma brucei*. J Cell Sci 95, 49–57.

Wordeman, L., 2010. How kinesin motor proteins drive mitotic spindle function: Lessons from molecular assays. Semin Cell Dev Biol 21, 260–268.

Wordeman, L., Wagenbach, M., Von Dassow, G., 2007. MCAK facilitates chromosome movement by promoting kinetochore microtubule turnover. J Cell Biol 179, 869–879.

Yam, C., He, Y., Zhang, D., Chiam, K.H., Oliferenko, S., 2011. Divergent strategies for controlling the nuclear membrane satisfy geometric constraints during nuclear division. Curr Biol 21, 1314–1319.

Yan, S., Myler, P.J., Stuart, K., 2001. Tetracycline regulated gene expression in Leishmania donovani. Mol Biochem Parasitol 112, 61–69.

Yang, Z., Tulu, U.S., Wadsworth, P., Rieder, C.L., 2007. Kinetochore dynein is required for chromosome motion and congression independent of the spindle checkpoint. Curr Biol 17, 973–980.

Yao, C., Luo, J., Hsiao, C.H.C., Donelson, J.E., Wilson, M.E., 2007. *Leishmania chagasi*: A tetracycline-inducible cell line driven by T7 RNA polymerase. Exp Parasitol 116, 205–213.

Yardimci, H., van Duffelen, M., Mao, Y., Rosenfeld, S.S., Selvin, P.R., 2008. The mitotic kinesin CENP-E is a processive transport motor. Proc Natl Acad Sci U S A 105, 6016–6021.

Yaro, M., Munyard, K.A., Stear, M.J., Groth, D.M., 2016. Combatting African Animal Trypanosomiasis (AAT) in livestock: The potential role of trypanotolerance. Vet Parasitol 225, 43–52.

Zhang, D., Oliferenko, S., 2013. Remodeling the nuclear membrane during closed mitosis. Curr Opin Cell Biol 25, 142–148.

Zhang, W.W., Matlashewski, G., 2015. CRISPR-Cas9-Mediated Genome Editing in Leishmania donovani. MBio 6, e00861.

Zhao, C., Omori, Y., Brodowska, K., Kovach, P., Malicki, J., 2012. Kinesin-2 family in vertebrate ciliogenesis. Proc Natl Acad Sci 109, 2388–2393.

Zhao, Z.-S., Lim, J.P., Ng, Y.-W., Lim, L., Manser, E., 2005. The GIT-associated kinase PAK targets to the centrosome and regulates Aurora-A. Mol Cell 20, 237–249.

Zomerdijk, J.C., Ouellette, M., ten Asbroek, A.L., Kieft, R., Bommer, A.M., Clayton, C.E., Borst, P., 1990. The promoter for a variant surface glycoprotein gene expression site in *Trypanosoma brucei*. EMBO J 9, 2791–2801.